Chapter A.7
Package Operations

TABLE OF CONTENTS

LIST OF TABLES

LIST OF FIGURES

A.7 PACKAGE OPERATIONS

NOTE: References in this chapter are shown as [1], [2], etc., and refer to the reference list in Section A.7.5. A glossary of terms used in this chapter is provided in Section A.7.6.

This chapter contains NUHOMS®-MP197HB cask loading and unloading procedures that are intended to show the general approach to cask operational activities. The procedures in this chapter are intended to show the types of operations that will be performed and are not intended to be limiting. Site specific conditions and requirements may require the use of different equipment and ordering of steps to accomplish the same objectives or acceptance criteria which must be met to ensure the integrity of the package.

A separate operations manual (OM) will be prepared for the NUHOMS®-MP197HB cask to describe the operational steps in greater detail. The OM, along with the information in this chapter, will be used to prepare the site-specific procedures that will address the particular operational considerations related to the cask.

A.7.1 NUHOMS®-MP197HB Package Loading

The use of the NUHOMS®-MP197HB cask to transport fuel offsite involves (1) preparation of the cask for use, (2) verification that the fuel assemblies loaded in the dry shielded canister (DSC) meet the criteria set forth in this document, and (3) installation of a DSC into the cask. Also included herein are procedures to prepare and load fuel in an empty DSC contained in a NUHOMS®-MP197HB cask and to close the DSC.

The use of the NUHOMS®-MP197HB cask to transport dry irradiated and/or contaminated non-fuel bearing solid materials in radioactive waste canisters (RWCs) involves (1) preparation of the cask for use, (2) verification that the waste to be loaded meet the criteria set forth in this document, and (3) loading of the RWC and waste into the cask.

Offsite transport involves (1) preparation of the cask for transport, (2) assembly verification leakage-rate testing of the packaging containment boundary, (3) placement of the cask onto a transportation vehicle, and (4) installation of the impact limiters.

During shipment, the packaging contains any one of the DSCs with its authorized contents as described in Chapter A.1, Appendices A.1.4.1 through A.1.4.9 or an RWC with dry irradiated and/or contaminated non-fuel bearing solid material as described in Appendix A.1.4.9A. Procedures are provided in this section for (1) transport of the cask/DSC/RWC directly from the plant spent fuel pool and (2) transport of a DSC/RWC which was previously stored in a NUHOMS® horizontal storage module (HSM). Section A.7.7 contains an appendix for each DSC model detailing its loading procedures. Table A.7-3 lists these appendices.

A.7.1.1 NUHOMS®-MP197HB Cask Preparation for Loading

Procedures for preparing the cask for use after receipt at the loading site are provided in this section and are applicable for shipment of DSCs loaded with fuel or of RWCs loaded with dry irradiated and/or contaminated non-fuel bearing solid materials.

Intentionally left blank

1. *R*emove the impact limiters from the cask.
2. *P*rior to removing the lid, sample the cask cavity atmosphere.
3. Remove the transportation skid personnel barrier and tie down assembly.
4. Take contamination smears on the outside surfaces of the cask. If necessary, decontaminate the cask.
5. O-ring seals shall be discarded after each use.
6. Install the front and rear trunnions, if required. *I*nstall the trunnion bolts and torque them *to 1000-1100 ft-lbs* following the torquing sequence shown in Figure A.7-1.
7. *L*ift the cask and place it on the onsite transfer trailer or upending frame, or lift the cask/transport skid and place them in the appropriate location.
8. *NOT USED.*
9. *NOT USED.*
10. If transporting any of the smaller diameter DSC models (NUHOMS®-24PT4, 32PT, 24PTH, 61BT, or 61BTH) or an RWC, verify that the MP197HB cask has been fitted with an internal aluminum sleeve (Refer to Drawing MP197HB-71-1014 provided in Chapter A.1, Appendix A.1.4.10.1). This step, if required, can be performed at any time prior to placing the DSC or RWC in the cask.
11. If transporting a NUHOMS®-69BTH DSC with heat load greater than 26 kW, verify that the removable external aluminum fins are available to be fitted to the cask after the cask is closed (Refer to Drawing MP197HB-71-1011 provided in Appendix A.1.4.10.1). Note that fins are not required to meet the 10 CFR 71 requirements and are optional.
12. For a specific DSC model to be loaded inside the MP197HB cask, verify the canister/basket type (A, B, C, D or E as applicable) is appropriate for the fuel to be transported.
13. The candidate intact, damaged and failed fuel assemblies to be transported in a specific DSC model must be evaluated *(by plant records or other means)* to verify that they meet the criteria of the applicable fuel specification as listed in Table A.7-2.
14. For the transportation of fuel within the NUHOMS®-32PT, 24PTH, 32PTH, 32PTH1, or 37PTH DSCs where burnup credit is employed for criticality safety, additional administrative controls to prevent misloading are also outlined in the applicable appendices of this chapter.

A.7.1.2 NUHOMS®-MP197HB Cask Wet Loading

NOTE: The wet loading procedure described in this section is applicable only when using the MP197HB cask for loading fuel from a spent fuel pool into any one of the DSCs listed in Chapter A.1 or for loading irradiated waste into a RWC. This section also provides steps for closure of the DSC/RWC.

Site specific conditions and requirements may require the use of different equipment and ordering of steps than those described below to accomplish the same objectives or acceptance criteria which must be met to ensure the integrity of the package.

1. Prior to being placed in service, the cask is to be cleaned or decontaminated as necessary.
2. *NOT USED.*
3. Remove the ram access closure plate, inspect the sealing surfaces, replace the old seals with new seals, lubricate and re-install the ram access closure plate.
4. *NOT USED.*
5. Engage the cask front trunnions with the lifting yoke using the plant crane, rotate the cask to a vertical orientation, lift the cask from the onsite transfer skid, and place the cask in the plant designated preparation area.
6. Install the shear key plug assembly.
7. If the cask lid has not already been removed, remove the bolts from the cask lid and lift the lid from the cask.
8. *Discard the used lid O-rings.*
9. *NOT USED.*
10. If loading any one of the smaller diameter DSC models (NUHOMS®-24PT4, 32PT, 24PTH, 61BT, or 61BTH) or RWCs from the MP197HB cask, install an unloading flange. Depending on the DSC model being loaded, verify that a DSC bottom spacer of appropriate height is placed at the bottom of the cask. The height of the DSC bottom spacer required for each type of DSC is listed in Table A.7-1.
11. Place an empty DSC in the cask.
12. If damaged fuel is to be loaded in the DSC, place the required number of bottom end caps into the cell locations that are to receive damaged fuel. For the NUHOMS®-24PT4 DSC only, verify that the failed fuel cans, required for loading damaged fuel assemblies if used, have replaced the guide sleeves at the locations specified for the specific configurations of the 24PT4 DSC basket.
13. If failed fuel is to be loaded in the DSC *(24PTH or 61BTH DSCs only)*, put the appropriate empty failed fuel cans in the appropriate locations.

13a. *If fuel and basket spacers are required, the height of the fuel and basket spacers required for each type of DSC is listed in Table A.7-1.*

14. Fill the cask/DSC annulus with water. *Install* the annulus seal.
15. Fill the DSC cavity with water. For the NUHOMS®-32PT, 24PTH, 32PTH, 32PTH1, and 37PTH DSCs, a minimum soluble boron concentration is required during loading and unloading operations.
16. *NOT USED.*
17. *NOT USED.*
18. *NOT USED.*
19. *NOT USED.*
20. *NOT USED.*
21. *NOT USED.*

A.7.1.2.1 DSC/RWC Wet Loading

The procedures for loading, vacuum drying, and sealing the DSC/RWC are described in detail in Appendices A.7.7.1 through A.7.7.10 as listed in Table A.7-3.
Following the completion of the wet loading activities described in a specific appendix listed in Table A.7-3, the MP197HB cask is prepared for downending as described in the next section.

A.7.1.2.2 Preparing the NUHOMS®-MP197HB Cask for Downending

1. Discard and install new drain port seals.
2. If transporting any one of the smaller diameter DSC models (NUHOMS®-24PT4, 32PT, 24PTH, 61BT, or 61BTH) or RWC, place a cask spacer ring at the top of the aluminum sleeve as shown in Drawing MP197HB-71-1014, Chapter A.1, Appendix A.1.4.10.1.
3. Verify that the lid O-ring seals are new.
4. *NOT USED.*
5. Install shims, if required.

5a. Install the DSC top spacer if required. The appropriate height of the DSC top spacer required for each type of DSC is listed in Table A.7-1.

6. Install the cask lid. Follow the torquing sequence shown in Figure A.7-1. *Torque to between 950 and 1040 ft-lbs.*
7. Install new cask vent port seals.
8. *I*nstall new cask test port seals.
9. Evacuate the cavity between the cask and the DSC and backfill with helium.
10. Perform the assembly verification leakage test following the procedure given in Section A.7.4.1.

A.7.1.2.3 NUHOMS®-MP197HB Cask Downending

NOTE: *A*lternate procedures may be developed *for plants with unique requirements.*

1. Remove the shear key plug assembly from the cask.
2. *L*ift the cask over the onsite transfer skid on the transfer trailer.
3. *NOT USED.*
4. Position the cask rear trunnions onto the onsite transfer skid pillow blocks.
5. *Downend the cask and secure it to the skid.*
6. *NOT USED.*
7. *NOT USED.*
8. *NOT USED.*
9. Prepare the cask for transportation in accordance with the procedure described in Section A.7.1.4.

A.7.1.3 NUHOMS®-MP197HB Cask Dry Loading (Transferring a Loaded DSC or RWC from an Overpack into an MP197HB Cask)

A number of NUHOMS® DSCs are currently being used for onsite storage of spent fuel inside the NUHOMS® horizontal storage modules (HSMs) or the advanced horizontal storage modules (AHSMs) under the provisions of 10 CFR 72.

This section summarizes the steps for transferring a previously loaded DSC under a 10 CFR 72 license from the HSM or AHSM (generally referred here as HSM) to the MP197HB cask for transportation. Depending on the most recent use of the cask, several of the initial steps listed below may not be necessary.

An RWC may be stored in an HSM, AHSM or other allowed overpack on the plant site. When the MP197HB cask is dry loaded with an RWC, operational steps similar to dry loading a DSC from an HSM into the MP197HB cask should be used depending on the storage overpack.

CAUTION:

Before initiating any steps described in this section:

- For the DSCs that are already in dry storage under the requirements of 10 CFR 72, the licensee shall review the loading records to ensure that the DSC was not damaged during the insertion or extraction process and that if necessary, appropriate evaluations were performed to verify the integrity of the DSC shell.
- If the storage license of a DSC has been extended beyond the initial licensed term of 20 years, the licensee shall verify that an appropriate time-limited aging analysis (TLAA) has been performed and an aging management program has been implemented to assure that the DSC, basket, and its contents are within the analyzed conditions. The TLAA should consider the effect of fatigue, radiation, depletion of neutron absorbing material, and environmental conditions including internal temperature and pressures. The aging management program should consider use of periodic in-service inspections of accessible canister surfaces to monitor for adverse indications along with radiation and contamination monitoring.
- The licensee shall perform an audit of spent fuel pool records from the time of canister loading for the identification of the loaded fuel assemblies, and
- The licensee shall compare the irradiation parameters of the loaded contents against those shown in Table A.6-17 to ensure compliance with the isotopic depletion analysis.

1. *V*erify that the contents are in compliance with the fuel specification requirements or waste requirements in the Certificate of Compliance (CoC). An independent check of this verification is also required.
2. *V*erify that the prerequisites for the preparation of the NUHOMS®-MP197HB cask for transport in Section A.7.1.1 have been met.
3. If loading any one of the smaller diameter DSC models (NUHOMS®-24PT4, 32PT, 24PTH, 61BT, or 61BTH) in the NUHOMS®-MP197HB cask, install an unloading flange. *V*erify that a DSC bottom spacer of appropriate height is placed at the bottom of the cask. The height of the DSC bottom spacer required for each type of DSC is listed in Table A.7-1.

4. Remove the ram access closure plate and the lid.
5. *NOT USED.*
6. *B*ring the onsite transfer trailer and the NUHOMS®- MP197HB cask to the ISFSI site.
7. Remove the HSM door and the DSC seismic restraint assembly from the HSM.
8. *NOT USED.*
9. *A*lign and dock the cask with the HSM.
10. Install the cask/HSM restraints.
11. Align the hydraulic ram cylinder in the ram trunnion support assembly.
12. Extend the ram hydraulic cylinder *and engage the grapple ring.*
13. *NOT USED.*
14. Retract the ram hydraulic cylinder until the DSC is fully retracted into the cask.
15. *NOT USED.*
16. Remove the hydraulic ram and ram trunnion support assembly.
17. Install the cask ram closure plate following the torquing sequence shown in Figure A.7-1.
18. Remove the cask/HSM restraints.
19. *M*ove the cask to the transfer position.
20. *NOT USED.*
21. *NOT USED.*
22. If transporting any one of the smaller diameter DSC models (NUHOMS®-24PT4, 32PT, 24PTH, 61BT, or 61BTH), place a cask spacer ring at the top of the aluminum sleeve as shown in Drawing MP197HB-71-1014, Chapter A.1, Appendix A.1.4.10.1.
23. Install shims, if required.

23a. Install the DSC top spacer *as specified* in Table A.7-1.

24. Install the cask lid following the torquing sequence shown in Figure A.7-1. *Torque to between 950 and 1040 ft-lbs.*
25. *NOT USED.*
26. *Install* new cask test port seals.
27. Evacuate the cavity between the cask and the DSC and backfill with helium.
28. Remove the shear key plug assembly from the cask.
29. Perform the assembly verification leakage test following the procedure given in Section A.7.4.1.
30. Prepare the cask for transportation in accordance with the procedure described in Section A.7.1.4.

A.7.1.4 NUHOMS®-MP197HB Cask Preparation for Transport

Once the NUHOMS®-MP197HB cask has been loaded using either the wet loading procedure described in Section A.7.1.2 or the dry loading procedure described in Section A.7.1.3 above, the following tasks are performed to prepare the cask for transportation. The cask is assumed to be seated horizontally in the onsite transfer skid. *Alternate procedures may be developed for plants with unique requirements.*

1. Verify that the cask surface removable contamination levels meet the requirements of 49 CFR 173.443 [2] and 10 CFR 71.87 [3].
2. Verify that the assembly verification leakage rate testing specified in Section A.7.4.1 has been performed. This test must be performed within 12 months prior to the shipment.

A.7.1.4.1 Placing the NUHOMS®-MP197HB Cask onto the Conveyance

The procedure for placement of the cask on the conveyance is given in this section. If cask is already on the transportation skid, rig the cask/skid, lift and place them on to the conveyance, then skip to Step 8.

1. *B*ring the cask and onsite transfer trailer to the conveyance.
2. *NOT USED.*
3. *NOT USED.*
4. *NOT USED.*
5. Place the cask onto the transportation skid.
6. Remove the cask upper and lower trunnions and install the trunnion plugs.
7. *NOT USED.*
8. If necessary, install the optional external aluminum fins.
9. Install the transportation skid tie-down straps.
10. Install the impact limiters on the cask *and torque the attachment bolts in accordance with the drawings in Chapter A.1, Appendix A.1.4.10.1.*
11. Remove the impact limiter hoist rings and replace them with hex bolts.
12. Install the cask tamperproof seals.
13. Install the transportation skid personnel barrier.
14. Perform a final radiation survey to assure the cask radiation levels do not exceed 49 CFR 173.441 [2] and 10 CFR 71.47 [3] requirements.
15. Verify that the temperature on all accessible surfaces is < 185°F.
16. Prepare the final shipping documentation and release the loaded cask for shipment.

A.7.2 NUHOMS®-MP197HB Package Unloading

Unloading the NUHOMS®-MP197HB cask after transport involves removing the cask from the conveyance and removing the DSC/RWC from the cask. The cask is designed to allow the DSC/RWC to be unloaded from the cask into a NUHOMS® staging module, hot cell or other

suitable overpack, and provisions exist to allow wet unloading into a fuel pool. The necessary procedures for these tasks are essentially the reverse of those described in Section A.7.1.

A.7.2.1 Receipt of Loaded NUHOMS®-MP197HB Package from Carrier

Procedures for receiving the loaded cask after shipment are described in this section. Procedures for receiving an empty cask are provided in Section A.7.1.1.

1. Verify that the tamperproof seals are intact.
2. Remove the tamperproof seals.
3. Remove the hex bolts from the impact limiters and replace them with the impact limiter hoist rings provided.
4. *R*emove the impact limiters from the cask.
5. Remove the transportation skid personnel barrier and tie-down straps.
6. Remove the external aluminum fins, if present.
7. Take contamination smears on the outside surfaces of the cask. If necessary, decontaminate the cask.
8. Install the front and rear trunnions *and torque them to 1000-1100 ft-lbs* following the torquing sequence shown in Figure A.7-1.
9. *NOT USED.*
10. *L*ift the cask from the conveyance. Place cask onto the onsite transfer trailer or other location.
11. *NOT USED.*
12. Transfer the cask to a staging module, fuel pool, dry cell or storage overpack and unload using the procedures described in the following sections.

A.7.2.2 Removal of Contents from NUHOMS®-MP197HB Cask

A.7.2.2.1 Unloading the NUHOMS®-MP197HB Cask to a Suitable Overpack

The procedure for unloading a DSC/RWC from the cask into an HSM or other authorized overpack is summarized in this section. This procedure is typical of NUHOMS® ISFSIs. *Alternate procedures may be developed for plants with unique requirements.*

1. *V*erify that the prerequisites for the preparation of the MP197HB cask in Section A.7.1.1 have been met.
2. If the shear key plug assembly is not in place, install the shear key plug assembly.
3. Position the onsite transfer trailer in front of the module face.
4. Sample the cask cavity atmosphere through the vent port. Flush the cask interior gases if necessary.
5. Remove the cask ram closure plate.

6. *NOT USED.*
7. Remove the HSM/overpack door.
8. *A*lign the cask with the HSM/overpack.
9. Remove the cask lid.
10. If unloading any one of the smaller diameter DSC models (NUHOMS®-24PT4, 32PT, 24PTH, 61BT, or 61BTH) or smaller RWCs from the MP197HB cask, install an unloading flange.
11. Dock the cask with the HSM/overpack and install the cask/HSM restraints.
12. *NOT USED.*
13. Extend the ram hydraulic cylinder *and engage the grapple ring.*
14. *NOT USED.*
15. Using the ram hydraulic cylinder move the DSC/RWC into the HSM/overpack.
16. *NOT USED.*
17. *NOT USED.*
18. Remove the cask/HSM restraints and move the cask *away* from the HSM/overpack.
19. Install the cask lid and cask ram closure plate, if required.
20. Install the HSM/overpack door and seismic restraint, as applicable.
21. *NOT USED.*
22. *NOT USED.*

A.7.2.2.2 Unloading the NUHOMS®-MP197HB Cask to a Fuel Pool

The procedure for unloading the cask and DSC/RWC to a fuel pool is summarized in this section. Site specific conditions and requirements may require the use of different equipment and ordering of steps than those descried below to accomplish the same objectives or acceptance criteria which must be met to ensure the integrity of the package. Note that the NUHOMS®-MP197HB cask or an alternate suitable cask may be used for onsite movements of the DSC/RWC.

1. *V*erify that the prerequisites for the preparation of the NUHOMS®-MP197HB cask in Section A.7.1.1 have been met.
2. Place the cask in the fuel receiving area.
3. *NOT USED.*
4. *R*otate the cask to a vertical orientation and place the cask in the decon pit.
5. If the shear key plug assembly is not already in place, install the shear key plug assembly.
6. Sample the cask cavity atmosphere. Flush the cask interior gases if necessary.
7. Remove the lid from the cask.
8. *NOT USED.*

9. If the cask contains any one of the smaller diameter DSC models (NUHOMS®-24PT4, 32PT, 24PTH, 61BT, or 61BTH) or RWC, remove the cask spacer ring at the top of the aluminum sleeve as shown in Drawing MP197HB-71-1014, Appendix A.1.4.10.1.
10. Fill the cask/DSC or cask/RWC annulus with water and install the cask/DSC or cask/RWC annulus seal.

After completion of the preparatory steps described above, follow the specific DSC unloading procedure as described in one of Appendices A.7.7.1 through A.7.7.9 as listed in Table A.7-4.

Section A.7.2.2.4 describes the procedures used for unloading of a NUHOMS®-MP197HB cask with an RWC.

A.7.2.2.3 Unloading the NUHOMS®-MP197HB Cask to a Dry Cell

The procedure for handling a DSC in a dry cell is highly dependent on the design of the dry cell and on the intended future use of the DSC. The procedure described below is intended to show the type of operations that will be performed and is not intended to be limiting.

1. Tow the onsite transfer trailer to the hot cell area.
2. *NOT USED.*
3. Using the cask lifting yoke, place the cask in the appropriate handling area.
4. Sample the cask cavity atmosphere. Flush the cask interior gases if necessary.
5. Install the shear key plug assembly, if required.
6. Remove the lid from the cask.
7. *NOT USED.*
8. Transfer the cask to the unloading area.
9. Remove the contents from the cask.
10. Decontaminate the cask as necessary.
11. *NOT USED.*

A.7.2.2.4 Horizontal Unloading of an RWC from the NUHOMS®-MP197HB Cask

This procedure is for handling a NUHOMS®-MP197HB cask with an RWC at a disposal site. The procedure described below is intended to show the type of operations that will be performed and is not intended to be limiting.

1. *NOT USED.*
2. Lift the cask and transfer it onto an unloading cradle.
3. *NOT USED.*
4. *NOT USED.*
5. *NOT USED.*
6. *R*emove the lid from the cask.

7. Install sealing surface protection, as appropriate.
8. Attach liner or waste removal tools.
9. Unload the cask contents into the disposal area.

A.7.3 Preparation of Empty Package for Transport

Previously used and empty NUHOMS®-MP197HB casks shall be prepared for transport per the requirements of 49 CFR 173.427 [2].

A.7.4 Other Operations

A.7.4.1 Leakage Testing of the Containment Boundary

The procedure for leakage testing of the cask containment boundary prior to shipment is given in this section. Assembly verification leakage testing shall conform to the requirements of ANSI N14.5 [1] or ISO -12807 [11]. A flow chart of the assembly verification leakage test is provided in Figure A.7-2. The order in which the leakage tests of the various seals are performed may vary. If more than one leakage detector is available then more than one seal may be tested at a time. Personnel performing the leakage test shall be specifically trained in leakage testing in accordance with SNT-TC-1A [7].

1. Remove the cask vent port plug.
2. Install the cask port tool in the cask vent port.
3. *O*pen the cask vent port.
4. Attach a suitable vacuum pump to the cask port tool.
5. Reduce the cask cavity pressure to below 1.0 psia.
6. *NOT USED.*
7. Fill the cask cavity with helium to atmospheric pressure.
8. Close the vent port bolt.
9. Remove the helium-saturated cask port tool and install a clean (helium free) cask port tool.
10. Connect a mass spectrometer leak detector to the cask port tool.
11. Evacuate the vent port until the vacuum is sufficient to operate the leakage detection equipment.
12. Perform the leakage test. If the leakage rate is greater than $1x10^{-7}$ ref·cm^3/s repair or replace the vent port bolt and/or seal as required and retest.

    NOTE: Upon removing the vent port bolt, it will be necessary to reduce the cask cavity pressure below 1.0 psia and refill with helium through the vent port.
13. Remove the leakage detection equipment.
14. Remove the cask port tool and replace the vent port plug.
15. Remove the lid test port plug.

16. Install the cask port tool in the lid test port.
17. *O*pen the lid test port.
18. Connect the vacuum pump to the cask port tool.
19. Connect the leakage detector to the cask port tool.
20. Evacuate the lid test port until the vacuum is sufficient to operate the leakage detection equipment per the manufacturer's recommendations. Perform a pressure rise leakage test to confirm leakage rate past the outer seal is less than $7x10^{-3}$ ref·cm^3/s of air.
21. Perform the helium leakage test. If the leakage rate is greater than $1x10^{-7}$ ref·cm^3/s repair or replace the cask lid or the cask lid O-ring seals as required and retest.

    NOTE: Upon removing and reinstalling the cask lid, it will be necessary to reduce the cask cavity pressure below 1.0 psia and refill with helium through the vent port. The vent port assembly verification leakage test must also be retested as described above.

22. Remove the leakage detection equipment.
23. Tighten the lid test port screw *in accordance with Drawing MP197HB-71-1002 in Chapter A.1, Appendix A.1.4.10.1.* Remove the cask port tool from the lid test port and replace the lid test port plug.
24. Remove the cask drain port plug.
25. Install the cask port tool in the cask drain port.
26. *V*erify that the cask drain port is closed.
27. Connect the vacuum pump to the cask port tool.
28. Connect the leakage detector to the cask port tool.
29. Evacuate the drain port until the vacuum is sufficient to operate the leakage detection equipment.
30. Perform the leakage test. If the leakage rate is greater than $1x10^{-7}$ ref·cm^3/s repair or replace the drain port bolt and/or seal as required and retest.

    NOTE: Upon removing the drain port bolt, it will be necessary to reduce the cask cavity pressure below 1.0 psia and refill with helium through the vent port. The vent port assembly verification test must also be retested as described above.

31. Remove the leakage detection equipment.
32. Tighten the drain port bolt *in accordance with Drawing MP197HB-71-1002 in Chapter A.1, Appendix A.1.4.10.1.* Remove the cask port tool from the cask drain port and replace the drain port plug.
33. Remove the bottom test port plug.
34. Install the cask port tool in the bottom test port.
35. *O*pen the bottom test port.
36. Connect the vacuum pump to the cask port tool.
37. Connect the leakage detector to the cask port tool.

38. Evacuate the bottom test port until the vacuum is sufficient to operate the leakage detection equipment. Perform a pressure rise leakage test to confirm leakage rate past the outer seal is less than $7x10^{-3}$ ref·cm^3/s of air.

39. Perform the helium leakage test. If the leakage rate is greater than $1x10^{-7}$ ref·cm^3/s repair or replace the cask ram access closure plate or the cask ram access closure plate O-ring seals as required and retest.

    NOTE: Upon removing the cask ram access closure plate, it will be necessary to reduce the cask cavity pressure below 1.0 psia and refill with helium through the vent port. The vent port assembly verification test must also be retested as described above.

40. Remove the leakage detection equipment.

41. Tighten the bottom test port bolt *in accordance with Drawing MP197HB-71-1002 in Chapter A.1, Appendix A.1.4.10.1*. Remove the cask port tool from the bottom test port and replace the bottom test port plug.

This concludes the assembly verification leakage test procedure.

Pages A.7-14 through A.7-16 are intentionally left blank.

A.7.5 References

1. ANSI N14.5-1997, "American National Standard for Radioactive Materials - Leakage Tests on Packages for Shipment," American National Standards Institute, Inc., New York, 1997.
2. Title 49, Code of Federal Regulations, Part 173 (49 CFR 173), "Shippers - General Requirements for Shipments and Packaging."
3. Title 10, Code of Federal Regulations, Part 71 (10 CFR 71), "Packaging and Transportation of Radioactive Material."
4. U.S. Nuclear Regulatory Commission, Office of the Nuclear Material Safety and Safeguards, "Safety Evaluation of VECTRA Technologies' Response to Nuclear Regulatory Commission Bulletin 96-04 for the NUHOMS®-24P and NUHOMS®-7P."
5. U.S. Nuclear Regulatory Commission Bulletin 96-04, "Chemical, Galvanic or Other Reactions in Spent Fuel Storage and Transportation Casks," July 5, 1996.
6. *Not Used.*
7. SNT-TC-1A, "American Society for Nondestructive Testing, Personnel Qualification and Certification in Nondestructive Testing."
8. Updated Final Safety Analysis Report *for* The Standardized Advanced NUHOMS® Horizontal Modular Storage System For Irradiated Nuclear Fuel (CoC 1029) Revision 3.
9. Not used.
10. Not used.
11. ISO-12807, "Safety Transport of Radioactive Materials – Leakage Testing on Packages," First Edition, 1996.

A.7.6 Glossary

The terms used in the above procedures are defined below.

annulus seal: *S*eal placed between the cask and DSC/RWC during operations in the fuel pool.

cask lifting yoke: Passive, open hook lifting yoke used for vertical lifts of the cask.

cask/HSM restraints: Provides the load path between the cask and HSM during DSC transfer operation.

conveyance: Any suitable conveyance such as a railcar, heavy haul trailer, barge, ship, etc.

horizontal storage module (HSM): Concrete shielded structure used for onsite storage of DSCs. HSM references herein refer to all models of HSM (e.g., HSM Model 80, Model 102, Model 152, Model 202, HSM-H, HSM-HS, AHSM, etc.) HSM also includes any other overpack authorized to accept a DSC or RWC via a horizontal transfer.

hydraulic ram: Hydraulic cylinder used to insert/withdraw DSCs to/from HSMs.

onsite transfer skid: Skid present on the onsite transfer trailer used to support the cask during onsite movements. Note in some cases the transportation skid may function as the onsite transfer skid.

onsite transfer trailer: A trailer used for onsite movements of the cask.

ram trunnion support assembly: Frame attached to the skid which provides an anchor for the hydraulic ram during DSC insertion and retrieval.

skid positioning system: Hydraulically operated alignment system that provides the interface between the onsite transfer trailer and the onsite transfer skid. It is used to align the skid (and cask) with the HSM prior to transfer.

Table A.7-1
DSC, Fuel, and Basket Spacer Nominal Heights for Each Type of DSC (in.)

Canister Type	61BT	61BTH		69BTH	24PTH			24PT4	32PT				32PTH	32PTH Type1	32PTH1			37PTH		RWC
		Type 1	Type 2		S	L	S-LC		S-100	S-125	L-100	L-125			S	M	L	S	M	
DSC bottom spacer height[1]	2.20	2.20	2.20	1.24	11.7	5.7	11.7	2.2	11.7	11.7	5.7	5.7	12.5	5.25	12.5	5.25	N/A	16.25	9.0	11.75
DSC top spacer height[1]	0.55	0.55	0.55	0.55	0.55	0.55	0.4	0.3	0.55	0.55	0.55	0.55	0.55	0.55	0.55	0.55	0.3	0.55	0.55	0.55
Fuel spacer height[2][3]	[2][3]	[2][3]	[2][3]	[2][3]	[2][3]	[2][3]	[2][3]	[2][3]	[2][3]	[2][3]	[2][3]	[2][3]	[2][3]	[2][3]	[2][3]	[2][3]	[2][3]	[2][3]	[2][3]	N/A
Basket spacer height[3][4]	N/A	N/A	N/A	N/A	N/A	N/A	N/A	0.5	N/A	N/A	N/A	N/A	1.75	1.75	1.75	1.75	1.75	1.5	1.75	N/A

[1] DSC top and bottom spacers can be combined to one spacer. If one spacer is used, it can be installed either on top or bottom of the DSC.
[2] Fuel spacer can be installed either on top or bottom of the fuel assembly. The height of the spacer *to* be determined using the *formula specified in Appendix A.2.13.14, Table A.2.13.14-2 at time of transport such that the maximum gap* is below 0.5".
[3] Fuel and basket spacers can be combined to one spacer.
[4] Basket spacer can be installed either on top or bottom of the basket.

APPENDIX A.7.7.1
NUHOMS®-24PT4 DSC Wet Loading and Unloading

Appendix A.7.7.1
NUHOMS®-24PT4 DSC Wet Loading and Unloading Procedures

NOTE: References in this appendix are shown as [1], [2], etc., and refer to the reference list in Section A.7.7.1.5. The term DSC as used in this appendix refers to the NUHOMS®-24PT4 DSC.

A.7.7.1.1 NUHOMS®-24PT4 DSC Fuel Loading

The starting condition for the following steps assumes completion of the cask preparation steps in Section A.7.1.2.

1. Lift the cask/DSC and position it over the cask loading area of the spent fuel pool.
2. Lower the cask into the fuel pool.
3. Place the cask in the location of the fuel pool *used for* the cask loading area.
4. Disengage the lifting yoke from the cask lifting trunnions and move the yoke clear of the cask.
5. The potential for fuel misloading is essentially eliminated through the implementation of procedural and administrative controls. The controls instituted to ensure that damaged and/or intact fuel assemblies are placed into a known cell location within a DSC will typically consist of the following:
    - A cask/DSC loading plan is developed to verify that the intact and damaged fuel assemblies meet the burnup, enrichment, and cooling time parameters of the applicable sections as listed in step 13 of Section A.7.1.1.
    - The loading plan is independently verified and approved before the fuel load.
    - A fuel movement schedule is then written, verified, and approved based upon the loading plan. All fuel movements from any rack location are performed under strict compliance with the fuel movement schedule.
    - If loading damaged fuel assemblies, verify that the required number of failed fuel cans for the 24PT4 DSC have replaced the guide sleeves at the authorized locations within the 24PT4 DSC basket.

been fully loaded, check and record the identity and location of each fuel assembly in the DSC.

8. After all the SFAs have been placed into the DSC and their identities verified, position the lifting yoke and the top shield plug (shield plug assembly) and lower the shield plug into the DSC. Optionally the shield plug may be installed using alternate rigging in lieu of the yoke.
9. Visually verify that the top shield plug is properly seated in the DSC.
10. *NOT USED.*
11. Raise the cask to the pool surface *using the cask trunnions and lifting yoke.*
12. *V*erify that *the top shield plug* is properly seated within the DSC. If not, lower the cask and reposition the top shield plug. Repeat steps 9 through 12 as necessary.
13. Continue to raise the cask from the pool until the top region of the cask is accessible.
14. Drain any excess water from the top of the DSC shield plug.
15. Check the radiation levels at the center of the top shield plug and around the perimeter of the cask.
16. As required for crane load limitations, drain water from the DSC. *Use 1 to 3 psig of* helium to backfill the DSC as water is being removed from the DSC cavity.
17. Lift the cask from the fuel pool. As the cask is raised from the pool.
18. Move the cask with loaded DSC to the plant designated preparation area.
19. *If w*ater *is* removed at step 16, *it* may be replaced with spent fuel pool water or equivalent.

A.7.7.1.2 NUHOMS®-24PT4 DSC Drying and Backfilling

1. Check the radiation levels *around* the perimeter of the cask. The cask exterior surface should be decontaminated as necessary. Temporary shielding may be installed as necessary to minimize personnel exposure.
2. *NOT USED.*
3. Disengage the top shield plug *from* the lifting yoke and position *the yoke* clear of the cask.
4. Decontaminate the exposed surfaces of the DSC *cylindrical* shell perimeter and remove the annulus seal.
5. *A*llow water from the annulus to drain out until the water level is approximately twelve inches below the top edge of the DSC shell. Take swipes around the outer *exposed* surface of the DSC shell and check for smearable contamination as required.

CAUTION: Radiation dose rates are expected to be high at the DSC vent and siphon port locations. Use proper ALARA practices (e.g., use of temporary

shielding, appropriate positioning of personnel, etc.) to minimize personnel exposure.

6. Prior to the start of the welding operations, drain approximately 60 gallons of water from the DSC. *Use 1 to 3 psig of helium* to backfill the DSC with an inert gas as water is being removed.

7. *NOT USED.*

8. Install the automated welding machine onto the inner top cover and place the inner top cover with the automated welding machine onto the DSC. Alternately, the inner top cover may be placed on the DSC separately or the inner top cover may be part of the shield plug; in these cases the automated welding machine is installed on the inner top cover already installed in the DSC.

9. Check radiation levels along the surface of the inner top cover plate. Temporary shielding may be installed as necessary.

10. Insert suitable tubing through the vent port such that it terminates just below the DSC top shield plug. Connect the tubing to a hydrogen monitor to allow continuous monitoring of the hydrogen atmosphere in the DSC cavity during welding of the inner top cover plate. Optionally, other methods may be used for continuous monitoring of the hydrogen atmosphere in the DSC cavity during welding of the inner top cover plate.

11. *Take precautions* to prevent debris and weld splatter from entering the annulus.

12. *W*eld the inner top cover plate to the DSC shell.

CAUTION: Continuously monitor the hydrogen concentration in the DSC cavity using the tube arrangement described in step 10 during the inner top cover plate cutting/welding operations. Verify that the measured hydrogen concentration does not exceed a safety limit of 2.4% [4] and [5]. If this limit is exceeded, stop all welding operations and purge the DSC cavity *with 2-3 psig* helium to reduce the hydrogen concentration safely below the 2.4% limit.

13. Perform *required* dye penetrant examination of the weld surface*(s)*.

14. *NOT USED.*

15. *R*emove remaining bulk water from the DSC cavity. *U*se helium to backfill the DSC as water is being removed from the DSC. Alternately, pressurized helium may be introduced through the vent port to *assist removal of* water from the DSC cavity through the siphon port.

16. Once the water stops flowing from the DSC, close the DSC siphon port and disengage the gas source.

17. Connect the VDS to *the cask.*

NOTE: Proceed cautiously when evacuating the DSC to avoid freezing consequences.

18. *S*tart the VDS and draw a vacuum on the DSC cavity. The cavity pressure should be reduced in steps *to optimize moisture removal and avoid freezing. During/between vacuum during steps,* the pump is valved off and the cavity pressure monitored. The

cavity pressure will rise as water and other volatiles in the cavity evaporate. When the cavity pressure stabilizes, the pump is valved in to continue the vacuum drying process. It may be necessary to repeat some steps, depending on the rate and extent of the pressure increase. Vacuum drying is complete when the pressure stabilizes for a minimum of 30 minutes at 3 torr or less.

NOTE: The user shall ensure that the vacuum pump is isolated from the canister cavity when demonstrating compliance with <3 torr for 30 minutes. Simply closing the valve between the canister and the vacuum pump is not sufficient, as a faulty valve allows the vacuum pump to continue to draw a vacuum on the canister. Turning off the pump, or opening the suction side of the pump to atmosphere are examples of ways to assure that the pump is not continuing to draw a vacuum on the canister.

CAUTION: Radiation dose rates are expected to be high at the vent and siphon port locations. Use proper ALARA practices (e.g., use of temporary shielding, appropriate positioning of personnel, etc.) to minimize personnel exposure.

19. Open the valve to the vent port and allow the helium to flow into the DSC cavity.
20. Pressurize the DSC cavity with helium to 6.0 +1.0/-0.0 psig.
21. Perform a helium leakage test on the top shield plug assembly and vent/siphon block and verify that a criterion of $\leq 1 \times 10^{-4}$ ref.cm^3/sec is met.
22. If a leak is found, repair the weld in accordance with the Code of Construction. Re-pressurize the 24PT4-DSC and repeat the helium leakage test.
23. Once no leaks are detected, depressurize the DSC cavity by releasing the helium through the VDS to the plant's spent fuel pool or radioactive waste system, or other appropriate system.
24. Re-evacuate the 24PT4 DSC cavity. The cavity pressure should be reduced in steps. *During/between vacuum drying steps,* the pump is valved off and the cavity pressure monitored. When the cavity pressure stabilizes, the pump is valved in to continue the vacuum drying process. Vacuum drying is complete when the pressure stabilizes for a minimum of 30 minutes at 3 torr.
25. Open the valve on the vent port and allow helium to flow into the DSC cavity to pressurize the 24PT4 DSC to 6.0 +1.0/-0.0 psig (stable for 30 minutes after filling).

    CAUTION: Radiation dose rates are expected to be high at the vent and siphon port locations. Use proper ALARA practices (e.g., use of temporary shielding, appropriate positioning of personnel, etc.) to minimize personnel exposure.

26. *NOT USED.*

A.7.7.1.3 NUHOMS®-24PT4 DSC Sealing Operations

1. Disconnect the VDS from the DSC. Seal weld the prefabricated covers over the vent and siphon ports, inject helium into the blind space just prior to completing welding, and perform *required* dye penetrant weld examination*(s)*.

NOTE: At licensee discretion, a strongback may be installed on the outer top cover plate to flatten the plate. This will require that the outer top cover plate to the 24PT4 DSC shell tack welds be made manually, as the AWS will not fit over the strongback. Remove the strongback after tack welding and install AWS prior to placing the outer top cover plate-weld root pass.

2. Install the outer top cover plate *with* the automated welding system onto the 24PT4 DSC.
3. Tack weld the outer top cover plate to the 24PT4 DSC shell. Weld outer top cover plate root pass. Perform dye penetrant examination of the root pass weld.
4. Weld out the outer top cover plate to the shell and perform *the required* dye penetrant examination on the weld surface*(s)*.
5. *NOT USED.*
6. *D*rain the water from the cask/DSC annulus.

The cask/DSC is now ready to be prepared for downending as described in Chapter A.7, Section A.7.1.2.2.

A.7.7.1.4 Unloading the NUHOMS®-24PT4 DSC to a Fuel Pool

CAUTION: The process of DSC unloading is similar to that used for DSC loading. DSC opening operations described below are to be carefully controlled in accordance with site procedures. This operation is to be performed under the site's standard health physics guidelines for welding, grinding, and handling of potentially highly contaminated equipment. These are to include the use of prudent housekeeping measures and monitoring of airborne particles. Procedures may require tenting, respirators, supplied air, or other measures to contain contamination and minimize the impact on the health and safety of workers.

1. *NOT USED.*
2. *R*emove the siphon cover plate.
3. *R*emove the vent cover plate.
4. Sample the DSC cavity atmosphere. If necessary, flush the DSC cavity gases to the site radwaste systems.

CAUTION: (a) The water fill rate must be regulated during this reflooding operation to ensure that the 24PT4 DSC vent pressure does not exceed 20 psig.

(b) Provide for continuous hydrogen monitoring of the 24PT4 DSC cavity atmosphere during all subsequent cutting operations to ensure that a safety limit of 2.4% hydrogen concentration is not exceeded [4] and [5]. Purge *with 2-3 psig* helium (or any other inert medium) as necessary to maintain the hydrogen concentration safely below this limit.

5. Fill the DSC with spent fuel pool water (or other plant-designated water source) through the siphon port with the vent port open and routed to the plant's off-gas system.

6. *Take precautions to prevent debris from entering* the cask/DSC annulus.
7. *R*emove the closure weld from the outer top cover plate.

CAUTION: Monitor the hydrogen concentration in the DSC cavity during this step to ensure that it does not exceed 2.4% by volume [4] and [5].

8. Remove the DSC outer top cover plate.
9. *R*emove the closure weld from the DSC inner top cover plate.
10. Remove the DSC inner top cover plate.
11. NOT USED
12. Remove excess material on the DSC inside shell surface which may interfere with top shield plug removal.
13. Clean the cask surface of dirt and debris that may have accumulated during transportation or weld removal.
14. *NOT USED.*
15. *NOT USED.*
16. Lower the cask into the fuel pool *using the upper trunnions and lifting yoke.*
17. Disengage the lifting yoke from the cask trunnions and remove the top shield plug.
18. Remove the fuel assemblies (or fuel cans as applicable for damaged fuel assemblies) from the DSC.
19. *R*emove the cask from the pool, and place it in the decon area.
20. Remove the water from the DSC cavity and cask/DSC annulus.
21. Remove the DSC from the cask.
22. Decontaminate the cask inner and outer surfaces as necessary.
23. *NOT USED.*

This page intentionally left blank

A.7.7.1.5 References

1. Not Used.

2. Not Used.

3. Not Used.

4. U.S. Nuclear Regulatory Commission, Office of the Nuclear Material Safety and Safeguards, "Safety Evaluation of VECTRA Technologies' Response to Nuclear Regulatory Commission Bulletin 96-04 for the NUHOMS®-24P and NUHOMS®-7P."

5. U.S. Nuclear Regulatory Commission Bulletin 96-04, "Chemical, Galvanic or Other Reactions in Spent Fuel Storage and Transportation Casks," July 5, 1996.

6. *Not Used.*

APPENDIX A.7.7.2
NUHOMS®-32PT DSC Wet Loading and Unloading

Appendix A.7.7.2
NUHOMS®-32PT DSC Wet Loading and Unloading Procedures

NOTE: References in this appendix are shown as [1], [2], etc., and refer to the reference list in Section A.7.7.2.5. The term DSC as used in this appendix refers to the NUHOMS®-32PT DSC.

A.7.7.2.1 NUHOMS®-32PT DSC Fuel Loading

The starting condition for the following steps assumes completion of the cask preparation steps in Section A.7.1.2.

1. Lift the cask/DSC and position it over the cask loading area of the spent fuel pool.
2. Lower the cask into the fuel pool.
3. Place the cask in the location of the fuel pool *used for* the cask loading area.
4. Disengage the lifting yoke from the cask lifting trunnions and move the yoke clear of the cask.
5. The potential for fuel misloading is essentially eliminated through the implementation of procedural and administrative controls. The controls instituted to ensure that intact spent fuel assemblies (SFAs) and control components (CCs), if applicable, are placed into a known cell location within a DSC will typically consist of the following:
   - A cask/DSC loading plan is developed to verify that the fuel assemblies, and CCs, if applicable, meet the burnup, enrichment and cooling time parameters of the applicable section as listed in step 13 of Section A.7.1.1. If poison rod assemblies (PRAs) are determined to be needed, record the number required and the DSC cell location for each of the PRAs on the loading plan.
   - The loading plan is independently verified and approved before the fuel load.
   - A fuel movement schedule is then written, verified and approved based upon the loading plan. All fuel movements from any rack location are performed under strict compliance with the fuel movement schedule.

5.A Since burnup credit is employed for demonstration of criticality safety, additional administrative controls are required for verification of fuel assembly burnup and to prevent misloading. Fuel loading plans developed in step 5 above shall also include the additional requirements shown in Section A.6.3.4.

6. Prior to loading of an SFA (and CC, if applicable) into the DSC, the identity of the assembly (and CC, if applicable) is to be verified by two individuals using an underwater video camera or other means. Verification of CC identification is optional if the CC has not been moved from the host fuel assembly since its last verification. Read and record the identification number from the fuel assembly (and CC, if applicable) and check this identification number against the DSC loading plan which indicates which fuel assemblies (and CCs, if applicable) are acceptable for transport.
7. Position the fuel assembly for insertion into the selected DSC compartment and load the fuel assembly. Repeat steps 6-7 for each SFA loaded into the DSC. If applicable, insert the required number of PRAs at specific locations called out in the loading plan. After the

DSC has been fully loaded, check and record the identity and location of each fuel assembly and CC, if applicable, in the DSC. Also record the location of each PRA inserted in the DSC (if applicable).

8. After all the SFAs, CCs, and PRAs, if applicable, have been placed into the DSC and their identities verified, lower the shield plug onto the DSC.
9. Visually verify that the top shield plug is properly seated in the DSC.
10. *NOT USED.*
11. Raise the cask to the pool surface *using the cask trunnions and lifting yoke.*
12. *V*erify that *the top shield plug* is properly seated within the DSC. If not, lower the cask and reposition the top shield plug. Repeat steps 9 through 12 as necessary.
13. Continue to raise the cask from the pool until the top region of the cask is accessible.
14. Drain any excess water from the top of the DSC shield plug.
15. Check the radiation levels at the center of the top shield plug and around the perimeter of the cask.
16. Water may be drained from the DSC back into the fuel pool or other suitable location to meet the weight limit on the crane. *Use 2 to 3 psig of* helium to backfill the DSC as water is being removed from the DSC.
17. Lift the cask from the fuel pool.
18. Move the cask with loaded DSC to the plant designated preparation area.
19. *If water is removed* at step 16, *it* may be replaced with spent fuel pool water or equivalent.

A.7.7.2.2 NUHOMS®-32PT DSC Drying and Backfilling

1. Check the radiation levels *around* the perimeter of the cask. The cask exterior surface should be decontaminated as necessary. Temporary shielding may be installed as necessary to minimize personnel exposure.
2. *NOT USED.*
3. Disengage the top shield plug *from* the lifting yoke and position *the yoke* clear of the cask.
4. Decontaminate the exposed surfaces of the DSC *cylindrical* shell perimeter and remove the annulus seal.
5. *A*llow water from the annulus to drain out until the water level is approximately twelve inches below the top edge of the DSC shell. Take swipes around the outer *exposed* surface of the DSC shell and check for smearable contamination as required.

CAUTION: Radiation dose rates are expected to be high at the DSC vent and siphon port locations. Use proper ALARA practices (e.g., use of temporary shielding, appropriate positioning of personnel, etc.) to minimize personnel exposure.

6. Prior to the start of the welding operations, drain a minimum of 750 gallons of water from the DSC. *Use 1 to 3 psig of* helium to backfill the DSC as water is being removed.

7. *NOT USED.*

8. Install the automated welding machine onto the inner top cover and place the inner top cover with the automated welding machine onto the DSC. Alternately, the inner top cover may be placed on the DSC separately or the inner top cover may be part of the shield plug; in these cases the automated welding machine is installed on the inner top cover already installed in the DSC.

9. Check radiation levels along the surface of the inner top cover plate. Temporary shielding may be installed as necessary.

10. Insert suitable tubing through the vent port such that it terminates just below the DSC top shield plug. Connect the tubing to a hydrogen monitor to allow continuous monitoring of the hydrogen atmosphere in the DSC cavity during welding of the inner top cover plate. Optionally, other methods may be used for continuous monitoring of the hydrogen atmosphere in the DSC cavity during welding of the inner top cover plate.

11. *Take precautions* to prevent debris and weld splatter from entering the annulus.

12. *W*eld the inner top cover plate to the DSC shell.

    CAUTION: Continuously monitor the hydrogen concentration in the DSC cavity using the tube arrangement described in step 10 during the inner top cover plate cutting/welding operations. Verify that the measured hydrogen concentration does not exceed a safety limit of 2.4% [4] and [5]. If this limit is exceeded, stop all welding operations and purge the DSC cavity *with 2-3 psig* helium to reduce the hydrogen concentration safely below the 2.4% limit.

13. Perform *required* dye penetrant examination of the weld surface*(s)*.

14. *NOT USED.*

15. *R*emove remaining bulk water from the DSC cavity. *U*se helium to backfill the DSC as water is being removed from the DSC. Alternately, pressurized helium may also be introduced through the vent port to *assist removal of* water from the DSC cavity through the siphon port.

16. Once the water stops flowing from the DSC, close the DSC siphon port and disengage the gas source.

17. Connect the VDS to *the cask.*

    NOTE: Proceed cautiously when evacuating the DSC to avoid freezing consequences.

18. *S*tart the VDS and draw a vacuum on the DSC cavity. The cavity pressure should be reduced in steps *to optimize moisture removal and avoid freezing. During/between vacuum drying steps,* the pump is valved off and the cavity pressure monitored. The cavity pressure will rise as water and other volatiles in the cavity evaporate. When the cavity pressure stabilizes, the pump is valved in to continue the vacuum drying process. It may be necessary to repeat some steps, depending on the rate and extent of the pressure

increase. Vacuum drying is complete when the pressure stabilizes for a minimum of 30 minutes at 3 mm Hg or less.

NOTE: The user shall ensure that the vacuum pump is isolated from the canister cavity when demonstrating compliance with <3 mm Hg for 30 minutes. Simply closing the valve between the canister and the vacuum pump is not sufficient, as a faulty valve allows the vacuum pump to continue to draw a vacuum on the canister. Turning off the pump, or opening the suction side of the pump to atmosphere are examples of ways to assure that the pump is not continuing to draw a vacuum on the canister.

CAUTION: Radiation dose rates are expected to be high at the vent and siphon port locations. Use proper ALARA practices (e.g., use of temporary shielding, appropriate positioning of personnel, etc.) to minimize personnel exposure.

19. Open the valve to the vent port and allow the helium to flow into the DSC cavity.

20. *NOT USED.*

21. *NOT USED.*

22. *NOT USED.*

23. *NOT USED.*

24. Re-evacuate the DSC cavity. The cavity pressure should be reduced in steps. *During/between vacuum drying steps,* the pump is valved off and the cavity pressure monitored. When the cavity pressure stabilizes, the pump is valved in to continue the vacuum drying process. Vacuum drying is complete when the pressure stabilizes for a minimum of 30 minutes at 3 mm Hg *or less.*

25. Open the valve on the vent port and allow helium to flow into the DSC cavity to pressurize the DSC to 2.5 ± 1.0 psig backfill pressure (stable for 30 minutes).

CAUTION: Radiation dose rates are expected to be high at the vent and siphon port locations. Use proper ALARA practices (e.g., use of temporary shielding, appropriate positioning of personnel, etc.) to minimize personnel exposure.

26. *NOT USED.*

A.7.7.2.3 NUHOMS®-32PT DSC Sealing Operations

1. Disconnect the VDS from the DSC. Seal weld the prefabricated covers over the vent and siphon ports, inject helium into the blind space just prior to completing welding, and perform *the required* dye penetrant weld examination*(s)*.

2. Install the outer top cover plate and the automated welding system onto the DSC.

3. Tack weld the outer top cover plate to the DSC shell. Place the outer top cover plate weld root pass.

4. Perform a helium leakage test of the inner top cover plate and vent/siphon port plate welds using the test port in the outer top cover plate and verify that the "leak-tight"

criterion is met. Verify that the personnel performing the leakage test are qualified in accordance with SNT-TC-1A [7]. Alternatively, this leakage test can be done with a test head following step 1.

5. If a leak is found, remove the outer cover plate root pass (if not using the test head), the vent and siphon port plugs and repair the inner cover plate welds. Then repeat applicable procedure steps from Section A.7.7.2.2, step 17.
6. Perform dye penetrant examination of the root pass weld. Weld out the outer top cover plate to the DSC shell and perform *the required* dye penetrant examination on the weld surface*(s)*.
7. Seal weld the prefabricated plug (when applicable) over the outer cover plate test port and perform dye penetrant weld examinations.
8. *NOT USED.*
9. *D*rain the water from the cask/DSC annulus.

The cask/DSC is now ready to be prepared for downending as described in Chapter A.7, Section A.7.1.2.2.

A.7.7.2.4 Unloading a NUHOMS®-32PT DSC to a Fuel Pool

CAUTION: The process of DSC unloading is similar to that used for DSC loading. DSC opening operations described below are to be carefully controlled in accordance with site procedures. This operation is to be performed under the site's standard health physics guidelines for welding, grinding, and handling of potentially highly contaminated equipment. These are to include the use of prudent housekeeping measures and monitoring of airborne particles. Procedures may require tenting, respirators, supplied air or other measures to contain contamination and minimize the impact on the health and safety of workers.

1. *NOT USED.*
2. *R*emove the siphon cover plate.
3. *R*emove the vent cover plate.
4. Sample the DSC cavity atmosphere. If necessary, flush the DSC cavity gases to the site radwaste systems.

CAUTION:
(a) The water fill rate must be regulated during this reflooding operation to ensure that the DSC vent pressure does not exceed 20.0 psig.

(b) Provide for continuous hydrogen monitoring of the DSC cavity atmosphere during all subsequent cutting operations to ensure that a safety limit of 2.4% is not exceeded [4] and [5]. Purge with *2-3 psig* helium (or any other inert medium) as necessary to maintain the hydrogen concentration safely below this limit.

5. Fill the DSC with spent fuel pool water (or other plant designated water source) through the siphon port with the vent port open and routed to the plant's off-gas system. Soluble boron requirements per step 5.A of Section A.7.7.2.1 are applicable for the pool and DSC cavity water.
6. *Take precautions to prevent debris from entering* the cask/DSC annulus.
7. *R*emove the closure weld from the outer top cover plate.

   CAUTION: Monitor the hydrogen concentration in the DSC cavity during this step to ensure that it does not exceed 2.4% by volume [4] and [5].
8. Remove the DSC outer top cover plate.
9. *R*emove the closure weld from the DSC inner top cover plate.
10. Remove the DSC inner top cover plate.
11. NOT USED
12. Remove excess material on the DSC inside shell surface which may interfere with top shield plug removal.
13. Clean the cask surface of dirt and debris that may have accumulated during transportation or weld removal.
14. *NOT USED.*
15. *NOT USED.*
16. Lower the cask into the fuel pool *using the upper trunnions and lifting yoke*.
17. Disengage the lifting yoke from the cask trunnions and remove the top shield plug.
18. Remove the fuel assemblies from the DSC.
19. *R*emove the cask from the pool, and place it in the decon area.
20. Remove the water from the DSC cavity and cask/DSC annulus.
21. Remove the DSC from the cask.
22. Decontaminate the cask inner and outer surfaces as necessary.
23. *NOT USED.*

This page left intentionally blank.

A.7.7.2.5 References

1. ANSI N14.5-1997, "American National Standard for Radioactive Materials - Leakage Tests on Packages for Shipment," American National Standards Institute, Inc., New York, 1997.

2. Not Used.

3. Not Used.

4. U.S. Nuclear Regulatory Commission, Office of the Nuclear Material Safety and Safeguards, "Safety Evaluation of VECTRA Technologies' Response to Nuclear Regulatory Commission Bulletin 96-04 for the NUHOMS®-24P and NUHOMS®-7P."

5. U.S. Nuclear Regulatory Commission Bulletin 96-04, "Chemical, Galvanic or Other Reactions in Spent Fuel Storage and Transportation Casks," July 5, 1996.

6. *Not Used.*

7. SNT-TC-1A, "American Society for Nondestructive Testing, Personnel Qualification and Certification in Nondestructive Testing."

APPENDIX A.7.7.3
NUHOMS®-24PTH DSC Wet Loading and Unloading

Appendix A.7.7.3
NUHOMS®-24PTH DSC Wet Loading and Unloading Procedures

NOTE: References in this appendix are shown as [1], [2], etc. and refer to the reference list in Section A.7.7.3.5. The term DSC as used in this appendix refers to the NUHOMS®-24PTH DSC.

The steps listed below are incorporated by reference into the CoC 9302 Conditions (paragraph 7.(c)) and shall not be deleted or altered in any way without a CoC revision approval from the NRC.

A.7.7.3.1 NUHOMS®-24PTH DSC Fuel Loading

The starting condition for the following steps assumes completion of the cask preparation steps in Section A.7.1.2.

1. Lift the cask/DSC and position it over the cask loading area of the spent fuel pool.
2. Lower the cask into the fuel pool.
3. Place the cask in the location of the fuel pool *used for* the cask loading area.
4. Disengage the lifting yoke from the cask lifting trunnions and move the yoke clear of the cask.
5. The potential for fuel misloading is essentially eliminated through the implementation of procedural and administrative controls. The controls instituted to ensure that failed, damaged and/or intact spent fuel assemblies (SFAs) and control components (CCs), if applicable, are placed into a known cell location within a DSC will typically consist of the following:
    - A cask/DSC loading plan is developed to verify that the intact, damaged and failed SFAs, and CCs, if applicable, meet the burnup, enrichment and cooling time parameters of the applicable sections as listed in step 13 of Section A.7.1.1.
    - The loading plan is independently verified and approved before the fuel load.
    - A fuel movement schedule is then written, verified and approved based upon the loading plan. All fuel movements from any rack location are performed under strict compliance with the fuel movement schedule.
    - If loading damaged fuel assemblies, verify that the required number of bottom end caps are installed in appropriate locations in the basket.
    - If loading failed fuel, verify that the required number of failed fuel cans are installed in the appropriate locations, or, once loaded with fuel, are installed in the appropriate locations in the basket.

5.A Since burnup credit is employed for demonstration of criticality safety, additional administrative controls are required for verification of fuel assembly burnup and to prevent misloading. Fuel loading plans developed in step 5 above shall also include the additional requirements shown in Section A.6.3.4.

6. Prior to loading of an SFA (and CC, if applicable) into the DSC, the identity of the SFA (and CC, if applicable) is to be verified by two individuals using an underwater video camera or other means. Verification of CC identification is optional if the CC has not

been moved from the host fuel assembly since its last verification. Read and record the identification number from the SFA (and CC, if applicable) and check this identification number against the DSC loading plan which indicates which SFAs (and CCs, if applicable) are acceptable for transport.

7. Position the fuel assembly for insertion into the selected DSC storage cell and load the fuel assembly. Repeat steps 6–7 for each SFA loaded into the DSC. If loading damaged fuel assemblies, place top end caps over each damaged fuel assembly placed into the basket. If loading failed fuel, ensure that the failed fuel can lids are installed. After the DSC has been fully loaded, check and record the identity and location of each fuel assembly and CC, if applicable, in the DSC.
8. After all the SFAs and CCs, if applicable, have been placed into the DSC and their identities verified, position the lifting yoke and the top shield plug (shield plug assembly) and lower the shield plug into the DSC. Optionally the shield plug may be installed using alternate rigging in lieu of the yoke.
9. Visually verify that the top shield plug is properly seated in the DSC.
10. *NOT USED.*
11. Raise the cask to the pool surface *using the cask trunnions and lifting yoke.*
12. *V*erify that *the top shield plug* is properly seated within the DSC. If not, lower the cask and reposition the top shield plug. Repeat steps 9 through 12 as necessary.
13. Continue to raise the cask from the pool until the top region of the cask is accessible.
14. Drain any excess water from the top of the DSC shield plug.
15. Check the radiation levels at the center of the top shield plug and around the perimeter of the cask.
16. As required for crane load limitations, drain water from the DSC. *Use 1 to 3 psig of* helium to backfill the DSC as water is being removed from the DSC cavity.
17. Lift the cask from the fuel pool.
18. Move the cask with loaded DSC to the plant designated preparation area.
19. *If w*ater *is* removed at step 16, *it* may be replaced with spent fuel pool water or equivalent.

A.7.7.3.2 NUHOMS®-24PTH DSC Drying and Backfilling

CAUTION: During performance of steps listed in this section, monitor the cask/DSC annulus water level and replenish as necessary to maintain cooling.

1. Check the radiation levels *around* the perimeter of the cask. The cask exterior surface should be decontaminated as necessary. Temporary shielding may be installed as necessary to minimize personnel exposure.
2. *NOT USED.*
3. Disengage the top shield plug *from* the lifting yoke and position *the yoke* clear of the cask.

4. Decontaminate the exposed surfaces of the DSC *cylindrical* shell perimeter and remove the annulus seal.

5. *A*llow water from the annulus to drain out until the water level is approximately twelve inches below the top edge of the DSC shell. Take swipes around the outer *exposed* surface of the DSC shell and check for smearable contamination as required.

   CAUTION: Radiation dose rates are expected to be high at the DSC vent and siphon port locations. Use proper ALARA practices (e.g., use of temporary shielding, appropriate positioning of personnel, etc.) to minimize personnel exposure.

6. Prior to the start of the welding operations, drain a minimum of 750 gallons of water from the DSC. *Use 1 to 3 psig of* helium to backfill the DSC gas as water is being removed from the DSC.

7. *NOT USED.*

8. Install the automated welding machine onto the inner top cover and place the inner top cover with the automated welding machine onto the DSC. Alternately, the inner top cover may be placed on the DSC separately or the inner top cover may be part of the shield plug; in these cases the automated welding machine is installed on the inner top cover already installed in the DSC.

9. Check radiation levels along the surface of the inner top cover plate. Temporary shielding may be installed as necessary.

10. Insert suitable tubing through the vent port such that it terminates just below the DSC top shield plug. Connect the tubing to a hydrogen monitor to allow continuous monitoring of the hydrogen atmosphere in the DSC cavity during welding of the inner top cover plate. Optionally, other methods may be used for continuous monitoring of the hydrogen atmosphere in the DSC cavity during welding of the inner top cover plate.

11. *Take precautions* to prevent debris and weld splatter from entering the annulus.

12. *W*eld the inner top cover plate to the DSC shell.

    CAUTION: Continuously monitor the hydrogen concentration in the DSC cavity using the tube arrangement described in step 10 during the inner top cover plate cutting/welding operations. Verify that the measured hydrogen concentration does not exceed a safety limit of 2.4% [4] and [5]. If this limit is exceeded, stop all welding operations and purge the DSC cavity *with 2-3 psig* helium to reduce the hydrogen concentration safely below the 2.4% limit.

13. Perform *required* dye penetrant examination of the weld surface*(s)*.

14. *NOT USED.*

15. *R*emove remaining bulk water from the DSC cavity. *U*se helium to backfill the DSC as water is being removed from the DSC. Alternately, pressurized helium may be introduced through the vent port to *assist removal* water from the DSC cavity through the siphon port.

16. Once the water stops flowing from the DSC, close the DSC siphon port and disengage the gas source.

17. Connect the VDS to *the cask.*

NOTE: Proceed cautiously when evacuating the DSC to avoid freezing consequences.

18. *S*tart the VDS and draw a vacuum on the DSC cavity. The cavity pressure should be reduced in steps *to optimize moisture removal and avoid freezing. During/between vacuum drying steps,* the pump is valved off and the cavity pressure monitored. The cavity pressure will rise as water and other volatiles in the cavity evaporate. When the cavity pressure stabilizes, the pump is valved in to continue the vacuum drying process. It may be necessary to repeat some steps, depending on the rate and extent of the pressure increase. Vacuum drying is complete when the pressure stabilizes for a minimum of 30 minutes at 3 mm Hg or less.

NOTE: The user shall ensure that the vacuum pump is isolated from the canister cavity when demonstrating compliance with <3 mm Hg for 30 minutes. Simply closing the valve between the canister and the vacuum pump is not sufficient, as a faulty valve allows the vacuum pump to continue to draw a vacuum on the canister. Turning off the pump, or opening the suction side of the pump to atmosphere are examples of ways to assure that the pump is not continuing to draw a vacuum on the canister.

CAUTION: Radiation dose rates are expected to be high at the vent and siphon port locations. Use proper ALARA practices (e.g., use of temporary shielding, appropriate positioning of personnel, etc.) to minimize personnel exposure.

19. Open the valve to the vent port and allow the helium to flow into the DSC cavity.

20. *NOT USED.*

21. *NOT USED.*

22. *NOT USED.*

23. *NOT USED.*

24. Re-evacuate the DSC cavity. The cavity pressure should be reduced in steps. *During/between vacuum during steps,* the pump is valved off and the cavity pressure monitored. When the cavity pressure stabilizes, the pump is valved in to continue the vacuum drying process. Vacuum drying is complete when the pressure stabilizes for a minimum of 30 minutes at 3 mm Hg or less.

25. Open the valve on the vent port and allow helium to flow into the DSC cavity to pressurize the DSC cavity to 2.5 ± 1.0 psig (stable for 30 minutes).

CAUTION: Radiation dose rates are expected to be high at the vent and siphon port locations. Use proper ALARA practices (e.g., use of temporary shielding, appropriate positioning of personnel, etc.) to minimize personnel exposure.

26. *NOT USED.*

A.7.7.3.3 NUHOMS®-24PTH DSC Sealing Operations

CAUTION: During performance of steps listed in this section, monitor the cask/DSC annulus water level and replenish as necessary to maintain cooling.

1. Disconnect the VDS from the DSC. Seal weld the prefabricated covers over the vent and siphon ports, inject helium into the blind space just prior to completing welding, and perform *the required* dye penetrant weld examination*(s)*.
2. Install the outer top cover plate and the automated welding system onto the DSC.
3. Tack weld the outer top cover plate to the DSC shell. Place the outer top cover plate weld root pass.
4. Perform a helium leakage test of the inner top cover plate and vent/siphon port plate welds using the test port in the outer top cover plate and verify that the "leak-tight" criterion is met. Verify that the personnel performing the leakage test are qualified in accordance with SNT-TC-1A [7]. Alternatively, this leakage test can be done with a test head following step 1 above.
5. If a leak is found, remove the outer cover plate root pass (if not using a test head), the vent and siphon port plugs and repair the inner cover plate welds. Then repeat the applicable procedure steps from Section A.7.7.3.2, step 17.
6. Perform dye penetrant examination of the root pass weld. Weld out the outer top cover plate to the DSC shell and perform *the required* dye penetrant examination on the weld surface*(s)*.
7. Seal weld the prefabricated plug (when applicable) over the outer cover plate test port and perform dye penetrant weld examinations.
8. *NOT USED.*
9. *D*rain the water from the cask/DSC annulus.

The cask/DSC is now ready to be prepared for downending as described in Chapter A.7, Section A.7.1.2.2.

A.7.7.3.4 Unloading the NUHOMS®- 24PTH DSC to a Fuel Pool

CAUTION: The process of DSC unloading is similar to that used for DSC loading. DSC opening operations described below are to be carefully controlled in accordance with site procedures. This operation is to be performed under the site's standard health physics guidelines for welding, grinding, and handling of potentially highly contaminated equipment. These are to include the use of prudent housekeeping measures and monitoring of airborne particles. Procedures may require tenting, respirators, supplied air or other measures to contain contamination and minimize the impact on the health and safety of workers.

1. *NOT USED.*
2. *R*emove the siphon cover plate.
3. *R*emove the vent cover plate.
4. Sample the DSC cavity atmosphere. If necessary, flush the DSC cavity gases to the site radwaste systems.

CAUTION: (a) The water fill rate must be regulated during this reflooding operation to ensure that the DSC vent pressure does not exceed 20.0 psig.

(b) Provide for continuous hydrogen monitoring of the DSC cavity atmosphere during all subsequent cutting operations to ensure that a safety limit of 2.4% is not exceeded [4] and [5]. Purge *with 2-3 psig* helium (or any other inert medium) as necessary to maintain the hydrogen concentration safely below this limit.

5. Fill the DSC with spent fuel pool water (or other plant-designated water source) through the siphon port with the vent port open and routed to the plant's off-gas system. Soluble boron requirements per step 5.A of Section A.7.7.3.1 are applicable for the pool and DSC cavity water.
6. *Take precautions to prevent debris from entering* the cask/DSC annulus.
7. *R*emove the closure weld from the outer top cover plate.

CAUTION: Monitor the hydrogen concentration in the DSC cavity during this step to ensure that it does not exceed 2.4% by volume [4] and [5].

8. Remove the DSC outer top cover plate.
9. *R*emove the closure weld from the DSC inner top cover plate.
10. Remove the DSC inner top cover plate.
11. NOT USED
12. Remove excess material on the DSC inside shell surface which may interfere with top shield plug removal.
13. Clean the cask surface of dirt and debris that may have accumulated during transportation or weld removal.
14. *NOT USED.*
15. *NOT USED.*
16. Lower the cask into the fuel pool *using the upper trunnions and lifting yoke.*
17. Disengage the lifting yoke from the cask trunnions and remove the top shield plug.
18. Remove the fuel assemblies (or fuel cans/end caps as applicable for failed/damaged fuel assemblies) from the DSC.
19. *R*emove the cask from the pool.
20. Remove the water from the DSC cavity and cask/DSC annulus.
21. Remove the DSC from the cask.
22. Decontaminate the cask as necessary.
23. *NOT USED.*

Pages A.7.7.3-7 and A.7.7.3-8 left intentionally blank.

A.7.7.3.5 References

1. ANSI N14.5-1997, "American National Standard for Radioactive Materials - Leakage Tests on Packages for Shipment," American National Standards Institute, Inc., New York, 1997.

2. Not Used.

3. Not Used.

4. U.S. Nuclear Regulatory Commission, Office of the Nuclear Material Safety and Safeguards, "Safety Evaluation of VECTRA Technologies' Response to Nuclear Regulatory Commission Bulletin 96-04 for the NUHOMS®-24P and NUHOMS®-7P."

5. U.S. Nuclear Regulatory Commission Bulletin 96-04, "Chemical, Galvanic or Other Reactions in Spent Fuel Storage and Transportation Casks," July 5, 1996.

6. *Not Used.*

7. SNT-TC-1A, "American Society for Nondestructive Testing, Personnel Qualification and Certification in Nondestructive Testing."

APPENDIX A.7.7.4
NUHOMS®-32PTH DSC Wet Loading and Unloading

Appendix A.7.7.4
NUHOMS®-32PTH DSC Wet Loading and Unloading Procedures

NOTE: References in this appendix are shown as [1], [2], etc., and refer to the reference list in Section A.7.7.4.5. The term DSC as used in this appendix refers to the NUHOMS®-32PTH DSC.

A.7.7.4.1 NUHOMS®-32PTH DSC Fuel Loading

The starting condition for the following steps assumes completion of the cask preparation steps in Section A.7.1.2.

1. Lift the cask/DSC and position it over the cask loading area of the spent fuel pool.
2. Lower the cask into the fuel pool.
3. Place the cask in the location of the fuel pool *used for* the cask loading area.
4. Disengage the lifting yoke from the cask lifting trunnions and move the yoke clear of the cask.
5. The potential for fuel misloading is essentially eliminated through the implementation of procedural and administrative controls. The controls instituted to ensure that damaged and/or intact spent fuel assemblies (SFAs) and control components (CCs), if applicable, are placed into a known cell location within a DSC will typically consist of the following:
   - A cask/DSC loading plan is developed to verify that the intact, damaged SFAs and CCs, if applicable, meet the burnup, enrichment and cooling time parameters of the applicable sections as listed in step 13 of Section A.7.1.1.
   - The loading plan is independently verified and approved before the fuel load.
   - A fuel movement schedule is then written, verified and approved based upon the loading plan. All fuel movements from any rack location are performed under strict compliance with the fuel movement schedule.
   - If loading damaged fuel assemblies, verify that the required number of bottom end caps are installed in appropriate locations in the basket.

5.A Since burnup credit is employed for demonstration of criticality safety, additional administrative controls are required for verification of fuel assembly burnup and to prevent misloading. Fuel loading plans developed in step 5 above shall also include the additional requirements shown in Section A.6.3.4.

6. Prior to loading of an SFA (and CCs, if applicable) into the DSC, the identity of the assembly (and CCs, if applicable) is to be verified by two individuals using an underwater video camera or other means. Verification of CC identification is optional if the CC has not been moved from the host SFA since its last verification. Read and record the identification number from the SFA (and CCs, if applicable) and check this identification number against the DSC loading plan which indicates which SFA (and CC, if applicable) are acceptable for transport.

7. Position the fuel assembly for insertion into the selected DSC compartment and load the fuel assembly. Repeat steps 6–7 for each SFA loaded into the DSC. After the DSC has been fully loaded, check and record the identity and location of each fuel assembly and CCs, if applicable, in the DSC. If loading damaged fuel assemblies, place top end caps over each damaged fuel assembly placed into the basket.
8. After all the SFAs and CCs, if applicable, have been placed into the DSC and their identities verified, lower the shield plug into the DSC.
9. Visually verify that the top shield plug is properly seated in the DSC.
10. *NOT USED.*
11. Raise the cask to the pool surface *using the cask trunnions and lifting yoke.*
12. *V*erify that *the top shield plug* is properly seated within the DSC. If not, lower the cask and reposition the top shield plug. Repeat steps 9 through 12 as necessary.
13. Continue to raise the cask from the pool until the top region of the cask is accessible.
14. Drain any excess water from the top of the DSC shield plug.
15. Check the radiation levels at the center of the top shield plug and around the perimeter of the cask.
16. As required for crane load limitations, drain water from the DSC. *Use 1 to 3 psig of* helium to backfill the DSC as water is being removed from the DSC cavity.
17. Lift the cask from the fuel pool.
18. Move the cask with loaded DSC to the plant designated preparation area.
19. *If water is removed* at step 16, *it* may be replaced with spent fuel pool water or equivalent.

A.7.7.4.2 NUHOMS®-32PTH DSC Drying and Backfilling

CAUTION: During performance of steps listed in this section, monitor the cask/DSC annulus water level and replenish as necessary to maintain cooling.

1. Check the radiation levels *around* perimeter of the cask. The cask exterior surface should be decontaminated as necessary. Temporary shielding may be installed as necessary to minimize personnel exposure.
2. *NOT USED.*
3. Disengage the top shield plug *from* the lifting yoke and position *the yoke* clear of the cask.
4. Decontaminate the exposed surfaces of the DSC *cylindrical* shell perimeter and remove the annulus seal.

5. *A*llow water from the annulus to drain out until the water level is approximately twelve inches below the top edge of the DSC shell. Take swipes around the outer *exposed* surface of the DSC shell and check for smearable contamination as required.

   CAUTION: Radiation dose rates are expected to be high at the DSC vent and siphon port locations. Use proper ALARA practices (e.g., use of temporary shielding, appropriate positioning of personnel, etc.) to minimize personnel exposure.

6. If water was not drained from the DSC earlier, remove up to 1300 gallons of water. Up to *1 to 3 psig* of helium gas may be applied at the vent port to assist the water pump down.

7. *NOT USED.*

8. Install the automated welding machine onto the inner top cover and place the inner top cover with the automated welding machine onto the DSC. Alternately, the inner top cover may be placed on the DSC separately or the inner top cover may be part of the shield plug; in these cases the automated welding machine is installed on the inner top cover already installed in the DSC.

9. Check radiation levels along the surface of the inner top cover plate.

10. Insert suitable tubing through the vent port such that it terminates just below the DSC top shield plug. Connect the tubing to a hydrogen monitor to allow continuous monitoring of the hydrogen atmosphere in the DSC cavity during welding of the inner top cover plate. Optionally, other methods may be used for continuous monitoring of the hydrogen atmosphere in the DSC cavity during welding of the inner top cover plate.

11. *Take precautions* to prevent debris and weld splatter from entering the annulus.

12. *W*eld the inner top cover plate to the DSC shell.

    CAUTION: Continuously monitor the hydrogen concentration in the DSC cavity using the tube arrangement described in step 10 during the inner top cover plate cutting/welding operations. Verify that the measured hydrogen concentration does not exceed a safety limit of 2.4% [4] and [5]. If this limit is exceeded, stop all welding operations and purge the DSC cavity *with 2-3 psig* helium to reduce the hydrogen concentration safely below the 2.4% limit.

13. Perform *required* dye penetrant examination of the weld surface*(s)*.

14. *NOT USED.*

15. *Remove* remaining water from the DSC.

16. Engage the helium supply and open the valve on the vent port and allow *up to 15 psig* helium to *assist removal of* water from the DSC cavity through the siphon port.

17. Once the water stops flowing from the DSC, close the DSC siphon port and disengage the gas source.

    NOTE: Proceed cautiously when evacuating the DSC to avoid freezing consequences.

18. Connect a vacuum pump/helium backfill manifold to the vent port or to both the vent and drain ports.

    Optionally, leak test the manifold and the connections to the DSC. The DSC may be pressurized to no more than 15 psig for leakage testing.

    When the cavity pressure stabilizes, the pump is valved in to complete the vacuum drying process. It may be necessary to repeat some steps, depending on the rate and extent of the pressure increase. Vacuum drying is complete when the pressure stabilizes for a minimum of 30 minutes at 3 mm Hg or less.

    NOTE: The user shall ensure that the vacuum pump is isolated from the canister cavity when demonstrating compliance with <3 mm Hg for 30 minutes. Simply closing the valve between the canister and the vacuum pump is not sufficient, as a faulty valve allows the vacuum pump to continue to draw a vacuum on the canister. Turning off the pump, or opening the suction side of the pump to atmosphere are examples of ways to assure that the pump is not continuing to draw a vacuum on the canister.

    CAUTION: Radiation dose rates are expected to be high at the vent and siphon port locations. Use proper ALARA practices (e.g., use of temporary shielding, appropriate positioning of personnel, etc.) to minimize personnel exposure.

19. If the DSC cavity pressure remains below the specified limit for the required duration with the pump isolated, continue to the next step. If not, repeat steps 18 and 19.

20. Purge air from the backfill manifold, open the isolation valve, and backfill the DSC cavity with helium to 16.5 to 18 psig and hold for 10 minutes.

21. Reduce the DSC cavity pressure to atmospheric pressure, or slightly over.

22. If the quick connect fittings were removed for vacuum drying, remove the vacuum line adapters from the ports, and re-install the quick connect fittings using suitable pipe thread sealant.

    CAUTION: Radiation dose rates are expected to be high at the vent and siphon port locations. Use proper ALARA practices (e.g., use of temporary shielding, appropriate positioning of personnel, etc.) to minimize personnel exposure.

23. Evacuate the DSC through the vent port quick connect fitting to a pressure 100 mbar or less.

24. Purge air from the backfill manifold, open the isolation valve, and backfill the DSC cavity with helium to 2.5 ± 1 psig (stable for 30 minutes).

25. *NOT USED.*

A.7.7.4.3 NUHOMS®-32PTH DSC Sealing Operations

CAUTION: During performance of steps listed in this section, monitor the cask/DSC annulus water level and replenish as necessary to maintain cooling.

1. Disconnect the VDS from the DSC. Weld the covers over the vent and drain ports, performing *the required* non-destructive examination of the weld surface*(s)*.
2. Install a temporary test head fixture (or any other alternative means). Perform a helium leakage test of the inner top cover/shield plug to the DSC shell welds and siphon/vent cover welds to demonstrate that these welds meet the "leak-light" criterion. If the leakage rate *is not met,* check and repair these welds. Verify that the personnel performing the leakage test are qualified in accordance with SNT-TC-1A [7].
3. Place the outer top cover plate onto the DSC. Install the automated welding machine onto the outer top cover plate.
4. Tack weld the outer top cover plate to the DSC shell. Place the outer top cover plate weld root pass.
5. If not previously performed, perform helium leakage test of the inner top cover plate and vent/siphon port plate welds using the test port in the outer top cover plate and verify that the "leak-tight" criterion is met. Verify that the personnel performing the leakage test are qualified in accordance with SNT-TC-1A [7]. Alternatively, this leakage test can be done with a test head in step 2.
    a. If a leak is found, remove the outer cover plate root pass (if not using a test head), the vent and siphon port plugs and repair the inner cover plate welds. Then repeat applicable procedure steps from Section A.7.7.4.2, step 18.
6. Perform dye penetrant examination of the root pass weld. Weld out the outer top cover plate to the DSC shell and perform *the required* dye penetrant examination on the weld surface*(s)*.
7. Seal weld the prefabricated plug (when applicable) over the outer cover plate test port and perform dye penetrant weld examinations.
8. *NOT USED.*
9. *D*rain the water from the cask/DSC annulus.

The cask/DSC is now ready to be prepared for downending as described in Chapter A.7, Section A.7.1.2.2.

A.7.7.4.4 Unloading a NUHOMS®-32PTH DSC to a Fuel Pool

CAUTION: The process of DSC unloading is similar to that used for DSC loading. DSC opening operations described below are to be carefully controlled in accordance with site procedures. This operation is to be performed under the site's standard health physics guidelines for welding, grinding, and handling of potentially highly contaminated equipment. These are to include the use of prudent housekeeping measures and monitoring of airborne particles. Procedures may require tenting, respirators, supplied air or other measures to contain contamination and minimize the impact on the health and safety of workers.

1. *NOT USED.*
2. *R*emove the siphon cover plate.
3. *R*emove the vent cover plate.
4. Sample the DSC cavity atmosphere. If necessary, flush the DSC cavity gases to the site radwaste systems.

CAUTION:

(a) The water fill rate must be regulated during this reflooding operation to ensure that the DSC vent pressure does not exceed 15.0 psig.

(b) Provide for continuous hydrogen monitoring of the DSC cavity atmosphere during all subsequent cutting operations to ensure that a safety limit of 2.4% is not exceeded [4] and [5]. Purge *with 2-3 psig* helium (or any other inert medium) as necessary to maintain the hydrogen concentration safely below this limit.

5. Fill the DSC with spent fuel pool water (or other plant-designated water source) through the siphon port with the vent port open and routed to the plant's off-gas system. Soluble boron requirements per step 5.A of Section A.7.7.4.1 are applicable for the pool and DSC cavity water. The vented cavity gas may include steam, water, and radioactive material, and should be routed accordingly. Monitor the vent pressure and regulate the water fill rate to ensure that the pressure does not exceed 15 psig.
6. Install the cask/DSC annulus.
7. *R*emove the closure weld from the outer top cover plate.

   CAUTION: Monitor the hydrogen concentration in the DSC cavity during this step to ensure that it does not exceed 2.4% by volume [4] and [5].
8. Remove the DSC outer top cover plate.
9. *R*emove the closure weld from the DSC inner top cover plate.
10. *NOT USED.*
11. NOT USED.
12. Remove excess material on the DSC inside shell surface which may interfere with top shield plug removal.

13. Clean the cask surface of dirt and debris that may have accumulated during transportation or weld removal.
14. *NOT USED.*
15. *NOT USED.*
16. *NOT USED.*
17. Lower the cask into the fuel pool *using the upper trunnions and lifting yoke.*
18. Disengage the lifting yoke from the cask trunnions and remove the top shield plug.
19. Remove the fuel assemblies (end caps as applicable for damaged assemblies) from the DSC.
20. *R*emove the cask from the pool, and place it in the decon area.
21. Remove the water from the DSC cavity and cask/DSC annulus.
22. Remove the DSC from the cask.
23. Decontaminate the cask as necessary.
24. *NOT USED.*

This page left intentionally blank.

A.7.7.4.5 References

1. ANSI N14.5-1997, "American National Standard for Radioactive Materials - Leakage Tests on Packages for Shipment," American National Standards Institute, Inc., New York, 1997.

2. Not Used.

3. Not Used.

4. U.S. Nuclear Regulatory Commission, Office of the Nuclear Material Safety and Safeguards, "Safety Evaluation of VECTRA Technologies' Response to Nuclear Regulatory Commission Bulletin 96-04 for the NUHOMS®-24P and NUHOMS®-7P."

5. U.S. Nuclear Regulatory Commission Bulletin 96-04, "Chemical, Galvanic or Other Reactions in Spent Fuel Storage and Transportation Casks," July 5, 1996.

6. *Not Used.*

7. SNT-TC-1A, "American Society for Nondestructive Testing, Personnel Qualification and Certification in Nondestructive Testing."

APPENDIX A.7.7.5
NUHOMS®-32PTH1 DSC Wet Loading and Unloading

Appendix A.7.7.5
NUHOMS®-32PTH1 DSC Wet Loading and Unloading Procedures

NOTE: References in this appendix are shown as [1], [2], etc. and refer to the reference list in Section A.7.7.5.5. The term DSC as used in this appendix refers to the NUHOMS®-32PTH1 DSC.

A.7.7.5.1 NUHOMS®-32PTH1 DSC Fuel Loading

The starting condition for the following steps assumes completion of the cask preparation steps in Section A.7.1.2.

1. Lift the cask/DSC and position it over the cask loading area of the spent fuel pool.
2. Lower the cask into the fuel pool.
3. Place the cask in the location of the fuel pool *used for* the cask loading area.
4. Disengage the lifting yoke from the cask lifting trunnions and move the yoke clear of the cask.
5. The potential for fuel misloading is essentially eliminated through the implementation of procedural and administrative controls. The controls instituted to ensure that damaged and/or intact spent fuel assemblies (SFAs) and control components (CCs), if applicable, are placed into a known cell location within a DSC will typically consist of the following:
   - A cask/DSC loading plan is developed to verify that the SFAs, and CCs, if applicable, meet the burnup, enrichment and cooling time parameters of the applicable sections listed in step 13 of Section A.7.1.1.
   - The loading plan is independently verified and approved before the fuel load.
   - A fuel movement schedule is then written, verified and approved based upon the loading plan. All fuel movements from any rack location are performed under strict compliance with the fuel movement schedule.
   - If loading damaged fuel assemblies, verify that the required number of bottom end caps are installed in appropriate basket locations.

5.A Since burnup credit is employed for demonstration of criticality safety, additional administrative controls are required for verification of fuel assembly burnup and to prevent misloading. Fuel loading plans developed in step 5 above shall also include the additional requirements shown in Section A.6.3.4.

6. Prior to loading of an SFA (and CC, if applicable) into the DSC, the identity of the assembly (and CC, if applicable) is to be verified by two individuals using an underwater video camera or other means. Verification of CC identification is optional if the CC has not been moved from the host fuel assembly since its last verification. Read and record the identification number from the SFA (and CC, if applicable) and check this identification number against the DSC loading plan which indicates which SFAs(and CCs, if applicable) are acceptable for transport.

7. Position the fuel assembly for insertion into the selected DSC compartment and load the fuel assembly. Repeat steps 6 through 7 for each SFA loaded into the DSC. If loading damaged fuel assemblies, place top end caps over each damaged fuel assembly placed into the basket. After the DSC has been fully loaded, check and record the identity and location of each SFA and CC, if applicable, in the DSC.
8. After all the SFAs, and CCs, if applicable, have been placed into the DSC and their identities verified, lower the shield plug onto the DSC.
9. Visually verify that the top shield plug is properly seated in the DSC.
10. *NOT USED.*
11. Raise the cask to the pool surface *using the cask trunnions and lifting yoke.*
12. *V*erify that *the top shield plug* is properly seated within the DSC. If not, lower the cask and reposition the top shield plug. Repeat steps 9 through 12 as necessary.
13. Continue to raise the cask from the pool until the top region of the cask is accessible.
14. Drain any excess water from the top of the DSC shield plug.
15. Check the radiation levels at the center of the top shield plug and around the perimeter of the cask.
16. Drain a minimum of 50 gallons of water. Optionally water may be drained from the DSC back into the fuel pool or other suitable location to meet the weight limit on the crane. *Use 1 to 3 psig of* helium to backfill the DSC with helium gas as water is being removed from the DSC.
17. Lift the cask from the fuel pool. Provisions shall be made to assure that air will not enter the DSC cavity.
18. Move the cask with loaded DSC to the plant designated preparation area.
19. *If water is removed* at step 16, *it* may be replaced with spent fuel pool water or equivalent.

A.7.7.5.2 NUHOMS®-32PTH1 DSC Drying and Backfilling

CAUTION: During performance of steps listed in this section, monitor the cask/DSC annulus water level and replenish as necessary to maintain cooling.

1. Check the radiation levels *around* the perimeter of the cask. The cask exterior surface should be decontaminated as necessary. Temporary shielding may be installed as necessary to minimize personnel exposure.
2. *NOT USED.*
3. Disengage the top shield plug *from* the lifting yoke and position *the yoke* clear of the cask.
4. Decontaminate the exposed surfaces of the DSC *cylindrical* shell perimeter and remove the annulus seal.

5. *A*llow water from the annulus to drain out until the water level is approximately twelve inches below the top edge of the DSC shell. Take swipes around the outer surface of the DSC shell and check for smearable contamination as required.

   CAUTION: Radiation dose rates are expected to be high at the DSC vent and siphon port locations. Use proper ALARA practices (e.g., use of temporary shielding, appropriate positioning of personnel, etc.) to minimize personnel exposure.

6. Prior to the start of the welding operations, drain approximately 900 gallons of water from the DSC. *Use 1 to 3 psig* helium to backfill the DSC with an inert gas as water is being removed from the DSC.

7. *NOT USED.*

8. Install the automated welding machine onto the inner top cover and place the inner top cover with the automated welding machine onto the DSC. Alternately, the inner top cover may be placed on the DSC separately or the inner top cover may be part of the shield plug; in these cases the automated welding machine is installed on the inner top cover already installed in the DSC.

9. Check radiation levels the surface of the inner top cover plate. Temporary shielding may be installed as necessary.

10. Insert suitable tubing through the vent port such that it terminates just below the DSC top shield plug. Connect the tubing to a hydrogen monitor to allow continuous monitoring of the hydrogen atmosphere in the DSC cavity during welding of the inner top cover plate. Optionally, other methods may be used for continuous monitoring of the hydrogen atmosphere in the DSC cavity during welding of the inner top cover plate.

11. *Take precautions* to prevent debris and weld splatter from entering the annulus.

12. *W*eld the inner top cover plate to the DSC shell.

    CAUTION: Continuously monitor the hydrogen concentration in the DSC cavity using the tube arrangement described in step 10 during the inner top cover plate cutting/welding operations. Verify that the measured hydrogen concentration does not exceed a safety limit of 2.4% [4] and [5]. If this limit is exceeded, stop all welding operations and purge the DSC cavity *with 2-3 psig* helium to reduce the hydrogen concentration safely below the 2.4% limit.

13. Perform *required* dye penetrant examination of the weld surface*(s)*.

14. *NOT USED.*

15. *R*emove remaining bulk water from the DSC cavity. *U*se helium to backfill the DSC as water is being removed from the DSC. Alternately, helium at up to 15.0 psig may be introduced through the vent port to *assist removal of* water from the DSC cavity through the siphon port.

16. Once the water stops flowing from the DSC, close the DSC siphon port and disengage the gas source.

17. Connect the VDS to *the cask.*

    NOTE: Proceed cautiously when evacuating the DSC to avoid freezing consequences.

18. *S*tart the VDS and draw a vacuum on the DSC cavity. The cavity pressure should be reduced in steps *to optimize the moisture removal and avoid freezing. During/between vacuum drying steps,* the pump is valved off and the cavity pressure monitored. The cavity pressure will rise as water and other volatiles in the cavity evaporate. When the cavity pressure stabilizes, the pump is valved in to continue the vacuum drying process. It may be necessary to repeat some steps, depending on the rate and extent of the pressure increase. Vacuum drying is complete when the pressure stabilizes for a minimum of 30 minutes at 3 mm Hg or less.

    NOTE: The user shall ensure that the vacuum pump is isolated from the canister cavity when demonstrating compliance with <3 mm Hg for 30 minutes. Simply closing the valve between the canister and the vacuum pump is not sufficient, as a faulty valve allows the vacuum pump to continue to draw a vacuum on the canister. Turning off the pump, or opening the suction side of the pump to atmosphere are examples of ways to assure that the pump is not continuing to draw a vacuum on the canister.

    CAUTION: Radiation dose rates are expected to be high at the vent and siphon port locations. Use proper ALARA practices (e.g., use of temporary shielding, appropriate positioning of personnel, etc.) to minimize personnel exposure.

19. Open the valve to the vent port and allow the helium to flow into the DSC cavity.

20. *NOT USED.*

21. *NOT USED.*

22. *NOT USED.*

23. *NOT USED.*

24. Re-evacuate the DSC cavity. The cavity pressure should be reduced in steps. *During/between vacuum drying steps,* the pump is valved off and the cavity pressure monitored. When the cavity pressure stabilizes, the pump is valved in to continue the vacuum drying process. Vacuum drying is complete when the pressure stabilizes for a minimum of 30 minutes at 3 mm Hg *or less.*

25. Open the valve on the vent port and allow helium to flow into the DSC cavity to pressurize the DSC to between 16.5 psig to 18.0 psig and hold for about 10 minutes. Depressurize the DSC cavity by releasing the helium through the VDS to plant fuel pool or radioactive waste system to a backfill pressure of 2.5 ± 1.0 psig (stable for 30 minutes).

    CAUTION: Radiation dose rates are expected to be high at the vent and siphon port locations. Use proper ALARA practices (e.g., use of temporary shielding, appropriate positioning of personnel, etc.) to minimize personnel exposure.

26. *NOT USED.*

A.7.7.5.3 NUHOMS®-32PTH1 DSC Sealing Operations

CAUTION: During performance of steps listed in this section, monitor the cask/DSC annulus water level and replenish as necessary to maintain cooling.

1. Disconnect the VDS from the DSC. Seal weld the prefabricated covers over the vent and siphon ports, inject helium into the blind space just prior to completing welding, and perform *the required* dye penetrant weld examination*(s)*.
2. Install outer top cover plate and the automated welding system onto the DSC.
3. Tack weld the outer top cover plate to the DSC shell. Place the outer top cover plate weld root pass.
4. Perform a helium leakage test of the inner top cover plate and vent/siphon port plate welds using the leak test port in the outer top cover plate and verify that the "leak-tight" criterion is met. Verify that the personnel performing the leakage test are qualified in accordance with SNT-TC-1A [7]. Alternatively, this leak test can be done with a test head following step 1.
5. If a leak is found, remove the outer cover plate root pass (if not using a test head), the vent and siphon port plugs and repair the inner cover plate welds. Then repeat applicable procedure steps from Section A.7.7.5.2, step 17.
6. Perform dye penetrant examination of the root pass weld. Weld out the outer top cover plate to the DSC shell and perform *the required* dye penetrant examination on the weld surface*(s)*.
7. Seal weld the prefabricated plug(when applicable) over the outer cover plate test port and perform dye penetrant weld examinations.
8. *NOT USED.*
9. *D*rain the water from the cask/DSC annulus.

The cask/DSC is now ready to be prepared for downending as described in Chapter A.7, Section A.7.1.2.2.

A.7.7.5.4 Unloading a NUHOMS®-32PTH1 DSC to a Fuel Pool

CAUTION: The process of DSC unloading is similar to that used for DSC loading. DSC opening operations described below are to be carefully controlled in accordance with site procedures. This operation is to be performed under the site's standard health physics guidelines for welding, grinding, and handling of potentially highly contaminated equipment. These are to include the use of prudent housekeeping measures and monitoring of airborne particles. Procedures may require tenting, respirators, supplied air or other measures to contain contamination and minimize the impact on the health and safety of workers.

1. *NOT USED.*
2. *R*emove the siphon cover plate.
3. *R*emove the vent cover plate.

4. Sample the DSC cavity atmosphere. If necessary, flush the DSC cavity gases to the site radwaste systems.

   CAUTION: (a) The water fill rate must be regulated during this reflooding operation to ensure that the DSC vent pressure does not exceed 20.0 psig.

   (b) Provide for continuous hydrogen monitoring of the DSC cavity atmosphere during all subsequent cutting operations to ensure that a safety limit of 2.4% is not exceeded [4] and [5]. Purge with *2-3 psig* helium (or any other inert medium) as necessary to maintain the hydrogen concentration safely below this limit.

5. Fill the DSC with spent fuel pool water (or other plant-designated water source) through the siphon port with the vent port open and routed to the plant's off-gas system. Soluble boron requirements per step 5.A of Section A.7.7.5.1 are applicable for the pool and DSC cavity water.

6. *Take precautions to prevent debris from entering* the cask/DSC annulus.

7. *R*emove the closure weld from the outer top cover plate.

   CAUTION: Monitor the hydrogen concentration in the DSC cavity during this step to ensure that it does not exceed 2.4% by volume [4] and [5].

8. Remove the DSC outer top cover plate.

9. *R*emove the closure weld from the DSC inner top cover plate.

10. Remove the DSC inner top cover plate.

11. NOT USED.

12. Remove excess material on the DSC inside shell surface which may interfere with top shield plug removal.

13. Clean the cask surface of dirt and debris that may have accumulated during transportation or weld removal.

14. *NOT USED.*

15. *NOT USED.*

16. Lower the cask into the fuel pool *using the upper trunnions and lifting yoke.*

17. Disengage the lifting yoke from the cask trunnions and remove the top shield plug.

18. Remove the fuel assemblies (end caps as applicable for damaged fuel assemblies) from the DSC.

19. *R*emove the cask from the pool.

20. Remove the water from the DSC cavity and cask/DSC annulus.

21. Remove the DSC from the cask.

22. Decontaminate the cask as necessary.

23. *NOT USED.*

Pages A.7.7.5-7 and A.7.7.5-8 left intentionally blank.

A.7.7.5.5 References

1. ANSI N14.5-1997, "American National Standard for Radioactive Materials - Leakage Tests on Packages for Shipment," American National Standards Institute, Inc., New York, 1997.
2. Not Used.
3. Not Used.
4. U.S. Nuclear Regulatory Commission, Office of the Nuclear Material Safety and Safeguards, "Safety Evaluation of VECTRA Technologies' Response to Nuclear Regulatory Commission Bulletin 96-04 for the NUHOMS®-24P and NUHOMS®-7P."
5. U.S. Nuclear Regulatory Commission Bulletin 96-04, "Chemical, Galvanic or Other Reactions in Spent Fuel Storage and Transportation Casks," July 5, 1996.
6. *Not Used.*
7. SNT-TC-1A, "American Society for Nondestructive Testing, Personnel Qualification and Certification in Nondestructive Testing."

APPENDIX A.7.7.6
NUHOMS®-37PTH DSC Wet Loading and Unloading

Appendix A.7.7.6
NUHOMS®-37PTH DSC Wet Loading and Unloading Procedures

NOTE: References in this appendix are shown as [1], [2], etc., and refer to the reference list in Section A.7.7.6.5. The term DSC as used in this appendix refers to the NUHOMS®-37PTH DSC.

A.7.7.6.1 NUHOMS®-37PTH DSC Fuel Loading

The starting condition for the following steps assumes completion of the cask preparation steps in Section A.7.1.2.

1. Lift the cask/DSC and position it over the cask loading area of the spent fuel pool.
2. Lower the cask into the fuel pool.
3. Place the cask in the location of the fuel pool *used for* the cask loading area.
4. Disengage the lifting yoke from the cask lifting trunnions and move the yoke clear of the cask.
5. The potential for fuel misloading is essentially eliminated through the implementation of procedural and administrative controls. The controls instituted to ensure that damaged and/or intact spent fuel assemblies (SFAs) and control components (CCs), if applicable, are placed into a known cell location within a DSC will typically consist of the following:
   - A cask/DSC loading plan is developed to verify that the intact, damaged fuel assemblies, and CCs, if applicable, meet the burnup, enrichment and cooling time parameters of the applicable sections as listed in step 13 of Section A.7.1.1.
   - The loading plan is independently verified and approved before the fuel load.
   - A fuel movement schedule is then written, verified and approved based upon the loading plan. All fuel movements from any rack location are performed under strict compliance with the fuel movement schedule.
   - If loading damaged fuel assemblies, verify that the required number of bottom end caps are installed in appropriate basket locations.

5.A Since burnup credit is employed for demonstration of criticality safety, additional administrative controls are required for verification of fuel assembly burnup and to prevent misloading. Fuel loading plans developed in step 5 above shall also include the additional requirements shown in Section A.6.3.4.

6. Prior to loading of an SFA (and CC, if applicable) into the DSC, the identity of the SFA (and CC, if applicable) is to be verified by two individuals using an underwater video camera or other means. Verification of CC identification is optional if the CC has not been moved from the host fuel assembly since its last verification. Read and record the identification number from the SFAs (and CCs, if applicable) and check this identification number against the DSC loading plan which indicates which SFAs (and CCs, if applicable) are acceptable for transport.
7. Position the fuel assembly for insertion into the selected DSC compartment and load the fuel assembly. Repeat steps 6–7 for each SFA loaded into the DSC. After the DSC has

been fully loaded, check and record the identity and location of each fuel assembly and CC, if applicable, in the DSC. If loading damaged fuel assemblies, place top end caps over each damaged fuel assembly placed into the basket.

8. After all the SFAs and CCs, if applicable, have been placed into the DSC and their identities verified, lower the shield plug into the DSC.
9. Visually verify that the top shield plug is properly seated in the DSC.
10. *NOT USED.*
11. Raise the cask to the pool surface *using the cask trunnions and lifting yoke.*
12. *V*erify *the top shield plug* is properly seated within the DSC. If not, lower the cask and reposition the top shield plug. Repeat steps 9 through 12 as necessary.
13. Continue to raise the cask from the pool until the top region of the cask is accessible.
14. Drain any excess water from the top of the DSC shield plug.
15. Check the radiation levels at the center of the top shield plug and around the perimeter of the cask.
16. As required for crane load limitations, drain water from the DSC back into the fuel pool or other suitable location. *Use 1 to 3 psig of* helium to backfill the DSC as water is being removed.
17. Lift the cask from the fuel pool.
18. Move the cask with loaded DSC to the plant designated preparation area.
19. *If water is removed* at step 16, *it* may be replaced with spent fuel pool water or equivalent.

A.7.7.6.2 NUHOMS®-37PTH DSC Drying and Backfilling

CAUTION: During performance of steps listed in this section, monitor the cask/DSC annulus water level and replenish as necessary to maintain cooling.

1. Check the radiation levels *around* the perimeter of the cask. The cask exterior surface should be decontaminated as necessary. Temporary shielding may be installed as necessary to minimize personnel exposure.
2. *NOT USED.*
3. Disengage the top shield plug *from* the lifting yoke and position *the yoke* clear of the cask.
4. Decontaminate the exposed surfaces of the DSC *cylindrical* shell perimeter and remove the annulus seal.
5. *A*llow water from the annulus to drain out until the water level is approximately twelve inches below the top edge of the DSC shell. Take swipes around the outer *exposed* surface of the DSC shell and check for smearable contamination as required.

CAUTION: Radiation dose rates are expected to be high at the DSC vent and siphon port locations. Use proper ALARA practices (e.g., use of temporary shielding, appropriate positioning of personnel, etc.) to minimize personnel exposure.

6. Prior to the start of the welding operations, drain a minimum of 100 gallons of water from the DSC. *Use 1 to 3 psig of* helium to backfill the DSC as water is being removed from the DSC.

7. *NOT USED.*

8. Install the automated welding machine onto the inner top cover and place the inner top cover with the automated welding machine onto the DSC. Alternately, the inner top cover may be placed on the DSC separately or the inner top cover may be part of the shield plug; in these cases the automated welding machine is installed on the inner top cover already installed in the DSC.

9. Check radiation levels along the surface of the inner top cover plate. Temporary shielding may be installed as necessary.

10. Insert suitable tubing through the vent port such that it terminates just below the DSC top shield plug. Connect the tubing to a hydrogen monitor to allow continuous monitoring of the hydrogen atmosphere in the DSC cavity during welding of the inner top cover plate. Optionally, other methods may be used for continuous monitoring of the hydrogen atmosphere in the DSC cavity during welding of the inner top cover plate.

11. *Take precautions* to prevent debris and weld splatter from entering the annulus.

12. *W*eld the inner top cover plate to the DSC shell.

CAUTION: Continuously monitor the hydrogen concentration in the DSC cavity using the tube arrangement described in step 10 during the inner top cover plate cutting/welding operations. Verify that the measured hydrogen concentration does not exceed a safety limit of 2.4% [4] and [5]. If this limit is exceeded, stop all welding operations and purge the DSC cavity *with 2-3 psig* helium to reduce the hydrogen concentration safely below the 2.4% limit.

13. Perform *required* dye penetrant examination of the weld surface*(s)*.

14. *NOT USED.*

15. *R*emove remaining bulk water from the DSC cavity. *U*se helium to backfill the DSC as water is being removed from the DSC. Alternately, helium at up to 15.0 psig may be introduced through the vent port to *assist removal of* the water from the DSC cavity through the siphon port.

16. Once the water stops flowing from the DSC, close the DSC siphon port and disengage the gas source.

17. Connect the VDS to *the cask.*

NOTE: Proceed cautiously when evacuating the DSC to avoid freezing consequences.

18. *S*tart the VDS and draw a vacuum on the DSC cavity. The cavity pressure should be reduced in steps *to optimize moisture removal and avoid freezing. During/between vacuum drying steps*, the pump is valved off and the cavity pressure monitored. The cavity pressure will rise as water and other volatiles in the cavity evaporate. When the cavity pressure stabilizes, the pump is valved in to continue the vacuum drying process. It may be necessary to repeat some steps, depending on the rate and extent of the pressure increase. Vacuum drying is complete when the pressure stabilizes for a minimum of 30 minutes at 3 mm Hg or less.

    NOTE: The user shall ensure that the vacuum pump is isolated from the canister cavity when demonstrating compliance with <3 mm Hg for 30 minutes. Simply closing the valve between the canister and the vacuum pump is not sufficient, as a faulty valve allows the vacuum pump to continue to draw a vacuum on the canister. Turning off the pump, or opening the suction side of the pump to atmosphere are examples of ways to assure that the pump is not continuing to draw a vacuum on the canister.

    CAUTION: Radiation dose rates are expected to be high at the vent and siphon port locations. Use proper ALARA practices (e.g., use of temporary shielding, appropriate positioning of personnel, etc.) to minimize personnel exposure.

19. Open the valve to the vent port and allow the helium to flow into the DSC cavity.

20. *NOT USED.*

21. *NOT USED.*

22. *NOT USED.*

23. *NOT USED.*

24. Re-evacuate the DSC cavity using the VDS. The cavity pressure should be reduced in steps. *During/between vacuum drying steps*, the pump is valved off and the cavity pressure monitored. When the cavity pressure stabilizes, the pump is valved in to continue the vacuum drying process. Vacuum drying is complete when the pressure stabilizes for a minimum of 30 minutes at 3 mm Hg *or less*.

25. Open the valve on the vent port and allow helium to flow into the DSC cavity to pressurize the DSC between 16.5 and 18.0 psig and hold for 10 minutes. Depressurize the DSC cavity to 2.5 ± 1.0 psig (stable for 30.0 minutes).

    CAUTION: Radiation dose rates are expected to be high at the vent and siphon port locations. Use proper ALARA practices (e.g., use of temporary shielding, appropriate positioning of personnel, etc.) to minimize personnel exposure.

26. *NOT USED.*

A.7.7.6.3 NUHOMS®-37PTH DSC Sealing Operations

CAUTION: During performance of steps listed in this section, monitor the cask/DSC annulus water level and replenish as necessary to maintain cooling.

1. Disconnect the VDS from the DSC. Seal weld the prefabricated covers over the vent and siphon ports, inject helium into the blind space just prior to completing welding, and perform *the required* dye penetrant weld examination*(s)*.
2. Install the outer top cover plate the automated welding system onto the DSC.
3. Tack weld the outer top cover plate to the DSC shell. Place the outer top cover plate weld root pass.
4. Perform a helium leakage test of the inner top cover plate and vent/siphon port plate welds using the test port in the outer top cover plate and verify that the "leak-tight" criterion is met. Verify that the personnel performing the leakage test are qualified in accordance with SNT-TC-1A [7]. Alternatively, this leakage test can be done with a test head following step 1 above.
5. If a leak is found, remove the outer cover plate root pass (if not using a test head), the vent and siphon port plugs and repair the inner cover plate welds. Then repeat applicable procedure steps from Section A.7.7.6.2, step 17.
6. Perform *the required* dye penetrant examination of the root pass weld. Weld out the outer top cover plate to the DSC shell and perform dye penetrant examination on the weld surface*(s)*.
7. Seal weld the prefabricated plug (when applicable) over the outer cover plate test port and perform dye penetrant weld examinations.
8. *NOT USED.*
9. *D*rain the water from the cask/DSC annulus.

The cask/DSC is now ready to be prepared for downending as described in Chapter A.7, Section A.7.1.2.2.

A.7.7.6.4 Unloading a NUHOMS®-37PTH DSC to a Fuel Pool

CAUTION: The process of DSC unloading is similar to that used for DSC loading. DSC opening operations described below are to be carefully controlled in accordance with site procedures. This operation is to be performed under the site's standard health physics guidelines for welding, grinding, and handling of potentially highly contaminated equipment. These are to include the use of prudent housekeeping measures and monitoring of airborne particles. Procedures may require tenting, respirators, supplied air or other measures to contain contamination and minimize the impact on the health and safety of workers.

1. *NOT USED.*
2. *R*emove the siphon cover plate.
3. *R*emove the vent cover plate.
4. Sample the DSC cavity atmosphere. If necessary, flush the DSC cavity gases to the site radwaste systems.

CAUTION: (a) The water fill rate must be regulated during this reflooding operation to ensure that the DSC vent pressure does not exceed 20.0 psig.

(b) Provide for continuous hydrogen monitoring of the DSC cavity atmosphere during all subsequent cutting operations to ensure that a safety limit of 2.4% is not exceeded [4] and [5]. Purge *with 2-3 psig* helium (or any other inert medium) as necessary to maintain the hydrogen concentration safely below this limit.

5. Fill the DSC with spent fuel pool water through the siphon port with the vent port open and routed to the plant's off-gas system. Soluble boron requirements per step 5.A of Section A.7.7.6.1 are applicable for the pool and DSC cavity water.
6. *Take precautions to prevent debris from entering* the cask/DSC annulus.
7. *R*emove the closure weld from the outer top cover plate.

CAUTION: Monitor the hydrogen concentration in the DSC cavity during this step to ensure that it does not exceed 2.4% by volume [4] and [5].

8. Remove the DSC outer top cover plate.
9. Remove the closure weld from the DSC inner top cover plate.
10. Remove the DSC inner top cover plate.
11. NOT USED
12. Remove excess material on the DSC inside shell surface which may interfere with top shield plug removal.
13. Clean the cask surface of dirt and debris that may have accumulated during transportation or weld removal.
14. *NOT USED.*
15. *NOT USED.*
16. Lower the cask slowly into the fuel pool *using the upper trunnions and lifting yoke.*
17. Disengage the lifting yoke from the cask trunnions and remove the top shield plug.
18. Remove the fuel assemblies (or end caps as applicable for damaged assemblies) from the DSC.
19. *R*emove the cask from the pool, and place it in the decon area.
20. Remove the water from the DSC cavity and cask/DSC annulus.
21. Remove the DSC from the cask.
22. Decontaminate the cask as necessary.
23. *NOT USED.*

Pages A.7.7.6-7 and A.7.7.6-8 left intentionally blank.

A.7.7.6.5 References

1. ANSI N14.5-1997,"American National Standard for Radioactive Materials - Leakage Tests on Packages for Shipment," American National Standards Institute, Inc., New York, 1997.
2. Not Used.
3. Not Used.
4. U.S. Nuclear Regulatory Commission, Office of the Nuclear Material Safety and Safeguards, "Safety Evaluation of VECTRA Technologies' Response to Nuclear Regulatory Commission Bulletin 96-04 for the NUHOMS®-24P and NUHOMS®-7P."
5. U.S. Nuclear Regulatory Commission Bulletin 96-04, "Chemical, Galvanic or Other Reactions in Spent Fuel Storage and Transportation Casks," July 5, 1996.
6. *Not Used.*
7. SNT-TC-1A, "American Society for Nondestructive Testing, Personnel Qualification and Certification in Nondestructive Testing."

APPENDIX A.7.7.7
NUHOMS®-61BT DSC Wet Loading and Unloading

Appendix A.7.7.7
NUHOMS®-61BT DSC Wet Loading and Unloading Procedures

NOTE: References in this appendix are shown as [1], [2], etc., and refer to the reference list in Section A.7.7.7.5. The term DSC as used in this appendix refers to the NUHOMS®-61BT DSC.

A.7.7.7.1 NUHOMS®-61BT DSC Fuel Loading

The starting condition for the following steps assumes completion of the cask preparation steps in Section A.7.1.2.

1. Lift the cask/DSC and position it over the cask loading area of the spent fuel pool.
2. Lower the cask into the fuel pool.
3. Place the cask in the location of the fuel pool *used for* the cask loading area.
4. Disengage the lifting yoke from the cask lifting trunnions and move the yoke clear of the cask.
5. The potential for fuel misloading is essentially eliminated through the implementation of procedural and administrative controls. The controls instituted to ensure that damaged and/or intact spent fuel assemblies (SFAs) are placed into a known cell location within a DSC will typically consist of the following:
   - A cask/DSC loading plan is developed to verify that the SFAs meet the burnup, enrichment and cooling time parameters of the applicable sections as listed in step 13 of Section A.7.1.1.
   - The loading plan is independently verified and approved before the fuel load.
   - A fuel movement schedule is then written, verified and approved based upon the loading plan. All fuel movements from any rack location are performed under strict compliance with the fuel movement schedule.
   - If loading damaged fuel assemblies, verify that the required number of bottom end caps are installed in appropriate fuel compartment tube locations before fuel load.

8. After all the SFAs have been placed into the DSC and their identities verified, place the hold down ring *if it is not integral to the basket.* Alternately, the hold down ring may be placed on the basket before loading the SFAs. *L*ower the shield plug onto the DSC.
9. Visually verify that the top shield plug is properly seated in the DSC.
10. *NOT USED.*
11. Raise the cask to the pool surface *using the cask trunnions and lifting yoke.*
12. *V*erify that *the top shield plug* is properly seated within the DSC. If not, lower the cask and reposition the top shield plug. Repeat steps 9 through 12 as necessary.
13. Continue to raise the cask from the pool until the top region of the cask is accessible.
14. Drain any excess water from the top of the DSC shield plug.
15. Check the radiation levels at the center of the top shield plug and around the perimeter of the cask.
16. As required for crane load limitations, drain water from the DSC back into the fuel pool or other suitable location to meet the weight limit on the crane. *Use 1 to 3 psig of* helium to backfill the DSC as water is being removed from the DSC.
17. Lift the cask from the fuel pool.
18. Move the cask with loaded DSC to the plant designated preparation area.
19. *If water is removed* at step 16, *it* may be replaced with spent fuel pool water or equivalent.

A.7.7.7.2 NUHOMS®-61BT DSC Drying and Backfilling

1. Check the radiation levels *around* the perimeter of the cask. The cask exterior surface should be decontaminated as necessary. Temporary shielding may be installed as necessary to minimize personnel exposure.
2. *NOT USED.*
3. Disengage the top shield plug *from* the lifting yoke and position *the yoke* clear of the cask.
4. Decontaminate the exposed surfaces of the DSC *cylindrical* shell perimeter and remove the annulus seal.
5. *A*llow water from the annulus to drain out until the water level is approximately twelve inches below the top edge of the DSC shell. Take swipes around the *exposed* surface of the DSC shell and check for smearable contamination as required.

   CAUTION: Radiation dose rates are expected to be high at the DSC vent and siphon port locations. Use proper ALARA practices (e.g., use of temporary shielding, appropriate positioning of personnel, etc.) to minimize personnel exposure.

6. Drain a minimum of 1100 gallons of water from the DSC. *Use 1 to 3 psig of* helium to backfill the DSC as water is being removed from the DSC.

7. *NOT USED.*

8. Install the automated welding machine onto the inner top cover and place the inner top cover with the automated welding machine onto the DSC. Alternately, the inner top cover may be placed on the DSC separately or the inner top cover may be part of the shield plug; in these cases the automated welding machine is installed on the inner top cover already installed in the DSC.

9. Check radiation levels along the surface of the inner top cover plate. Temporary shielding may be installed as necessary.

10. Insert suitable tubing through the vent port such that it terminates just below the DSC top shield plug. Connect the tubing to a hydrogen monitor to allow continuous monitoring of the hydrogen atmosphere in the DSC cavity during welding of the inner top cover plate. Optionally, other methods may be used for continuous monitoring of the hydrogen atmosphere in the DSC cavity during welding of the inner top cover plate.

11. *Take precautions* to prevent debris and weld splatter from entering the annulus.

12. *T*ack weld the inner top cover plate to the DSC shell. Complete the inner top cover plate weld to the DSC shell.

    CAUTION: Continuously monitor the hydrogen concentration in the DSC cavity using the tube arrangement described in step 10 during the inner top cover plate cutting/welding operations. Verify that the measured hydrogen concentration does not exceed a safety limit of 2.4% [4] and [5]. If this limit is exceeded, stop all welding operations and purge the DSC cavity *with 2-3 psig* helium to reduce the hydrogen concentration safely below the 2.4% limit.

13. Perform *required* dye penetrant examination of the weld surface*(s)*.

14. Place the strongback on the inner top cover plate and is oriented such that:

15. *NOT USED.*

16. *R*emove remaining bulk water from the DSC cavity. *U*se helium to backfill the DSC as water is being removed from the DSC. Alternately, helium (up to 10 psig) may also be used on the vent port and allow helium to *assist removal of* the water from the DSC cavity through the siphon port.

17. Once the water stops flowing from the DSC, close the DSC siphon port and disengage the gas source.

18. Connect the VDS to *the cask.*

    NOTE: Proceed cautiously when evacuating the DSC to avoid freezing consequences.

19. *S*tart the VDS and draw a vacuum on the DSC cavity. The cavity pressure should be reduced in steps *to optimize moisture removal and avoid freezing. During/between vacuum drying steps,* the pump is valved off and the cavity pressure monitored. The cavity pressure will rise as water and other volatiles in the cavity evaporate. When the cavity pressure stabilizes, the pump is valved in to continue the vacuum drying process. It may be necessary to repeat some steps, depending on the rate and extent of the pressure increase. Vacuum drying is complete when the pressure stabilizes for a minimum of 30 minutes at 3 mm Hg or less.

NOTE: The user shall ensure that the vacuum pump is isolated from the canister cavity when demonstrating compliance with <3 mm Hg for 30 minutes. Simply closing the valve between the canister and the vacuum pump is not sufficient, as a faulty valve allows the vacuum pump to continue to draw a vacuum on the canister. Turning off the pump, or opening the suction side of the pump to atmosphere are examples of ways to assure that the pump is not continuing to draw a vacuum on the canister.

CAUTION: Radiation dose rates are expected to be high at the vent and siphon port locations. Use proper ALARA practices (e.g., use of temporary shielding, appropriate positioning of personnel, etc.) to minimize personnel exposure.

20. Open the valve to the vent port and allow the helium to flow into the DSC cavity.
21. *NOT USED.*
22. *NOT USED.*
23. *NOT USED.*
24. *NOT USED.*
25. Re-evacuate the DSC cavity. The cavity pressure should be reduced in steps. *During/between vacuum drying steps,* the pump is valved off and the cavity pressure monitored. When the cavity pressure stabilizes, the pump is valved in to continue the vacuum drying process. Vacuum drying is complete when the pressure stabilizes for a minimum of 30 minutes at 3 mm Hg *or less.*
26. Open the valve on the vent port and allow helium to flow into the DSC cavity to pressurize the DSC to 2.5 ± 1.0 psig backfill pressure (stable for 30 minutes).

    CAUTION: Radiation dose rates are expected to be high at the vent and siphon port locations. Use proper ALARA practices (e.g., use of temporary shielding, appropriate positioning of personnel, etc.) to minimize personnel exposure.

27. *NOT USED.*
28. Remove the strongback.

A.7.7.7.3 NUHOMS®-61BT DSC Sealing Operations

1. Disconnect the VDS from the DSC. Seal weld the prefabricated covers over the vent and siphon ports, inject helium into the blind space just prior to completing welding, and perform *the required* dye penetrant weld examination*(s)*.
2. Install the outer top cover plate and the automated welding system onto the DSC. .
3. Tack weld the outer top cover plate to the DSC shell. Place the outer top cover plate weld root pass.
4. Perform helium leakage test of the inner top cover plate and vent/siphon port plate welds using the test port in the outer top cover plate and verify that the "leak-tight" criterion is met. Verify that the personnel performing the leak test are qualified in accordance with SNT-TC-1A [7]. Alternatively, this leak test can be done with a test head following step 1.

5. If a leak is found, remove the outer cover plate root pass, the vent and siphon port plugs and repair the inner cover plate welds. Then repeat applicable procedure steps from Section A.7.7.7.2, step 18.
6. Perform *the required* dye penetrant examination of the root pass weld. Weld out the outer top cover plate to the DSC shell and perform dye penetrant examination on the weld surface*(s)*.
7. Seal weld the prefabricated plug (when applicable) over the outer cover plate test port and perform dye penetrant weld examinations.
8. *NOT USED.*
9. *D*rain the water from the cask/DSC annulus.

The cask/DSC is now ready to be prepared for downending as described in Chapter A.7, Section A.7.1.2.2.

A.7.7.7.4 Unloading the NUHOMS®-61BT DSC to a Fuel Pool

CAUTION: The process of DSC unloading is similar to that used for DSC loading. DSC opening operations described below are to be carefully controlled in accordance with site procedures. This operation is to be performed under the site's standard health physics guidelines for welding, grinding, and handling of potentially highly contaminated equipment. These are to include the use of prudent housekeeping measures and monitoring or airborne particles. Procedures may require tenting, respirators, supplied air or other measures to contain and minimize the spread of and impact on the health and safety of workers due to contamination.

1. *NOT USED.*
2. *R*emove the siphon cover plate.
3. *R*emove the vent cover plate.
4. Sample the DSC cavity atmosphere. If necessary, flush the DSC cavity gases to the site radwaste systems.

CAUTION: (a) The water fill rate must be regulated during this reflooding operation to ensure that the DSC vent pressure does not exceed 20.0 psig.

(b) Provide for continuous hydrogen monitoring of the DSC cavity atmosphere during all subsequent cutting operations to ensure that a safety limit of 2.4% is not exceeded [4] and [5]. Purge *with 2-3 psig* helium (or any other inert medium) as necessary to maintain the hydrogen concentration safely below this limit.

5. Fill the DSC with spent fuel pool water (or other plant designated water source) through the siphon port with the vent port open.
6. *Take precautions to prevent debris from entering* the cask/DSC annulus.
7. *R*emove the closure weld from the outer top cover plate.

CAUTION: Monitor the hydrogen concentration in the DSC cavity during this step to ensure that it does not exceed 2.4% by volume [4] and [5].

8. Remove the DSC outer top cover plate.
9. *R*emove the DSC inner top cover plate.
10. Remove the DSC inner top cover plate.
11. NOT USED.
12. Remove excess material on the DSC inside shell surface which may interfere with top shield plug removal.
13. Clean the cask surface of dirt and debris that may have accumulated during transportation or weld removal.
14. *NOT USED.*
15. *NOT USED.*
16. Lower the cask slowly into the fuel pool *using the upper trunnions and lifting yoke.*
17. Disengage the lifting yoke from the cask trunnions and remove the top shield plug and hold down ring.
18. Remove the fuel assemblies (end caps as applicable for damaged fuel assemblies) from the DSC.
19. *R*emove the cask from the pool.
20. Remove the water from the DSC cavity and cask/DSC annulus.
21. Remove the DSC from the cask.
22. Decontaminate the cask as necessary.
23. *NOT USED.*

This page left intentionally blank.

A.7.7.7.5 References

1. ANSI N14.5-1997, "American National Standard for Radioactive Materials - Leakage Tests on Packages for Shipment," American National Standards Institute, Inc., New York, 1997.
2. Not Used.
3. Not Used.
4. U.S. Nuclear Regulatory Commission, Office of the Nuclear Material Safety and Safeguards, "Safety Evaluation of VECTRA Technologies' Response to Nuclear Regulatory Commission Bulletin 96-04 for the NUHOMS®-24P and NUHOMS®-7P."
5. U.S. Nuclear Regulatory Commission Bulletin 96-04, "Chemical, Galvanic or Other Reactions in Spent Fuel Storage and Transportation Casks," July 5, 1996.
6. *Not Used.*
7. SNT-TC-1A, "American Society for Nondestructive Testing, Personnel Qualification and Certification in Nondestructive Testing."

APPENDIX A.7.7.8
NUHOMS®-61BTH DSC Wet Loading and Unloading

Appendix A.7.7.8
NUHOMS®-61BTH DSC Wet Loading and Unloading Procedures

NOTE: References in this appendix are shown as [1], [2], etc. and refer to the reference list in Section A.7.7.8.5. The term DSC as used in this appendix refers to the NUHOMS®-61BTH DSC.

A.7.7.8.1 NUHOMS®-61BTH DSC Fuel Loading

The starting condition for the following steps assumes completion of the cask preparation steps in Section A.7.1.2.

1. Lift the cask/DSC and position it over the cask loading area of the spent fuel pool.
2. Lower the cask into the fuel pool.
3. Place the cask in the location of the fuel pool *used for* the cask loading area.
4. Disengage the lifting yoke from the cask lifting trunnions and move the yoke clear of the cask.
5. The potential for fuel misloading is essentially eliminated through the implementation of procedural and administrative controls. The controls instituted to ensure that failed, damaged and/or intact spent fuel assemblies (SFAs) are placed into a known cell location within a DSC, will typically consist of the following:
   - A cask/DSC loading plan is developed to verify that the failed, damaged and/or intact SFAs meet the burnup, enrichment and cooling time parameters of the applicable sections as listed in step 13 of Section A.7.1.1.
   - The loading plan is independently verified and approved before the fuel load.
   - A fuel movement schedule is then written, verified and approved based upon the loading plan. All fuel movements from any rack location are performed under strict compliance with the fuel movement schedule.
   - If loading damaged fuel assemblies, verify that the required number of bottom end caps are installed in appropriate fuel compartment tube locations before fuel load.

damaged fuel assemblies, place top end caps over each damaged fuel assembly placed into the basket. If loading failed fuel, ensure that the FFC lids are installed. After the DSC has been fully loaded, check and record the identity and location of each fuel assembly in the DSC.

8. a. After all the SFAs have been placed into the DSC and their identities verified, place the hold-down ring or optional top grid assembly as applicable. If using the hold down ring, it may be placed on the basket before loading the SFAs.

   b. *L*ower the shield plug into the DSC.

9. Visually verify that the top shield plug is properly seated in the DSC.

10. *NOT USED.*

11. Raise the cask to the pool surface.

12. *V*erify that *the top shield plug* properly seated within the DSC. If not, lower the cask and reposition the top shield plug. Repeat steps 9 through 12 as necessary.

13. Continue to raise the cask from the pool.

14. Drain any excess water from the top of the DSC shield plug back to the fuel pool. Check the radiation levels at the center of the top shield plug and around the perimeter of the cask.

15. Drain water as needed from the DSC back into the fuel pool or other suitable location to meet the crane load limits. *Use 1 to 3 psig of* helium to backfill the DSC as water is being removed from the DSC.

16. Lift the cask from the fuel pool.

17. Move the cask with loaded DSC to the plant designated preparation area.

18. *If w*ater *is* removed at step 15, *it* may be replaced with spent fuel pool water or equivalent.

A.7.7.8.2 NUHOMS®-61BTH DSC Drying and Backfilling

CAUTION: During performance of steps listed in this section, monitor the cask/DSC annulus water level and replenish as necessary to maintain cooling.

1. Check the radiation levels *around* the perimeter of the cask. The cask exterior surface should be decontaminated as necessary. Temporary shielding may be installed as necessary to minimize personnel exposure.

2. *NOT USED.*

3. Disengage the top shield plug *from* the lifting yoke and position *the yoke* clear of the cask.

4. Decontaminate the exposed surfaces of the DSC *cylindrical* shell perimeter and remove the annulus seal.

5. *A*llow water from the annulus to drain out until the water level is approximately twelve inches below the top edge of the DSC shell. Take swipes around the outer *exposed* surface of the DSC shell and check for smearable contamination as required.

   CAUTION: Radiation dose rates are expected to be high at the DSC vent and siphon port locations. Use proper ALARA practices (e.g., use of temporary shielding, appropriate positioning of personnel, etc.) to minimize personnel exposure.

6. Prior to the start of the welding operations, drain approximately 1100 gallons of water from the DSC. *Use 1 to 3 psig of* helium to backfill the DSC as water is being removed from the DSC.

7. *NOT USED.*

8. Install the automated welding machine onto the inner top cover and place the inner top cover with the automated welding machine onto the DSC. Alternately, the inner top cover may be placed on the DSC separately or the inner top cover may be part of the shield plug; in these cases the automated welding machine is installed on the inner top cover already installed in the DSC.

9. Check radiation levels along the surface of the inner top cover plate. Temporary shielding may be installed as necessary.

10. Insert suitable tubing through the vent port such that it terminates just below the DSC top shield plug. Connect the tubing to a hydrogen monitor to allow continuous monitoring of the hydrogen atmosphere in the DSC cavity during welding of the inner top cover plate. Optionally, other methods may be used for continuous monitoring of the hydrogen atmosphere in the DSC cavity during welding of the inner top cover plate.

11. *Take precautions* to prevent debris and weld splatter from entering the annulus.

12. *T*ack weld the inner top cover plate to the DSC shell. Complete the inner top cover plate weld to the DSC shell.

    CAUTION: Continuously monitor the hydrogen concentration in the DSC cavity using the tube arrangement described in step 10 during the inner top cover plate cutting/welding operations. Verify that the measured hydrogen concentration does not exceed a safety limit of 2.4% [4] and [5]. If this limit is exceeded, stop all welding operations and purge the DSC cavity *with 2-3 psig* helium to reduce the hydrogen concentration safely below the 2.4% limit.

13. Perform dye penetrant examination of the weld surface.

14. If loading a Type 2 61BTH DSC skip to step *16*; otherwise, *install* the strongback on the inner top cover plate.

15. *NOT USED.*

16. *R*emove remaining bulk water from the DSC cavity. *U*se helium to backfill the DSC as water is being removed from the DSC. Alternately, helium (at up to 10.0 psig for Type 1 DSC or 15.0 psig for Type 2 DSC) may be introduced through the vent port to *assist removal of* the water from the DSC.

17. Once the water stops flowing from the DSC, close the DSC siphon port and disengage the gas source.

18. Connect the VDS to *the cask.*

NOTE: Proceed cautiously when evacuating the DSC to avoid freezing consequences.

19. *S*tart the VDS and draw a vacuum on the DSC cavity. The cavity pressure should be reduced in steps *to optimize moisture removal and avoid freezing. During/between vacuum drying steps,* the pump is valved off and the cavity pressure monitored. The cavity pressure will rise as water and other volatiles in the cavity evaporate. When the cavity pressure stabilizes, the pump is valved in to continue the vacuum drying process. It may be necessary to repeat some steps, depending on the rate and extent of the pressure increase. Vacuum drying is complete when the pressure stabilizes for a minimum of 30 minutes at 3 mm Hg or less.

NOTE: The user shall ensure that the vacuum pump is isolated from the canister cavity when demonstrating compliance with <3 mm Hg for 30 minutes. Simply closing the valve between the canister and the vacuum pump is not sufficient, as a faulty valve allows the vacuum pump to continue to draw a vacuum on the canister. Turning off the pump, or opening the suction side of the pump to atmosphere are examples of ways to assure that the pump is not continuing to draw a vacuum on the canister.

CAUTION: Radiation dose rates are expected to be high at the vent and siphon port locations. Use proper ALARA practices (e.g., use of temporary shielding, appropriate positioning of personnel, etc.) to minimize personnel exposure.

20. Open the valve to the vent port and allow the helium to flow into the DSC cavity.

21. *NOT USED.*

22. *NOT USED.*

23. *NOT USED.*

24. *NOT USED.*

25. Re-evacuate the DSC cavity. The cavity pressure should be reduced in steps. *During/between vacuum drying steps,* the pump is valved off and the cavity pressure monitored. When the cavity pressure stabilizes, the pump is valved in to continue the vacuum drying process. Vacuum drying is complete when the pressure stabilizes for a minimum of 30 minutes at 3 mm Hg or less.

26. Open the valve on the vent port and allow helium to flow into the DSC cavity to pressurize the DSC between 14.5 to 16.0 psig for 61BTH Type 1 and 18.5 to 20.0 psig for 61BTH Type 2 DSC and hold for 10 minutes. Depressurize the DSC cavity to 2.5 psig ± 1.0 psig backfill pressure (stable for 30 minutes).

CAUTION: Radiation dose rates are expected to be high at the vent and siphon port locations. Use proper ALARA practices (e.g., use of temporary shielding, appropriate positioning of personnel, etc.) to minimize personnel exposure.

27. *NOT USED.*

28. If installed, remove the strongback.

A.7.7.8.3 NUHOMS®-61BTH DSC Sealing Operations

CAUTION: During performance of steps listed in this section, monitor the cask/DSC annulus water level and replenish as necessary to maintain cooling.

1. Disconnect the VDS from the DSC. Seal weld the prefabricated covers over the vent and siphon ports, inject helium into the blind space just prior to completing welding, and perform *the required* dye penetrant weld examination*(s)*.
2. Install the outer top cover plate and the automated welding system onto the DSC.
3. Tack weld the outer top cover plate to the DSC shell. Place the outer top cover plate weld root pass.
4. Perform helium leakage test of the inner top cover plate and vent/siphon port plate welds using the test port in the outer top cover plate and verify that the "leak-tight" criterion is met. Verify that the personnel performing the leakage test are qualified in accordance with SNT-TC-1A [7]. Alternatively, this leakage test can be done with a test head following step 1 above.
5. If a leak is found, remove the outer cover plate root pass (if not using a test head), the vent and siphon port plugs and repair the inner cover plate welds. Then install the strongback (if used) and repeat procedure steps from A.7.7.8.2, step 18.
6. Perform dye penetrant examination of the root pass weld. Weld out the outer top cover plate to the DSC shell and perform *the required* dye penetrant examination on the weld surface*(s)*.
7. Install and seal weld the prefabricated plug (when applicable) over the outer cover plate test port and perform dye penetrant weld examinations.
8. *NOT USED.*
9. *D*rain the water from the cask/DSC annulus.

The cask/DSC is now ready to be prepared for downending as described in Chapter A.7, Section A.7.1.2.2.

A.7.7.8.4 Unloading a NUHOMS®-61BTH DSC to a Fuel Pool Using the NUHOMS®-MP197HB Cask

CAUTION: The process of DSC unloading is similar to that used for DSC loading. DSC opening operations described below are to be carefully controlled in accordance with site procedures. This operation is to be performed under the site's standard health physics guidelines for welding, grinding, and handling of potentially highly contaminated equipment. These are to include the use of prudent housekeeping measures and monitoring of airborne particles. Procedures may require tenting, respirators, supplied air or other measures to contain contamination and minimize the impact on the health and safety of workers.

1. *NOT USED.*
2. *R*emove the siphon cover plate.
3. *R*emove the vent cover plate.
4. Sample the DSC cavity atmosphere. If necessary, flush the DSC cavity gases to the site radwaste systems.

   CAUTION: (a) The water fill rate must be regulated during this reflooding operation to ensure that the DSC vent pressure does not exceed 20.0 psig.

   (b) Provide for continuous hydrogen monitoring of the DSC cavity atmosphere during all subsequent cutting operations to ensure that a safety limit of 2.4% is not exceeded [4] and [5]. Purge *with 2-3 psig* helium as necessary to maintain the hydrogen concentration safely below this limit.
5. Fill the DSC with spent fuel pool water (or other plant-designated water source) through the siphon port with the vent port open.
6. *Take precautions to prevent debris from entering* the cask/DSC annulus.
7. *R*emove the closure weld from the outer top cover plate.

   CAUTION: Monitor the hydrogen concentration in the DSC cavity during this step to ensure that it does not exceed 2.4% by volume [4] and [5].
8. Remove the DSC outer top cover plate.
9. *R*emove the closure weld from the DSC inner top cover plate.
10. Remove the DSC inner top cover plate.
11. NOT USED
12. Remove excess material on the DSC inside shell surface which may interfere with top shield plug removal.
13. Clean the cask surface of dirt and debris that may have accumulated during transportation or weld removal.
14. *NOT USED.*
15. *NOT USED.*
16. Lower the cask into the fuel pool *using the upper trunnions and lifting yoke.*
17. Disengage the lifting yoke from the cask trunnions and remove the top shield plug.
18. Remove the holddown ring (if not integral to the basket).
19. Remove the fuel assemblies (or fuel cans/end caps as applicable for failed/damaged fuel assemblies) from the DSC.
20. *R*emove the cask from the pool.
21. Remove the water from the DSC cavity and cask/DSC annulus.
22. Remove the DSC from the cask.

23. Decontaminate the cask as necessary.
24. *NOT USED.*

This page left intentionally blank.

A.7.7.8.5 References

1. *ANSI N14.5-1997, "American National Standard for Radioactive Materials - Leakage Tests on Packages for Shipment," American National Standards Institute, Inc., New York, 1997.*
2. *Not Used.*
3. *Not Used.*
4. *U.S. Nuclear Regulatory Commission, Office of the Nuclear Material Safety and Safeguards, "Safety Evaluation of VECTRA Technologies' Response to Nuclear Regulatory Commission Bulletin 96-04 for the NUHOMS®-24P and NUHOMS®-7P."*
5. *U.S. Nuclear Regulatory Commission Bulletin 96-04, "Chemical, Galvanic or Other Reactions in Spent Fuel Storage and Transportation Casks," July 5, 1996.*
6. *Not Used.*
7. *SNT-TC-1A, "American Society for Nondestructive Testing, Personnel Qualification and Certification in Nondestructive Testing."*

APPENDIX A.7.7.9
NUHOMS®-69BTH DSC Wet Loading and Unloading

Appendix A.7.7.9
NUHOMS®-69BTH DSC Wet Loading and Unloading Procedures

NOTE: References in this appendix are shown as [1], [2], etc., and refer to the reference list in Section A.7.7.9.5. The term DSC as used in this appendix refers to the NUHOMS®-69BTH DSC.

A.7.7.9.1 NUHOMS®-69BTH DSC Fuel Loading

The starting condition for the following steps assumes completion of the cask preparation steps in Section A.7.1.2.

1. Lift the cask/DSC and position it over the cask loading area of the spent fuel pool.
2. Lower the cask into the fuel pool.
3. Place the cask in the location of the fuel pool *used for* the cask loading area.
4. Disengage the lifting yoke from the cask lifting trunnions and move the yoke clear of the cask.
5. The potential for fuel misloading is essentially eliminated through the implementation of procedural and administrative controls. The controls instituted to ensure that damaged and/or intact spent fuel assemblies (SFAs) are placed into a known cell location within a DSC will typically consist of the following:
   - A cask/DSC loading plan is developed to verify that the intact and damaged fuel assemblies meet the burnup, enrichment and cooling time parameters of the applicable sections as listed in step 13 of Section A.7.1.1.
   - The loading plan is independently verified and approved before the fuel load.
   - A fuel movement schedule is then written, verified and approved based upon the loading plan. All fuel movements from any rack location are performed under strict compliance with the fuel movement schedule.
   - If loading damaged fuel assemblies, verify that the required number of bottom end caps are installed in appropriate locations in the basket.
6. Prior to loading of an SFA into the DSC, the identity of the assembly is to be verified by two individuals using an underwater video camera or other means. Read and record the identification number from the SFA and check this identification number against the DSC loading plan which indicates which SFAs are acceptable for transport.
7. Position the fuel assembly for insertion into the selected DSC fuel compartment and load the fuel assembly. Repeat steps 6 through 7 for each SFA loaded into the DSC. If loading damaged fuel assemblies, place top end caps over each damaged fuel assembly placed into the basket. After the DSC has been fully loaded, check and record the identity and location of each fuel assembly in the DSC.
8. After all the SFAs have been placed into the DSC and their identities verified, install the hold down ring *if it is not integral to the basket.* Alternately, the hold down ring may be placed before loading the SFAs.

   Lower the shield plug into the DSC.

Intentionally left blank

9. Visually verify that the top shield plug is properly seated in the DSC.
10. *NOT USED.*
11. Raise the cask to the pool surface.
12. *V*erify that *the top shield plug* is properly seated within the DSC. If not, lower the cask and reposition the top shield plug. Repeat steps 9 through 12 as necessary.
13. Continue to raise the cask from the pool until the top region of the cask is accessible.
14. Drain any excess water from the top of the DSC shield plug.
15. Check the radiation levels at the center of the top shield plug and around the perimeter of the cask.
16. As required for crane load limitations, drain water from the DSC. *Use 1 to 3 psig of* helium to backfill the DSC as water is being removed.
17. Lift the cask from the fuel pool.
18. Move the cask with loaded DSC to the plant designated preparation area.
19. *If w*ater *is* removed at step 16, *it* may be replaced with spent fuel pool water or equivalent.

A.7.7.9.2 NUHOMS®-69BTH DSC Drying and Backfilling

CAUTION: During performance of steps listed in this section, monitor the cask/DSC annulus water level and replenish as necessary to maintain cooling.

1. Check the radiation levels *around* the perimeter of the cask. The cask exterior surface should be decontaminated as necessary. Temporary shielding may be installed as necessary to minimize personnel exposure.
2. *NOT USED.*
3. Disengage top shield plug *from* the lifting yoke and position *the yoke* clear of the cask.
4. Decontaminate the exposed surfaces of the DSC *cylindrical* shell perimeter and remove the annulus seal.
5. *A*llow water from the annulus to drain out until the water level is approximately twelve inches below the top edge of the DSC shell. Take swipes around the outer *exposed* surface of the DSC shell and check for smearable contamination as required.

CAUTION: Radiation dose rates are expected to be high at the DSC vent and siphon port locations. Use proper ALARA practices (e.g., use of temporary shielding, appropriate positioning of personnel, etc.) to minimize personnel exposure.

6. Prior to the start of the welding operations, drain a minimum of 100 gallons of water from the DSC. *Use 1 to 3 psig of* helium to backfill the DSC as water is being removed.
7. *NOT USED.*

8. Install the automated welding machine onto the inner top cover and place the inner top cover with the automated welding machine onto the DSC. Alternately, the inner top cover may be placed on the DSC separately or the inner top cover may be part of the shield plug; in these cases the automated welding machine is installed on the inner top cover already installed in the DSC.

9. Check radiation levels along the surface of the inner top cover plate. Temporary shielding may be installed as necessary.

10. Insert suitable tubing through the vent port such that it terminates just below the DSC top shield plug. Connect the tubing to a hydrogen monitor to allow continuous monitoring of the hydrogen atmosphere in the DSC cavity during welding of the inner top cover plate. Optionally, other methods may be used for continuous monitoring of the hydrogen atmosphere in the DSC cavity during welding of the inner top cover plate.

11. *Take precautions* to prevent debris and weld splatter from entering the annulus.

12. *W*eld the inner top cover plate to the DSC shell.

CAUTION: Continuously monitor the hydrogen concentration in the DSC cavity using the tube arrangement described in step 10 during the inner top cover plate cutting/welding operations. Verify that the measured hydrogen concentration does not exceed a safety limit of 2.4% [4] and [5]. If this limit is exceeded, stop all welding operations and purge the DSC cavity *with 2-3 psig* helium to reduce the hydrogen concentration safely below the 2.4% limit.

13. Perform *required* dye penetrant examination of the weld surface*(s)*.

14. *NOT USED.*

15. *R*emove remaining bulk water from the DSC cavity. *U*se helium to backfill the DSC as water is being removed from the DSC. Alternately, helium at up to 15.0 psig may be introduced through the vent port to *assist removal of* the water from the DSC cavity through the siphon port.

16. Once the water stops flowing from the DSC, close the DSC siphon port and disengage the gas source.

17. Connect the VDS to *the cask.*

NOTE: Proceed cautiously when evacuating the DSC to avoid freezing consequences.

18. *S*tart the VDS and draw a vacuum on the DSC cavity. The cavity pressure should be reduced in steps *to optimize moisture removal and avoid freezing. During/between vacuum drying steps,* the pump is valved off and the cavity pressure monitored. The cavity pressure will rise as water and other volatiles in the cavity evaporate. When the cavity pressure stabilizes, the pump is valved in to continue the vacuum drying process. It may be necessary to repeat some steps, depending on the rate and extent of the pressure increase. Vacuum drying is complete when the pressure stabilizes for a minimum of 30 minutes at 3 mm Hg or less.

NOTE: The user shall ensure that the vacuum pump is isolated from the canister cavity when demonstrating compliance with <3 mm Hg for 30 minutes.

Simply closing the valve between the canister and the vacuum pump is not sufficient, as a faulty valve allows the vacuum pump to continue to draw a vacuum on the canister. Turning off the pump, or opening the suction side of the pump to atmosphere are examples of ways to assure that the pump is not continuing to draw a vacuum on the canister.

CAUTION: Radiation dose rates are expected to be high at the vent and siphon port locations. Use proper ALARA practices (e.g., use of temporary shielding, appropriate positioning of personnel, etc.) to minimize personnel exposure.

19. Open the valve to the vent port and allow the helium to flow into the DSC cavity.
20. *NOT USED.*
21. *NOT USED.*
22. *NOT USED.*
23. *NOT USED.*
24. Re-evacuate the DSC cavity. The cavity pressure should be reduced in steps *During/between vacuum drying steps*, the pump is valved off and the cavity pressure monitored. When the cavity pressure stabilizes, the pump is valved in to continue the vacuum drying process. Vacuum drying is complete when the pressure stabilizes for a minimum of 30 minutes at 3 mm Hg *or less*.
25. Open the valve on the vent port and allow helium to flow into the DSC cavity to pressurize the DSC between 16.5 and 18.0 psig and hold for 10 minutes. Depressurize the DSC cavity to 2.5 ± 1.0 psig (stable for 30 minutes).

    CAUTION: Radiation dose rates are expected to be high at the vent and siphon port locations. Use proper ALARA practices (e.g., use of temporary shielding, appropriate positioning of personnel, etc.) to minimize personnel exposure.

26. *NOT USED.*

A.7.7.9.3 NUHOMS®-69BTH DSC Sealing Operations

CAUTION: During performance of steps listed in this section, monitor the cask/DSC annulus water level and replenish as necessary to maintain cooling.

1. Disconnect the VDS from the DSC. Seal weld the prefabricated covers over the vent and siphon ports, inject helium into the blind space just prior to completing welding, and perform *the required* dye penetrant weld examination*(s)*.
2. Install the outer top cover plate and the automated welding system onto the DSC.
3. Tack weld the outer top cover plate to the DSC shell. Place the outer top cover plate weld root pass.
4. Perform a helium leakage test of the inner top cover plate and vent/siphon port plate welds using the test port in the outer top cover plate and verify that the "leak-tight" criterion is met. Verify that the personnel performing the leakage test are qualified in

accordance with SNT-TC-1A [7]. Alternatively, this leakage test can be done with a test head following Step 1 above.

5. If a leak is found, remove the outer cover plate root pass (if not using a test head), the vent and siphon port plugs and repair the inner cover plate welds. Then repeat applicable procedure steps from Section A.7.7.9.2, step 17.

6. Perform dye penetrant examination of the root pass weld. Weld out the outer top cover plate to the DSC shell and perform *the required* dye penetrant examination on the weld surface*(s)*.

7. Seal weld the prefabricated plug (when applicable) over the outer cover plate test port and perform dye penetrant weld examinations.

8. *NOT USED.*

9. *D*rain the water from the cask/DSC annulus.

The cask/DSC is now ready to be prepared for downending as described in Chapter A.7, Section A.7.1.2.2.

A.7.7.9.4 Unloading a NUHOMS®-69BTH DSC to a Fuel Pool

CAUTION: The process of DSC unloading is similar to that used for DSC loading. DSC opening operations described below are to be carefully controlled in accordance with site procedures. This operation is to be performed under the site's standard health physics guidelines for welding, grinding, and handling of potentially highly contaminated equipment. These are to include the use of prudent housekeeping measures and monitoring of airborne particles. Procedures may require tenting, respirators, supplied air or other measures to contain contamination and minimize the impact on the health and safety of workers.

1. *NOT USED.*

2. *R*emove the siphon cover plate.

3. *R*emove the vent cover plate.

4. Sample the DSC cavity atmosphere. If necessary, flush the DSC cavity gases to the site radwaste systems.

CAUTION: (a) The water fill rate must be regulated during this reflooding operation to ensure that the DSC vent pressure does not exceed 20.0 psig.

(b) Provide for continuous hydrogen monitoring of the DSC cavity atmosphere during all subsequent cutting operations to ensure that a safety limit of 2.4% is not exceeded [4] and [5]. Purge *with 2-3 psig* helium (or any other inert medium) as necessary to maintain the hydrogen concentration safely below this limit.

5. Fill the DSC with spent fuel pool water (or other plant-designated water source) through the siphon port with the vent port open and routed to the plant's off-gas system.

6. *Take precautions to prevent debris from entering* the cask/DSC annulus.
7. *R*emove the closure weld from the outer top cover plate.

   CAUTION: Monitor the hydrogen concentration in the DSC cavity during this step to ensure that it does not exceed 2.4% by volume [4] and [5].
8. Remove the DSC outer top cover plate.
9. *R*emove the closure weld from the DSC inner top cover plate.
10. Remove the DSC inner top cover plate.
11. NOT USED
12. Remove excess material on the DSC inside shell surface which may interfere with top shield plug removal.
13. Clean the cask surface of dirt and debris that may have accumulated during transportation or weld removal.
14. *NOT USED.*
15. *NOT USED.*
16. Lower the cask slowly into the fuel pool *using the upper trunnions and lifting yoke.*
17. Disengage the lifting yoke from the cask trunnions and remove the top shield plug and hold-down ring, as applicable.
18. Remove the fuel assemblies (or end caps as applicable for damaged assemblies) from the DSC.
19. *R*emove the cask from the pool.
20. Remove the water from the DSC cavity and cask/DSC annulus.
21. Remove the DSC from the cask.
22. Decontaminate the cask as necessary.
23. *NOT USED.*

This page left intentionally blank.

A.7.7.9.5 References

1. *ANSI N14.5-1997, "American National Standard for Radioactive Materials - Leakage Tests on Packages for Shipment," American National Standards Institute, Inc., New York, 1997.*
2. *Not Used.*
3. *Not Used.*
4. *U.S. Nuclear Regulatory Commission, Office of the Nuclear Material Safety and Safeguards, "Safety Evaluation of VECTRA Technologies' Response to Nuclear Regulatory Commission Bulletin 96-04 for the NUHOMS®-24P and NUHOMS®-7P."*
5. *U.S. Nuclear Regulatory Commission Bulletin 96-04, "Chemical, Galvanic or Other Reactions in Spent Fuel Storage and Transportation Casks," July 5, 1996.*
6. *Not used.*
7. *SNT-TC-1A, "American Society for Nondestructive Testing, Personnel Qualification and Certification in Nondestructive Testing."*

APPENDIX A.7.7.10
Radioactive Waste Canister (RWC) Wet Loading Procedures

Appendix A.7.7.10
Radioactive Waste Canister (RWC) Wet Loading Procedures

Note: The procedure outlined below applies to the final loading of either the RWC-W or the RWC-B prior to release for shipment. Both versions of the RWC have a top shield plug and an outer top cover plate. Both the plug and the plate are welded in place prior to transport.

A.7.7.10.1 Wet Loading of the RWC

The starting condition for the following steps assumes completion of the cask preparation steps in Section A.7.1.2.

1. Lift the cask and position it over the cask loading area of the spent fuel pool.
2. Lower the cask into the fuel pool.
3. Place the cask in the location of the fuel pool *used for* the cask loading area.
4. Disengage the lifting yoke from the cask lifting trunnions and move the yoke clear of the cask.
5. *L*oad the RWC cavity. Record contents and location on the cask loading report to the extent practical.
6. Install the liner shield plug (RWC-W), as applicable, and then install the RWC top shield plug.
7. *NOT USED.*
8. *NOT USED.*
9. Inspect the shield plug/lid to verify that it is properly seated within the RWC. Repeat steps 6 through 8 as necessary.
10. *NOT USED.*
11. Drain any excess water from the top of the RWC back to the fuel pool.
12. Check the radiation levels at the center of the top shield plug and around the perimeter of the cask.
13. *NOT USED.*
14. Lift the cask from the fuel pool.
15. Move the cask to the plant designated preparation area.

Intentionally left blank

A.7.7.10.2 RWC Drying and Backfilling

1. Check the radiation levels along the perimeter of the cask. The cask exterior surface should be decontaminated as necessary. Temporary shielding may be installed as necessary to minimize personnel exposure.
2. *NOT USED.*
3. Disengage top shield plug *from* the lifting yoke and position *the yoke* clear of the cask.
4. Decontaminate the exposed surfaces of the RWC *cylindrical* shell perimeter and remove the annulus seal.
5. *A*llow water from the annulus to drain out until the water level is approximately twelve inches below the top edge of the RWC shell. Take swipes around the outer *exposed* surface of the RWC shell and check for smearable contamination as required.

   CAUTION: Radiation dose rates are expected to be high at the RWC vent and siphon port locations. Use proper ALARA practices (e.g., use of temporary shielding, appropriate positioning of personnel, etc.) to minimize personnel exposure.

6. Prior to the start of welding operations drain approximately 100 gallons of water from the RWC.
7. *NOT USED.*
8. Install the automated welding machine onto the top shield plug.
9. Check radiation levels along the surface of the top shield plug. Temporary shielding may be installed as necessary.
10. *Take precautions* to prevent debris and weld splatter from entering the annulus.
11. *W*eld the top shield to the RWC shell.
12. Perform *required* dye penetrant examination of the weld surface*(s)*.
13. *NOT USED.*
14. *R*emove remaining bulk water from the RWC cavity.
15. Once the water stops flowing from the RWC, close the RWC siphon port and disengage the gas source.
16. Connect the VDS to *the cask.*
17. *S*tart the VDS and draw a vacuum on the RWC cavity until dry. That is, until a vacuum of approximately 10 mbar can be maintained for 10 minutes.
18. *Use* air or helium to pressurize the RWC to 2.5 ± 1.0 psig backfill pressure (stable for 30 minutes).

    CAUTION: Radiation dose rates are expected to be high at the vent and siphon port locations. Use proper ALARA practices (e.g., use of temporary shielding, appropriate positioning of personnel, etc.) to minimize personnel exposure.

19. Close the line connected to the vent port.

A.7.7.10.3 RWC Sealing Operations

1. Disconnect the VDS from the RWC. Seal weld the prefabricated covers over the vent and siphon ports and perform *the required* dye penetrant weld examination*(s)*.
2. Install the outer top cover plate and the automated welding system onto the RWC.
3. Tack weld the outer top cover plate to the RWC shell. Place the outer top cover plate weld root pass.
4. Perform dye penetrant examination of the root pass weld. Weld out the outer top cover plate to the RWC shell and perform *the required* dye penetrant examination on the weld surface*(s)*.
5. Remove the automated welding machine from the RWC.
6. *D*rain the water from the cask/RWC annulus.

The cask/RWC is now ready to be prepared for downending as described in Chapter A.7, Section A.7.1.2.2.

Chapter A.8
Acceptance Tests and Maintenance Program

TABLE OF CONTENTS

Chapter A.8
Acceptance Tests and Maintenance Program

NOTE: References in this Chapter are shown as [1], [2], etc. and refer to the reference list in Section A.8.3.

A.8.1 Acceptance Tests

The following reviews, inspections, and tests shall be performed on the NUHOMS®-MP197HB packaging prior to initial transport. Many of these tests will be performed at the fabricator's facility prior to delivery of the cask or dry shielded canister (DSC) to the utility for use. Tests will be performed in accordance with written procedures.

A.8.1.1 Visual Inspection and Measurements

Visual inspections are performed at the fabricator's facility to ensure that the packaging conforms to the drawings and specifications. The visual inspections include:

- cleanliness inspections,
- visual weld inspections as required by ASME Code [1],
- inspection of sealing surface finish, and
- dimensional inspections for conformance with the drawings included in Chapter A.1, Appendix A.1.4.10.

A.8.1.2 Weld Examinations

The structural materials are chemically and physically tested to confirm that the required properties are met.

To the maximum extent practical, all welding is performed using qualified processes and qualified personnel, according to the ASME Boiler and the Pressure Vessel Code [1]. Base materials and welds are examined in accordance with the ASME Boiler and Pressure Vessel Code requirements. NDE requirements for welds are specified on the drawings provided in Appendix A.1.4.10. All NDE is performed in accordance with written procedures. The inspection personnel are qualified in accordance with SNT-TC-1A [2].

The containment welds of the NUHOMS®-MP197HB cask, and the NUHOMS®-DSCs are designed, fabricated, tested and inspected in accordance with ASME B&PV Code Subsection NB. Welds of the noncontainment structure are inspected as per the NDE acceptance criteria of ASME B&PV Code, Subsection NF.

The NUHOMS®-DSC fuel baskets are designed, fabricated, and inspected in accordance with the ASME B&PV Code Subsection NG. Fusion weld tests as required are shown on drawings provided in Appendix A.1.4.10.

Alternatives to the code are described in Chapter A.2, Section A.2.1.4 and Appendix A.2.13.13.

A.8.1.3 Structural and Pressure Tests

A.8.1.3.1 Load Tests

Two sets of trunnions are provided for the NUHOMS®-MP197HB transport package lifting. One set of trunnions has double shoulders (non-single failure proof). The other set of trunnions has a single shoulder (single failure proof). Only one set of trunnions is used depending on site and transfer operation requirements. The trunnions are fabricated and tested in accordance with ANSI N14.6 [3]. A load test of 3.0 times the design lift load (for single failure proof trunnions) or 1.5 times the design lift load (for non-single failure proof trunnions) is applied to the trunnions for a period of ten minutes, to ensure that the trunnions can perform satisfactorily.

A force equal to 1.5 times the impact limiter weight will be applied to the hoist rings of each impact limiter for a period of ten (10) minutes. At the conclusion of the test, the impact limiter hoist rings will be visually examined for defects and permanent deformation.

A.8.1.3.2 Pressure Tests

A pressure test is performed on the NUHOMS®-MP197HB packaging assembly at a pressure between 40.0 and 45.0 psig. This is well above 1.5 times the maximum normal operating pressure of 12.7 psig (Chapter A.3, Table A.3-20). The test pressure is held for a minimum of 10 minutes. The test is performed in accordance with ASME B&PV Code, Section III, Subsection NB, Paragraph NB-6200 or NB-6300. All visible joints/surfaces are visually examined for possible leakage after application of the pressure.

In addition, a bubble leakage test is performed on the resin enclosure. The purpose of this test is to identify any potential leakage passages in the enclosure welds.

A.8.1.4 Containment Boundary Leakage Tests

A.8.1.4.1 MP197HB Cask Leakage Tests

Leakage tests are performed on the MP197HB cask containment boundary prior to first use, typically at the fabricator's facility. The fabrication verification leakage test can be separated into the following five tests: 1) cask leakage integrity, 2) cask vent port closure bolt seal integrity, 3) cask drain port closure bolt seal integrity, 4) cask lid seal integrity, and 5) ram access closure plate seal integrity. These tests are usually performed using the helium mass spectrometer method. Alternative methods are acceptable, provided that the required sensitivity is achieved. The leakage test is performed in accordance with ANSI N14.5 [4] or ISO-12807 [11]. The personnel performing the leakage test are qualified in accordance with SNT-TC-1A [2].

Cask Leakage Integrity Test

Prior to lead pour and final machining of the inner shell, the cylindrical portion of the containment boundary, including the bottom end closure, will be leakage tested in accordance with the requirements of ANSI N14.5 [4] or ISO-12807 [11], using temporary closures and seals for the ram access cover plate and lid. Because the inner shell will not be accessible for leakage testing after lead is poured, leakage testing will be performed during the fabrication process, as permitted by ANSI N14.5 Table 1 [4].

If a leakage is discovered, the source will be determined, repaired, and the shells retested to ensure that the measured leakage rate is less than $1x10^{-7}$ ref cm^3/s.

The test will be performed in conjunction with the non-destructive examination of the inner shell welds in accordance with ASME B&PVC Code, Section III, Subsection NB. An MT or PT examination of every weld layer in the shell-to-top-forging closure weld and an MT or PT examination of all final machined weld surfaces of the inner shell will be performed per the Code.

Fabrication Verification Leakage Tests

The fabrication verification leakage tests include the following:

- Cask vent port closure bolt seal integrity
- Cask drain port closure bolt seal integrity
- Cask lid seal integrity
- Cask ram access closure plate seal integrity

The tests will be performed as described in Chapter A.7, Section A.7.4.1, in accordance with the ANSI N 14.5 [4] or ISO-12807 [11]. The acceptance criterion requires each component to be individually leaktight, that is, the leakage rate must be less than $1x10^{-7}$ ref cm^3/s.

A.8.1.4.2 NUHOMS® DSCs Leakage Test

The containment boundary of a NUHOMS® DSC is leakage tested to verify it is leaktight in accordance with ANSI N14.5 [4] or ISO-12807 [11]. The leakage tests are typically performed using the helium mass spectrometer method. Alternative methods are acceptable, provided that the required sensitivity is achieved. Following completion of the welding of the DSC inner top cover plate and siphon and vent cover plates, these welds are leakage tested to $\leq 1.0 \times 10^{-7}$ ref cm^3/s.

If the leakage rate exceeds this criteria, the inner top cover plate seal weld and siphon and vent cover plate welds will be inspected and repaired where necessary.

For the 24PT4 DSC, the leakage test requirements outlined in CoC 1029 are used to demonstrate leaktightness in lieu of the above criteria.

A.8.1.5 MP197HB Cask Component and Material Tests

A.8.1.5.1 Valves, Rupture Discs, and Fluid Transport Devices

There are no valves, rupture discs, or couplings in the containment of the NUHOMS®-MP197HB packaging.

A.8.1.7 Neutron Absorber Tests

The neutron absorber used for criticality control in the DSC baskets may consist of any of the following types of material. Depending on the DSC model, these neutron absorber materials may be used alone or be paired with aluminum:

(a) Boron-aluminum alloy (borated aluminum)

(b) Boron carbide/Aluminum metal matrix composite (MMC)

(c) Boral®

These materials only serve as neutron absorber for criticality control and as heat conduction paths. The MP197HB packaging safety analyses do not rely upon their mechanical strength. The radiation and temperature environment in the cask is not sufficiently severe to damage these metallic/ceramic materials. To assure performance of the neutron absorber's design function only the presence of B10 and the uniformity of its distribution need to be verified, with testing requirements specific to each material. The boron content of these materials is given in the Appendices A.1.4 for each DSC type.

References to metal matrix composites throughout this chapter are not intended to refer to Boral®, which is described later in this section.

A.8.1.7.1 Boron Aluminum Alloy (Borated Aluminum)

The material is produced by direct chill (DC) or permanent mold casting with boron precipitating *primarily* as a uniform fine dispersion of discrete AlB_2 or TiB_2 particles in the matrix of aluminum or aluminum alloy *(other boron compounds, such as AlB_{12}, can also occur)*. For extruded products, the TiB_2 form of the alloy shall be used. For rolled products, either the AlB_2, the TiB_2, or a hybrid may be used.

Boron is added to the aluminum in the quantity necessary to provide the specified minimum B10 areal density in the final product. The amount required to achieve the specified minimum B10 areal density will depend on whether boron with the natural isotopic distribution of the isotopes B10 and B11, or boron enriched in B10 is used. In no case shall the boron content in the aluminum or aluminum alloy exceed 5% by weight.

The criticality calculations take credit for 90% of the minimum specified B10 areal density of borated aluminum. The basis for this credit is the B10 areal density acceptance testing, which shall be as specified in Section A.8.1.7.6. The specified acceptance testing assures that at any location in the material, the minimum specified areal density of B10 will be found with 95% probability and 95% confidence.

A.8.1.7.2 Boron Carbide/Aluminum Metal Matrix Composites (MMC)

The material is a composite of fine boron carbide particles in an aluminum or aluminum alloy matrix. The material shall be produced by either direct chill casting, permanent mold casting, powder metallurgy, or thermal spray techniques. The boron carbide content shall not exceed 40% by volume. The boron carbide content for MMCs with an integral aluminum cladding shall not exceed 50% by volume.

The final MMC product shall have density greater than 98% of theoretical density demonstrated by qualification testing, with no more than 0.5 volume % interconnected porosity. For MMC with an integral cladding, the final density of the core shall be greater than 97% of theoretical density demonstrated by qualification testing, with no more than 0.5 volume % interconnected porosity of the core and cladding as a unit of the final product.

Boron carbide particles for the products considered here *shall be smaller than* 40 microns or less. No more than 10% of the particles shall be over 60 microns.

Prior to use in the DSC, MMCs shall pass the qualification testing specified in Section A.8.1.7.7, and shall subsequently be subject to the process controls specified in Section A.8.1.7.8.

The criticality calculations take credit for 90% of the minimum specified B10 areal density of MMCs. The basis for this credit is the B10 areal density acceptance testing, which is specified in Section A.8.1.7.6. The specified acceptance testing assures that at any location in the final product, the minimum specified areal density of B10 will be found with 95% probability and 95% confidence.

A.8.1.7.3 Boral®

This material consists of a core of aluminum and boron carbide powders between two outer layers of aluminum, mechanically bonded by hot-rolling an "ingot" consisting of an aluminum box filled with blended boron carbide and aluminum powders. The core, which is exposed at the edges of the sheet, is slightly porous. *Before rolling, at least 80% by weight of the B_4C particals in BORAL® shall be smaller than 200 microns.* The nominal boron carbide content shall be limited to 65% (+ 2% tolerance limit) of the core by weight.

The criticality calculations take credit for 75% of the minimum specified B10 areal density of Boral®. B10 areal density will be verified by chemical analysis and by certification of the B10 isotopic fraction for the boron carbide powder, or by neutron transmission testing. Areal density testing is performed on a coupon taken from the sheet produced from each ingot. If the measured areal density is below that specified, all the material produced from that ingot will be either rejected, or accepted only on the basis of alternate verification of B10 areal density for each of the final pieces produced from that ingot.

A.8.1.7.4 Visual Inspections of Neutron Absorbers

Neutron absorbers shall be 100% visually inspected in accordance with the Certificate Holder's QA procedures. Material that does not meet the following acceptance criteria shall be reworked, repaired, or scrapped. Blisters shall be treated as non-conforming. Inspection of MMCs with an integral aluminum cladding shall also include verification that the matrix is not exposed through the faces of the aluminum cladding and that solid aluminum is not present at the edges. For Boral, visual inspection shall verify that there are no cracks through the cladding, exposed core on the face of the sheet, or solid aluminum at the edge of the sheet.

A.8.1.7.5 Other Visual Inspections Criteria (non-CoC Conditions)

For borated aluminum and MMCs, visual inspections shall follow the recommendations in Aluminum Standards and Data, Chapter 4 "Quality Control, Visual Inspection of Aluminum Mill Products and Castings"[12]. Local or cosmetic conditions such as scratches, nicks, die lines, inclusions, abrasion, isolated pores, or discoloration are acceptable.

A.8.1.7.6 Specification for Acceptance Testing of Neutron Absorbers by Neutron Transmission

A.8.1.7.6a Neutron Transmission acceptance testing procedures shall be subject to approval by the Certificate Holder. Test coupons shall be removed from the rolled or extruded production material at locations that are systematically or probabilistically distributed throughout the lot. Test coupons shall not exhibit physical defects that would not be acceptable in the finished product, or that would preclude an accurate measurement of the coupon's physical thickness.

Any plate which is thinner than the statistically derived minimum thickness from Section A.8.1.7.6a or the minimum design thickness, whichever is greater, shall be treated as non-conforming, with the following exception. Local depressions are acceptable, so long as they total no more than 0.5% of the area on any given plate, and the thickness at their location is not less than 90% of the minimum design thickness. *Edge effects due to manufacturing operations such as shearing, deburring, and chamfering need not be included in this determination.*

Non-conforming material shall be evaluated for acceptance in accordance with the Certificate Holder's QA procedures.

A.8.1.7.7 Specification for Qualification Testing of Metal Matrix Composites

A.8.1.7.7.1 Applicability and Scope

Metal matrix composites (MMCs) acceptable for use in the DSCs are described in Section A.8.1.7.2.

Prior to initial use in a spent fuel transport system, such MMCs shall be subjected to qualification testing that will verify that the product satisfies the design function. Key process controls shall be identified per Section A.8.1.7.8 so that the production material is equivalent to or better than the qualification test material. Changes to key processes shall be subject to qualification before use of such material in a spent fuel dry storage or transport system.

ASTM test methods and practices are referenced below for guidance. Alternative methods may be used with the approval of the certificate holder.

A.8.1.7.7.2 Design Requirements

In order to perform its design functions the product must have at a minimum sufficient strength and ductility for manufacturing and for the normal and accident conditions of the transport system. This is demonstrated by the tests in Section A.8.1.7.7.4. It must have a uniform distribution of boron carbide. This is demonstrated by the tests in Section A.8.1.7.7.5.

A.8.1.7.7.3 Durability

There is no need to include accelerated radiation damage testing in the qualification. Such testing has already been performed on MMCs, and the results confirm what would be expected of materials that fall within the limits of applicability cited above. Metals and ceramics do not experience measurable changes in mechanical properties due to fast neutron fluences typical over the lifetime of spent fuel transport, about 10^{15} neutrons/cm^2.

The need for thermal damage and corrosion (hydrogen generation) testing shall be evaluated case-by-case based on comparison of the material composition and environmental conditions with previous thermal or corrosion testing of MMCs.

Thermal damage testing is not required for unclad MMCs consisting only of boron carbide in an aluminum 1100 matrix, because there is no reaction between aluminum and boron carbide below 842°F, well above the basket temperature under normal conditions of transport[1].

Corrosion testing is not required for MMCs (clad or unclad) consisting only of boron carbide in an aluminum 1100 matrix, because testing on one such material has already been performed by Transnuclear[2].

A.8.1.7.7.3.1 Delamination Testing of Clad MMC

Clad MMCs shall be subjected to thermal damage testing following water immersion to ensure that delamination does not occur under normal conditions of storage. *This testing shall include conditions to simulate water conditions of the pool and heating temperatures for storage. An example of such a test would be: (1) immerse a specimen at least 6 x 6 inches in water under pressure ≥30 psig for at least 24 hours, (2) place the specimen in a vacuum furnace preheated to at least 300°F and evacuate the furnace. Acceptance criterion for the test shall be no blistering or delamination of the cladding.*

A.8.1.7.7.4 Required Qualification Tests and Examinations to Demonstrate Mechanical Integrity

At least three samples, one each from approximately the two ends and middle of the qualification material run shall be subject to:

a) room temperature tensile testing (ASTM- B557[3]) demonstrating that the material has the following tensile properties:
   - Minimum yield strength, 0.2% offset: 1.5 ksi
   - Minimum ultimate strength: 5 ksi
   - Minimum elongation in 2 inches: 0.5%

As an alternative to the elongation requirement, ductility may be demonstrated by bend testing per ASTM E290[4]. The radius of the pin or mandrel shall be no greater than three times the material thickness, and the material shall be bent at least 90 degrees without complete fracture,

b) Testing to verify more than 98% of theoretical density for non-clad MMCs and 97% for the matrix of clad MMCs. Testing or examination for interconnected porosity on the faces and edges of unclad MMC, and on the edges of clad MMC shall be performed by a means to be approved by the Certificate Holder. The maximum interconnected porosity is 0.5 volume %, and for at least one sample,

---

1 Sung, C., "Microstructural Observation of Thermally Aged and Irradiated Aluminum/Boron Carbide (B_4C) Metal Matrix Composite by Transmission and Scanning Electron Microscope," 1998.

2 Boralyn testing submitted to the NRC under docket 71-1027, 1998.

3 ASTM B557 Standard Test Methods of Tension Testing Wrought and Cast Aluminum and Magnesium-Alloy Products

4 ASTM E290, Standard Methods for Bend Testing of Materials for Ductility.

c) For MMCs with an integral aluminum cladding, thermal durability testing demonstrating that after a minimum 24 hour soak in either pure or borated water, then insertion into a preheated oven at approximately 825°F for a minimum of 24 hours, the specimens are free of blisters and delamination and pass the mechanical testing requirements described in test 'a' of this section.

A.8.1.7.7.5 Required Tests and Examinations to Demonstrate B10 Uniformity

Uniformity of the boron distribution shall be verified either by:

a) Neutron radioscopy of material from the ends and middle of the test material production run, verifying no more than 10% difference between the minimum and maximum B10 areal density, or
b) Quantitative testing for the B10 areal density, B10 density, or the boron carbide weight fraction, on locations distributed over the test material production run, verifying that one standard deviation in the sample is less than 10% of the sample mean. Testing may be performed by a neutron transmission method similar to that specified in Section A.8.1.7.6, or by chemical analysis for boron carbide content in the composite.

A.8.1.7.7.6 Approval of Procedures

Qualification procedures shall be subject to approval by the Certificate Holder.

A.8.1.7.8 Specification for Process Controls for Metal Matrix Composites

This section provides process controls to ensure that the material delivered for use is equivalent to the qualificaion test material.

A.8.1.7.8.1 Applicability and Scope

Key processing changes shall be subject to qualification prior to use of the material produced by the revised process. The Certificate Holder shall determine whether a complete or partial re-qualification program per Section A.8.1.7.7 is required, depending on the characteristics of the material that could be affected by the process change.

A.8.1.7.8.2 Definition of Key Process Changes

Key process changes are those which could adversely affect the uniform distribution of the boron carbide in the aluminum, reduce density, reduce corrosion resistance, or reduce the mechanical strength or ductility of the MMC.

A.8.1.7.8.3 Identification and Control of Key Process Changes

The manufacturer shall provide the Certificate Holder with a description of materials and process controls used in producing the MMC. The Certificate Holder and manufacturer shall identify key process changes as defined in Section A.8.1.7.8.2.

A.8.1.7.9 Neutron Absorber for DSCs Already Loaded and DSCs Under Fabrication

The neutron absorber tests and acceptance criteria as described in Section A.8.1.7.1 through Section A.8.1.7.8 are only applicable to all the canister types that will be loaded in the spent fuel pool using the MP197HB cask. However, for canister types which are already in service under 10CFR Part72, the neutron absorber material acceptance requirements for each specific canister type as described in the applicable 10CFR Part72 approved certificate of compliance are applicable.

A.8.1.8 *Cask* Thermal Tests

The thermal evaluation of the MP197HB cask described in Chapter A.3 is performed using very conservative and bounding assumptions. Gaps between the components are modeled in the thermal analysis to account for possible gaps expected during fabrication. Gaps are assumed to be present during NCT and HAC post fire cases when calculating heat flow out of the cask and gaps are assumed closed when calculating heat flow into the cask (i.e., during the HAC fire). The calculated cladding temperatures are much lower than the cladding temperature limit, assuring large margins to the limits. The cladding temperatures reported for the DSCs are very conservative because the allowed heat loads for a given DSC are reduced until the calculated DSC shell temperature in the MP197HB cask is below that calculated for storage conditions in the applicable 10 CFR Part 72 license. The reported cladding temperature is that of the higher heat load allowed under storage conditions with the same or higher DSC shell temperature.

However, to provide additional assurance that the thermal performance of the fabricated cask is equal to or exceeds the theoretical performance reported in the SAR, a thermal test is performed after fabrication of MP197HB cask.

Heat dissipation for the MP197HB cask to the ambient occurs three-dimensionally with a significant portion of the design heat load being radially dissipated through the neutron shield region of the cask body. The cask top and bottom ends beyond the neutron shield region are covered by the impact limiters. Due to limited contact between the thermal shields and the cask end plates (cask bottom plate and cask lid) and the insulating properties of wood within the impact limiters, the heat dissipation in the axial direction is largely restricted and is insignificant in comparison to the radial heat dissipation.

The thermal test measures the effective thermal conductivity of a cask in the radial direction over an approximately 10-ft exposed length within the neutron shield region. These measured thermal conductivities will be used as thermal input into the ANSYS model described in the SAR, Chapter A.3, Section A.3.3.1.1 for the NCT thermal analysis. The temperature distribution computed with the measured conductivity of the cask is then compared against the corresponding values in the SAR, Chapter A.3, Table A.3-8, and A.3-10 to demonstrate the thermal performance of the fabricated cask is equal to or exceeds the theoretical performance reported in the SAR.

A.8.1.9 Neutron Absorber Thermal Conductivity Testing

Acceptance testing shall conform to ASTM E1225, ASTM E1461, or equivalent method, performed at room temperature on coupons taken from the rolled or extruded production material. Initial sampling shall be one test per lot, and may be reduced if the first five tests meet

the specified minimum thermal conductivity. For cast products, the lot shall be defined by the heat or ingot. For other products, the lot shall be defined as material produced in a single production campaign using the same heat or lots of aluminum and boron carbide feed materials.

If a thermal conductivity test result is below the specified minimum, at least four additional tests shall be performed on the material from that lot. If the mean value of those tests, including the original test, falls below the specified minimum, the associated lot shall be rejected.

After twenty five tests of a single type of material, with the same aluminum alloy matrix, the same boron content, and the same primary boron phase, e.g., B_4C, TiB_2, or AlB_2, if the mean value of all the test results less two standard deviations meets the specified thermal conductivity, no further testing of that material is required. This exemption may also be applied to the same type of material if the matrix of the material changes to a more thermally conductive alloy (e.g., from 6000 to 1000 series aluminum), or if the boron content is reduced without changing the boron phase.

The measured thermal conductivity values shall satisfy the minimum required conductivities as shown in Section A.3.2.1, Table 17 for HLZC #1, #2 and #3, and in Section A.3.2.1, Table 19 for HLZC #4.

In cases where the specified thickness of the neutron absorber may vary, the equations introduced in Section A.3.3.1.5 shall be used to determine the minimum required effective thermal conductivity.

The thermal conductivity test requirement does not apply to aluminum that is paired with the neutron absorber.

A.8.2 Maintenance Program

A.8.2.1 Structural and Pressure Tests

Within 14 months prior to any lift of a NUHOMS®-MP197HB transport package, the front trunnions shall be subject to either of the following:

- A test load equal to 300% of the maximum service load per ANSI N14.6 [3], paragraph 7.3.1(a) for single failure proof trunnions or a test load equal to 150% of the maximum service load per ANSI N14.6 [3], paragraph 7.3.1(b) for non-single failure proof trunnions. After sustaining the test load for a period of not less than 10 minutes, accessible critical areas shall be subjected to visual inspection for defects, and all components shall be inspected for permanent deformation.
- Dimensional testing, visual inspection and nondestructive examination of accessible critical areas of the trunnions including the bearing surfaces in accordance with Paragraph 6.3.1 of ANSI N14.6 [3].

A.8.2.2 Leakage Tests

The following containment boundary components shall be subject to periodic maintenance, and preshipment leakage testing in accordance with ANSI N14.5 [4] or ISO-12807 [11]:

- Lid
- Ram Access Closure Plate
- Vent Port
- Drain Port

Test	Frequency	Acceptance Criteria	Typical Method (ANSI N14.5 TABLE A-1, [4])
Periodic	Within 12 months prior to shipment	Each component individually ≤ 1×10^{-7} ref cm^3/s	(He) A.5.3 A.5.4
Pre-shipment	Before each shipment, after the contents are loaded and the package is closed	No detected leakage, sensitivity of 10^{-3} ref cm^3/s or better, unless seal is replaced.	A.5.1 A.5.2 A.5.8 A.5.9
Maintenance	After maintenance, repair, or replacement of containment components, including inner seals	Each component individually ≤ 1×10^{-7} ref cm^3/s	(He) A.5.3 A.5.4

No leakage tests are required prior to shipment of an empty NUHOMS®-MP197HB packaging.

A.8.3 References

1. ASME Boiler and Pressure Vessel Code, Section III, 2004 Edition including 2006 addenda. (For the MP197HB; various editions apply to specific DSCs. See Chapter A.2 for specific applications).
2. SNT-TC-1A, "American Society for Nondestructive Testing, Personnel Qualification and Certification in Nondestructive Testing."
3. ANSI N14.6-1993, "American National Standard for Special Lifting Devices for Shipping Containers Weighing 10,000 Pounds or More for Nuclear Materials," New York.
4. ANSI N14.5-1997, "American National Standard for Leakage Tests on Packages for Shipment of Radioactive Materials."
5. Not Used.
6. Not Used.
7. Not Used.
8. Not Used.
9. Not Used.
10. Not Used.
11. ISO-12807, "Safe transport of radioactive material - Leakage testing on packages," First Edition, 1996.
12. "Aluminum Standards and Data, 2003," The Aluminum Association.
13. Natrella, "Experimental Statistics," Dover, 2005.
14. *ASTM E1225, "Thermal Conductivity of Solids by Means of the Guarded-Comparative-Longitudinal Heat Flow Technique."*
15. *ASTM E1461, "Thermal Diffusivity of Solids by the Flash Method."*

Enclosure 9 to TN E-30577

Report of dose rate measurements performed on two TN-32 storage casks (associated with RAI 5-2)

N50-T23-286

October 6, 1998

Ms. Tara J. Neider
Vice President, Engineering
Transnuclear, Inc.
Four Skyline Drive
Hawthorne, New York 10532-2120

Dear Ms. Neider:

Radiation Survey Measurements
Purchase Orders BNT-403169 and BNT-544677
TN-32 Spent Fuel Storage Casks
Surry and North Anna Power Stations

Neutron and gamma radiation surveys were obtained from casks TN-32.05 and TN-32.07 at Surry Power Station on September 30, 1998. Two different forms were used to record the data. One form was developed for field measurements. The data from the field measurements were then transcribed to Surry Radiological Survey maps, which also identify the instruments used to make the measurements. The survey data, on both sets of forms, are included as Attachment 1. The neutron measurements recorded on these forms have not been corrected for the cask surface neutron spectrum. Therefore, all neutron measurements recorded on the attached forms must be divided by two to properly reflect the actual neutron dose rates. Additionally, the fuel assemblies in cask TN-32.05 have BPRAs whereas the fuel assemblies in cask TN-32.07 do not.

In addition, axial and azimuthal sweeps were performed along the surface of the casks to determine if the effect of the cobalt-60 in the Inconel grid spacers or neutron streaming through the aluminum resin boxes could be measured. A constant gamma dose rate was measured during the axial sweeps (over three feet in length) and azimuthal sweeps on both casks. Therefore, the effect of cobalt-60 in the grid spacers was not evident. Also, I confirmed that all fuel assemblies loaded in these two casks were manufactured with Inconel grid straps, and not Zircaloy grid straps.

The azimuthal sweep (as well as the axial sweep) indicated a slight variation in neutron dose rates. The variations ranged from 2 mr/hr (uncorrected) for the azimuthal sweep and 6 mr/hr (uncorrected) for the axial sweep. The variations in azimuthal neutron surface dose rates were not coincident with the pitch of the aluminum resin boxes, and neutron streaming through the aluminum resin boxes was not observed. The variation in neutron dose rate observed in the axial sweep is likely to be the result of other factors such as the varying axial neutron source term from the fuel and scattering from the concrete, rather than the aluminum resin boxes.

Provided as Attachment 2 are copies of the signed ISFSI Fuel Certifications and Cask Loading Maps for TN-32.05 and TN-32.07. These forms identify the average neutron and gamma source emission rates for the fuel assemblies loaded into casks TN-32.05 and TN-32.07. The loading maps indicate the positions where the fuel assemblies are loaded in the casks. For reference, the trunnions are located on the North-South axis.

Please feel free to contact me at (804) 273-3243 if you have any questions regarding these data.

Very truly yours,

Tom A. Brookmire

Tom A. Brookmire
Senior Staff Engineer

Attachments

cc: Ms. Adelaide Giantelli – Transnuclear, Inc.

bc: Mr. N. P. Wolfhope - IN/3SW (w/o Attachments)
Mr. D. P. Batalo – IN/3SW
Mr. T. A. Brookmire – IN/3SW
FPA File 5.2.7 - IN/3SW
Records Mgt. NP-50 & NP-2884 - IN/GW

ATTACHMENT 1
NEUTRON AND GAMMA SURVEYS
TN-32.05 AND TN-32.07
SEPTEMBER 30, 1998

Enclosure 9 to TN-E-30577

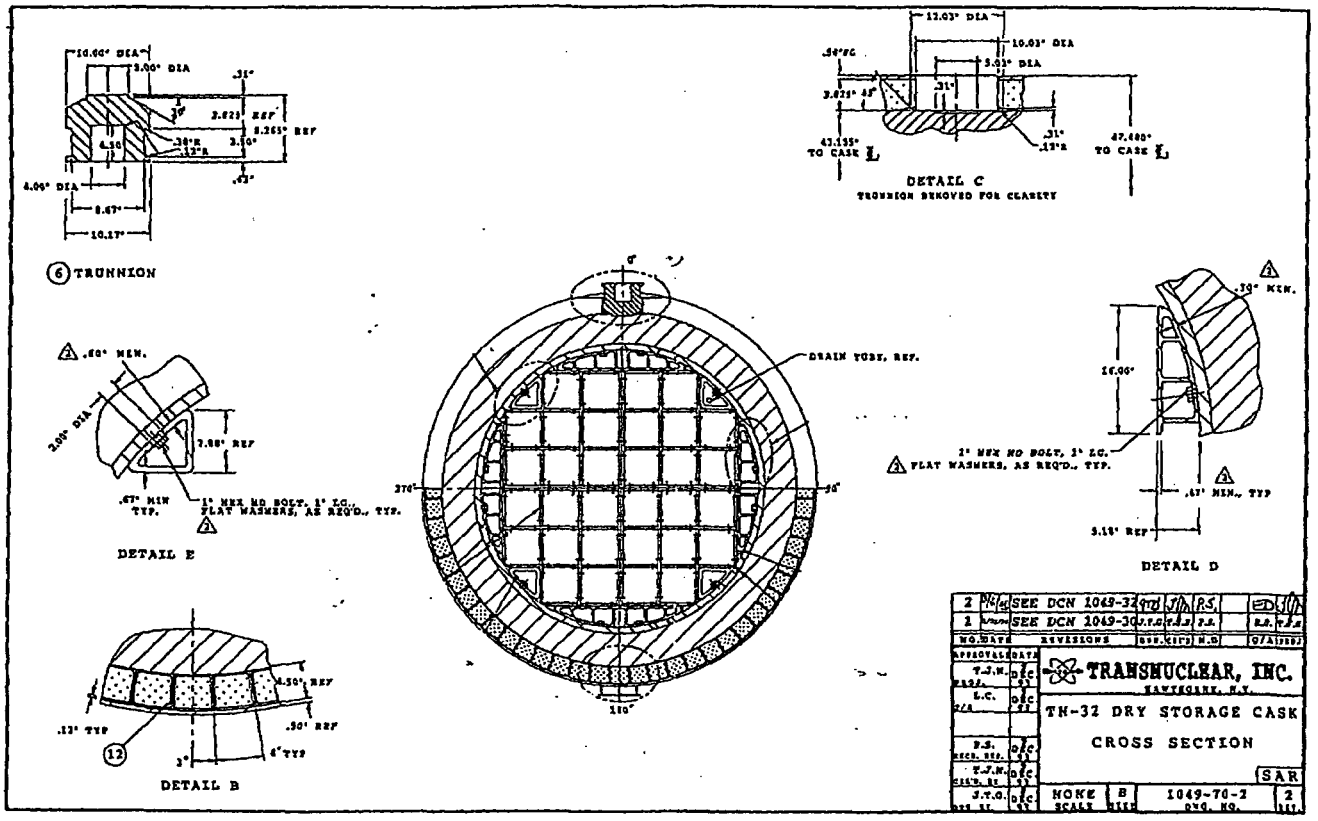

9/30/98 TN-32-05

	NEUTRON	GAMMA
CIRC.	18-20	7
Long.	20-26	9
BACKGROUND	0.2	0.8

AT ANY HEIGHT

A) CIRCUMFERENTIAL SWEEP OVER ≥ 12" TO SEE IF CAN DETECT THE ALUM. BOXES.

B) LONGITUDINAL SWEEP OF ≥ 3 FT. TO SEE IF CAN DETECT GRID SPACERS.

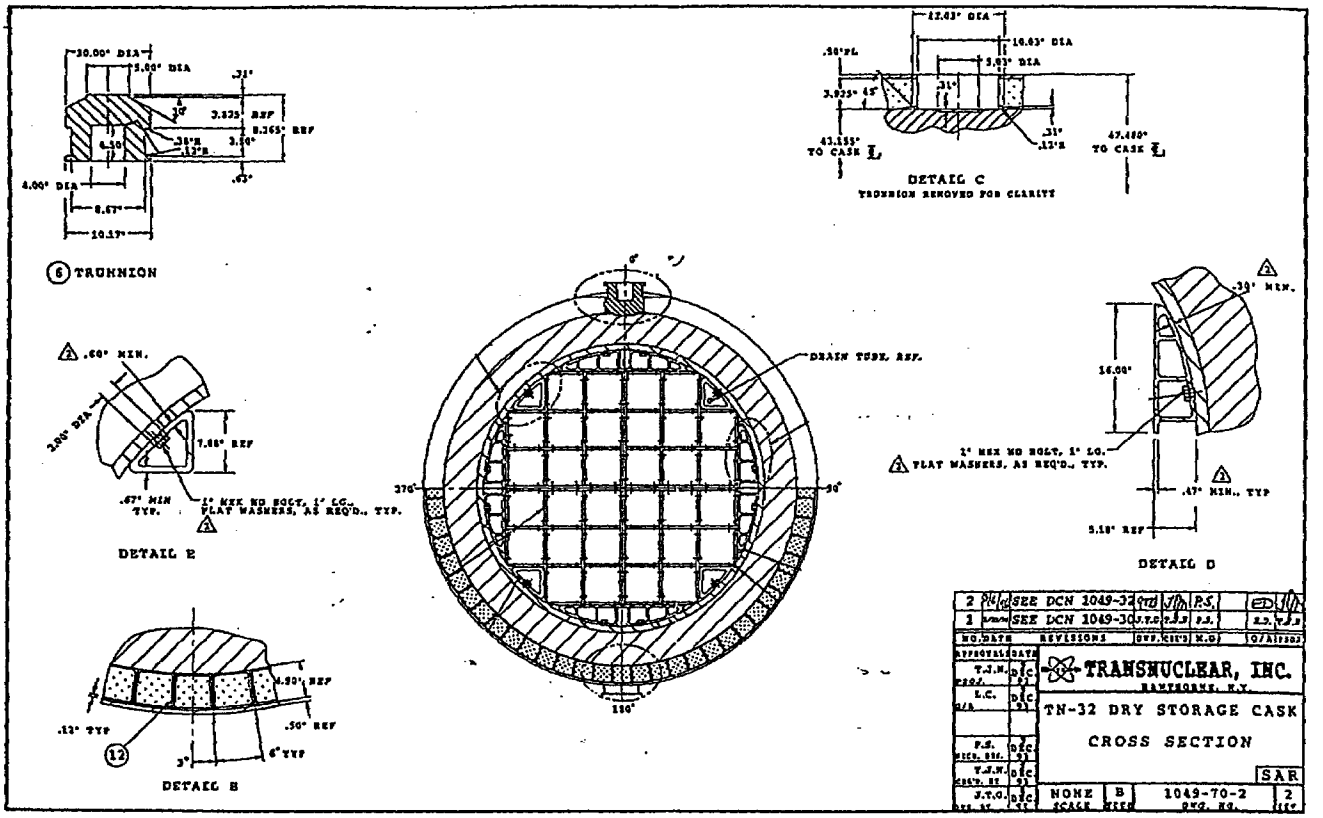

9/30/98 TN-32-07

CIRC.	NEUTRON 16-18	13 5
LONG.	14-16	5
BACKGROUND	0.2	0.8

AT ANY HEIGHT

A) CIRCUMFERENTIAL SWEEP OVER ≥ 12"
TO SEE IF CAN DETECT THE ALUM. BOXES.

B) LONGITUDINAL SWEEP of ≥ 3 ft.
TO SEE IF CAN DETECT GRID SPACERS.

CASK ID # TN-32-05

DATE 9/30/98

NEUTRON

DOSE POINTS AT SURFACE, 18 in. & 1 METER

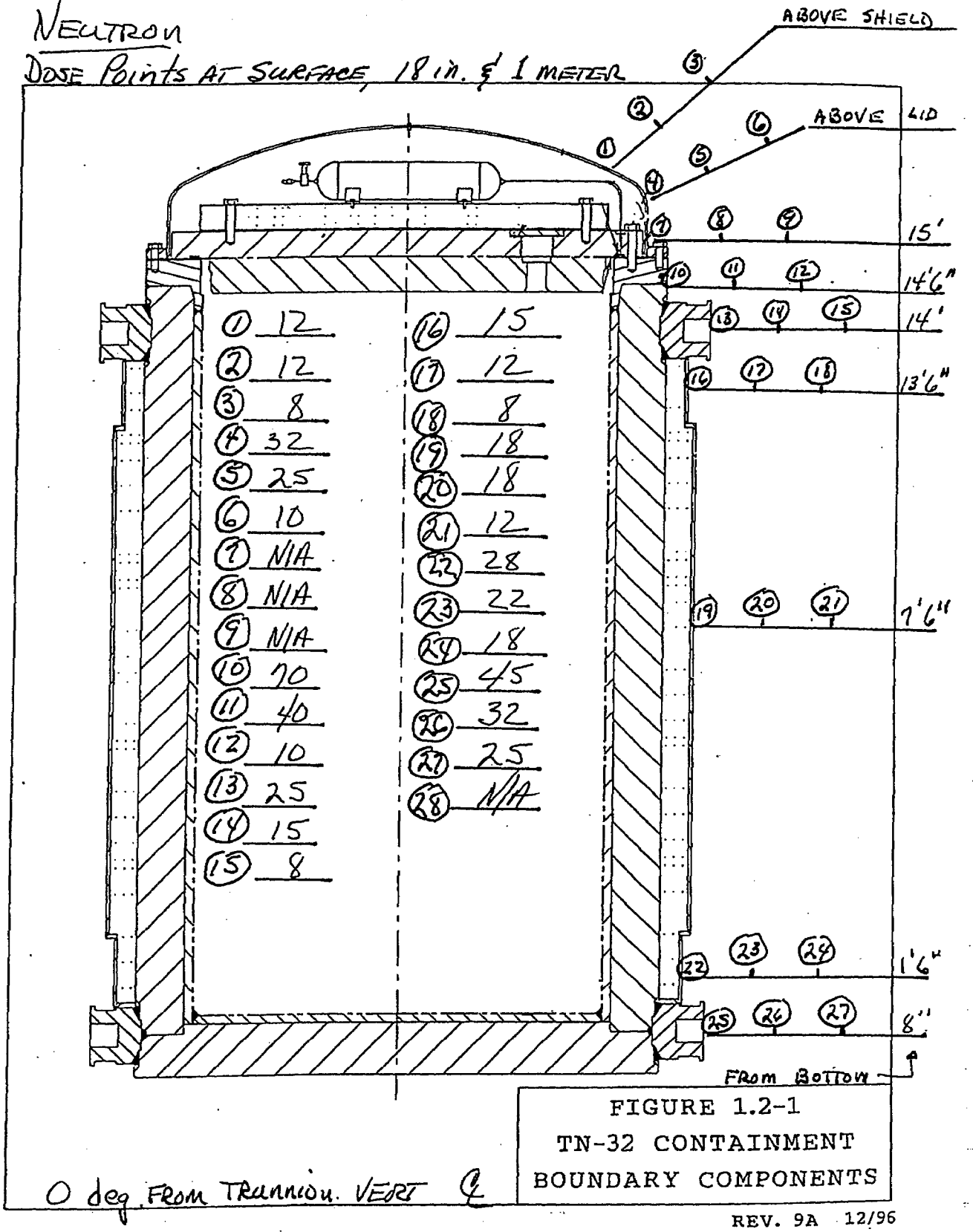

FIGURE 1.2-1
TN-32 CONTAINMENT
BOUNDARY COMPONENTS

REV. 9A 12/96

CASK ID # TN-32-05

DATE 9/30/98

NEUTRON

DOSE POINTS AT SURFACE, 18 in. & 1 METER

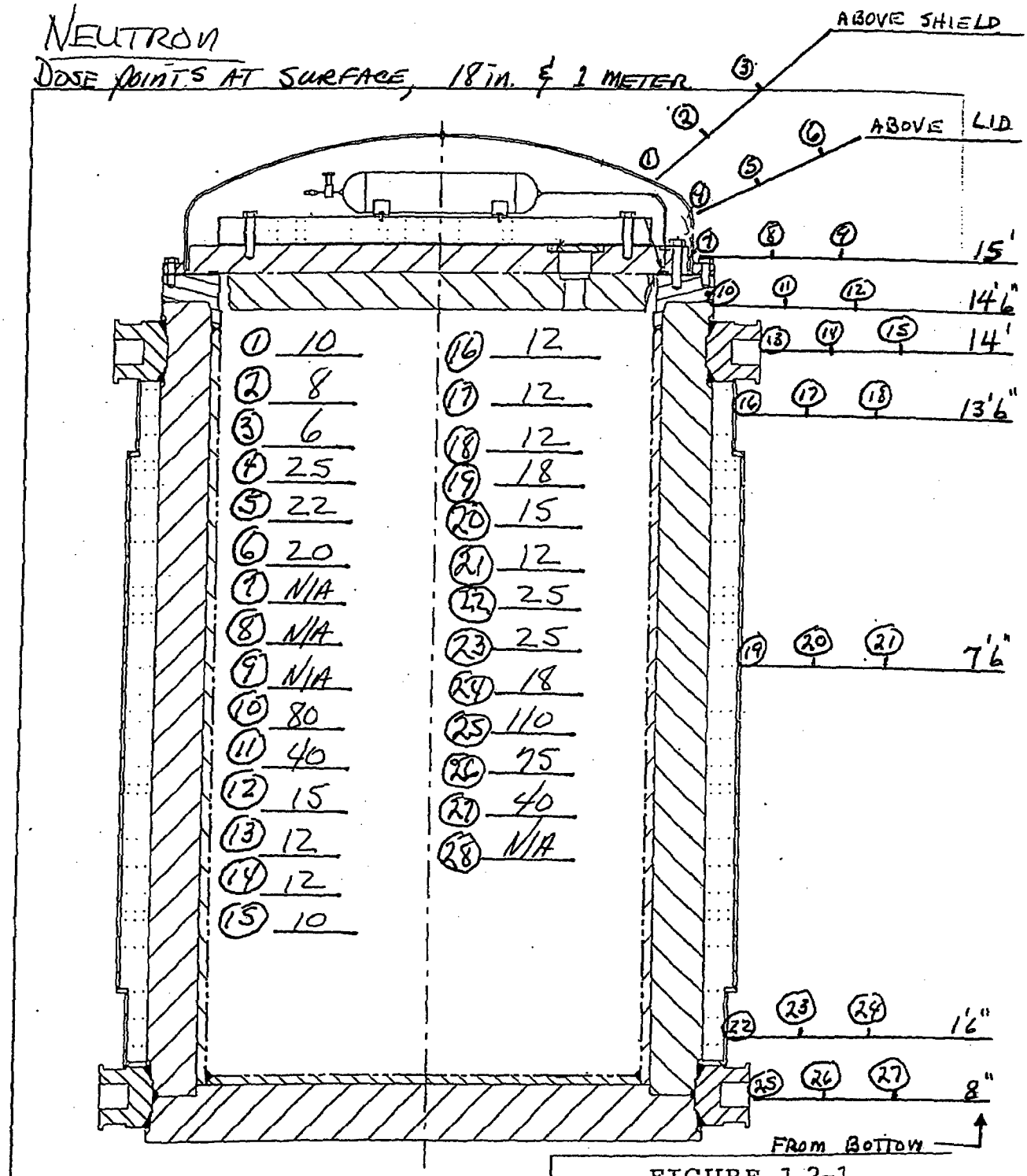

90 deg From Trunnion VERT ℄

FIGURE 1.2-1
TN-32 CONTAINMENT
BOUNDARY COMPONENTS

REV. 9A 12/96

CASK ID # TN-32-05

DATE 9/30/98

BETA, GAMMA

DOSE POINTS AT SURFACE, 18 in. & 1 METER

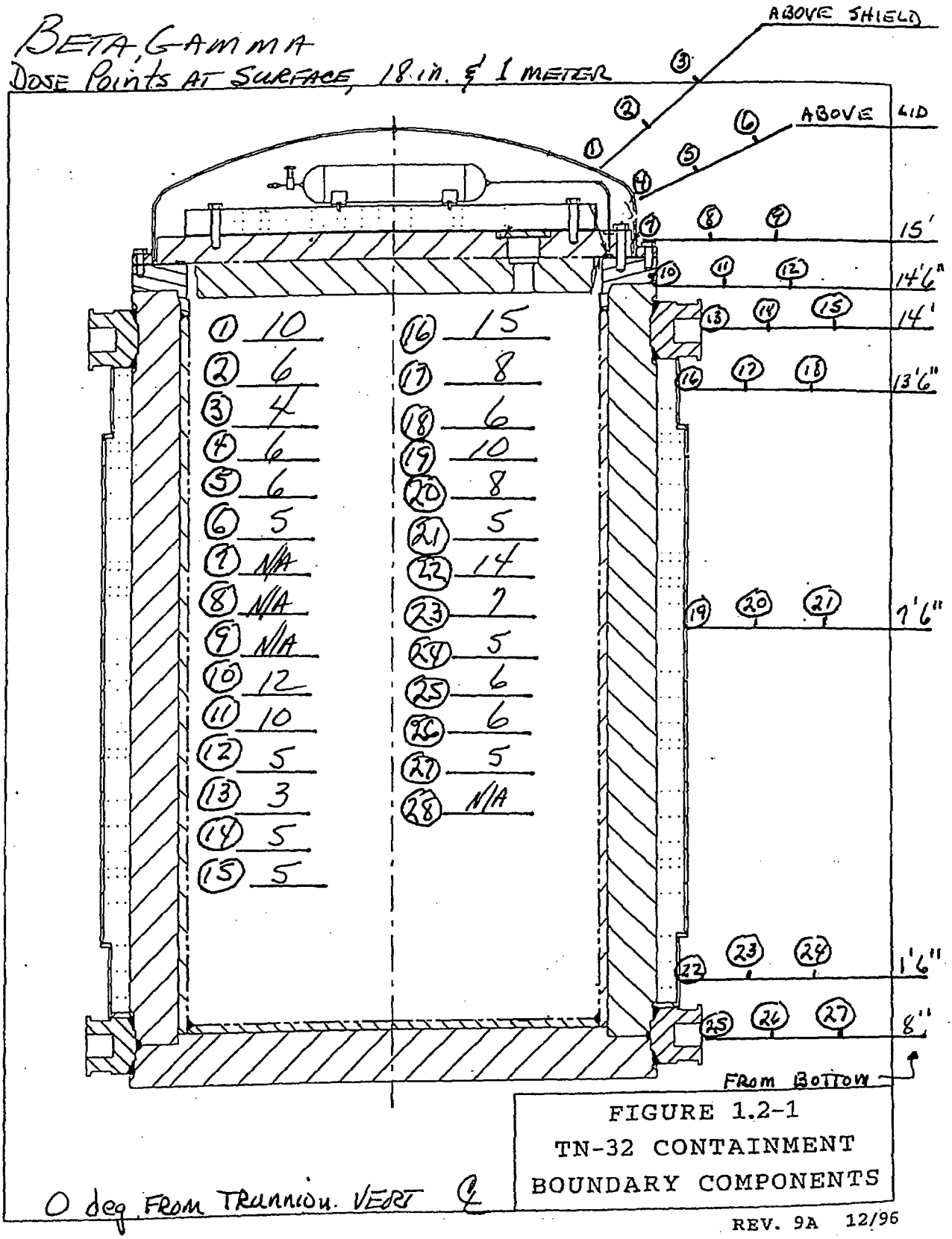

FIGURE 1.2-1
TN-32 CONTAINMENT
BOUNDARY COMPONENTS

REV. 9A 12/96

CASK ID # TN-32-05

DATE 9/30/98

BETA, GAMMA

DOSE POINTS AT SURFACE, 18 in. & 1 METER

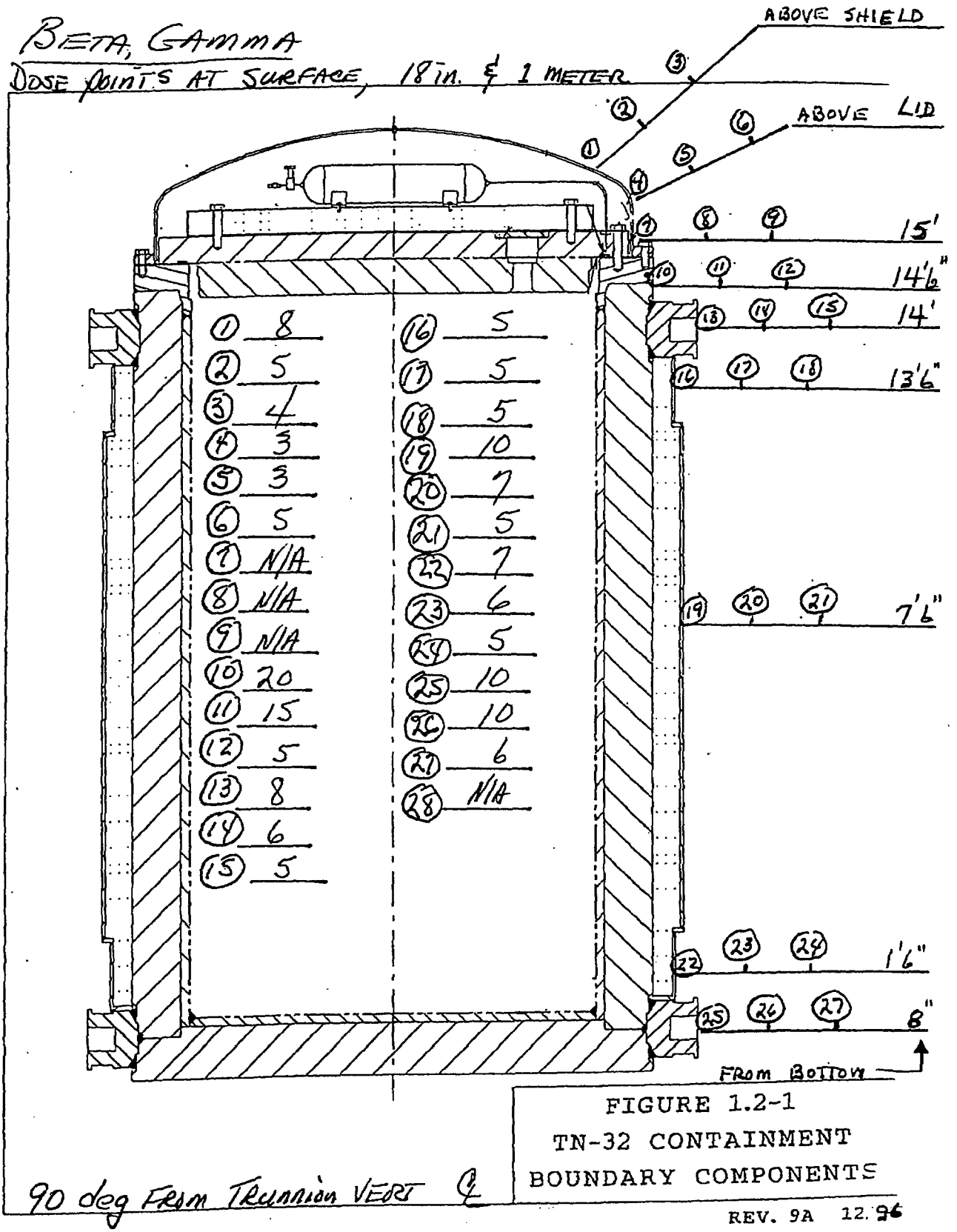

FIGURE 1.2-1
TN-32 CONTAINMENT
BOUNDARY COMPONENTS

REV. 9A 12.96

CASK ID # TN-32-07

DATE 9/30/98

NEUTRON

DOSE POINTS AT SURFACE, 18 in. & 1 METER

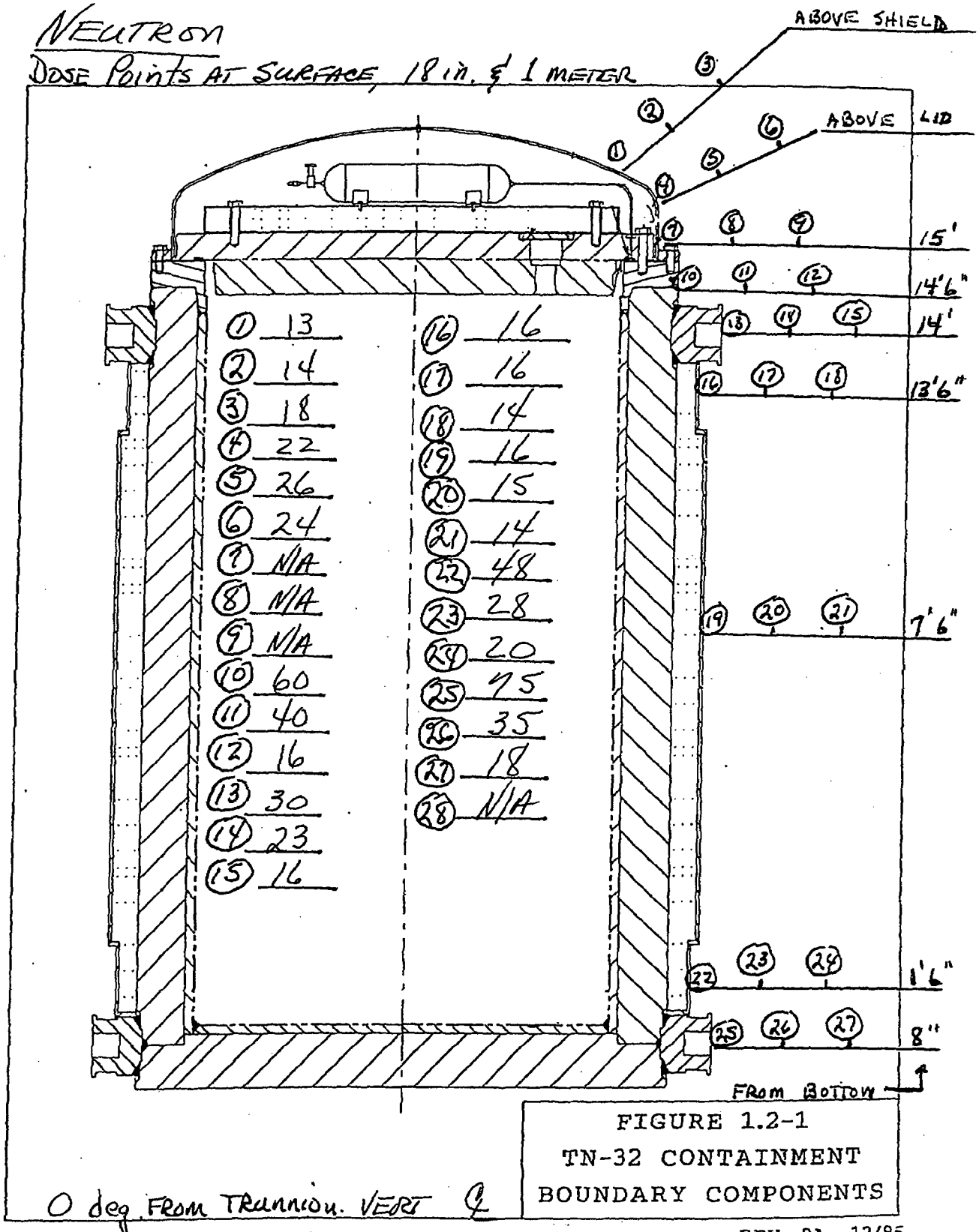

FIGURE 1.2-1
TN-32 CONTAINMENT
BOUNDARY COMPONENTS

REV. 9A 12/96

CASK ID # TN-32-07

DATE 9/30/98

NEUTRON

DOSE POINTS AT SURFACE, 18in. & 1 METER

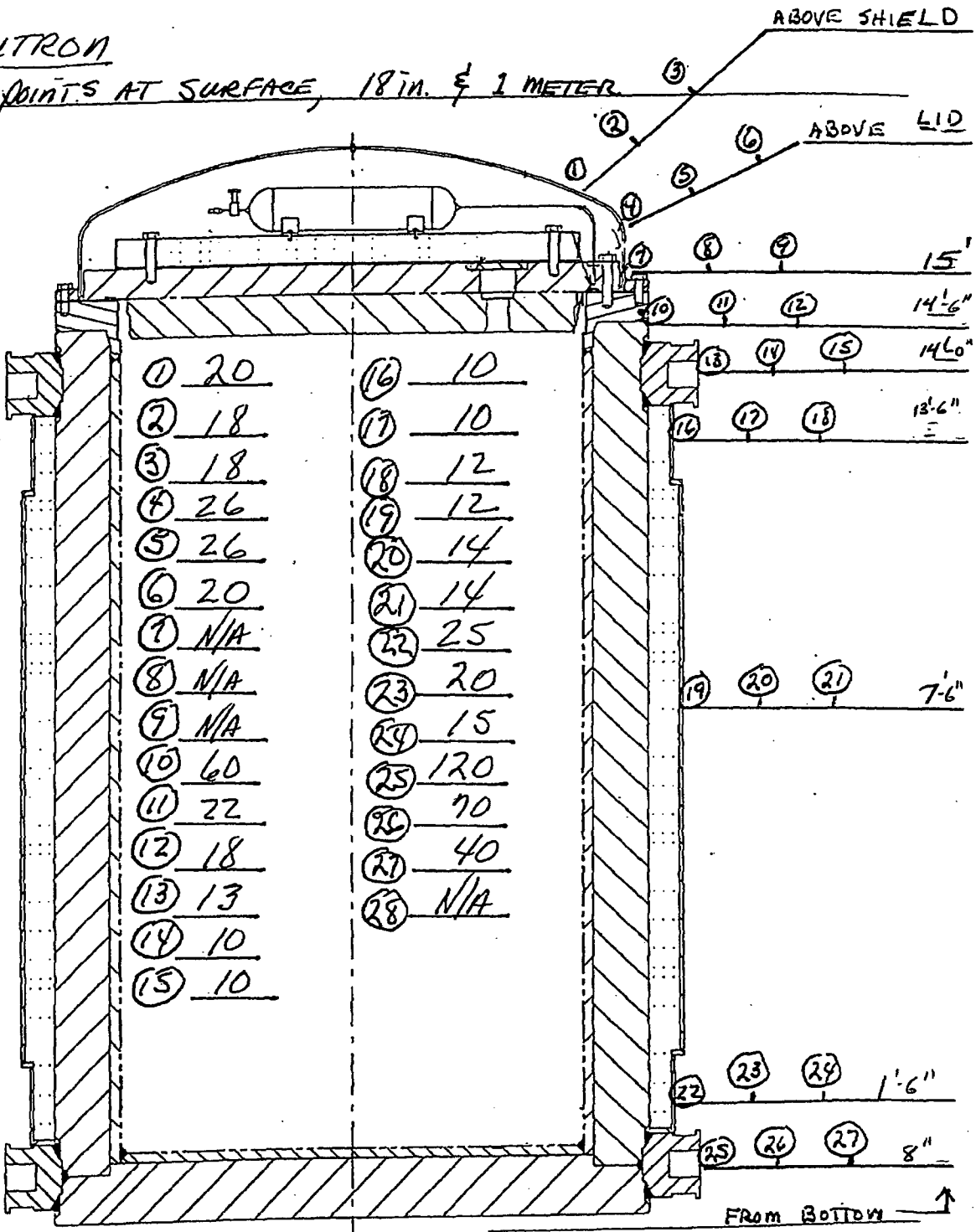

90 deg From Trunnion VERT ℄

FIGURE 1.2-1
TN-32 CONTAINMENT
BOUNDARY COMPONENTS

REV. 9A 12.

CASK ID # TN-32-07

DATE 9/30/98

BETA, GAMMA

DOSE POINTS AT SURFACE, 18 in. & 1 METER

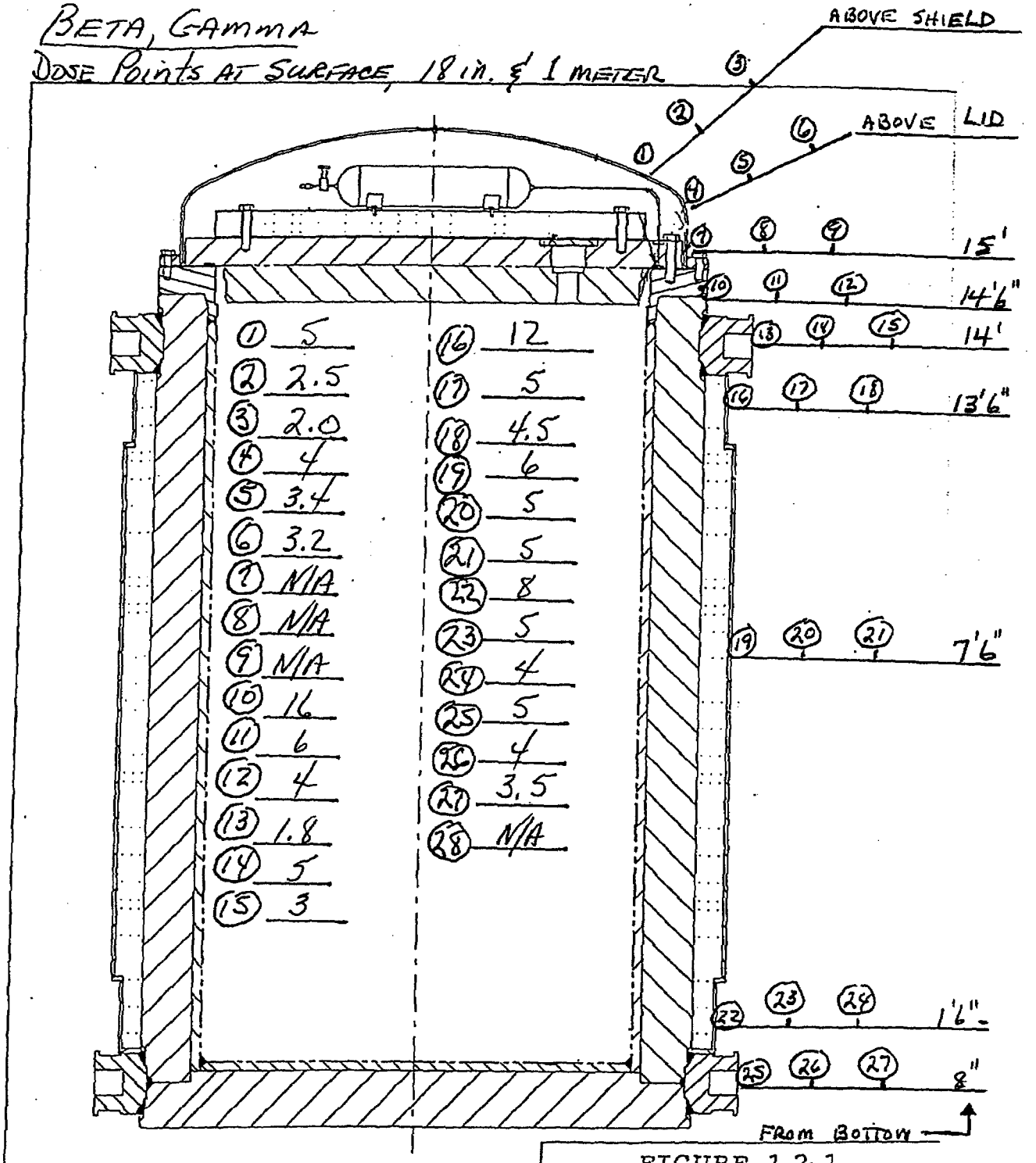

FIGURE 1.2-1
TN-32 CONTAINMENT
BOUNDARY COMPONENTS

REV. 9A 12/98

CASK ID # TN-32-07

DATE 9/30/98

BETA, GAMMA

DOSE POINTS AT SURFACE, 18 IN. & 1 METER

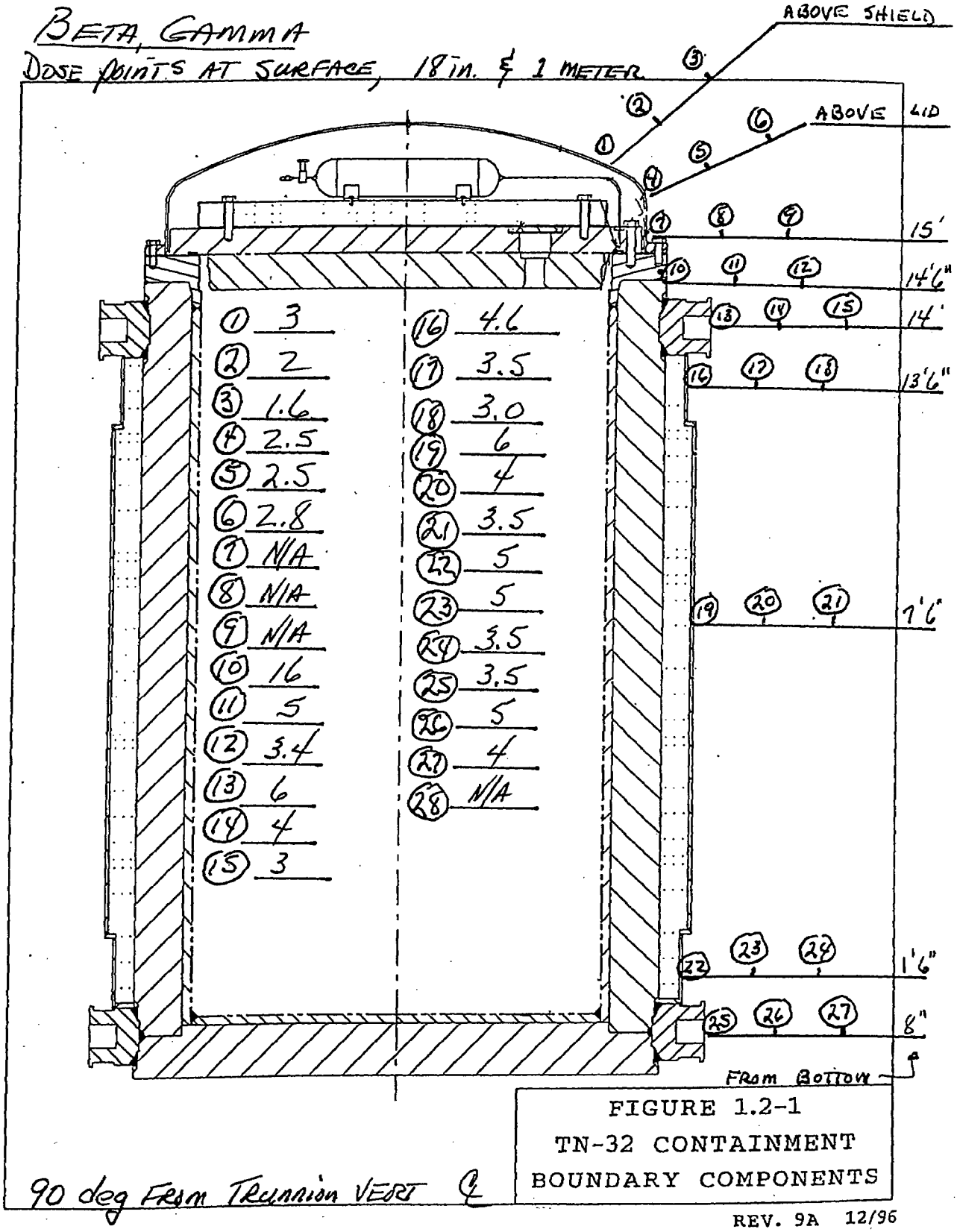

1	3	16	4.6
2	2	17	3.5
3	1.6	18	3.0
4	2.5	19	6
5	2.5	20	4
6	2.8	21	3.5
7	N/A	22	5
8	N/A	23	5
9	N/A	24	3.5
10	16	25	3.5
11	5	26	5
12	3.4	27	4
13	6	28	N/A
14	4		
15	3		

FIGURE 1.2-1
TN-32 CONTAINMENT
BOUNDARY COMPONENTS

REV. 9A 12/96

Enclosure 9 to TN-E-30577

ISFSI FUEL CERTIFICATION, REV. 0
TN-32, NO. 07

Technical Specifications Limits

Initial Enrichment	≤ 3.85 w/o U235
Burnup	≤ 40,000 MWD/MTU
Decay Heat/Fuel Assembly	≤ 847 Watts
Time Since Discharge	≥ 2,555 Days
Intact, Unconsolidated Surry Fuel Only	

Other Parameters

Fuel Rod Internal Pressure After 2,555 Days	≤ 126.3 Bar
Gamma Source/Cask	≤ 2.31E+17 Photons/Sec
Neutron Source/Cask	≤ 4.84E+09 Neutrons/Sec

F/A ID	Insert Component ID	Initial Enrichment (w/o)	Burnup MWD/MTU	Heat At 3/1/98 (Watts)	Days From Discharge To 3/1/98	Fuel Rod Pressure (Bar)	Gamma Source (P/Sec)	Neutron Source (N/Sec)
4C0	N/A	3.40	37,198	667	2,703	85.7	2.96E+15	1.30E+08
2C4	N/A	3.40	38,384	729	2,703	92.7	3.32E+15	1.55E+08
2E2	N/A	3.60	36,536	793	2,703	94.0	3.69E+15	1.69E+08
5E4	N/A	3.60	39,964	793	2,703	94.0	3.69E+15	1.69E+08
0P1	N/A	3.61	32,646	525	4,729	85.0	2.36E+15	5.96E+07
4P4	N/A	3.61	32,267	525	4,729	85.0	2.36E+15	5.96E+07
5P2	N/A	3.61	30,280	480	4,729	85.0	2.18E+15	4.18E+07
5P4	N/A	3.61	32,824	525	4,729	85.0	2.36E+15	5.96E+07
5P5	N/A	3.61	30,119	480	4,729	85.0	2.18E+15	4.18E+07
6P5	N/A	3.61	32,658	525	4,729	85.0	2.36E+15	5.96E+07
6P7	N/A	3.61	35,702	580	4,729	85.0	2.57E+15	8.67E+07
0P8	N/A	3.61	36,410	669	3,459	83.4	3.01E+15	1.22E+08
1P2	N/A	3.61	36,677	669	3,459	83.4	3.01E+15	1.22E+08
1P8	N/A	3.61	37,426	669	3,459	83.4	3.01E+15	1.22E+08
2P0	N/A	3.61	39,431	708	3,459	83.4	3.15E+15	1.48E+08
2P1	N/A	3.61	38,908	708	3,459	83.4	3.15E+15	1.48E+08
2P2	N/A	3.61	36,478	669	3,459	83.4	3.01E+15	1.22E+08
2P4	N/A	3.61	38,731	708	3,459	83.4	3.15E+15	1.48E+08
2P6	N/A	3.61	37,745	669	3,459	83.4	3.01E+15	1.22E+08
3P1	N/A	3.61	38,650	708	3,459	83.4	3.15E+15	1.48E+08
3P4	N/A	3.61	36,716	669	3,459	83.4	3.01E+15	1.22E+08
4P2	N/A	3.61	38,447	708	3,459	83.4	3.15E+15	1.48E+08
4P3	N/A	3.61	37,305	669	3,459	83.4	3.01E+15	1.22E+08
4P6	N/A	3.61	36,868	669	3,459	83.4	3.01E+15	1.22E+08
5P3	N/A	3.61	38,616	708	3,459	83.4	3.15E+15	1.48E+08
5P8	N/A	3.61	38,643	708	3,459	83.4	3.15E+15	1.48E+08
0R8	N/A	3.59	36,837	662	3,459	86.8	3.04E+15	1.12E+08
5R2	N/A	3.59	36,377	662	3,459	86.8	3.04E+15	1.12E+08
5R6	N/A	3.59	36,386	662	3,459	86.8	3.04E+15	1.12E+08
5R9	N/A	3.59	36,583	662	3,459	86.8	3.04E+15	1.12E+08
1R4	N/A	3.59	37,363	660	3,613	89.8	3.01E+15	1.16E+08
0S8	N/A	3.60	32,611	593	3,459	92.2	2.84E+15	6.62E+07
Totals				20,831			9.417E+16	3.67E+09

This is to certify that the Surry Power Station fuel assemblies listed above for the TN-32 storage cask No. 7 do not exceed Technical Specifications and other limits

Tom A Brookens — Prepared — 5-13-98 Date

alblack — Reviewed — 5/13/98 Date

Andrew Kreider — Reviewed — 5/14/98 Date

Brian K. Nahan — Reviewed — 5/14/98 Date

N.P. Wolfhope — Approved — 5/15/98 Date

Enclosure 9 to TN-E-30577

CASK LOADING MAP, REV. 0
TN-32, NO. 07

[redacted] No.	
F/A ID	
Insert ID	
Comment	

EAST

	1 4P4 No Insert	2 5P2 No Insert	3 5P4 No Insert	4 3P4 No Insert	
5 0P1 No Insert	6 0P8 No Insert	7 2C4 No Insert	8 2E2 No Insert	9 1P8 No Insert	10 6P5 No Insert
11 6P7 No Insert	12 4C0 No Insert	13 1P2 No Insert	14 2P1 No Insert	15 2P0 No Insert	16 5P5 No Insert
17 2P2 No Insert	18 2P4 No Insert	19 4P2 No Insert	20 3P1 No Insert	21 5E4 No Insert	22 0R8 No Insert
23 4P3 No Insert	24 4P6 No Insert	25 5P3 No Insert	26 5P8 No Insert	27 2P6 No Insert	28 5R2 No Insert
	29 5R6 No Insert	30 5R9 No Insert	31 1R4 No Insert	32 0S8 No Insert	

WEST

Tom A Brookins Prepared	5-13-98 Date	_____ Loaded	_____ Date
B W Hahn Reviewed ABB 5/13/98	5/14/98 Date	_____ Checked	_____ Date
N. P. Wolfhope Approved	5/15/98 Date		

Enclosure 9 to TN-E-30577

SURRY POWER STATION

ersion 10/20/94 **RADIOLOGICAL SURVEY MAP AND RECORD** (REV 0)

Location	Date	Time
MAP # 901 ISFSF	9-30-98	1300

PURPOSE: ☐ Routine ■ Non-Routine ☐ RWP, RWP# _____

TYPE: ☐ Gamma ☐ Beta ■ Neutron ☐ Smear, GA ☐ Smear, LA ☐ Smear, HP ☐ Air Sample

REACTOR POWER	
Unit 1	Unit 2
98	100

Instrument Model	Serial #
LUDLUM	44441
LUDLUM	35960

☐ All GA smears < 1000 DPM/100cm² except as noted on map or smear worksheet.
☐ All GA smears < 1000 DPM/100cm²
☐ All LA smears < 1000 DPM/ft²
☐ All HP smears < 1 HP/smear
☐ Air particulate + I_2 < 0.1 DAC
☐ All GA smears in DPM/100cm²
☐ All HP smears in HPs/smear
☐ All Gamma readings in mrem/hr.
■ All Neutron readings in mrem/hr.
☐ All Beta readings in mrad/hr.
☐ _____

Comments:
ALL DOSE RATES ARE NEUTRON ONLY

LUDLUM CAL DUE 01-99

Survey RWP
98-1-0002

Survey Team Dose, mrem
(SRD/DAD or calculated) 3

Submitted By (Printed Name, Signature)
MARK R. DOLL

Reviewed By (Printed Name, Signature)

Date Reviewed 10-1-98

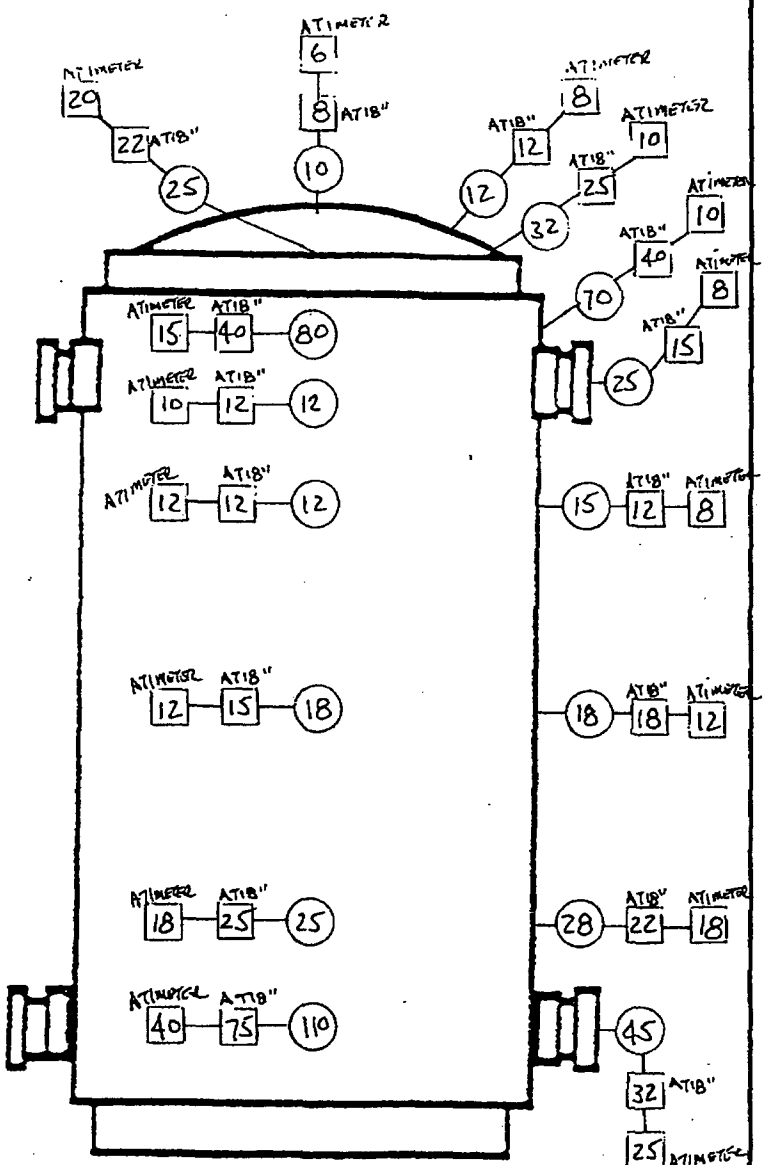

INFORMATION ONLY

CASK ID # TN-32-05

LDWA - Low Dose Waiting Area
LHRA - Locked High Radiation Area
HRA - High Radiation Area
RA - Radiation Area
HPA - Hot Particle Area
CA - Contaminated Area
ARA - Airborne Radioactivity Area
RM - Radioactive Material(s)
CAM - Continuous Air Monitor
(F) - Frisking Station
RCAB - Radiological Control Area Boundary
NDCR - Neutron Dose Calculation Required

☐ Gen. Area; ◯ Contact; △ GA Smear; ◇ LA Smear; △* HP Smear; AS Air Sample Location; LCK Locked Gate; ~~XXXX~~ Barrier

Enclosure 9 to TN-E-30577

OW 24-02-09
ersion 10/20/94

SURRY POWER STATION
RADIOLOGICAL SURVEY MAP AND RECORD

FORM HP-1032.010-1
(REV 0)

Location		Date	Time
MAP # 901	ISFSF	9-30-98	1300

PURPOSE: ☐ Routine ■ Non-Routine ☐ RWP, RWP# _____

TYPE: ■ Gamma ☐ Beta ☐ Neutron ☐ Smear, GA ☐ Smear, LA ☐ Smear, HP ☐ Air Sample

REACTOR POWER	
Unit 1	Unit 2
98	100

Instrument Model	Serial #
RSO-50-E	204
RSO-50-E	206

☐ All GA smears < 1000 DPM/100cm² except as noted on map or smear worksheet.
☐ All GA smears < 1000 DPM/100cm²
☐ All LA smears < 1000 DPM/ft²
☐ All HP smears < 1 HP/smear
☐ Air particulate + I_2 < 0.1 DAC
☐ All GA smears in DPM/100cm²
☐ All HP smears in HPs/smear
■ All Gamma readings in mrem/hr.
☐ All Neutron readings in mrem/hr.
☐ All Beta readings in mrad/hr.
☐ _____

Comments:
ALL DOSE RATES ARE GAMMA ONLY

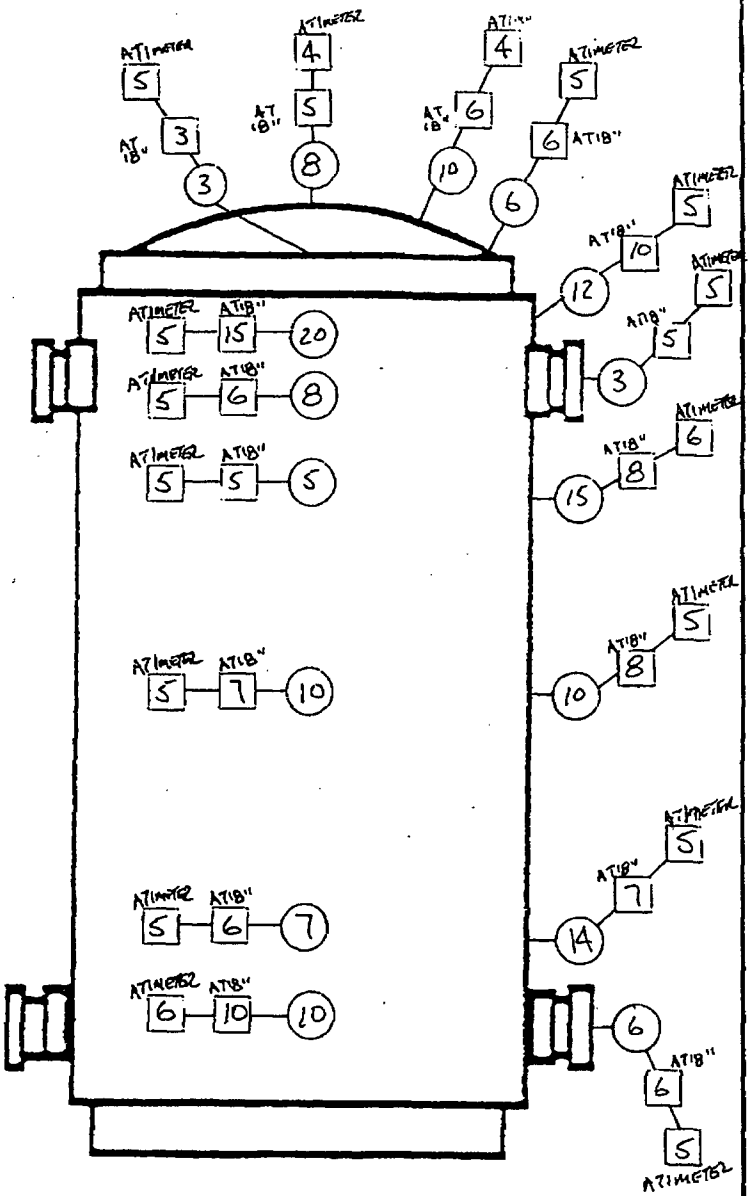

CASK # TN-32-05

Survey RWP
98-1-0002

Survey Team Dose, mrem
(SRD/DAD or calculated) 3

Submitted By (Printed Name, Signature)
MARK R. DOLAN

Reviewed By (Printed Name, Signature)

Date Reviewed 10-1-98

LDWA - Low Dose Waiting Area
LHRA - Locked High Radiation Area
HRA - High Radiation Area
RA - Radiation Area
HPA - Hot Particle Area
CA - Contaminated Area
ARA - Airborne Radioactivity Area
RM - Radioactive Material(s)
CAM - Continuous Air Monitor
(F) - Frisking Station
RCAB - Radiological Control Area Boundary
NDCR - Neutron Dose Calculation Required

☐ Gen. Area; ◯ Contact; △ GA Smear; ◇ LA Smear; △* HP Smear; AS Air Sample Location; LCK Locked Gate; ~~XXXX~~ Barrier

Enclosure 9 to TN-E-30577

SURRY POWER STATION
RADIOLOGICAL SURVEY MAP AND RECORD

HP-1032...
FORM HP-1032.010-1
(REV 0)

... 24-02-09
... 10/20/94

...ation MAP # 901 ISFSF	Date 9-30-98	Time 1300

...POSE: ☐ Routine ■ Non-Routine ☐ RWP, RWP#______

...: ☐ Gamma ☐ Beta ■ Neutron ☐ Smear, GA ☐ Smear, LA ☐ Smear, HP ☐ Air Sample

REACTOR POWER: Unit 1 98 / Unit 2 100

...strument Model	Serial #
Ludlum	44441
Ludlum	35960
~~...250 50E~~	~~204~~
~~...250 50E~~	~~206~~

- ☐ All GA smears < 1000 DPM/100cm^2 except as noted on map or smear worksheet.
- ☐ All GA smears < 1000 DPM/100cm^2
- ☐ All LA smears < 1000 DPM/ft^2
- ☐ All HP smears < 1 HP/smear
- ☐ Air particulate + I_2 < 0.1 DAC
- ☐ All GA smears in DPM/100cm^2
- ☐ All HP smears in HPs/smear
- ☐ All Gamma readings in mrem/hr.
- ■ All Neutron readings in mrem/hr.
- ☐ All Beta readings in mrad/hr.

...ments:
All Dose Rates are
Neutron only.

Ludlum cal Due 01-99

...ey RWP
98-1-0002

...ey Team Dose, mrem
(...D DAD or calculated) 3

...itted By (Printed Name, Signature)
Mark R. Dolan [signature]

...ewed By (Printed Name, Signature)
[signature]

... Reviewed 10-1-98

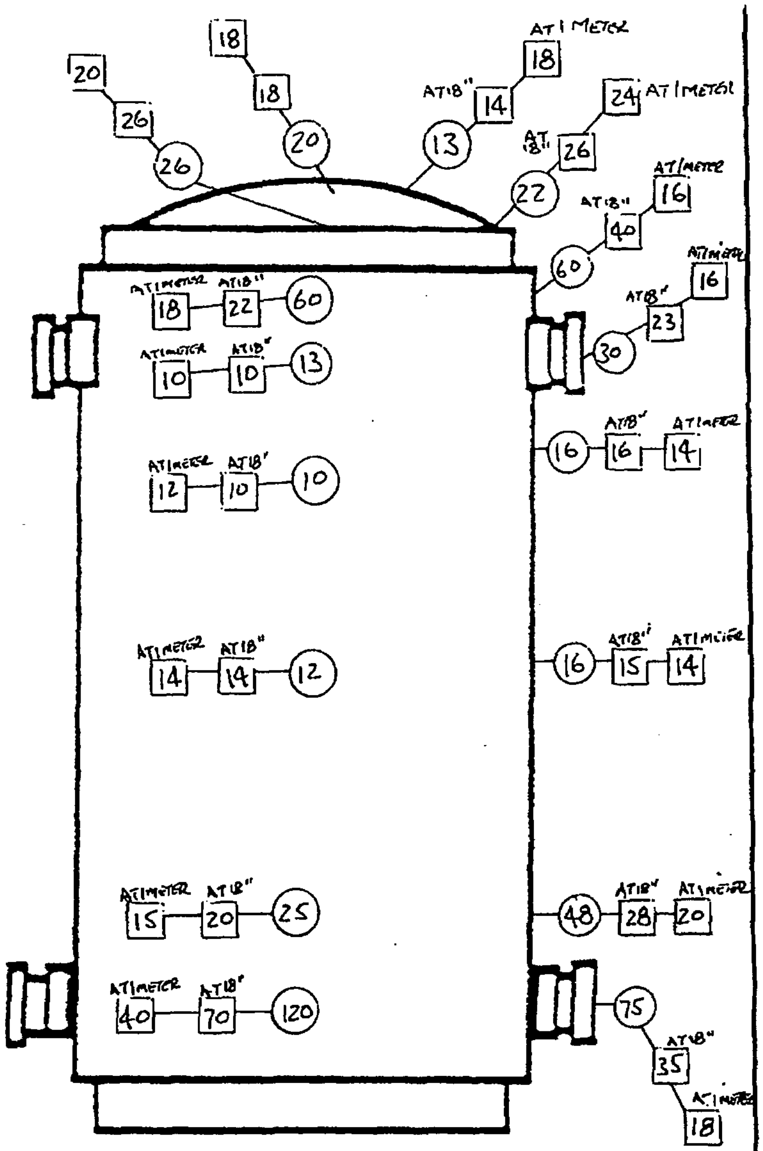

INFORMATION ONLY

CASK ID# TN-32-07

LDWA - Low Dose Waiting Area	HPA - Hot Particle Area	CAM - Continuous Air Monitor
LHRA - Locked High Radiation Area	CA - Contaminated Area	(F) - Frisking Station
HRA - High Radiation Area	ARA - Airborne Radioactivity Area	RCAB - Radiological Control Area Boundary
RA - Radiation Area	RM - Radioactive Material(s)	NDCR - Neutron Dose Calculation Required

... Gen. Area; ○ Contact; △ GA Smear; ◇ LA Smear; △* HP Smear; AS Air Sample Location; LCK Locked Gate; ~~XXXX~~ Barrier

...tion		Date	Time
MAP # 901	ISFSI	9-30-98	1300

...POSE: ☐ Routine ■ Non-Routine ☐ RWP, RW...

...PE: ■ Gamma ☐ Beta ☐ Neutron ☐ Smear, GA ☐ Smear, LA ☐ Smear, HP ☐ Air Sample

REACTOR POWER	
Unit 1	Unit 2
98	100

...nstrument Model	Serial #
RSO-50-E	204
RSO-50-E	206

All GA smears < 1000 DPM/100cm² except as noted on map or smear worksheet.
All GA smears < 1000 DPM/100cm²
All LA smears < 1000 DPM/ft²
All HP smears < 1 HP/smear
Air particulate + I_2 < 0.1 DAC
All GA smears in DPM/100cm²
All HP smears in HPs/smear
All Gamma readings in mrem/hr.
All Neutron readings in mrem/hr.
All Beta readings in mrad/hr.

...mments: All DOSE RATES ARE GAMMA ONLY

...rvey RWP 98-1-0002

...rvey Team Dose, mrem (...RD/DAD or calculated) 3

...bmitted By (Printed Name, Signature) [signature]

...viewed By (Printed Name, Signature) [signature]

...te Reviewed 10-1-98

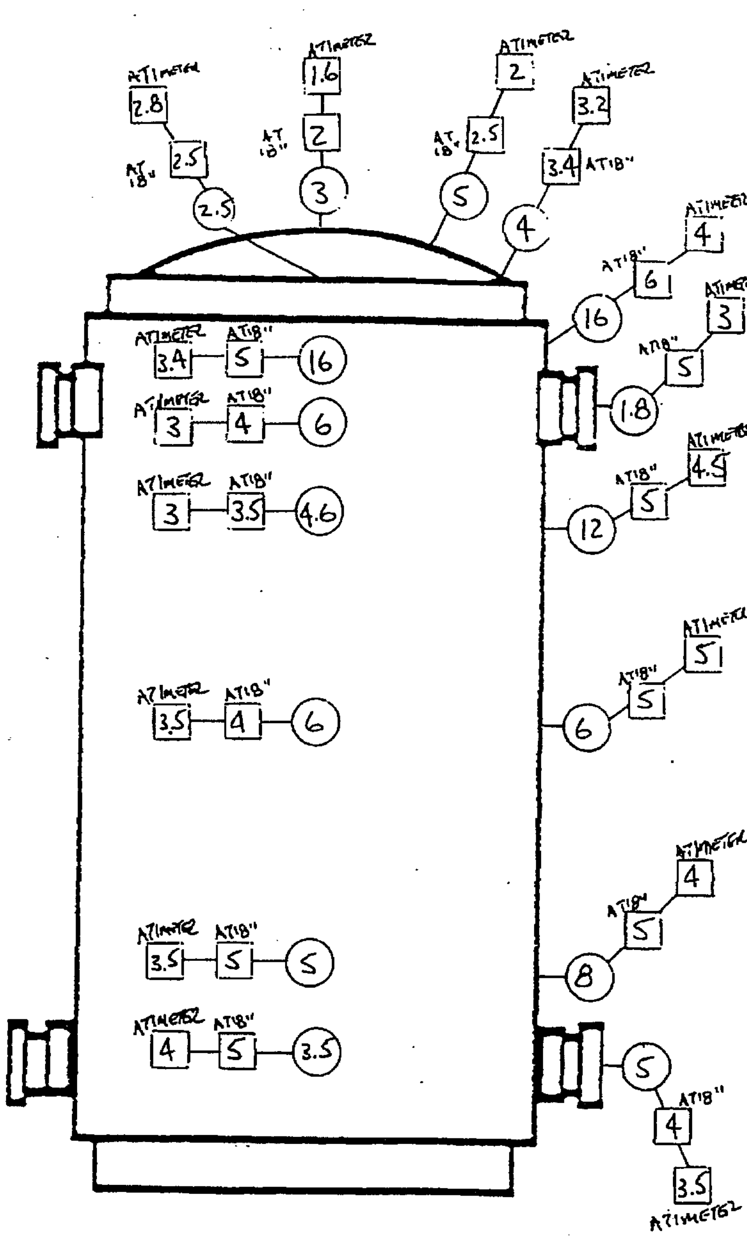

INFORMATION ONLY

CASK # TN-32-07

LDWA - Low Dose Waiting Area
LHRA - Locked High Radiation Area
HRA - High Radiation Area
RA - Radiation Area
HPA - Hot Particle Area
CA - Contaminated Area
ARA - Airborne Radioactivity Area
RM - Radioactive Material(s)
CAM - Continuous Air Monitor
Ⓕ - Frisking Station
RCAB - Radiological Control Area Boundary
NDCR - Neutron Dose Calculation Required

☐ Gen. Area; ○ Contact; △ GA Smear; ◇ LA Smear; △* HP Smear; AS Air Sample Location; LCK Locked Gate; -XXXX- Barrier

ATTACHMENT 2
ISFSI FUEL CERTIFICATIONS AND CASK LOADING MAPS
TN-32.05 AND TN-32.07

ISFSI FUEL CERTIFICATION, REV. 1
TN-32, NO. 05

Technical Specification Limits

Initial Enrichment	≤ 3.85 w/o U235
Burnup	≤ 40,000 MWD/MTU
Decay Heat/Fuel Assembly	≤ 847 Watts
Time Since Discharge	≤ 2,555 Days
Intact, Unconsolidated Surry Fuel Only	

Other Parameters

Fuel Rod Internal Pressure After 2,555 Days	≤ 126.3 Bar
Gamma Source/Cask	≤ 2.31E+17 Photons/Sec
Neutron Source/Cask	≤ 4.84E+09 Neutrons/Sec

F/A ID	Insert Component ID	Initial Enrichment (w/o)	Burnup MWD/MTU	Heat At 12/1/97 (Watts)	Days From Discharge To 12/1/97	Fuel Rod Pressure (Bar)	Gamma Source (P/Sec)	Neutron Source (N/Sec)
0P3	16P181	3.61	35,535	597	4,639	85.0	2.65E+15	9.44E+07
0P4	20P97	3.61	35,989	597	4,639	85.0	2.65E+15	9.44E+07
1P3	20P29	3.61	36,351	597	4,639	85.0	2.65E+15	9.44E+07
2P5	12P89	3.61	35,955	597	4,639	85.0	2.65E+15	9.44E+07
2P9	16P158	3.61	36,208	597	4,639	85.0	2.65E+15	9.44E+07
3P3	4P51	3.61	37,978	644	4,076	86.3	2.87E+15	1.17E+08
3P9	16P245	3.61	35,465	597	4,639	85.0	2.65E+15	9.44E+07
4P7	8P130	3.61	37,548	644	4,076	86.3	2.87E+15	1.17E+08
5P8	8P108	3.61	36,908	644	4,076	86.3	2.87E+15	1.17E+08
6P0	16PA40	3.61	36,381	597	4,639	85.0	2.65E+15	9.44E+07
6P1	20P121	3.61	37,655	644	4,076	86.3	2.87E+15	1.17E+08
0S3	BP002	3.60	36,039	679	3,369	92.2	3.22E+15	1.05E+08
0S5	16P174	3.60	35,257	679	3,369	92.2	3.22E+15	1.05E+08
0S7	16P89	3.60	35,113	679	3,369	92.2	3.22E+15	1.05E+08
1S1	16P177	3.60	35,680	679	3,369	92.2	3.22E+15	1.05E+08
1S6	16P180	3.60	35,702	679	3,369	92.2	3.22E+15	1.05E+08
1S7	4P40	3.60	36,115	679	3,369	92.2	3.22E+15	1.05E+08
1S8	BP041	3.60	35,419	679	3,369	92.2	3.22E+15	1.05E+08
2S0	16P198	3.60	35,390	679	3,369	92.2	3.22E+15	1.05E+08
2S3	BP017	3.60	36,098	679	3,369	92.2	3.22E+15	1.05E+08
2S4	16P172	3.60	35,675	679	3,369	92.2	3.22E+15	1.05E+08
2S5	BP038	3.60	35,514	679	3,369	92.2	3.22E+15	1.05E+08
2S6	BP014	3.60	35,098	679	3,369	92.2	3.22E+15	1.05E+08
2S7	16P244	3.60	35,902	679	3,369	92.2	3.22E+15	1.05E+08
3S0	17PA08	3.60	35,270	679	3,369	92.2	3.22E+15	1.05E+08
3S3	BP033	3.60	35,804	679	3,369	92.2	3.22E+15	1.05E+08
3S8	4P52	3.60	35,754	679	3,369	92.2	3.22E+15	1.05E+08
3S9	BP044	3.60	35,745	679	3,369	92.2	3.22E+15	1.05E+08
4S1	BP015	3.60	35,780	679	3,369	92.2	3.22E+15	1.05E+08
4S3	BP060	3.60	36,006	679	3,369	92.2	3.22E+15	1.05E+08
4S8	12P261	3.60	35,776	679	3,369	92.2	3.22E+15	1.05E+08
5S0	16P242	3.60	36,096	679	3,369	92.2	3.22E+15	1.05E+08
Totals				21,014			9.77E+16	3.33E+09

This is to certify that the Surry Power Station fuel assemblies listed above for the TN-32 storage cask No. 5 do not exceed Technical Specification and other limits

JMM 12/10/97 BH Barker 12/10/97
Prepared Date

Reviewed Date 12/10/97

Reviewed 12/10/97 Date

Reviewed 12/10/97 Date

Approved Kenny J. Bashore 12-10-97 Date

CASK LOADING MAP, REV. 0
TN-32, NO. 05

Cell No.
F/A ID
Insert ID
Comment

EAST

	1 0P3 16P181	2 0P4 20P97	3 1P3 20P29	4 2P5 12P69	
5 2P9 16P158	6 3P3 4P51	7 3P9 16P245	8 4P7 8P130	9 5P6 8P108	10 6P0 16PA40
11 6P1 20P121	12 0S3 BP002	13 0S5 16P174	14 0S7 16P89	15 1S1 16P177	16 1S6 16P180
17 1S7 4P40	18 1S8 BP041	19 2S0 16P198	20 2S3 BP017 Debris/No EV	21 2S4 16P172	22 2S5 BP038
23 2S6 BP014	24 2S7 16P244	25 3S0 17PA08	26 3S3 BP033	27 3S8 4P52	28 3S9 BP044
	29 4S1 BP015	30 4S3 BP060	31 4S8 12P261	32 5S0 16P242	

WEST

Prepared	Date	Loaded	Date
Reviewed	Date	Checked	Date
Approved	Date		

Enclosure 10 to TN E-30577

Presentation made to the ASTM C26 committee in 2008
(associated with RAIs 5-1 and 8-1)

Enclosure 10 to
TN E-30577

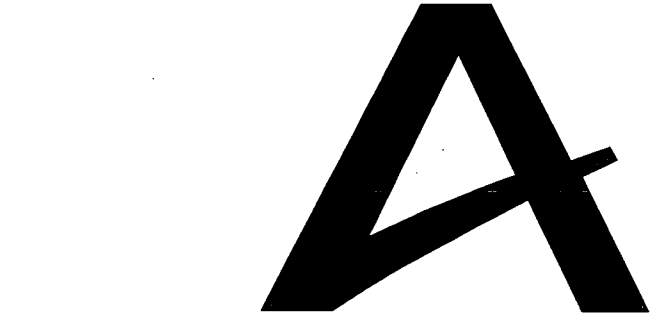

AREVA

AREVA

Enclosure 10 to
TN E-30577

Ageing Tests of Neutron Shielding Materials for Transport Storage Casks

Hervé ISSARD

AREVA TN International

C26 Second Seminar on Accelerated Testing of Materials in Spent Nuclear Fuel and High Level Waste Storage Systems

Tampa, Florida January 31 – February 1, 2008

AREVA

Enclosure 10 to
TN E-30577

Summary

- *Background*
- *Neutron shielding materials for transport storage casks*
- *Long term behaviour of Neutron shielding materials*
- *Ageing tests of neutron shielding materials*
- *Conclusion*

Neutron Shielding Materials for Transport Storage Casks

Enclosure 10 to
TN E-30577

- ***Background:***
- ***Transport and Storage casks are needed for Spent fuel, Mox fuel, vitrified wastes, taking into account increased burn ups***
- ***Casks designs have to withstand the severe temperature conditions coming from conservative ambient assumptions and from envelop values of the residual heat of the spent fuels.***
- ***AREVA-TN international research and development has consequently developed and characterized neutron shielding materials showing high shielding capabilities for a range of temperature corresponding to the needs.***

Neutron shielding material for transport storage casks

Enclosure 10 to
TN E-30577

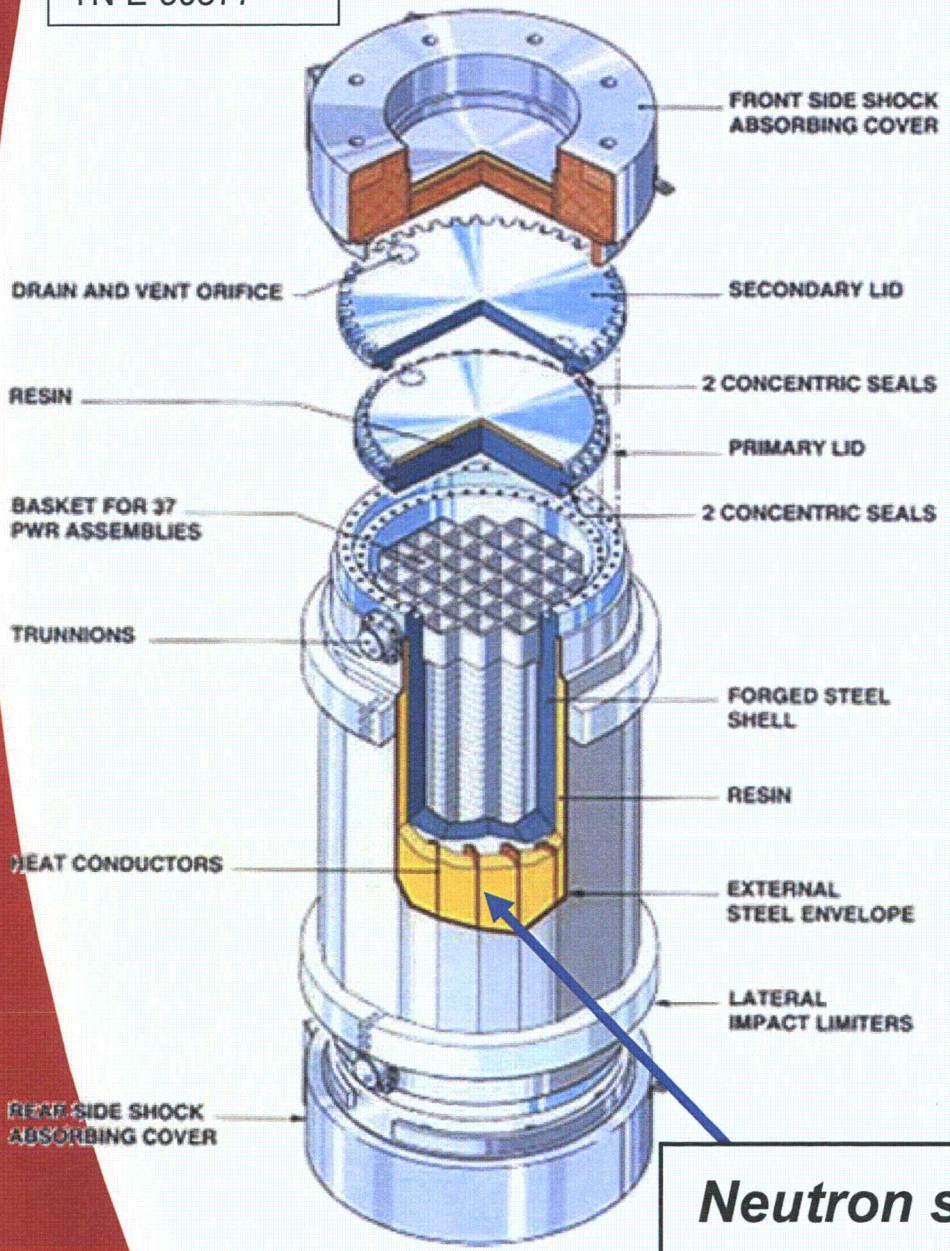

Locations	*Cask cover* *Main section of cask*
Function	*Radioprotection* *Sub-criticality*

Neutron shielding material for transport storage casks

Enclosure 10 to
TN E-30577

- **Shielding material made of polyester resin used in United States:**
  - **TN40 or TN68 metal casks**
  - **NUHOMS ® transfer casks**

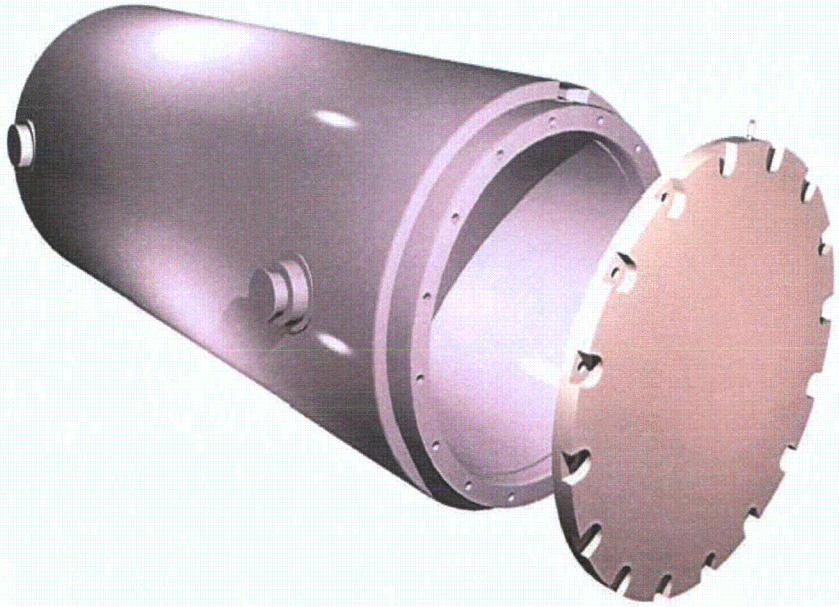

Nuhoms® OP197 transfer cask

AREVA

Enclosure 10 to
TN E-30577

Neutron shielding material for transport storage casks

▶ Specification of neutron shielding materials :

- ◇ Shielding/attenuation efficiency, in case of transport compliance with IAEA safety standards TS-R-1.
- ◇ Radiation and heat resistance during the period considered for the casks : storage or transport.
- ◇ Quality and homogeneity of the shielding material.
- ◇ Fire resistance, with self extinction property.
- ◇ Thermal characteristics - expansion coefficient, conductivity .
- ◇ Environment: minimize the impact on the environment and human health.

Neutron shielding material for transport storage casks

Formulation of neutron shielding materials by TN International:

- Thermosetting matrix (polyester or vinylester), advantages: hydrogen content, infusible, water resistant and temperature resistant. The cross linking of the polymer leads to a rigid 3 dimensional lattice, solid and resisting to transport or storage conditions
- Mineral fillers : Alumine hydroxyde ($Al(OH)_3$) and zinc borate. Advantages: economical, contain hydrogen, Boron (neutron capture) and good for fire resistance
- Vyal- B material has been patented by TN International:
  - WO 03/050822 (19-06-2003)
  - US 7,160,486 (09-01-2007)

Long term behaviour of Neutron shielding materials

Long term behaviour of Vyal-B neutron shielding material:

- The shielding capacity depends on the variations of the atomic concentrations of Hydrogen and Boron in the resin
- Initial atomic concentrations:
  - $[H] \geq 5.10^{22} atoms/cm^3$
  - $[B] \geq 9.10^{20} atoms/cm^3$
- Study was carried out to justify the long term behaviour of resin Vyal-B and the shielding capacity after 40 years of storage
- Modification of atomic concentrations may occur due to
  - Radiation effects
  - Thermal effects

Long term behaviour of Neutron shielding materials

Radiation degradation of neutron shielding materials

- Evaluated for use in nuclear reactors (CERN data)
- Mechanisms depends on type of polymer : break of the main chain, cross linking, production of unsaturated bonds and oxidization
- Degradation starts at more than 10^{15} n/cm^2 as fast neutron fluence, corresponding to a dose of 10^6 Gy
- Curve for unsaturated polyester: S ultimate flexural strength , D deflexion at break, M modulus of elasticity

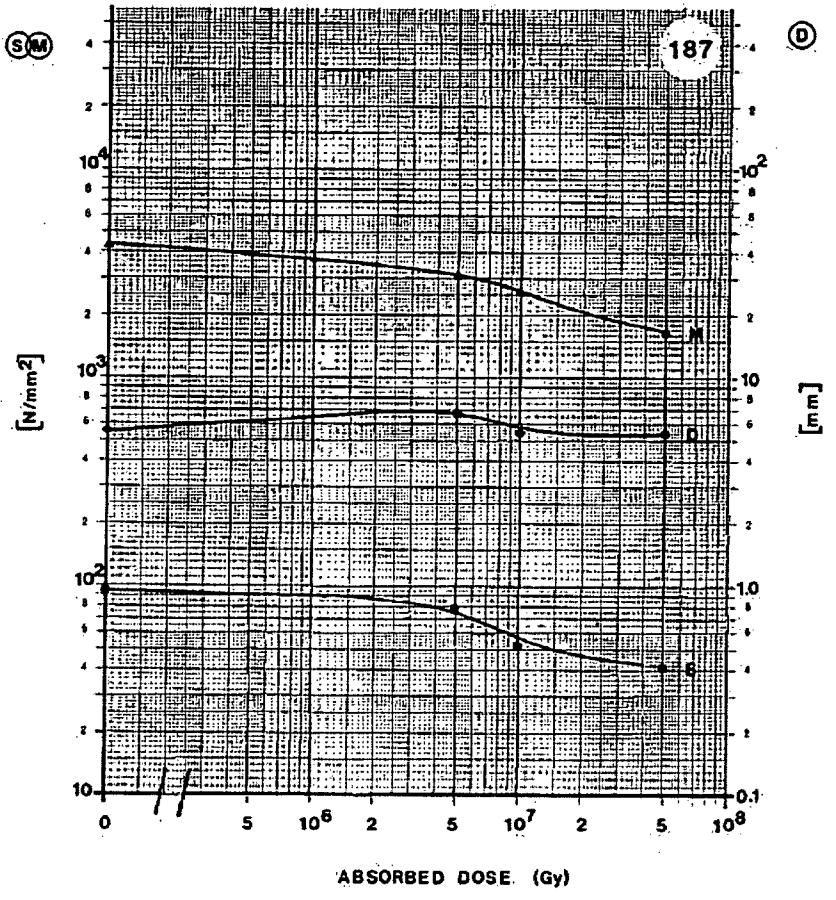

Long term behaviour of Neutron shielding materials

- **Radiation degradation of Vyal-B neutron shielding material**
  - **Fluence level for neutron shielding of packages is 10^{11} n/cm^2 for 40 years of continuous use = dose : 10^3 Gy**
  - **Radiation degradation of neutron shielding of interim storage packages is negligible**
- **Depletion of Boron 10 in the resin Vyal-B ?**
  - **Total neutron capture is less than 10^{13} atoms/cm^3**
  - **Initial Boron 10 content of resin : approx 10^{20} atoms/cm^3**
  - **Conclusion: no depletion**

Ageing Tests of Neutron Shielding Materials for Transport Storage Casks

- Thermal degradation of neutron shielding materials
- For Vyal-B qualification for storage conditions, experiments were carried out, with the following test specification :
  - Ageing tests in oven at different temperatures 150, 160 and 170°C
  - Total test duration for each test: 7 months
  - Specimen with different geometry S/V: blocks and pellets
  - Weight loss measurements
  - Chemical analysis of H and B
- Purpose of these accelerated tests:
  - To check the evolution of shielding performance

Ageing Tests of Neutron Shielding Materials for Transport Storage Casks

▶Long term behaviour at different temperatures

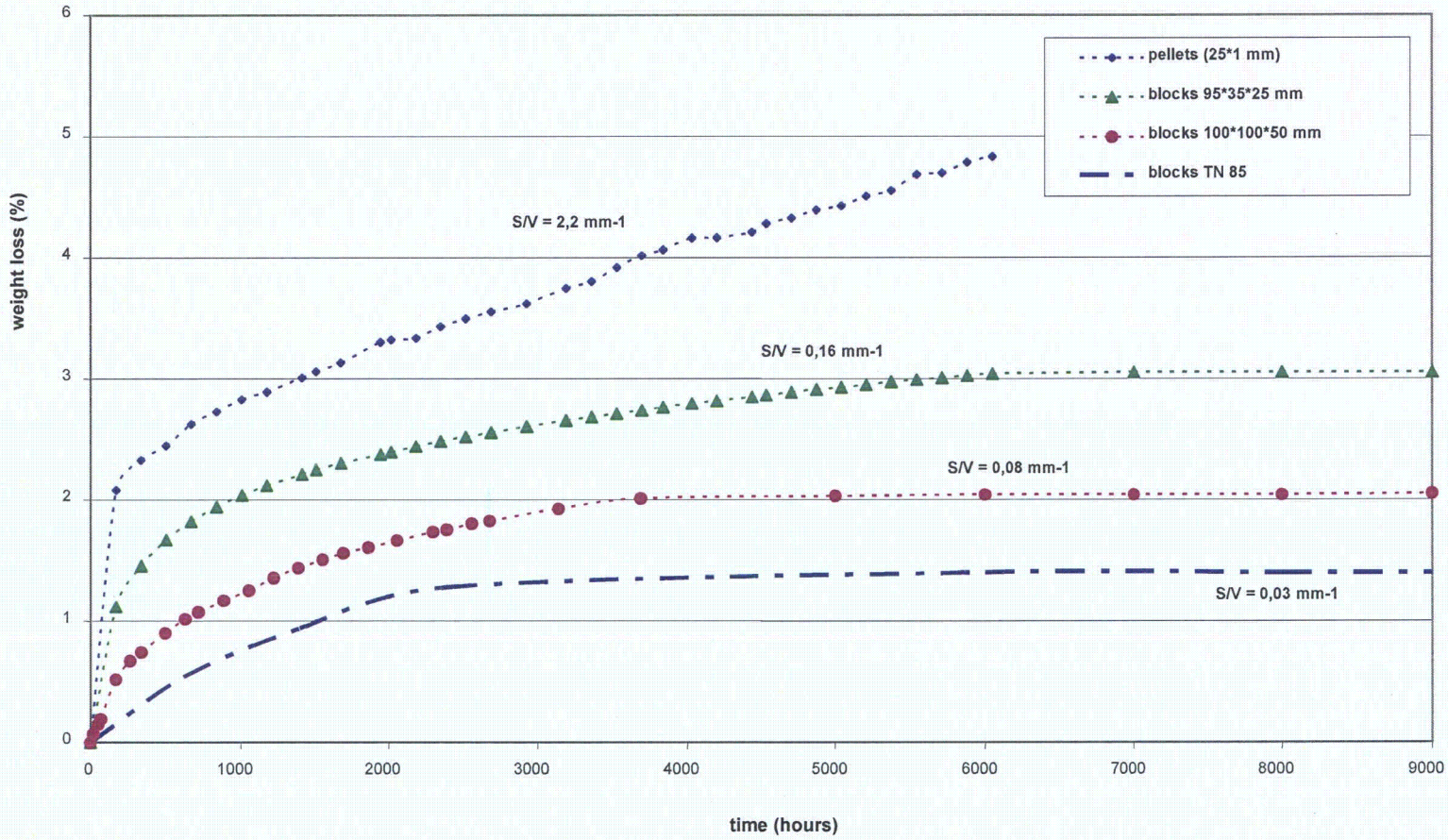

Results: Weight loss trends for different Vyal B samples exposed at 160°C

Minimum loss when S/V is small (= general cask designs)

Diffusion limited phenomenon

Enclosure 10 to
TN E-30577

Ageing Tests of Neutron Shielding Materials for Transport Storage Casks

▶ Degradation Mechanism

- ◇ Mainly oxidation of polymer matrix, but for high temperatures, Aluminium hydroxide may release water, mechanism become complex above 170°C
- ◇ Boron content unchanged
- ◇ Under a specific temperature, oxidation occurs only on specimen surface, above this temperature, we observe cracks which can propagate and oxidation can penetrate in the specimen. This temperature shall be considered when selecting the maximum continuous operating temperature in storage
- ◇ Remark : In cask designs the neutron shielding material is in a closed box, no oxygen ingress; tests are therefore very conservative

Ageing Tests of Neutron Shielding Materials for Transport Storage Casks

After testing at different temperatures, for 7 months the observations and measurements show that the degradation of resin Vyal-B is superficial : no evolution was observed inside the « block » samples

- From micrographic observations made by TN International on aged specimen at T<160°C, volume of oxidized resin correspond to a layer of maximum 0.5 mm
- We estimate the oxidized layer to less than 5 mm for the whole storage period

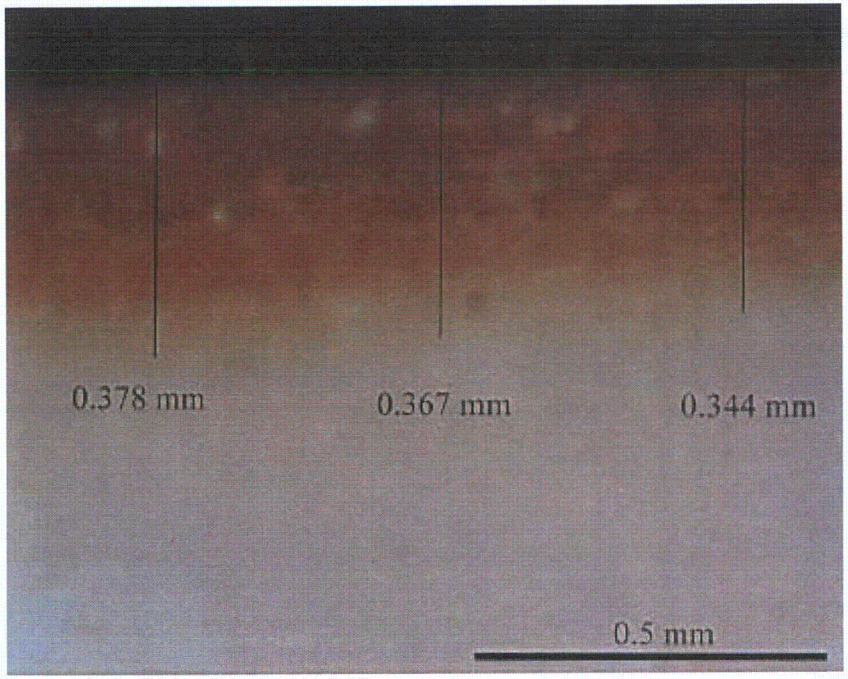

Thickness of oxidized layer

Ageing Tests of Neutron Shielding Materials for Transport Storage Casks

- **After accelerated tests 160°C, infrared analysis (red) of thin samples compared to initial analysis (blue) : modification**

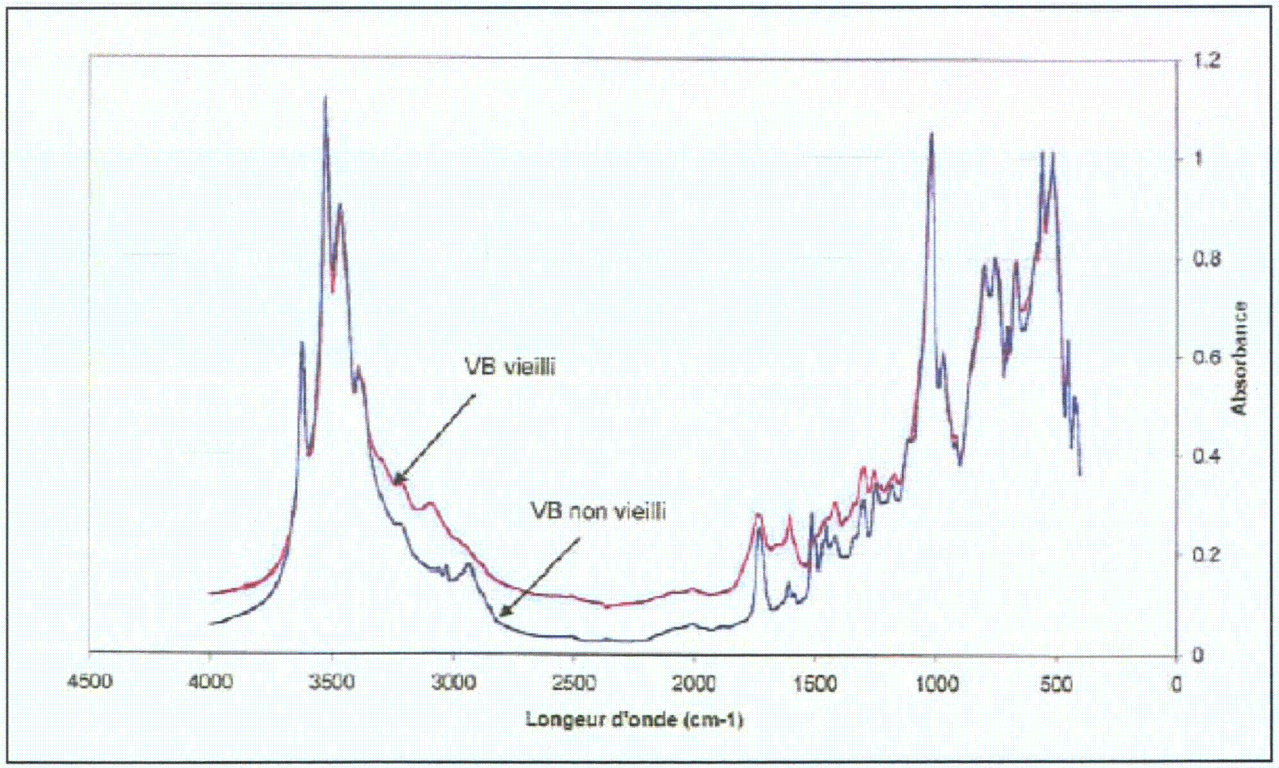

Ageing Tests of Neutron Shielding Materials for Transport Storage Casks

- **After accelerated tests 160°C, infrared analysis (red) of block samples compared to initial analysis (blue) : no modification**

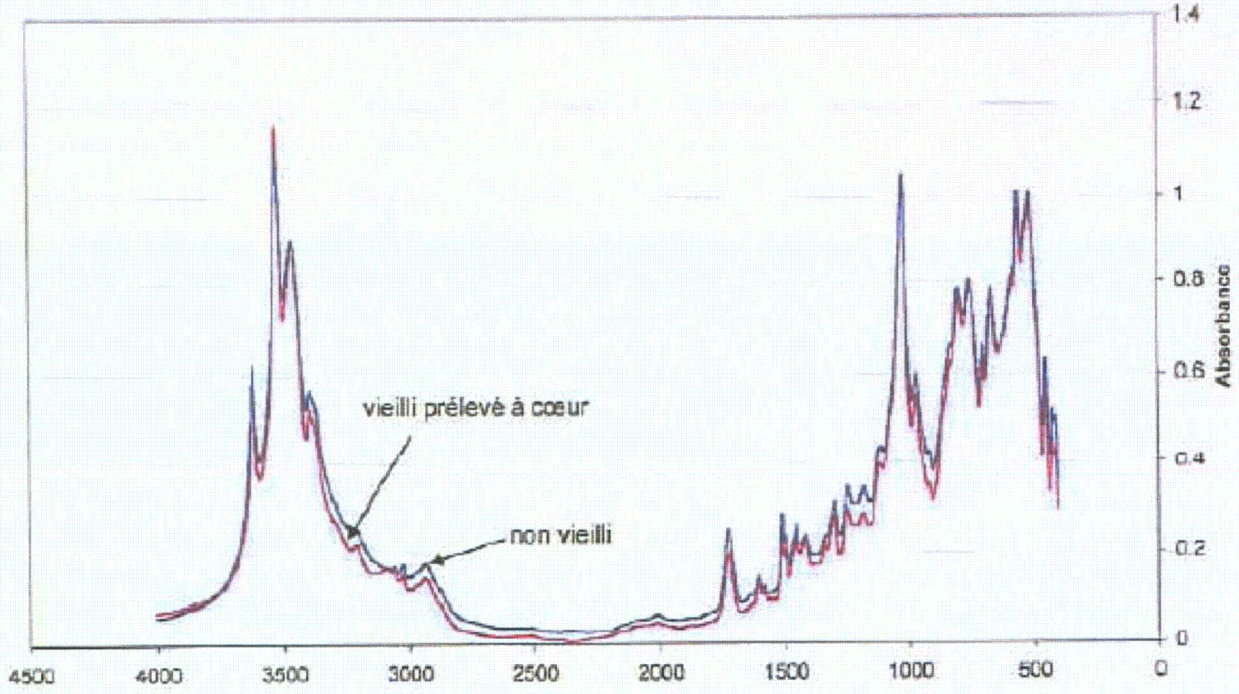

Ageing Tests of Neutron Shielding Materials for Transport Storage Casks

- **Weight loss trends for thin Vyal B resin samples exposed at 150°C, 160°C and 170°C (Ø = 25 mm ; thickness = 1mm)**

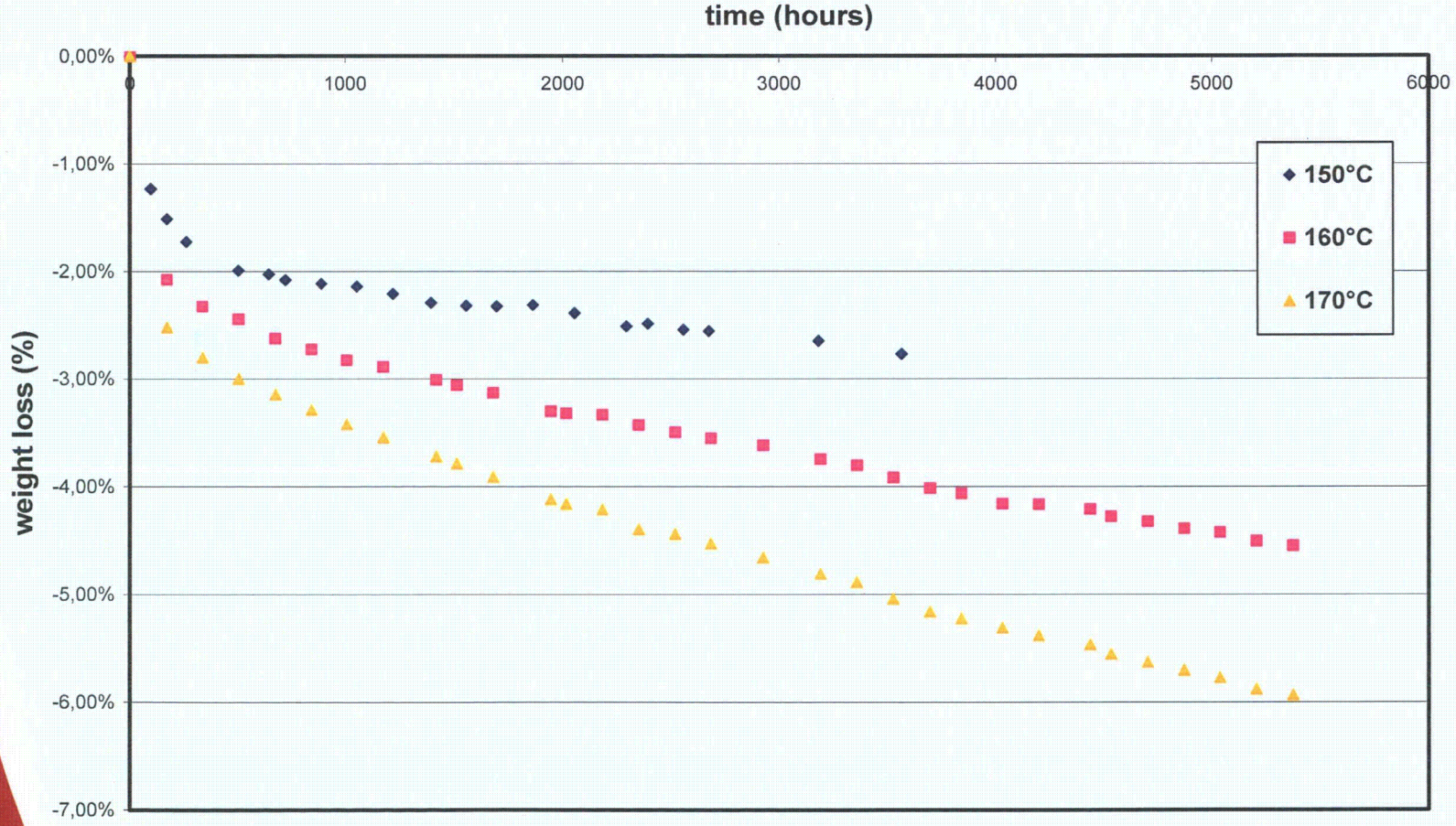

Ageing Tests of Neutron Shielding Materials for Transport Storage Casks

- **Arrhenius trends : ln(exposure time) = f(1/T) (data from previous curve, thin samples)**

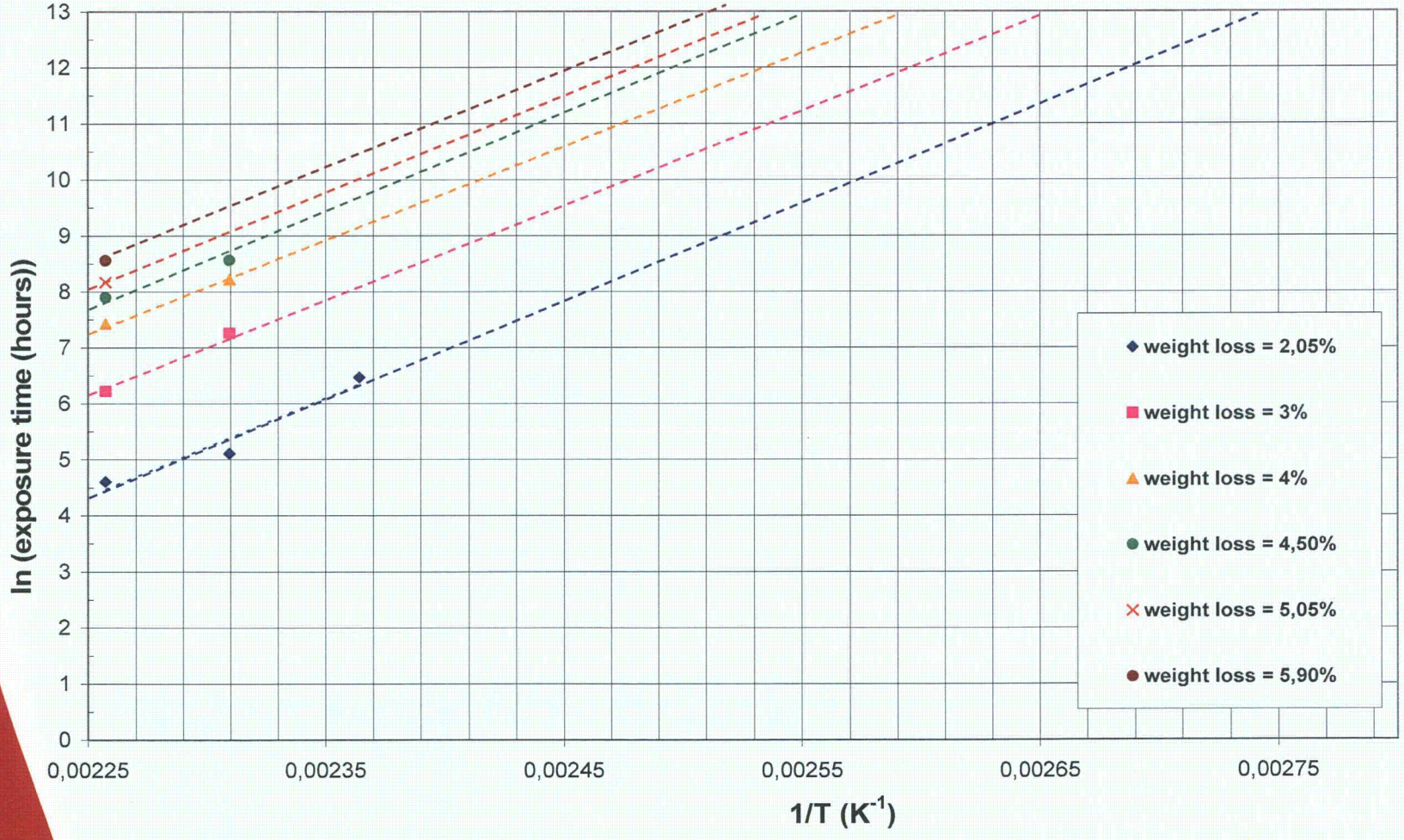

Ageing Tests of Neutron Shielding Materials for Transport Storage Casks

- **Assessment of variations of atomic concentrations in casks**
  - **In the layer of maximum thickness 5 mm, Hydrogen loss (X) and density loss are given by the curve, built with assumption of arrhenius type phenomenon.**
  - **Except this layer, as observed on specimen, we consider no degradation**
  - **We can calculate the final atomic concentrations, to be used in safety analysis.**

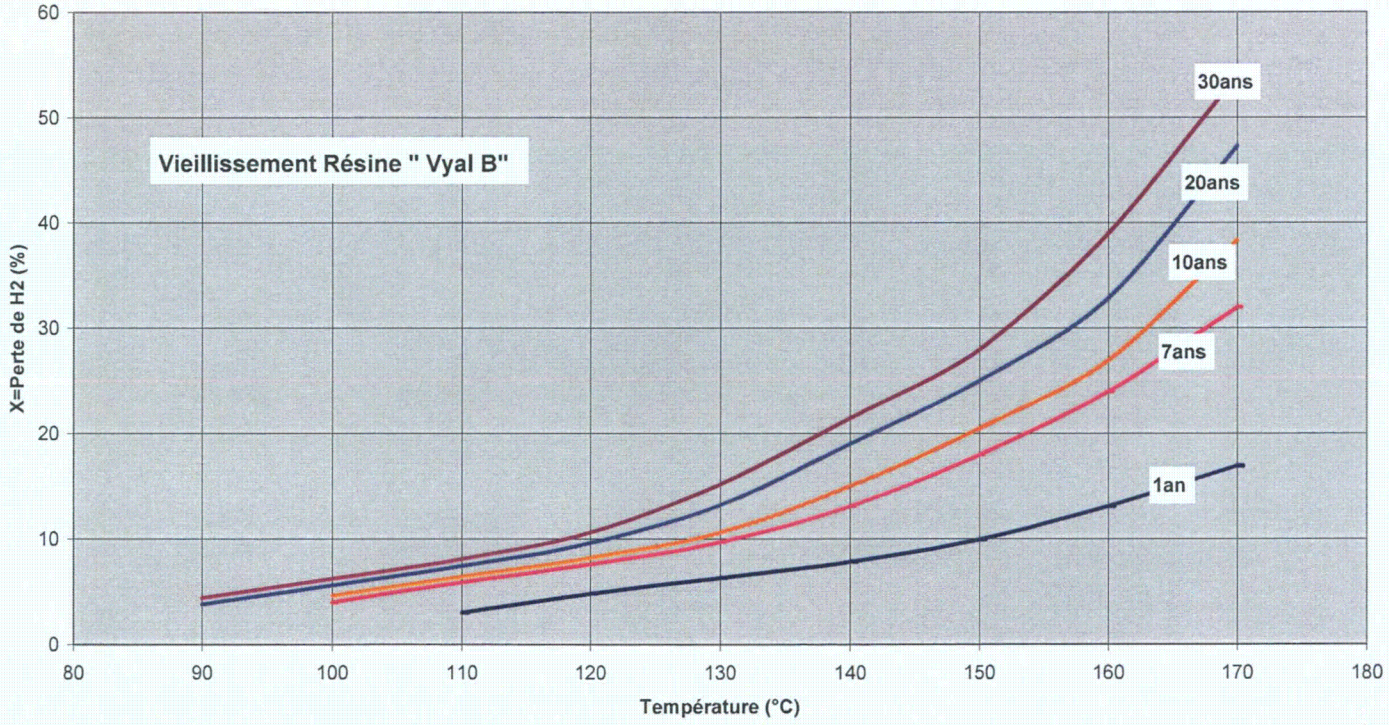

- **Example: Hydrogen content of Vyal-B for vitrified waste package after an exposure at 130°C for 40 years decreases of 0.1%**

AREVA

Enclosure 10 to
TN E-30577

Ageing Tests of Neutron Shielding Materials for Transport Storage Casks

- **Experimental checking of the good behaviour of neutron shielding material in a cask in actual conditions***
  - **Samples taken from Cask TN17 n°704 for spent fuel transport after use during 17 years (resin is polyester based and similar, but not Vyal-B)**

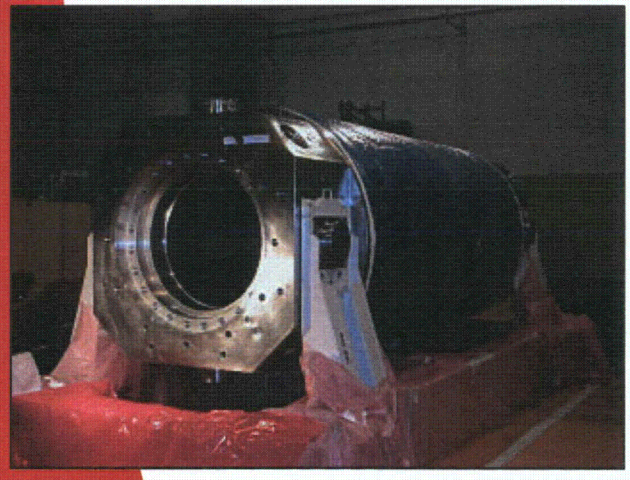

»VIEW OF THE FLASK BEFORE SAMPLINGS

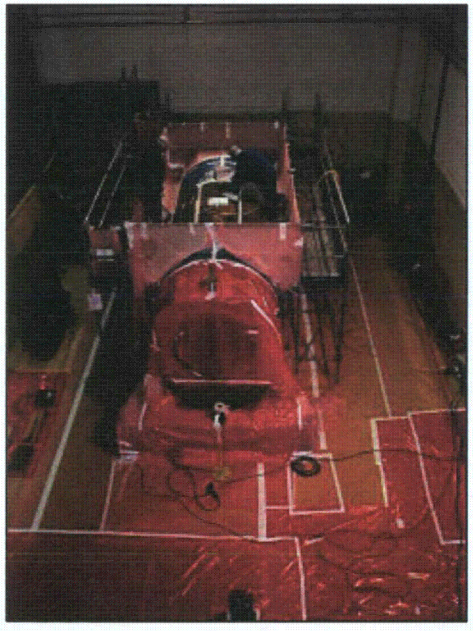

»TOP VIEW OF THE WORK AREA

»SAMPLE N°1
»BODY TOP SIDE DURING
»FINS + RESIN REMOVAL

Remark: temperatures are less severe than in safety analysis

Ageing Tests of Neutron Shielding Materials for Transport Storage Casks

- **Experimental checking of the good behaviour of neutron shielding material in a transport cask TN17 n°704**
  - **Analysis of density of Neutron shielding Samples : measured : 1.514 (criteria : 1.4), no evolution**
  - **Chemical analysis Hydrogen and Boron : conform, no evolution**

»SAMPLE N°1
»FINS CUTTING + RESIN DEBURING

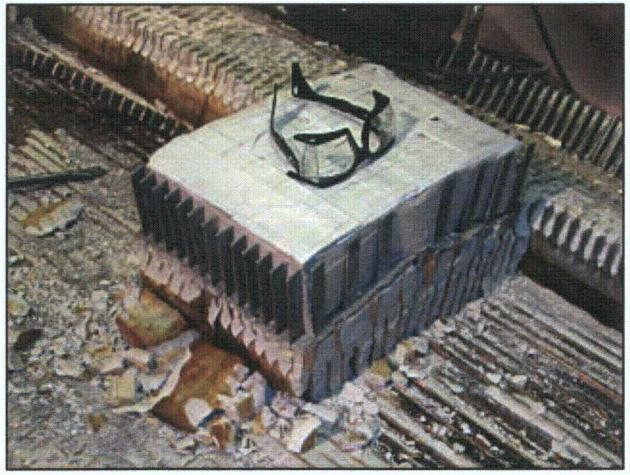

»SAMPLE N°1
»DELIMITATION DURING FINS + RESIN REMOVAL

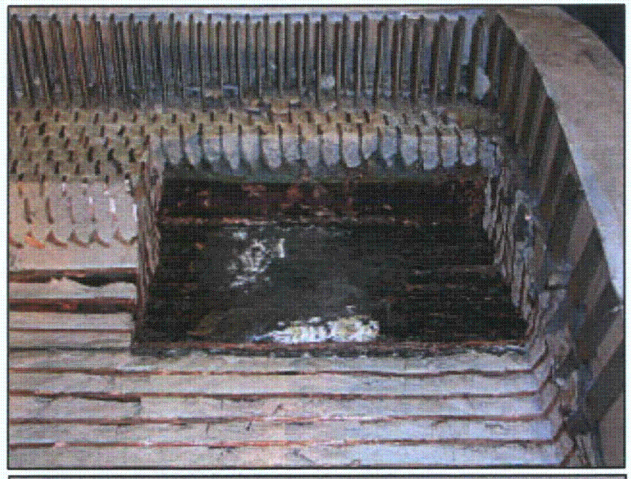

»SAMPLE N°1
»VIEW OF THE DIFFERENT SHIELDING LEVELS

Ageing Tests of Neutron Shielding Materials for Transport Storage Casks

Conclusions

- Through exposition tests of samples at different temperatures (150°C to 170°C), assessment of long term behaviour of Vyal-B shielding material has been carried out. The accelerated tests results give the variations of chemical composition and density. Considering a degradation mechanism limited to an outer layer and using the relation between time and temperature for the degradation of this layer (Arrhenius), the final composition after the complete storage period can be determined
- The new chemical composition after ageing tests are compared to the minimum values complying with the regulatory shielding requirements.
- A maximal temperature of long term use for the Vyal-B neutron shielding material is confirmed equal to 160°C.
- Samples taken from actual casks after use show satisfactory results for shielding performance
- Shielding material from TN International is now qualified for use in transport and storage casks in Germany, United States, France, Belgium, and other countries.

Discussion of MP197HB compliance with ISG-19

Interim Staff Guidance (ISG-19) "Moderator Exclusion under Hypothetical Accident Conditions and Demonstrating Subcriticality of Spent Fuel under the Requirements of 10CFR 71.55 (e)" provides guidance on two basic approaches and criteria acceptable to show subcriticality under 10 CFR 71.55(e).

- Approval based on reconfigured fuel by showing that the reconfigured fuel is subcritical, assuming water inleakage and performing a criticality evaluation of bounding reconfigured fuel geometries.
- Approval based on moderator exclusion by showing that there is no water inleakage under HAC and demonstrating through physical testing the water exclusion boundary so that damage to the fuel would be inconsequential from a reactivity control perspective.

The MP197HB Transportation Package is designed to transport both low and high burnup fuel assemblies. The current licensing application is not requesting the package to be approved based on moderator exclusion under HAC 10 CFR 71.55(e). However the MP197HB package and DSC design meet the guidelines of ISG-19 by demonstrating that there is no water inleakage under HAC.

Double containment boundaries are provided in the MP197HB transport package; (1) the MP197HB transport cask where the containment boundary consists of a cylindrical shell, bottom plate with a ram access penetration, cask body flange, bottom and top cover plates (lids) with associated seals and bolts, and vent and drain port closure bolts and seals, and (2) the canister of the DSC where the primary containment boundary consists of the shell, inner top and inner bottom cover plates, the siphon and vent block, the siphon and vent port cover plates, and the associated welds. The outer top cover plate and associated welds form a redundant containment closure boundary.

In lieu of demonstrating moderator exclusion through physical drop test, the structural integrity of the MP197HB and DSC are demonstrated through analyses. The analyses for the MP197HB transport cask containment boundary, presented in chapter A.2 (specifically Appendices A.2.13.1, A.2.13.2, A.2.13.3, A.2.13.6, and A.2.13.14), demonstrate the integrity of the containment boundary and the closure system. The closure bolts are evaluated in accordance with NUREG/CR-6007. Furthermore the average closure bolt tensile stress due to the secondary impact of the DSC and fuel assemblies during an end drop is also determined by an LS-DYNA dynamic analysis. The resulting stresses are below the smaller value of 0.7 Su or Sy.

The analyses for all of the DSCs to be transported in the MP197HB are presented in Appendix A.2.13.7, showing the integrity of the closure system during 10 CFR 71 HAC conditions.

The analyses of the cask and DSCs confirm that the containments of both the cask and DSCs are maintained and inleakage of water is not credible after HAC drop events.

In addition to the analyses, the containments of both the MP197HB cask and DSCs are leakage tested during fabrication and loading. The leakage tests of the MP197HB and DSCs containments are specified in SAR Section A.8.1.4.

Again, even though the current application is not requesting the package to be approved based on moderator exclusion under HAC 10 CFR 71.55(e), the SAR does include the following:

1. The integrity of the MP197HB and DSCs containment boundaries are maintained by analyses.
2. Leakage tests of the MP197HB and DSCs containment boundaries are performed.
3. The basket geometries also remain intact by analyses performed in Appendix A.2.13.8.

Therefore, it can be concluded that the package design as described in the SAR ensures moderator exclusion consistent with the intended level of safety provided by ISG-19.

Listing of Disk Numbering and Contents for Computer Files
Contained on Enclosure 13 DVDs
(all files are Proprietary)

Disk ID No. (size)	Discipline	System/ Component	File Series (topics)	Number of Files
DVD No. 1 (Enclosure 13) (3.49 GB for Structural)	Structural	Fuel	001-10x10 - Directory (A.2.13.11 – input and output files for fuel end drop analyses for the 10x10 fuel rod with maximum 55g deceleration for 30 ft end drop with 2020 psi internal pressure- LSDYNA analysis)	40
DVD No. 2 (Enclosure 13) (3.98 GB for Structural)	Structural	Fuel	002-14x14 - Directory (A.2.13.11 – input and output files for fuel end drop analyses for the 14x14 fuel rod with maximum 55g deceleration for 30 ft end drop with 2020 psi internal pressure- LSDYNA analysis)	41
	Structural	Fuel	003- BWR 90 E Reduc-Directory (A.2.13.11 – input and output files for 9x9 fuel side drop with E reduced by 90%, no pellet gap and internal pressure of 2020 psi-ANSYS analysis)	3
	Structural	Fuel	004- BWR Accident Modified- Directory (A.2.13.11 input and output files for 9x9 fuel Accident side drop-ANSYS analysis)	4
	Structural	Fuel	005- PWR 90 E Reduc- Directory (A.2.13.11 – input and output files for 14x14 fuel side drop with E reduced by 90%, no pellet gap and internal pressure of 2020 psi-ANSYS analysis)	3
	Structural	Fuel	006-PWR Accident Modified- Directory (A.2.13.11 input and output files for 14x14 fuel Accident side drop-ANSYS analysis)	4
DVD No. 2 (Enclosure 13) (234MB for Criticality)	Criticality	32PTH WE14 & WE17	• CSAS25 inputs for WE14, WE17 using DARWIN and SAS2H isotopic correction factors • CSAS25 inputs for WE14, WE17 for fission products "bounding" approach • CSAS25 inputs for WE14, WE17 for Actinides bias sensitivity study SAS2H / measured	324
	Criticality	24PTH, 32PT, 32PTH 37PTH WE17 Misload Fuel Sensitivity	• Misload sensitivity study • Misload analysis multiple underburned fuels • Misload analysis single high reactivity fuels • Misload analysis poison rod fuel assembly	96

STRUCTURAL AND MATERIALS

2-1 Provide information on how the spacers between fuel and Dry Shielded Canisters (DSC) will be installed for DSCs loaded under storage licenses and/or other transport CoCs.

Table A.2.13.14-2 specifies the various spacer heights ranges to limit fuel-to-DSC gaps which affect Hypothetical Accident Conditions (HAC) drop considerations. However, it is not clear to the staff how these spacers will be implemented for DSCs loaded previously regarding considerations for transportation in the MP-197HB.

This information is needed to verify compliance with 10 CFR 71.73(c)(1).

Response to 2-1

Table A.2.13.14-1 and Table A.2.13.14-2 specify the gap requirements between (1) the canisters (DSCs) and the inner surfaces of the cask ends and (2) the fuel assemblies and the inner surfaces of the DSC cavity. All DSCs loaded into the casks will meet the allowable gaps using cask spacers if necessary. The fuel assemblies will be loaded into the DSCs with internal spacers, if necessary, to keep the gap size within limits. Loaded DSCs that are currently in storage will only be shipped if the gaps between the fuel assemblies and the inner surfaces of the ends of the cavity meet the above-mentioned limits.

SAR Section A.1.2.3.1 has been revised to reflect this change.

2-2 Clarify the approach taken regarding fuel cladding integrity under HAC conditions, given the status of the TN-40 application cited in response to RAI 2-30 and 2-38.

The TN-40 review has not been finalized. Therefore, open questions regarding the methodology at this time are still open for the MP-197HB as well.

This information is needed to verify compliance with 10 CFR 71.55(e)(1).

Response to 2-2

Per the methodology used in the TN-40 Transport application, fuel end drop analyses are updated for both PWR and BWR fuel assemblies by applying the maximum g-load to the cask-ground spring representing the impact limiter. The results are provided in the updated Appendix A.2.13.11.

2-3 Update the relevant results tables in the Safety Analysis Report (SAR).

Updated results from the revised structural analyses, applicable to various tables throughout the application, (e.g., crush depths in Table A.2.13.12-8), are not provided in the updated application.

This information is needed to verify compliance with 10 CFR 71.71(c)(7) and 71.73(c)(1).

Response to 2-3

Based on the revised structural analyses, all the relevant results tables in the SAR have been verified throughout the application. Some of the results were not affected by the revised structural analyses. For instance, the crush depths in Table A.2.13.12-8 are identical in the original and the revised LS-DYNA impact limiter analyses.

2-4 Clarify the magnitude of g-loads for the HAC side drop basket analysis for the 32PTH1 basket.

Table A.2.13.8.1 lists the g-load for the 32PTH1 as 55 g, while for the 32PTH it is 75 g. However, Tables A.2.13.8-24 through A.2.13.8-26 list very similar results for maximum stresses for the two similar baskets. It is unlikely that such a different loading would produce such similar effects.

This information is needed to verify compliance with 10 CFR 71.73(c)(1).

Response to 2-4

Even though the maximum stress results are similar for the 32PTH and 32PTH1 baskets, the applied g-loads are 75g and 55g respectively. There are several reasons for similar stress results, they are as follows:

- *For both the 32PTH and 32PTH1 DSCs, no distinctions of secondary or peak stress were made after the analysis. The maximum stress intensity at the surface was compared against the membrane plus bending allowable and maximum stress intensity in the middle was compared against the membrane allowable. Since no distinction was made the controlling stresses are typically secondary or peak stresses due to the provided gap at basket to canister and canister to cask interface for thermal growth. These gaps are modeled explicitly in the analysis via contact elements in ANSYS; as the loading increases these gaps are closed and redistribution of the load occurs, causing the maximum stress intensity to remain relatively constant.*

- *Even though the 32PTH and 32PTH1 basket designs are similar, the maximum assembly weight for the 32PTH is 1585 lbs versus 1715 lbs for the 32PTH1. Thus the load in the 32PTH1 basket is higher than the 32PTH basket analysis at the same g-load.*

- *Bilinear elastic-plastic material properties are used in the analysis; due to this, once the stress surpasses the yield stress value the increase in stress is much lower relative to the load.*

2-5 Remove the use of foreign code material as an alternative to American Society for Testing and Materials (ASTM), or American Society of Mechanical Engineers (ASME) code material for cask systems to be used in the United States. Specify exact alternative code material or properties of the code materials that have to meet specifications of the US code material such as yields, elongation, ultimate strength, etc.

A number of the drawings (notes and/or materials lists) include a statement that foreign specifications can be used.

This information is needed to satisfy the requirements of 10 CFR 71.111.

Response to 2-5

Notes allowing the use of foreign code material as an alternative to United States standards have been removed.

2-6 Reduce the maximum allowable assembly burnup for the 69BHT canister to 62.5 GWd/MTU peak rod average in Table A1.4.9-4, or provide justifications for the use of the temperatures in Interim Staff Guidance – 11 (ISG-11), Revision 3, "Cladding Considerations for Transportation and Storage of Spent Fuel."

Staff asked this same RAI in the 1st round (2-19). The applicant's justification was that there would be longer cooling times and the fast neutrons were the same, thus there was no thermal issue. The maximum assembly burnup allowable, if the temperature limits delineated in ISG-11, Revision 3, are invoked, is 62.5 GWd/MTU. This is based on creep and hydriding considerations. The burnup will affect the cladding oxide thickness, the cladding hydrogen content, and the fission gas release. All these will affect the cladding stress, and potentially the ductility, and creep. There is insufficient data on these parameters for the various fuels and claddings to substantiate these effects for reactor operations, hence the knowledge of these parameters for use in cladding stress calculations and creep calculations is insufficient for transportation applications. Table A.1.2.9-4 lists burnups as high as 70 GWd/MTU.

This information is needed to meet the requirements of 10 CFR 71.55(d)(1) and (2).

Response to 2-6

The maximum allowable assembly burnup for the MP197HB has been reduced to 62.5 GWd/MTU. SAR Table A1.4.9-4 has been revised accordingly. Note that other portions of the application still use 70 GWd/MTU as a basis for some evaluations as they are considered bounding for the 62.5 GWd/MTU maximum.

2-7 Show that the mechanical properties calculated using the Geelhood and Beyer correlations in SAR Section A2.13.11.1, apply to cladding with radial hydrides. Compare the ductility of cladding with radial hydrides with the stress imposed during a side drop, i.e., hoop plus crush stress.

Most of the DSCs have either been approved for storage of high burnup fuel or are asking for approval to transport high burnup fuel. The presence of radial hydrides is expected, since 1) the cladding will have had to undergo a drying cycle, and 2) most cladding, other than M5, has both hydrogen contents >200 wppm, with hoop stresses increased by the larger increase in fission gases at high burnup.

The applicant drew on the results of two papers, one by Chu and another by Aomi, to attempt to make the case that the formation of radial hydrides did little to decrease the yield and ultimate strength of the cladding in the axial direction and only decreased them by 20% in the hoop direction. The staff accepts the conclusion for the axial direction, but rejects the conclusions for the hoop direction. Chu's work was conducted at applicable temperatures, stresses and hydrogen contents but only used charged unirradiated

samples. The morphology of the initially charged samples (Chu, Fig. 4a) is completely different from the hydride morphology that occurs in irradiated cladding, and includes the artifacts of the circumferential hydrides in the body of the cladding, which if not dissolved, form a barrier to the propagation of radial hydrides and lowering of the yield stress. As a result, the results and conclusions from Chu's work cannot be generalized to irradiated cladding. Aomi uses burnups up to 59 GWd/MTU but conducts hydride orientation only up to a temperature of 300°C and stresses only up to 70 MPa. Both conditions are too low to place a significant amount of hydrides into the radial direction although they form a preponderance of the hydrides in the body of the cladding. In addition, the cooling rate of 30 C/hr is too fast to allow for significant growth of the hydrides. Shorter hydrides have a lower chance to affect the yield strength. As a result, the reduced yield strengths calculated from these two papers, while only slightly lower than that calculated by Geelhood and Beyer, are rejected by the staff.

The proposed reduced yield stress was compared to the hoop stress in the cladding. The radial hydrides are important during the side drop where there are both hoop and crush stresses. Both must be accounted for when determining the stability of the cladding.

This same argument has been made by the applicant in the past and was rejected by the staff.

This information is needed to meet the requirements of 10 CFR 71.55(b)(1).

Response to 2-7

The high burnup fuel assemblies will only be transported directly from the pool. The hoop stress evaluation is updated to reflect the crush stress during side drop and is presented in SAR Appendix A.2.13.11, Section A.2.13.11.4. The potential for radial hydride formation during loading/vacuum drying operation is discussed in the following paragraphs.

A temperature history for typical fuel cladding in the 69BTH DSC is shown in Figure 2-1. As shown in the figure, the maximum fuel cladding temperature within the 69BTH DSC increases monotonically during the loading/vacuum drying operations. Once the loading/vacuum drying operations are completed and the DSC/TC annulus is drained and filled with helium, the maximum fuel cladding temperature continues to rise further until it reaches NCT equilibrium at approximately 472 °F (244 °C), after about 70 hours. Another small temperature rise occurs when the DSC/TC annulus is drained and filled with helium. After that, the cladding temperature during NCT is quasi-constant, i.e., is subject only to ambient temperature fluctuations.

In order to analyze this cladding temperature history from the point of view of hydride radial re-orientation, the hydride dissolution and precipitation solvi are employed. As is well known, a hysteresis exists between hydride dissolution during heat-up and hydride precipitation during cool-down stages. At a given temperature, the hydrogen concentration in solution in equilibrium with dissolving hydride, TSSD (Terminal Solid Solubility at Dissolution), is less than that in equilibrium with precipitating hydride, TSSP (Terminal Solid Solubility at Precipitation). In this solid system, the chemical potential of hydrogen in a hydride undergoing dissolution is significantly lower than the chemical potential of hydrogen in a hydride that is precipitating.

The following example is reproduced from [2.1] and is illustrated in Figure 2-2 (Figure 2.8 of [2.1]):

"The effect of thermal history on the concentration of hydrogen in solution of a specimen containing, for example, 60 ppm, can be illustrated by examining what occurs when the specimen is taken through a specific temperature sequence through heating and cooling. Referring to Fig. 2.8 [2.1], as

the temperature is increased from room temperature, the hydrogen concentration increases following the curve along AB. When the temperature begins to decrease, the concentration in solution is assumed not to change until the precipitation solvus is reached at point C. On further cooling, the concentration in solution drops following the precipitation solvus (TSSP) until point D. If the temperature is now increased again, the concentration in solution does not increase until the TSSD curve is reached."

The cladding hydrogen concentration – temperature variation during the loading/vacuum drying stage and the following NCT phase is illustrated in Figure 2-3 below. The TSSD, dissolution limit, and TSSP, precipitation limit, have been taken from Reference [2.2], and are valid for irradiated Zircaloy.

During the heat-up phase of loading/vacuum drying dissolution of some of the hydrides present at pool conditions (~ 150 °F or 66 °C) are dissolved and the hydrogen in solution follows the red line on the lower TSSD curve up to the final maximum possible temperature during NCT at 674 °F (357 °C). In general the peak temperature for cold -40 °F ambient condition and hot 100 °F ambient condition can be in the range 570 °F to 674 °F (299 °C to 357 °C) respectively, (see Figure 2-1 for NCT temperatures) .

Also as seen from Figure 2-1, the fuel cladding temperature fluctuation within the 69BTH DSC is only due to the change in the ambient conditions:

- *Temperature variation between 100°F and -20°F ambient conditions is (674°F -582 °F) = 92°F (51°C).*
- *Temperature variation between 100°F and -40°F ambient conditions is (674°F -570 °F) = 104°F (58°C).*

As seen above, the temperature fluctuations in the 69BTH DSC due to changes in ambient temperatures are well below the 117°F (65 °C) limit specified in ISG-11, Rev.3 [2.3]. These temperature fluctuations given above have significant conservatism in that the ambient temperature changes considered for this evaluation are significantly larger than those that would occur during a typical transport cycle.

Assuming a year long transport, the maximum variation in temperature would be the extremes of the NCT ambient giving a cladding temperature variation of 104°F (58°C) when the ambient temperature change is 140°F (from 100°F to -40°F). As shown in Figure 2-3 as the horizontal blue line, this temperature variation does not allow the cladding temperature to reach the precipitation solvus during cool down. Consequently there is no onset of additional hydride precipitation. Therefore, the 10 thermal cycle limit specified in ISG-11, Rev.3 does not apply to 69BTH DSC. Note, also, the maximum temperature fluctuation due to changes in ambient temperatures in the 69BTH DSC, 104°F (58°C), are also below the 117°F (65°C) specified in ISG-11, Rev.3 [2.3].

Thus, no additional precipitation of hydrides occurs during the temperature cycles associated with NCT and therefore, no radial re-orientation of hydrides occurs during the loading/vacuum drying or transport.

Therefore, material properties calculated using the Geelhood and Beyer correlation in SAR Appendix A.2.13.11, Section A.2.13.11.1 are used for the cladding structural evaluation.

References (references 2.1 and 2.2 are included in this submittal as Enclosures 15 and 16. respectively)

2.1 *IAEA-TECDOC-1410, "Delayed Hydride Cracking in Zirconium Alloys in Pressure Tube Nuclear Reactors," Final Report of a Coordinated Research Project 1998-2002, October 2004.*

2.2 *A. McMinn, E.C. Darby and J.S. Schofield, "The Terminal Solubility of Hydrogen in Zirconium Alloys", Proc. 12th Int. Symp. on Zr in the Nucl. Ind., Toronto, ON., 1998, ASTM-STP-1354, pp: 173-195.*

2.3 *ISG 11, Revision 3, "Cladding Considerations for the Transportation and Storage of Spent Fuel", November 2003.*

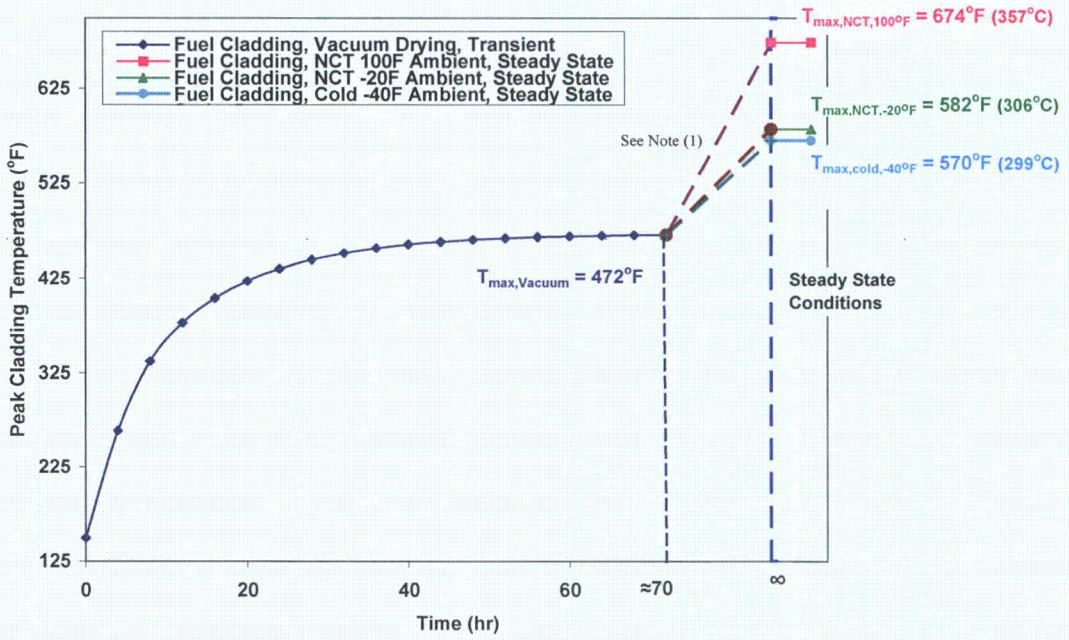

(1) The dashed lines showing the heat-up curves are only for illustrating that the final maximum fuel cladding temeprature after vacuum drying will increase until a steady state temperature is achieved for NCT that will be between the lines shown for NCT at 100°F and NCT -20°F ambient conditions.

Figure 2-1
Temperature Time History for 69BTH DSC, 32 kW during Loading/Vacuum Drying Operations

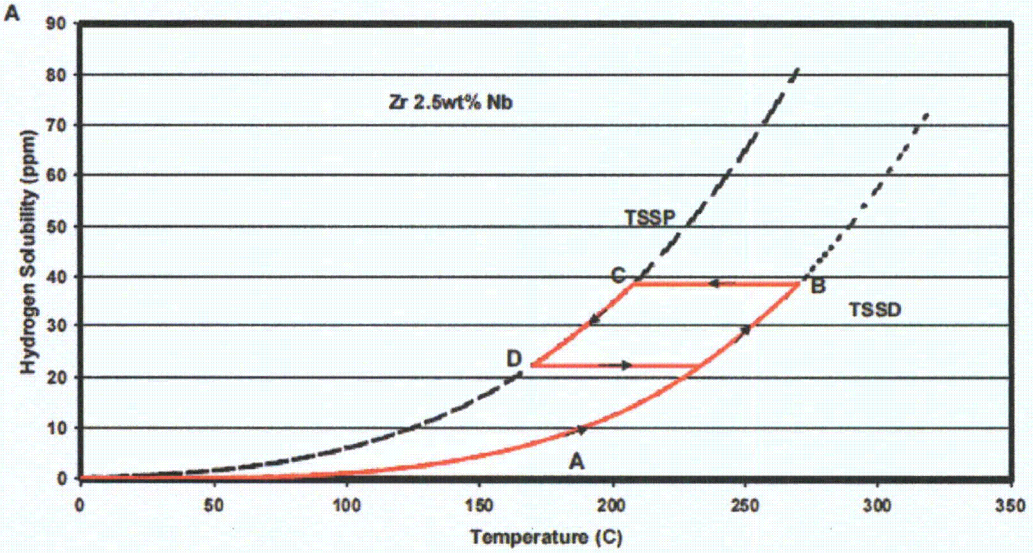

Figure 2-2
Hydride Evolution during a Heating/Cooling Cycle

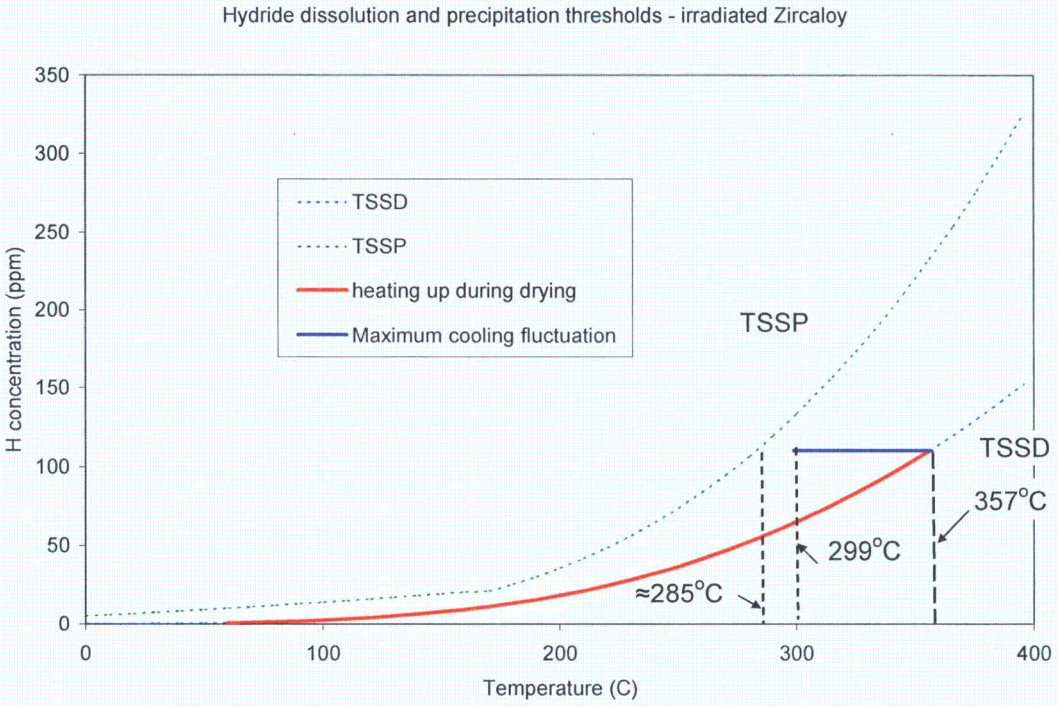

Figure 2-3
Heat-up Phase during Loading/Vacuum Drying Operations,
Followed by Heating/Cooling Cycles during NCT

2-8 Amend the SAR referring to the neutron absorbing materials used for criticality control to be consistent with recent amendments (e.g., CoC No. 1030, Amendment 1).

a) Modify SAR Section A.8.1.7.1. The direct chill of an Al-Ti-B melt could precipitate other phases, e.g., AlB_{12}. The current language in the Technical Specifications (TS) would not permit such phases to act as the principle neutron absorbing material and may create a non-compliance issue with the TS, as the TS relate to transportation.

b) Specify In SAR Section A.8.1.7.2 that the boron carbide particles shall have an average size of 40 microns or less. Particle sizes may be determined by mesh size. The current language, which is that boron carbide particles "typically have an average size...," is vague and open to interpretation.

c) Specify In SAR Section A.8.1.7.3 that at least 80% by weight of the boron carbide particles should be less than 200 microns in size. This requirement is to control the final particle size of the boron carbide in the Boral plates after rolling, which affects neutron streaming.

d) Add a discussion of the thermal conductivity qualification testing of the neutron absorbers to the SAR. The thermal conductivity of the neutron absorbers influences the temperatures distribution of all the components of the entire package, and hence the component performance. No qualification testing protocol was included in this application, consistent with previous applications.

e) Describe in SAR Section A.8.1.7.7.3.1, the delamination testing protocol. The delamination testing mentioned in the SAR is not described for the staff to evaluate. Delamination of clad neutron absorbers during drying may lead to unanalyzed geometries or deformations making retrievability of the fuel problematic.

This information is needed to determine compliance with 10 CFR 71.55(b).

Response to 2-8

a) Section A.8.7.1 has been revised to allow the formation other phases of the Al-Ti-B melt in addition to those currently listed.

b) Section 8.1.7.2 has been revised to require the average particle size be less than 40 microns.

c) Section 8.1.7.3 has been revised to require at least 80% of the B_4C particles be smaller than 200 microns.

d) A description of the thermal qualification testing to be performed on the neutron absorbers has been added

e) Section A.8.1.7.7.3.1 has been expanded to provide a description of the delamination testing to be performed on the clad MMC.

2-9 Revise the SAR to add a plan to ensure, for any DSC that has spent an extended time in storage, that the contents and DSC itself meet all the requirements in the CoC. This plan should include inspections to obtain data or analysis to support: 1) the mechanical and thermal properties of the components of the DSCs related to safety, and 2) the contents, have not degraded during the storage period. Provide evidence that removal of the DSC from the storage overpack will not damage the DSC, and impact safety.

a) Describe how loading records will ensure that DSC damage is not done during the extraction process. Clarify what "appropriate evaluations" as indicated in the initial response, will be conducted.

b) Provide evidence that high burnup fuel in storage for 20 or more years will remain in its analyzed condition. To the staff's knowledge, the analysis on the condition of high burnup fuel after storage has not been experimentally confirmed.

c) Provide a discussion of how Time Limited Aging Analysis (TLAA) will be performed, and describe the aging management program that will be incorporated into the storage license to assure the condition of the basket, neutron absorbers, and fuel contents. Take into accounts comments in RAI M.3.

d) Describe how the applicant will ensure that if there is a storage license renewal beyond 20 years, the aging management plan will include periodic in-service inspections of the accessible canister surfaces as indicated at the end of the 1st round RAI response. Indicate the type of in-service inspections that will be required and what kind of damage will they look for. This section of the application is unique, as it will link a storage renewal application with a future transportation application for the first time.

All the mechanical and thermal properties of the materials of construction of the DSC used in this Part 71 analysis are for pristine materials. Many of the DSCs were constructed and loaded many years ago and are in storage. The materials properties used for the evaluation of the safety systems and contents of the DSCs that have already been in storage service must be representative of the conditions at the time of transport, not at the time of the loading of the DSC. A number of the issues were satisfactorily addressed in the initial RAI response. The issues cited above were not sufficiently resolved.

This information is needed to meet any thermal, shielding, criticality, or structural requirements of 10 CFR Part 71 where the materials properties are integral to the response of the system.

Response to 2-9

A plan will be established to ensure that any DSC that has been in extended storage (i.e., greater than 20 years), will meet the requirements of the CoC and the supporting analyses. This plan will include descriptions of inspections to be performed, data to be obtained, or evaluations required to verify that the mechanical and thermal properties of the DSCs and the basket material have not degraded sufficiently during storage to affect the qualification basis for transportation. The following elements are integral to the implementation of this plan.

1) *The conditions during insertion of the canister into the HSM (and withdrawal there from), including alignment tolerance of the HSM and transfer cask, and ram hydraulic pressure (among other conditions), are specified in the operating procedures, monitored during implementation, and typically recorded. In addition, a review of local environmental records will be performed to identify off-normal conditions such as flooding, dust storms, seismic activity, and similar events. Canisters which have been inserted into and removed from the HSM with records that indicate compliance to the alignment and hydraulic pressure values may be transported with no further action. Canisters whose records indicate a deviation from these specifications or which have been subjected to off-normal conditions will be investigated further to determine if they meet the original design conditions. If conformance cannot be conclusively demonstrated, appropriate mitigating actions will be taken prior to transport.*

2) *This license application is revised now to exclude post-storage high burnup fuel as an allowable payload.*

3) *When the current 10 CFR 72 certificates of compliance (CoC) for the canisters which are in storage are submitted to NRC for renewal, draft NUREG-1927 "Standard Review Plan for Renewal of Independent Spent Fuel Storage Installation License and Dry Storage System Certificate of Compliance" will be used. The TLAA will be based on information provided in draft NUREG-1927. NRC has approved license extensions for two licensees that are using NUHOMS® systems. TN has performed the TLAA analyses for these licensees. TN will use similar methods and draft NUREG-1927 to perform the TLAA in support of the CoC renewal.*

4) *The storage CoC license renewal application will include an appropriate aging management program that is consistent with applicable information from draft NUREG-1927 for the NUHOMS® system.*

Note that the requirements of items 1, 3 and 4 above ensure that any DSC in storage will meet all of the requirements of this transportation CoC.

2-10 Describe the methodology used to determine the size of the gap between the fuel assembly and the DSC.

The gaps between the fuel assemblies and the DSC are given in Tables A.2.13.14-1 and 2. The size of the gap will depend on the dimensions of the DSC and the expected growth of the assembly, which depends on the burnup during irradiation. Without the expected growth of the assembly being stated, there is no way for the staff to determine if the stated gaps are the most limiting for determining the deformation of the assemblies during a hypothetical accident.

This information is necessary to meet the requirements of 10 CFR 71.73(c)(1).

Response to 2-10

In order to calculate the axial gap between the fuel assembly and DSC at time of transport, the following equation will be used to determine the spacer length to be used and to ensure that the axial gap between the fuel assembly and DSC will meet the transport requirement.

$(L_C + \Delta L_C) - (L_F + \Delta L_F) - (L_S + \Delta L_S) - L_R = \text{Gap} < 0.5"$

L_C = DSC cavity length, in.
ΔL_C = DSC cavity length thermal growth, in.
L_F = cold (room temperature), un-irradiated length of the fuel assembly, in.
ΔL_F = fuel assembly thermal growth, in.
L_S = fuel spacer length, in.
ΔL_S = fuel spacer thermal growth, in.
L_R = fuel assembly irradiation growth, in

The length of the DSC cavity, DSC cavity length thermal growth, fuel assembly length, fuel assembly thermal growth, fuel spacer length, and fuel spacer thermal growth can be calculated using the analyzed temperatures at the time of transport.

The fuel assembly irradiation growth depends on the fuel assembly burnup and will be provided by the client or will be calculated based on the burnup values and using irradiation growth models.

Using this methodology will ensure that proper spacer length can be sized to maintain the axial gap less than 0.5". This 0.5" gap also bounds the gap used for the fuel cladding accident end drop analysis.

SAR Table A.2.13.14-2 has been revised to reflect this change.

SHIELDING

5-1 Demonstrate that the neutron shield will retain a uniform layer for the purpose of effective neutron shielding the under hypothetical accident conditions.

In its response to RAI 5-4, the applicant states: "Tests have shown that the neutron shielding material retains more than 60% of its principal contents (hydrogen, boron) following design basis fire accident..." In its response to RAI 5-6, the applicant further states: "The results of the fire tests performed during the testing of the resin indicate that a small layer gets charred under direct fire exposure and this layer is likely to be much smaller when there is no direct exposure to fire." The applicant further states: "The charring is localized ..."

The staff's concerns, however, were not only with how much of the content would be retained or whether the tubes will detach or not. Another chief concern is if the neutron shielding material will be able to retain a uniform neutron shielding layer as assumed in the shielding model. A localized charring and further cracking of the resin may create neutron streaming paths that result in "localized" hot spots that void the effectiveness of the neutron shielding layer. The applicant is requested to demonstrate that the neutron shield will retain a uniform layer for the purpose of effective neutron shielding.

This information is needed for the staff to determine if the package design meets the regulatory requirements of 10 CFR 71.51.

Response to 5-1

Proprietary Information Withheld Pursuant to 10 CFR 2.390

Proprietary Information Withheld Pursuant to 10 CFR 2.390

5-2 Provide shielding analyses that explicitly model the walls of the aluminum tubes that contain the neutron shield resin.

In its response to first round RAI 5-1, the applicant explained in detail the structural design of the resin tubes. From these explanations, it appears that the walls between two adjacent tubes will form an approximately 0.24 inch aluminum wall. Because aluminum has a much lower neutron absorption cross section than boron and a much lower slowing down power than the hydrogen and oxygen in the resin, these aluminum layers between the adjacent resin tubes may result in neutron streaming paths. It was not clear how these aluminum tube walls were treated in shielding analyses of the MP-197 packages. The applicant is requested to provide information on how the aluminum tube walls were treated in the shielding models with adequate justification.

This information is needed for the staff to determine if the package design meets the regulatory requirements of 10 CFR 71.47 and 71.51.

Response to 5-2

As described in SAR Appendix A.5, Section A.5.3.1.1 and Section A.5.3.2, the neutron shielding material (VYAL-B) is encased in a 0.12-inch thick aluminum box. The boxes are arranged in such a fashion that there is approximately 0.24-inch aluminum material present between adjacent resin blocks. The neutron shielding resin and the aluminum are homogenized using a volume weighted average and the homogenized material composition is shown in SAR Table A.5-18.

This neutron shielding configuration has been incorporated in all of Transnuclear's metal cask storage designs for more than 15 years. Detailed surface dose rate measurements have been performed for the TN-32 storage cask to quantify the neutron streaming (if any) due to the aluminum boxes. Enclosure 9 provides the details of such measurements performed on two TN-32

storage casks. These measurements indicate that the aluminum boxes did not present possible neutron streaming paths through their walls.

In addition, a sensitivity evaluation is performed to determine the effect of using a homogenized resin/aluminum "layer" on the calculated dose rates on and around the MP197HB TC. The MCNP model was revised to include the actual configuration of resin/aluminum boxes as shown in Figure 5-2-1, below. Detailed mesh tallies were placed at both the cask surface and at 2m from the impact limiters. The results of this evaluation indicate that the maximum increase in the calculated dose rate at the cask surface is approximately 6%. The results of this evaluation also indicate that the maximum increase in the calculated dose rate at 2m from the cask surface is approximately 5%.

The methodology employed to determine the design basis dose rates – in particular the application of the axial neutron source distribution is conservative by more than 10% as shown in SAR Chapter A.5, Section A.5.5.6.1. Therefore, it is expected that the use of a homogenized model combined with a bounding use of the axial neutron source distribution sufficiently covers the increase in "calculated" dose rates using the discrete resin/aluminum box configuration. Further, detailed measurements do not indicate any measurable variation in the dose rates specifically due to the resin/aluminum box configuration. Therefore, there is reasonable assurance that the calculated dose rates using a homogenized neutron shielding layer and a conservative source distribution results in bounding dose rates. SAR Appendix A.5, Section A.5.3.2 is revised to include a discussion on the sensitivity analysis.

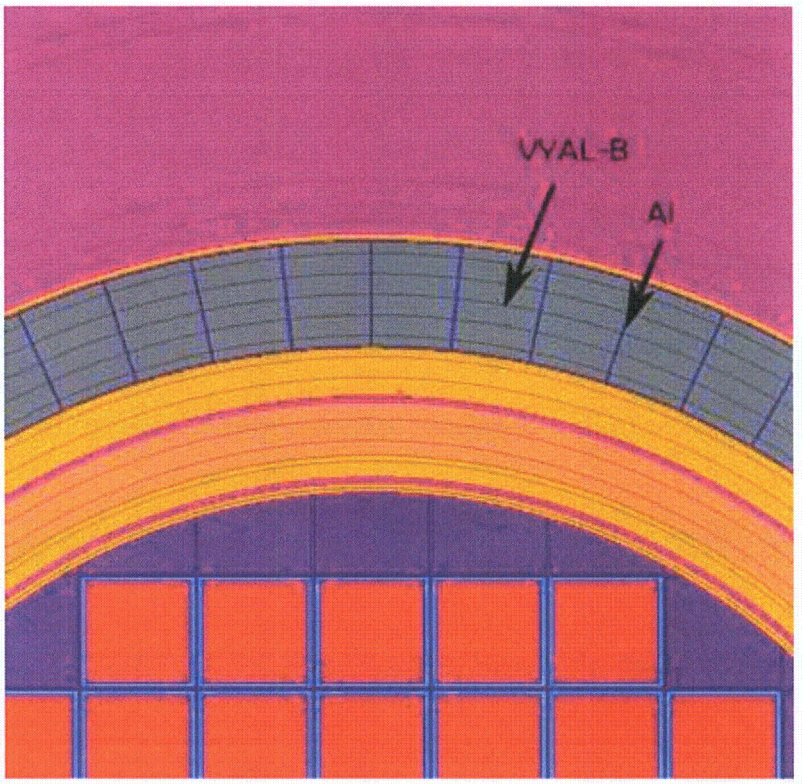

Figure 5-2-1: MCNP Model Plot Showing the Neutron Shielding and Aluminum Boxes

5-3 Demonstrate via calculations that the MP197HB cask loaded with the 69BTH DSC containing design basis BWR fuel assemblies bounds all contents.

The staff requested, in the original RAI 5-3, which was transmitted to the applicant on December 2, 2009, that the applicant demonstrate that a MP197HB cask loaded with the 69BTH DSC containing design basis BWR fuel assemblies bounds all contents. In its response to the RAI, the applicant explained the bases on which it determined that the 69BTH DSC containing design basis BWR fuel assemblies bounds all contents with respect to the shielding safety analysis. However, the response used mainly qualitative discussion rather than calculations, and the discussions focused solely on a fuel load of a single fuel assembly. From the perspective of shielding safety analysis, the source terms (both neutron and gamma) are the determining factors for bounding design basis fuel. As such, the combination of total fuel quantity, burnup, cooling time, and initial enrichment are the major parameters that affect the source terms. The applicant is requested to demonstrate that the selected design basis content bounds all of the nine different cask designs, including those that contain damaged fuel and/or non-fuel hardware.

This information is needed for the staff to determine if the package design meets the regulatory requirements of 10 CFR 71.47 and 71.51.

Response to 5-3

As discussed in the response to the original RAI 5-3, the 69BTH DSC containing the design basis BWR fuel assemblies is evaluated to determine the dose rates on and around the MP197HB Transport Cask under NCT and HAC. This determination is made based on the fuel qualification calculations documented in SAR Appendix A.5, Section A.5.5 that determine the allowable combinations of burnup, enrichment and cooling time (BECT) for the various PWR and BWR fuel assemblies within the various DSCs. In addition to the total fuel quantity and BECT combinations, the dose rates are also influenced by the shielding properties of baskets and DSCs within which these sources are placed. This implies that the strongest radiological sources may not result in the highest dose rates when they are surrounded with superior shielding in comparison to other source/shielding configurations. Therefore, a selection of the design basis shielding configurations are not governed solely by maximization of the radiological sources but rather a determination of a combination of radiological sources and a shielding configuration that result in bounding dose rates. This forms the basis for the fuel qualification methodology employed in the MP197HB shielding calculations. Response functions are determined as part of the fuel qualification calculations for each DSC content of the cask. Therefore, the differences in the geometry and materials between the various DSCs and the total fuel quantity and BECT combinations of the fuel assembly payloads are accounted for in the fuel qualification calculations.

The fuel qualification is based on limiting the maximum calculated dose rate at 2m for NCT to within the applicable Part 71 limits and provides a reasonable assurance that all the DSCs and their allowable contents are "equivalent" in terms of dose rates at NCT. At HAC, it is assumed that the neutron shielding of the cask is severely degraded. Therefore, the HAC dose rates are nearly entirely dominated by the neutron source terms. Since the 69BTH DSC payload has the bounding neutron source term (due to the highest allowable burnup of 70 GWD/MTU) it represents the bounding payload for HAC.

Additional justification is provided in the responses to RAI Items 5-8, 5-9, 5-10 and 5-12 that describe the methodology employed to determine the source term and shielding models (DSC and fuel payload) employed for NCT and HAC. This includes calculation of NCT dose rates for all payloads and demonstrating the bounding nature of the source terms employed for HAC.

Based on discussions with the staff, SAR Appendix A.5, Section A.5.1.1 is modified to refer to an "evaluated" configuration to determine dose rates instead of a "bounding evaluation".

5-4 Demonstrate via calculations that the source terms calculated using SAS2H are conservative.

In its response to the staff's RAI 5-8, transmitted to the applicant on December 2, 2009, and subsequent RSI 5-1, the applicant revised the SAR to provide qualitative sensitivity analyses to justify that the source terms calculated using SAS2H are conservative. However, the applicant did not provide any quantitative analyses to demonstrate that the calculated source terms are conservative and the calculated dose rates will not exceed the regulatory limits, e.g., 10 mrem/hr at 2 meters from the surface of the cask or enclosure. In fact, Table A.5-1a of revision 8 of the SAR shows that the maximum dose rate at two meters from the assumed railcar is 9.4 mrem/hr. The margin for safety is only 6%. Review of publications on SA2H validation against experimental data indicates that SAS2H underpredicts the concentrations of many isotopes that are important to shielding by over 10%. Given this fact, the applicant is requested to demonstrate with code benchmark results that the accumulated errors in the dose rates, including errors and uncertainties in source terms and dose rate calculations using the MCNP code will not exceed 6%. An analysis of the uncertainties associated with Monte Carlo method for shielding calculations will be helpful to the staff for determining if the cask design meets 10 CFR 71.47 and 71.51 requirements, given the fact that MCNP is a Monte Carlo method particle transport calculation code.

This information is needed for the staff to determine if the package design meets the regulatory requirements of 10 CFR 71.47 and 71.51.

Response to 5-4

Proprietary Information Withheld Pursuant to 10 CFR 2.390

Proprietary Information Withheld Pursuant to 10 CFR 2.390

5-5 Provide data to demonstrate that the uncertainty of SAS2H calculated gamma and neutron sources is 10% and 5%, respectively.

In its response to the staff's, RSI 5-1, transmitted to the applicant on June 17, 2010, the applicant states that the uncertainty of the SAS2H calculated gamma and neutron sources is 10% and 5%, respectively. In addition, the applicant states: "A more direct validation of source term calculations is to measure the dose rate from these sources. Numerous measurements from various spent fuel storage and transportation systems have indicated that the measured dose rates are typically lower than the calculated dose rates." The staff's review of the isotopes estimated by SA2H that are important to shielding indicates that many of them are underestimated by a large percentage. For example, the isotopic concentration for Cm-244, the major neutron emitter and high energy gamma emitter (average energy = 7.25 MeV and 9 MeV groups), is underestimated by as much as 21% and 12.5% for the TMI and REBUS samples, respectively. For the design basis fuel, the major gamma emitters, Cs-134 (average energy = 0.9 MeV group) were underestimated by 23%, 34.6% for two TMI samples,

20.8% for the Calvert Cliffs sample, 19.7% for the Takahama-3 sample, and 14.4% for the ARIANE sample, respectively. The applicant also referenced NUREG/CR-6701 and ORNL/TM-13315 for validation of SAS2H at burnups up to 75 GWd/MTU. The staff reviewed these publications and found they are not applicable to the TN MP197 package because (1) the only sample with burnup of 73 GWd/MTU used in NUREG/CR-6701 was taken from a reconstituted fuel assembly and (2) the maximum burnup for all benchmark data in ORNL/TM-13315 is 34 GWd/MTU. The staff also consulted the appropriate authors at Oak Ridge National Laboratory; the answer is stated that these reports were never intended to be used as basis to support that the validated range of SAS2H is up to 75 GWd/MTU. In addition, NUREG/CR-6701 and a presentation on CASMO validation presented during a recent Electric Power Research Institute Workshop on Light Water Reactor Physics Methods shows that the uncertainties of the calculated isotopic concentrations increase as the fuel assembly burnup increases. However, in the revised SAR and responses to the RAIs, no quantitative data were provided on the relationship between these uncertainties and fuel burnup. For these reasons, the applicant is requested to demonstrate that the gamma and neutron sources calculated for the MP-197 package shielding analysis are within 10% and 5%, respectively, for isotopes that are important to shielding. Additionally, the applicant should provide documentation to support the validation range of the SAS2H code up to 75 GWd/MTU.

The applicant is recommended to provide supporting data that the staff may not be aware of and make justification for the accuracy of the SAS2H source term calculation for high burnup fuels.

This information is needed for the staff to determine if the package design meets the regulatory requirements of 10 CFR 71.47 and 71.51.

Response to 5-5

There are many isotopes that contribute to the intensity of design basis gamma radiation sources among which, ^{134}Cs is not the major contributor. As specified in SAR Section A.5.5.1, primary gamma radiation (PGR) dose rate is essentially contributed by PGR sources in 1.0 to 3.0 MeV energy range. Any contribution from other energy groups results in a statistically insignificant change to the resulting dose rates. Therefore, even a large deviation (either under or over prediction) in the concentration of isotopes determined with SAS2H that contribute to intensity of PGR source in the 7.25 and 9.0 MeV energy groups has no impact on the calculated dose rates.

PGR dose rate is largely due to 1.0 to 1.66 MeV energy group when considering PGR sources from assemblies at cooling times greater than 5.0 years. ^{134}Cs, half-life 2.065 years, decays via β^- emission (27%, 88.6 keV maximum, 23.1 keV average energy; 70%, 668 keV maximum, 210 keV average energy) and gamma emission (abs intensities: 97.6% 605 keV; 85.5% 796 keV; 15.4% 569 keV) to ^{134}Ba, half-life stable. The contribution of PGR source energy groups in less than 1.0 MeV range to the PGR dose rate is negligible for the shielding configurations under consideration.

Differences between the measured concentration of isotopes in spent fuel samples and calculated with SAS2H are discussed in Section A.5.5.7. Their effect on dose rates near the transportation cask is also addressed in the section. More discussion is added to Section A.5.2 regarding applicability of SAS2H code to higher (up to 75 GWd/MTU) burn-ups, including validation and associated uncertainties.

5-6 Provide justification for why the neutron sources, as a function of the axial burnup profile, were not proportional to the fourth power of burnup

Table A.5-15 of the revised SAR provides BWR axial peaking factors for neutron and gamma sources. A simple calculation of the peaking factor for neutron source along the axial direction seems to indicate that the neutron source is not proportional to the fourth power of local burnup. In comparison, Table A.5-16 shows that the neutron source for PWR fuel is proportional to the fourth power of burnup. On page A.5-7a of the revised SAR, the applicant states: "The ratio of the true total neutron source in an assembly to the neutron source calculated by SAS2H/ORIGEN-S for an average assembly burnup is 1.326 and 1.152 for BWR and PWR assemblies, respectively." However, it is not clear how these numbers are derived and what the bases are for these conclusions. Furthermore, the ratio for BWR fuel was used in Table A.5.-15, but not used for the PWR source determination in the same table. It is not clear why the same rule was not applied to both BWR and PWR fuel. The applicant is requested to provide justification for why the source term provided in this table does not follow the physical law.

This information is needed for the staff to determine if the package design meets the regulatory requirements of 10 CFR 71.47 and 71.51.

Response to 5-6

Appendix A.5, Section A.5.2.1 of the SAR contains a description of the determination of the axial peaking factors for both BWR and PWR fuel. This section is changed to make it clearer as to how the BWR axial peaking factors were determined. A new table (Table A.5-37) and figure (Figure A.5-17) have been added to provide justification for the BWR peaking factors.

5-7 Demonstrate that dose rates under normal conditions of transport will not change significantly for fuel with natural uranium blankets, even though the source terms in the enriched fuel regions increases significantly for such fuel.

In its RAI 5-19, transmitted to the applicant on December 2, 2009, the staff requested the applicant explain how the natural uranium blankets were treated in the source term calculation and cask dose rate calculations. In the applicant's response, the applicant concluded that the natural uranium blankets caused the source terms to increase significantly, but the impact to dose rates of the cask is insignificant. This conclusion, however, appears to be in conflict with the basis of the "response function" method used for fuel qualification. The fundamental assumption of the "response function" method is that there exists a linear relationship between the outside dose rates and source terms in the cask. The applicant is requested to demonstrate its conclusion with detailed calculations.

This information is needed for the staff to determine if the package design meets the regulatory requirements of 10 CFR 71.47 and 71.51.

Response to 5-7

Proprietary Information Withheld Pursuant to 10 CFR 2.390

Proprietary Information Withheld Pursuant to 10 CFR 2.390

5-8 Pertinent to the response function method, explain why the response function calculated with a cask under normal conditions of transport can be used to determine the design basis HAC source terms.

In its response to the staff's RAI 5-18, transmitted to the applicant on December 2, 2009, and subsequent RSI 5-3, and the follow-up conference call on the RSIs, the applicant stated that the response function was not used for shielding analysis for the cask under hypothetical accident conditions. However, on page A.5-26 of Revision 8 of the SAR, the applicant states: "In summary, the response functions are calculated using the NCT shielding configuration models for the fuel qualification (to determine acceptable BECT combinations for various payloads). The neutron dose rates calculated using the response functions employed to determine the design basis HAC source terms to ensure that the fuel qualification methodology also ensures that the dose rates are within acceptable limits under HAC." There appears to be an inconsistency between these responses to the same question. The applicant is requested to explain exactly how the response functions calculated under normal conditions of transport were used in the safety analyses for the cask under hypothetical accident conditions and provide justification for such uses. Review of original RAI 5-18 and RSI-3 may be helpful to address the staff's concerns.

This information is needed for the staff to determine if the package design meets the regulatory requirements of 10 CFR 71.47 and 71.51.

Response to 5-8

An additional section (Section A.5.5.8.4) is added to Appendix A.5 of the SAR which addresses this RAI.

5-9 Pertinent to the response function method, provide:

a) Detailed information on the definition of the response function, including the mathematical formulation and analytical derivation of the equations,

b) Technical basis for this method, i.e., how and why this approach produces reliable and accurate results, and

c) Validation and verification of the method, or

d) Publications and references that have demonstrated the validity of the methodology.

In response to the staff's RAI 5-18, the applicant revised the SAR to add some discussions on the response function method. However, the response to RAI 5-18 and the revised SAR do not address the above questions. Specifically, the response to the RAI did not provide any discussion on why this method is valid and reliable for casks loaded with various contents. The response did not provide any discussion on why the complicated particle transport problem can be simplified as a simple arithmetic problem so that the fuel qualification can be determined using a simple spreadsheet data table. The fundamental question is to demonstrate that the particle transport problem related to shielding calculations of the cask is independent of the material composition in the cask fuel region. The applicant is requested to (1) provide detailed information on the definition of the response function, including the mathematical formulation and analytical derivation of the equations, (2) technical basis for this method, i.e., how and why this approach works, and (3) validation and verification of the method or, (4) publications and references that have demonstrated the validity of the methodology.

This information is needed for the staff to determine if the package design meets the regulatory requirements of 10 CFR 71.47.

Response to 5-9

Existing Section A.5.5.8 of the SAR is renumbered as Section A.5.5.9, and a new Section A.5.5.8 is added to Appendix A.5 of the SAR, which addresses this RAI.

5-10 Explain exactly how the response function was used for determination of the design basis HAC source terms and provide justification for why such an approach is acceptable.

On page A.5-26 of the revised SAR, the applicant states: "The neutron dose rates calculated using the response functions are employed to determine the design basis HAC source terms to ensure that the fuel qualification methodology also ensures that the dose rates are within acceptable limits under HAC." In its response to RSI-3 of the acceptance review of the response to the RAI, the applicant states: "From the NCT dose rate results, the source with largest neutron dose rate fraction was selected as the bounding HAC source. This occurs for a burnup of 70 GWd/MTU and enrichment of 4.3% U-235, where the neutron fraction of the total NCT dose rate is 85%." However, it is not clear how the source giving highest neutron fraction of NCT dose rate will necessarily be that which will produce the highest neutron dose rate under HAC. In particular, if the neutron shielding material is highly effective, the neutron dose rate will be small for all practical purposes. Under HAC, both gamma shield and neutron shield will lose some shielding capabilities. There is no clear nexus between these two scenarios. The applicant is requested to clarify exactly how the response function was used for determination of the design basis HAC source terms and provide justification for

why such an approach is acceptable. A detailed description for the two types of base models, as mentioned in the last paragraph of page A.5-12, for both NCT and HAC, and the input/output files will be helpful for the staff to make the determination that the package meets the regulatory requirements.

In addition, the applicant is requested to provide code validation results that demonstrate that SAS2H is validated to 70 GWd/MTU burnup.

Also, the applicant should demonstrate the need for packages for spent fuel with burnups up to 70 GWd/MTU, given the fact that the Office of Nuclear Reactor Regulations limits maximum assembly burnup to 62.5 GWd/MTU.

This information is needed for the staff to determine if the package design meets the regulatory requirements of 10 CFR 71.51.

Response to 5-10

While it is true that the gamma shield will lose some shielding capabilities, the impact on the neutron shielding is substantially greater in the HAC model analyzed in the shielding calculations. It is conservatively assumed in the shielding calculation models that 75% of neutron-shielding is lost during the HAC. The response to RAI Item 5-8 addresses this request. Also, a discussion useful for addressing this request is presented in the response to RAI Item 5-3.

The validation of the SAS2H module to determine source terms at higher burnups (up to 80 GWd/MTU) is illustrated in Appendix A.5, Section A.5.2 of the SAR

The need for the requested burnup limit for the MP197HB transport package is discussed in the response to RAI 2-6.

5-11 Demonstrate that SAS2H can model fuel assemblies with low enriched or natural uranium blankets.

On page A.5-33 of the revised SAR, the applicant states that the use of axial blankets could be explicitly accounted for in the source term calculation by running SAS2H for each of the axial regions of the core. However, it was not clear how the power density and depletion environment were modeled in the source term calculations given the behavior of the neutron flux in the interface zones of the normal enrichment zone and low enrichment zone. In addition, the neutron flux in the low enrichment blanketed core is severely skewed. A model with local burnup may not be able to capture the flux distortion along the axial direction of the fuel assembly, and there is no axial burnup peaking factor that covers the fuel assemblies with natural uranium or lightly enriched uranium blankets. It was also not clear how the 3D effects were treated in a supercell model code such as SAS2H. The applicant is requested to demonstrate that SAS2H can model fuel assemblies with low enriched or natural uranium blankets.

This information is needed for the staff to determine if the package design meets the regulatory requirements of 10 CFR 71.47.

Response to 5-11

Proprietary Information Withheld Pursuant to 10 CFR 2.390

Proprietary Information Withheld Pursuant to 10 CFR 2.390

This evaluation is documented in SAR Appendix A.5, Section A.5.5.6.1.B.

5-12 Provide justification for the conclusion that the extra conservatisms discussed in Section A.5.5.7 of the revised SAR will bound the uncertainties associated with the SAS2H source term calculations.

Section A.5.5.7 of the SAR discusses the uncertainties associated with the source terms calculated by the SAS2H code. However, some of the conservatisms discussed may not actually be present. For example, the fact that cobalt-60 contents for newer fuel designs are lower than in older designs may not be considered as conservatism, because the CoC, once approved, will not prohibit users from loading a cask with high-cobalt-60 fuel assemblies. Unless the CoC explicitly prohibits high cobalt-60 fuel from the authorized contents, this conservatism is not available as additional conservatism to dose rates. The same is true for other parameters listed on page A.5-34b of the revised SAR. The applicant is requested to provide justification for the conclusion that the listed conservatisms would compensate for the uncertainties of the SAS2H source term calculations.

This information is needed for the staff to determine if the package design meets the regulatory requirements of 10 CFR 71.47 and 71.51.

Response to 5-12

A detailed evaluation that quantifies the conservatisms that can be credited such that the calculated dose rates on and around the MP197HB cask (accounting for all major uncertainties) are below the applicable Part 71 limits is documented in Appendix A.5, Section A.5.8 of the SAR.

5-13 Correct the statement on page A.5-4a regarding the dose rate limit to the package accessible surface.

On page A.5-4a of the revised SAR, the applicant states: "External dose rate at any point on the outer accessible surface of the package under normal conditions: 1000 mrem/hr (max)." This is inaccurate because 10 CFR 71.47 requires the package surface dose

rate to be 1000 mrem/hr only when the package is enclosed in a transport vehicle. The applicant is requested to revise this statement to make it consistent with 10 CFR 71.47.

This information is needed for the staff to determine if the package design meets the regulatory requirements of 10 CFR 71.47.

Response to 5-13

The statement has been corrected. The statement is now located on SAR Page A.5-4b and reads "External dose rate at any point on the outer accessible surface of the package under normal conditions: 200 mrem/hr (max)."

5-14 Verify the reference to Table 5.2-7 on page A.5-7 and make corrections as necessary. Page A.5-7 of the revised SAR references Table A.5-7. The staff was unable to find this table. The applicant is requested to provide information on the location of this table.

This information is needed for the staff to determine if the package design meets the regulatory requirements of 10 CFR 71.47 and 71.51.

Response to 5-14

The referenced table (Table 5.2-7) is in the MP197 base SAR (Please refer to ADAMS Accession Number ML063190444). Note that the MP197HB safety analysis is documented in Appendix A of the SAR.

CRITICALITY

Unless otherwise stated, the following information is required in order to ensure that the Model No. TN NUHOMS®MP-197HB package will meet the criticality safety requirements of 10 CFR 71.55 and 71.59, and that fissile material is packaged as if unknown properties have credible values that will cause the maximum neutron multiplication, per 10 CFR 71.83.

6-1 Revise Section A.6.2.4.A of the application, *Axial Burnup Distribution*, to clarify the number and burnup ranges of the axial profiles used in the criticality analysis.

The last paragraph in Section A.6.2.4.A states that the fourth profile is used in the criticality analysis for burnups greater than 42 GWd/MTU and greater than 4.0 weight percent initial enrichment. The fourth profile given in Table A.6-3 is for greater than 38 GWd/MTU, and does not state an initial enrichment limit. The application should be revised to clarify the burnup and enrichment limits for the fourth profile used in the criticality analysis.

Response to 6-1

The last paragraph in SAR Appendix A.6, Section A.6.2.4.A is revised to delete the statement in question, to be consistent with the use of the fourth profile given in Table A.6-3. The fourth profile is employed at burnups greater than 38 GWd/MTU and does not include an enrichment limit.

6-2 Revise Section A.6.2.7.4, *Reactivity Effect of Specific Power During Depletion*, to either add a bias correction for burnups lower than 35 GWd/MTU, or justify that one is not necessary.

Section A.6.2.7.4 states that a bias of 0.0035 is appropriate for burnups lower than 35 GWd/MTU, as shown in Table A.6-36. This section then states that bias is not necessary since the SAS2H calculations are benchmarked to the DARWIN code with the same specific power. This conclusion is not supported by the text of this paragraph.

Revise this section to either use a more appropriate bounding specific power during depletion at low burnups, or to apply the 0.0035 bias determined for the burnup range.

Response to 6-2

A specific power bias of 0.0035 is conservatively applied to all the burnup values in the loading curves. Appendix A.6, Section A.6.2.7.4 of the SAR is revised to include this discussion. In addition, the specific power bias is added to Section A.6.3.4.1.1 and Appendices A.6.5.4, A.6.5.5, A.6.5.6, and A.6.5.7.

6-3 Revise Section A.6.3.2.1, *SAS2H Fuel Depletion Benchmark Evaluation*, to justify using best-estimate correction factors without adjusting for uncertainty. Additionally, revise this section to justify crediting absorber isotopes with small numbers of radiochemical assay samples for depletion code validation.

Table A.6-10 of the application contains both the mean correction factor and standard deviation, but the standard deviation does not appear to be included to adjust the final isotopic correction factors for uncertainty. The isotopic correction factors should be adjusted to include the uncertainty, or this section should be revised to justify not doing so. Additionally, some credited isotopes have small numbers (i.e., less than 30) of radiochemical assay measurements used for depletion code validation. These small data sets should be subjected to a normality test to determine if the resulting isotopic correction factor values should be adjusted based on uncertainties determined using small-sample statistics.

Response to 6-3

Proprietary Information Withheld Pursuant to 10 CFR 2.390

Appendix A.6, Section A.6.3.2.1 is revised to include the uncertainty evaluation.

6-4 Revise Section A.6.3.2.1, *SAS2H Fuel Depletion Benchmark Evaluation*, to include a trending analysis of the SAS2H calculated correction factors independent of the DARWIN scaling factor adjustment.

Table A.6-10 of the application presents single values of the TN SAS2H average correction factor, with no dependence on trending parameters important to the depletion analysis (e.g., burnup or enrichment). Section A.6.3.2.1 should be revised to include a trending analysis which demonstrates that the average correction factors do not have significant trends, or they should be adjusted to account for trends.

Response to 6-4

The SAS2H isotopic correction factors (ICFs) are independent of sample enrichment and burnup. Plots of ICFs against their burnup-to-enrichment (BE) ratios are made and described in Appendix A.6, Section A.6.3.2.1 of the SAR. The plots are given in Figure A.6-8 with the associated values shown in Table A.6-37.

6-5 Revise Section A.6.3.2.1, *SAS2H Fuel Depletion Benchmark Evaluation*, to clarify how the isotopic scaling factors from DARWIN benchmarks were calculated, and how these scaling factors were applied to the SAS2H isotopic correction factor results.

The second paragraph on page A.6-17 of this section states that "A set of correction factors, based on the average ratios (DARWIN/SAS2H) for all three assembly types, was determined and these factors are shown in Table A.6-11." It is not clear, however, exactly how these correction factors were determined. Additionally, it is not clear how the isotopic scaling factors determined from the DARWIN calculations were used to adjust the SAS2H correction factors. This section should be revised to clarify these two issues.

Response to 6-5

Proprietary Information Withheld Pursuant to 10 CFR 2.390

Appendix A.6, Section A.6.3.2.1 is revised to provide this clarification.

Unless otherwise stated, the following information is required in order for the staff to ensure that the Model No. TN NUHOMS® MP-197 package will meet the criticality safety

requirements of 10 CFR 71.55 and 10 CFR 71.59 when loaded with the contents described in the application.

6-6 Revise Section A.6.3.2.2, *CSAS25 Criticality Benchmark Evaluation*, to justify that the critical benchmarks sufficiently cover the burnup range modeled in the criticality calculations.

For applicability of the critical benchmark experiments, this section claims that the highest "credited" burnup corresponds to the lowest burned axial segment of the highest average burnup assembly, or 26.2 GWd/MTU at the top end of a 50 GWd/MTU assembly average burnup. In fact, the analysis is "crediting" the highest burned sections of the fuel as well, which may be significantly above the 50 GWd/MTU assembly average. This section should be revised to justify that the critical benchmarks sufficiently cover the burnup range modeled in the criticality calculations.

Response to 6-6

Proprietary Information Withheld Pursuant to 10 CFR 2.390

6-7 Revise Section A.6.3.4.1.2, *Single Fresh Assembly Misload Evaluation*, to justify the basket type and fuel assembly placement chosen for this evaluation.

This section states that the NUHOMS-32PT DSC basket is used for the evaluation due to low number of poison plates, but does not demonstrate that this is the most reactive case. Provide an analysis of a similar misload in another canister (e.g., 37PTH) to demonstrate that the 32PT is the most sensitive to a misload. This section also states that the misload evaluation is performed with the misloaded assembly in periphery of basket where there is no poison plate. This section should be revised to justify that this assumption is conservative compared to placing assembly in the center of basket. Additionally, this section does not state what the enrichment of the fresh assembly used in the evaluation is. Revise the application to provide this information. Note that although the basket may be administratively limited in the enrichment of the assembly that can be loaded, there may be higher enrichment fuel available in the pool for misloading. The misload analysis should consider the maximum reactivity assembly that may be misloaded.

Response to 6-7

Proprietary Information Withheld Pursuant to 10 CFR 2.390

This is discussed in Appendix A.6, Section A.6.3.4.1.2 of the SAR.

6-8 Revise Section A.6.3.4.1.3, *Multiple Underburned Assemblies Misload Evaluation*, to state why Yankee Rowe, San Onofre 1, Haddam Neck, Maine Yankee, Zion 1 & 2, Indian Point 1, Rancho Seco, and Trojan were excluded from the misload evaluation.

It is not clear that these assembly types are specifically excluded as allowable contents in the NUHOMS-MP-197 package.

Response to 6-8

Proprietary Information Withheld Pursuant to 10 CFR 2.390

This is discussed in Appendix A.6, Section A.6.3.4.1.3 of the SAR.

6-9 Revise Section A.6.3.4.1.3, *Multiple Underburned Assemblies Misload Evaluation*, to justify the basket type chosen for the misload evaluation.

This section states that the NUHOMS-32PTH1 DSC Type C basket is used for the misload evaluation as it is the most common in use. This analysis should consider the basket that is likely to be most sensitive to such a misload. Note that for the single fresh assembly evaluation, the NUHOMS-32PT was considered to be the most sensitive due to the low number of poison plates. Note also that although the 32PTH1 DSC may be the most common PWR canister in use today, this may not be the case in the future as utilities transition to higher density cask systems.

Response to 6-9

Proprietary Information Withheld Pursuant to 10 CFR 2.390

This is discussed in Appendix A.6, Section A.6.3.4.1.3 of the SAR.

6-10 Revise the application to include a reduction in the reactor record burnup value by the uncertainty in that value.

It is not clear that uncertainties in reactor record burnup values are included when evaluating whether or not candidate fuel assemblies meet the appropriate loading curve burnup value. Interim Staff Guidance-8 (ISG-8), Revision 2, *Burnup Credit in the Criticality Safety Analyses of PWR Spent Fuel in Transport and Storage Casks*, recommends that the assembly burnup value to be used for loading acceptance (termed the assigned burnup loading value) should be the confirmed reactor record value as adjusted by reducing that value by its associated uncertainty.

Response to 6-10

The uncertainty associated with burnup and enrichment to evaluate the candidate fuel assemblies against the requirements of the burnup loading curve is not included in the criticality analysis. However, the loading requirements shown in SAR Table A.1.4.2-7 for the 32PT DSC, Table A.1.4.3-8 and Table A.1.4.3-8A for the 24PTH DSC, Table A.1.4.4-8 and Table A.1.4.4-8A for the 32PTH DSC, Table A.1.4.5-8 and Table A.1.4.5-8A for the 32PTH1 DSC and Table A.1.4.6-6 for the 37PTH DSC include the recommended considerations for uncertainty. These requirements are shown below:

"Use burnup and enrichment to lookup minimum cooling time in years. Licensee is responsible for ensuring that uncertainties in fuel enrichment and burnup are conservatively applied in determination of actual values for these parameters (uncertainty in enrichment to be added and uncertainty in burnup to be subtracted)".

6-11 For canister loading curves crediting 40 years of cooling, revise the application to include a transportation cooling time limit of 160 years, beyond which the package would need to be reevaluated for criticality safety prior to transportation.

ISG-8 contains a maximum cooling time credit of 40 years, due to the fact that reactivity will decrease after this point until about 100 years, and then rise again to roughly the same reactivity at about 200 years. At the time ISG-8 was published, this transportation window of between 40 to 200 years was considered sufficient to allow transportation of most spent fuel. The NRC has recently undertaken an effort to identify issues related to potential long-term storage of dual-purpose spent fuel storage casks and transportation packages, considering a potential storage time frame of 300 years or more. Given this recent focus on long-term storage, staff considers it prudent to condition spent fuel transportation package certificates of compliance to require a re-evaluation of burnup credit if fuel is in storage for a period of time in which the reactivity may be higher than when originally evaluated.

Response to 6-11

The SAR (Appendix A.1.4.2 through Appendix A.1.4.6) is revised to include a cooling time limit of 160 years for DSCs where burnup credit is applied to the criticality evaluations.

6-12 Revise the damaged fuel configuration for the NUHOMS-61BT DSC to consider rod pitch expansion and loss of rods from the lattice.

Rod pitch expansion and loss of rods from the fuel lattice was considered for every other DSC for which damaged fuel is an allowable content, and was shown to be the most reactive condition of the damaged fuel. The NUHOMS-61BT criticality analysis appears to consider only single- and double-ended rod shear in the damaged fuel criticality analysis. The application should be revised to either demonstrate that these two configurations are more reactive for the NUHOMS-61BT DSC, or revise the evaluation to consider rod pitch expansion and loss of rods from the lattice, consistent with the other DSC damaged fuel evaluations.

Response to 6-12

Proprietary Information Withheld Pursuant to 10 CFR 2.390

6-13 Revise the application to clarify the damaged fuel configuration for the WE 14x14 class fuel assemblies in the NUHOMS-32PTH/32PTH1 DSC.

Section A.6.5.4.4.2.C discusses the determination of the most reactive WE 17x17 class damaged fuel assembly, but does not include a similar evaluation of the WE 14x14 class fuel assembly. Without such an analysis, it is unclear how the WE 14x14 assembly class acceptable average initial enrichment and burnup combinations for damaged fuel, given in Table A.6.5.4-15, were determined. The application should be revised to show how damaged WE 14x14 class fuel assemblies were modeled in the criticality analysis. Note that this information may also be necessary to clarify the modeling of damaged WE 14x14 class fuel assemblies in the NUHOMS-24PTH and -37PTH DSCs.

Response to 6-13

Proprietary Information Withheld Pursuant to 10 CFR 2.390

Proprietary Information Withheld Pursuant to 10 CFR 2.390

6-14 Revise this section of the application to clarify the number of damaged fuel assemblies allowed to be shipped in the 24PTH DSC. Additionally, clarify whether or not CE 16x16 fuel assemblies are intended as allowable contents.

Section A.6.5.5.2 of the application, *Package Fuel Loading*, states that "a maximum of 8 damaged and remaining intact (for a total of 24) PWR fuel assemblies can also be transported within the NUHOMS-24PTH DSC. Section A.6.5.5.3 of the application, *Criticality Results*, states that the DSC can transport "up to 12 damaged (up to 8 failed)" fuel assemblies. The application should be revised to be consistent in all sections that discuss damaged/failed fuel. Additionally, Table A.1.4.3-2 of the application does not list CE 16x16 fuel assemblies as allowable contents, while they are listed in the loading curves described in Tables A.6.5.5-9 and A.6.5.5-10 of the application. The application should be revised to clarify whether or not CE 16x16 fuel assemblies are intended as allowable contents.

This information is needed to ensure that the contents of the Model No. TN NUHOMS MP-197 package are adequately described, per the requirements of 10 CFR 71.33.

Response to 6-14

A maximum of 12 damaged assemblies are allowed for transport within the 24PTH DSC. SAR Appendix A.6.5.5, Section A.6.5.5.2 is revised to provide this clarification.

CE 16x16 class fuel assemblies are not authorized for transport within the 24PTH DSC. The SAR is revised to delete all references to CE 16x16 class fuel assemblies in Appendix A.6.5.5 and Appendix A.1.4.3.

6-15 Revise the application to clarify the loading requirements for damaged fuel in the NUHOMS-24PTH DSC.

Table A.6.5.5-10 provides the acceptable average initial enrichment and burnup combinations for damaged fuel loaded in the NUHOMS-24PTH DSC. It is not clear, however, if these limits are applied to the damaged fuel only, or for all fuel in the DSC when damaged fuel is loaded. The application should be revised to clarify the damaged and intact fuel loading requirements.

This information is needed to ensure that the contents of the Model No. TN NUHOMS MP-197 package are adequately described, per the requirements of 10 CFR 71.33.

Response to 6-15

For the 24PTH DSC, the limits shown in Table A.6.5.5-10 are applicable to all fuel assemblies (intact, damaged and failed) whenever damaged and/or failed assemblies are loaded.

The SAR is revised to provide this clarification in Appendix A.6.5.5 and Appendix A.1.4.3.

PACKAGE OPERATIONS

7-1 Provide technical justification that Chapter 7 and Chapter 8 are not required to be referenced in their entirety in the CoC.

The applicant marked only part of the Operating Procedures and Acceptance Tests and Maintenance Programs as conditions of the CoC. The staff reviewed the proposed justifications and they are not sufficient. In particular, given the potential aging of the materials used in the cask because of prolonged storage before shipment, the entire Operating Procedures and Acceptance Tests and Maintenance Programs are required as conditions in the CoC. The example the applicant provided as rationale for not including the entirety of Chapter 7 and 8 is not relevant and not the common practice (see NUREG-1617, Section 8.2.4; NUREG-1609, Section 7.5; and ISG-20).

This information is needed for the staff to determine if the package design meets the regulatory requirements of 10 CFR 71.47, 71.85, and 71.87.

Response to 7-1

Chapters A.7 and A.8 have been revised and now may be referenced in their entirety in the CoC.

For this licensing action, CoC mark-ups of suggested changes have been provided informally, as a courtesy, to the NRC staff via the project manager. Changed CoC mark-ups reflecting these Chapters A.7 and A.8 changes will be provided informally, as a courtesy, as before.

7-2 Modify Chapter 7, A.7.1.5 to add dose rate measurements and calculation of Transport Index as part of the procedures.

Section A.7.1.5 of the SAR defines the operating procedures for the NUHOMS MP-197 packages. However, it appears that the dose rate measurements and calculation of the Transport Index were not included in the operating procedures. The applicant is requested to revise Chapter 7 of the SAR to add dose rate measurements and calculation of Transport Index as part of the procedures.

This information is needed for the staff to determine if the package design meets the regulatory requirements of 10 CFR 71.47, 71.83, and 71.87.

Response to 7-2

Chapter 7, Section 7.1.5 has been updated to include all required pre-shipment radiation measurements. However, similarly to Section A.7.1.4 of Chapter A.7, no Transport Index is calculated. Because this is an exclusive use shipment, the TI is assumed to be greater than 10 and is not required under 10CFR 71.47 (b).

ACCEPTANCE TESTS AND MAINTENANCE PROGRAM

8-1 Provide evaluations of the neutron shielding material that include radiation effects as well as thermal effects in combination.

RAI 8-2, provided previously, requested test results that demonstrate the neutron shield will not degrade over time. Radiation from the package contents will also affect the neutron shielding material. The response did not include results of evaluations/tests for radiation effects combined with thermal effects. This information is important in understanding the neutron shield performance over time. Additionally, the application should address a time frame of greater than 20 years, since the canisters loaded with spent fuel could be in storage for a longer period of time. Otherwise, a neutron shield maintenance test of adequate periodicity should be included in Chapter A.8 of the application due to the possible use of a package for greater than 20 years.

This information is needed for the staff to determine if the package design meets the regulatory requirements of 10 CFR 71.83 and 71.87.

Response to 8-1

The neutron shielding material, VyalB is a thermosetting matrix with hydrogen content, infusible, water resistant and temperature resistant. The cross linking of the polymer leads to a rigid 3 dimensional lattice, solid and resisting to transport or storage conditions. Mineral fillers include alumina trihydrate and zinc borate, providing hydrogen, boron (neutron capture) and good fire resistance.

The neutron shielding material has been subjected to considerable testing in order to demonstrate its long-term performance. The testing has included both nuclear and thermal testing with attention paid to long term effects as one of the uses for this material is in storage casks. This testing is described in Enclosure 10 , a presentation made to the ASTM C26 committee in 2008.

The thermal testing included long term tests at elevated temperatures to evaluate thermal degradation. These tests, as described in Enclosure 10, showed a thin layer of oxidized material formed at the surface of the test samples but no loss of hydrogen or mechanical damage below the oxidized layer. Surface cracks appeared after long-term testing at 170° C but not at the long term operating limit of 160° C. These tests and other described demonstrate that the thermal capability of VyalB exceeds the requirements imposed by the MP197HB design.

Tests of the ability of VyalB to withstand a radiation environment were also conducted and are described in Enclosure 10. The mechanisms of radiation degradation of neutron shielding materials can include breaking of the main polymer chain, cross linking, production of unsaturated bonds and oxidization. Testing results show that degradation starts at more than 10^{15} n/cm^2 fast neutron fluence, corresponding to a dose of 10^6 Gy. This fluence is far greater than the shielding material would experience when used in a transport cask application where the fluence level for is expected to be approximately 10^{11} n/cm^2 after 40 years of continuous use.

Based on results of the thermal and radiation testing, it can be concluded that VyalB will provide sufficient shielding when subjected to long term exposure to both environments since the effects of either (especially neutron fluence) are minimal.

Note also that this application is for a transport cask where the exposure to either neutron fluence or elevated temperatures is limited. Thus long-term test results translate to extremely long transport cask lifetimes.

Enclosure 15 to TN E-30577

IAEA-TECDOC-1410, *Delayed hydride cracking in zirconium alloys in pressure tube nuclear reactors,* October 2004, (associated with RAI 2-7)

IAEA-TECDOC-1410

Delayed hydride cracking in zirconium alloys in pressure tube nuclear reactors

Final report of a coordinated research project
1998–2002

IAEA
International Atomic Energy Agency

October 2004

IAEA-TECDOC-1410

Delayed hydride cracking in zirconium alloys in pressure tube nuclear reactors

Final report of a coordinated research project
1998–2002

IAEA
International Atomic Energy Agency

October 2004

The originating Section of this publication in the IAEA was:

Nuclear Power Technology Development Section
International Atomic Energy Agency
Wagramer Strasse 5
P.O. Box 100
A-1400 Vienna, Austria

DELAYED HYDRIDE CRACKING IN ZIRCONIUM ALLOYS IN PRESSURE TUBE NUCLEAR REACTORS
IAEA, VIENNA, 2004
IAEA-TECDOC-1410
ISBN 92–0–110504–5
ISSN 1011–4289

Printed by the IAEA in Austria
October 2004

FOREWORD

This report documents the work performed in the Coordinated Research Project (CRP) on Hydrogen and Hydride Degradation of the Mechanical and Physical Properties of Zirconium Alloys. The Project consisted of hydriding samples of Zr-2.5 Nb pressure tube materials used in CANDU-type and RBMK reactors, the measurement of delayed hydride cracking (DHC) rates under specified conditions, and analysis of hydrogen concentrations. The project was overseen by a supervisory group of experts in the field who provided advice and assistance to the participants as required.

All of the research work undertaken as part of the CRP is described in this report, which includes a review of the state of the art in understanding crack propagation by DHC and details of the experimental procedures that produced the most consistent set of DHC rates reported in an international round-robin exercise to this date. All of the participants and many of their co-workers in the laboratories involved in the CRP contributed results and material used in the drafting of this report, which contains compilations of all of the results, their analysis, discussions of their interpretation and conclusions and recommendations for further work.

The research was coordinated in three laboratories in industrialized Member States and seven laboratories in developing Member States. Besides the basic goal of transfer of "know-how" at the laboratory level from some experienced laboratories and the supervisory group to those starting off in the field, the CRP was set up to harmonize experimental methodologies in an attempt to produce consistent data sets, both in the results from a particular laboratory and from one laboratory to another. DHC is sensitive to the local microstructure and internal stress in the area of the crack tip as well as to the temperature history and stress state of the sample. Thus it was clear from the outset that to obtain consistency in the results and their interpretation from laboratory to laboratory, it would be necessary for each participant to work with samples of the same, well-characterized materials and to develop and follow a standard set of experimental protocols.

The basic scope of the programme was originally formulated by the IAEA with the help of the supervisory group in March 1998. It was based on the materials and experimental procedures developed over several decades at the host laboratory of the CRP, the Chalk River Laboratories (CRL) of Atomic Energy of Canada Limited (AECL). The CRP began formally with the signing of contracts and agreements in the second half of 1998. The first research coordination meeting (RCM) was held in December 1998. At this RCM, standard compact tension samples and rings cut from a single CANDU Zr-2.5Nb pressure tube were given to each participant together with detailed instructions for the measurement of DHC and for hydriding samples to a given target concentration. The second RCM was held in Pitesti, Romania, in June 2000 and at that meeting each participant was given a ring of RBMK channel tube material, kindly provided by the Lithuanian participant, for testing within the framework of the CRP. Later in 2000, each participant was provided with a bottle containing 10 standard pellets of Zr-2.5Nb material provided by the host laboratory for hydrogen analysis in a round-robin exercise. The third and final RCM was held in July 2002 in Studsvik, Sweden. Supervisory group meetings were also held at appropriate times to review the results obtained. The CRP was completed and documented at the end of 2002.

The IAEA wishes to thank all of the participants in the CRP for their contributions to this publication. In particular, the IAEA is grateful to the host laboratory (CRL, Canada) that generously provided most of the materials and standard samples for testing during the CRP.

Special thanks are also due to C.E. Coleman (AECL, Canada) who represented the host laboratory and led the supervisory group and to M. Roth (Pitesti, Romania) and V. Grigoriev (Studsvik, Sweden) for their outstanding contributions to the CRP in organizing the RCMs at their institutes. The IAEA officer responsible for this publication was I.G. Ritchie of the Division of Nuclear Fuel Cycle and Waste Technology.

EDITORIAL NOTE

CONTENTS

CHAPTER 1

INTRODUCTION

Zirconium alloys are used in water reactors because of their low capture cross-section for thermal neutrons and good mechanical and corrosion properties. Early in their application, hydrogen was identified as an embrittling agent. The source of the embrittlement was hydride precipitates that formed as platelets [1.1] Usually, low ductility was found below about 150°C with impact testing or in tensile testing when the normal to the hydride plates was parallel to the tensile stress. Much effort was expended in keeping the hydrogen concentration low and ensuring that any hydrides were in a benign orientation. Results from a few laboratory experiments hinted that zirconium alloys may also fracture by a time-dependent mechanism involving hydrogen, but the first practical confirmation of such a mechanism was the cracking of experimental fuel cladding made from Zr-2.5 Nb [1.2]. Cracks were found in the heat-affected zone in the weld between the cladding and its end-cap after several months of storage at room temperature. Hydrides were associated with the cracks and the process was called Delayed Hydride Cracking – DHC.[1] A factor contributing to the fracture was high residual tensile stress from the welding.

Later, high residual stresses were shown to be responsible for DHC in Zr-2.5 Nb pressure tubes. In CANDU, the pressure tubes are about 6 m long, 104 mm inside diameter and 4 mm thick and are made from cold-worked material. They are joined to the reactor at their ends by a mechanical joint. The tube end is placed inside a thick-walled tube of 403 stainless steel containing three internal, circumferential grooves and the pressure tube is internally rolled to make a seal at the grooves; this configuration is called a rolled-joint. If the rolls are advanced too far, part of the pressure tube is deformed without support from the stainless steel and large residual tensile stresses, up to 700 MPa, arise. Consequently, cracks may initiate. When a crack penetrates the tube wall, heat-transport water leaks and is detected, and the reactor is shutdown. Once the leaking tubes are identified, they are removed and replaced. Twenty tubes out of 780 in Pickering Units 3 and 4 leaked [1.3]. The cracks initiated on the inside surface and grew by DHC radially and axially in a series of bands, Fig. 1.1. The interpretation was that the cracks grew at low temperatures by DHC, but once the reactor was at power and the pressure tubes were at a high temperature, >250°C, cracking stopped because the low hydrogen concentration, <15 ppm, was all in solution. The crack surface oxidized. Cracking continued during subsequent reactor shutdowns and the stopped crack continued to oxidize during power production. Each band on the fracture surface corresponded with a reactor shutdown and period of operation, with cracking at the expected rates for DHC at the temperature of the shutdown [1.4]. To prevent further occurrences of such cracking, depending on the reactor, the residual stresses were minimized by stress-relief or redesign of the rolled-joint [1.5].

Cracking in the pressure tubes in RBMK reactors had a similar cause. These tubes have a length of about 8 m, an inside diameter of 80 mm and a wall thickness of 4 mm, and the Zr-2.5 Nb is partly recrystallized. The final stage of fabrication involved straightening that induced residual tensile stresses of about 350 MPa. Twenty tubes out of a population of 20,000 leaked because of cracking by DHC initiated on the outside surface. Most of the failures were in the first two years of operation of the Kursk and Chernobyl reactors [1.6].

[1] In the literature on zirconium alloys, the time-dependent cracking involving hydrogen has had several names but the accepted one is delayed hydride cracking or DHC.

Similar cracking was observed in guide tubes. Stress relief after straightening has prevented further cracking.

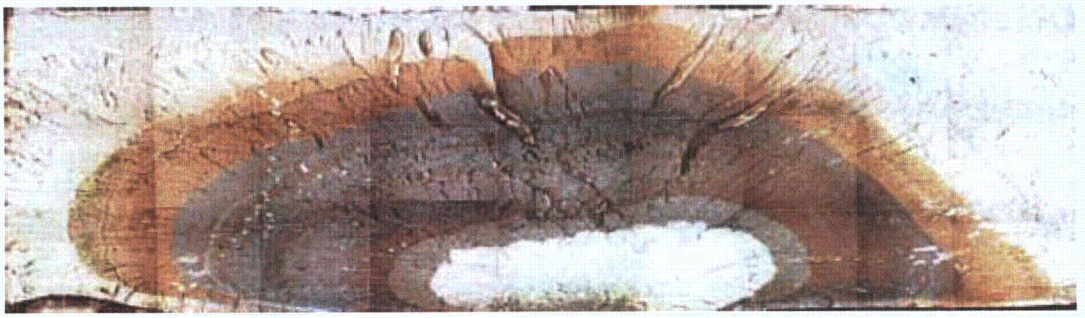

Fig. 1.1. Through-wall crack in a CANDU Zr-2.5 Nb pressure tube, showing oxidized crack growth bands. The crack initiated at the inside surface just inboard of the rolled joint.

These failures prompted much research on the phenomenology and mechanisms of DHC in zirconium alloys. Although no new cracks have been observed in CANDU or RBMK reactors during the past 18 years, as the reactors age the spectre of DHC looms because of increasing hydrogen concentration from corrosion and potential mechanical damage to the surfaces of the pressure tubes. Thus constant vigilance is required. The results of the research are used to determine the life of the pressure tubes due to both crack initiation and subsequent DHC propagation. Should a crack initiate and penetrate the tube wall, water leaking from the through-wall crack is detected and the reactor must be capable of being shut-down before the critical crack length is reached and the pressure tube ruptures. This sequence is the basis for Leak-Before-Break (LBB) [1.7]. The values required to support LBB are knowledge of the length of the crack at leakage, the critical crack length for rupture and the velocity of DHC in the axial direction of a tube. The latter quantity is the focus of this project. The IAEA set up a co-ordinated research programme (CRP) on Hydrogen and Hydride Induced Degradation of the Mechanical and Physical Properties of Zirconium-based Alloys the objective of which was to transfer "know-how" on laboratory practices to member states who have pressure tube reactors but were unfamiliar with DHC testing. The participating Institutes in the CRP are listed in Table 1.1[2]. The major goal of the programme was to establish a uniform and consistent laboratory practice to determine the DHC velocity in the axial direction of pressure tubes to be followed internationally so that meaningful inter-laboratory comparison of the results could be made. Two reference materials were tested – CANDU cold-worked Zr-2.5 Nb and RBMK Zr-2.5 Nb in the TMT-1 heat-treated condition. Participants were encouraged to test examples of their own material for comparison with the reference materials.

As an extension of this CRP, preliminary development of a test method for fuel cladding is in progress [1.8]. In some Zircaloy nuclear fuel cladding used in boiling water reactors (BWR), hydride cracking is strongly implicated in long splits that allowed substantial leakage of fission products [1.9–1.11]. Cladding in BWRs is usually a tube with diameter of about

[2] The names of the participating Institutes and their usual acronyms are given in the list of Contributors, page 101. For simplicity in the text participants are simply referred to by their country and the Republic of Korea is given as ROK.

TABLE 1.1 Participating Institutes, countries and their reactor types of interest

INSTITUTE[2]	COUNTRY	REACTOR TYPE
CNEA	Argentina	CANDU, PWR (D_2O moderated)
AECL	Canada	CANDU
NPIC	China	CANDU, PWR
BARC	India	Indian HWR
KAERI	ROK	CANDU, PWR
LEI	Lithuania	RBMK
PINSTECH	Pakistan	CANDU
INR	Romania	CANDU
VNINM	Russia	RBMK, WWER
STUDSVIK	Sweden	BWR, PWR, surveillance on RBMK

10 mm, wall thickness of about 0.6 mm and length of about 4 m. The Zircaloy is usually recrystallized and in some designs of fuel rod the inside surface is lined with another zirconium alloy or pure zirconium, to prevent stress corrosion cracking by fission products, such as iodine [1.12]. If the cladding wall is penetrated during operation, for example by fretting, water from the heat-transport system can enter the fuel cavity where, because of the low pressure, steam is produced. Much hydrogen is generated because the steam oxidizes the fuel and the inside surface of the cladding, reducing the partial pressure of oxygen and leaving a gas rich in hydrogen. This process is called "oxygen starvation". At some distance from the primary defect the gas stream becomes almost pure hydrogen, and with break down of the protective oxide layer, copious quantities of hydrogen may be absorbed by the cladding [1.13]. Sometimes, "sunbursts" of hydride are formed on the inside surface. Although the pure Zr liner was often found to be completely corroded, and therefore contributed hydrogen to the inventory and stress through expansion via the oxide, it is not a necessary requirement for the secondary damage because unlined fuel cladding behaves in a similar manner. With fuel expansion during fuel shuffling, the hydrided cladding is stressed which leads to crack initiation. The cracks grow through-wall and may be over 1 m long. The fractures are characterized by brittle regions in "striations" or "chevrons", with the crack front often leading towards the outside surface of the cladding [1.14]. The lower bounds of the crack velocities were in the range 4×10^{-8} to 5×10^{-7} $m.s^{-1}$ based on assuming constant growth rates in the time between first detection of the defect and removal of the fuel. The mechanism of cracking appears to be a form of DHC [1.10, 1.15] perhaps exacerbated by a continuous additional supply of hydrogen from the steam inside the fuel element [1.16]. Careful reactor core management can mitigate the consequences of a primary defect by controlling the fuel expansion.

In this report, in Chapter 2 background to DHC is provided to show the technical basis for the test procedures, Chapter 3 describes the materials, specimen preparation and test methods, and an interlaboratory comparison of hydrogen analysis, the test results are discussed in Chapter 4, possible future work on fuel cladding is described in Chapter 5 while in Chapter 6 conclusions and recommendations are made.

REFERENCES TO CHAPTER 1

[1.1] MUDGE, W.L, Effect of hydrogen on the embrittlement of zirconium and zirconium-tin alloys, Symposium on Zirconium and Zirconium alloys, ASM, Metals Park, OH, (1953) 146–167.

[1.2] SIMPSON, C.J., ELLS, C.E., Delayed hydrogen embrittlement of Zr-2.5wt.%Nb, J. Nucl. Mater., **52**, (1974) 289–295.

[1.3] PERRYMAN, E.C.W., Pickering pressure tube cracking experience, Nucl. Energy, **17**, (1978) 95–105.

[1.4] CAUSEY, A.R., URBANIC, V.F., COLEMAN, C.E., In-reactor oxidation of crevices and cracks in cold-worked Zr-2.5 wt.% Nb, J. Nucl. Mater., **71**, (1977) 25–35.

[1.5] DUNN, J.T., KAKARIA, B.K., GRAHAM, J., JACKMAN, A.H., CANDU-PHW fuel channel replacement experience, AECL-Report, AECL-7538, Atomic Energy of Canada, Ltd., Sheridan Park, Mississauga, Ontario, (1982)

[1.6] PLATONOV, P.A., RYAZANTSEVA, A.V., SAENKO, G.P., KNIZHNIKOV, Y.N.,VIKTOROV, V.F., The study of the cause of cracking in zirconium alloy fuel channel tubes, Poster paper at ASTM Zirconium in the Nuclear Industry – 8th International Symposium, available as AECL report RC-87, (1988).

[1.7] MOAN, G.D., COLEMAN, C.E., PRICE, E.G., RODGERS, D.K., SAGAT, S., leak-before-break in the pressure tubes of CANDU reactors, Int. J. Press. Ves. Piping., **43**, (1990) 1–21.

[1.8] GRIGORIEV, V., JAKOBSSON, R., Application of the pin-loading tension test to measurements of delayed hydride cracking velocity in Zircaloy cladding, Studsvik Report SKI 00:57, (2000).

[1.9] JONSSON, A., HALLSTADIUS, L., GRAPENGIESSER, B., LYSELL, G., Failure of a barrier rod in Oskarshamn, in Fuel in the '90's, International Topical Meeting on LWR Fuel Performance, Avignon, France, ANS and ENS, (1991), 371–377.

[1.10] SCHRIRE, D., GRAPENGIESSER, B., HALLSTADIUS, L., LUNDHOLM, I., LYSELL, G., FRENNING, G., RONNBERG,G., JONSSON, A., Secondary defect behaviour in ABB BWR fuel, International Topical Meeting on LWR Fuel Performance, West Palm Beach, ANS, (1994) 398–409.

[1.11] ARMIJO, J.S., Performance of failed BWR fuel, International Topical Meeting on LWR Fuel Performance, West Palm Beach, ANS, (1994), 410–422.

[1.12] ARMIJO, J.S., COFFIN, L.F., ROSENBAUM, H.S., Development of zirconium-barrier fuel cladding, Zirconium in the Nuclear Industry – 10th International Symposium, ASTM STP 1245, eds, A.M. Garde and E.R. Bradley, ASTM, West Conshohocken, PA, (1994), 3–18.

[1.13] CLAYTON, J.C., Internal hydriding in irradiated defected Zircaloy fuel rods, Zirconium in the Nuclear Industry – 8th International Symposium, ASTM STP 1023, eds. F.P. Van Swam and C.M. Eucken, ASTM, West Conshohocken, PA, (1989), 266–288.

[1.14] LYSELL, G., GRIGORIEV, V., Characteristics of axial splits in failed BWR fuel rods, Ninth International Symposium on Environment Degradation of Materials in Nuclear Power Systems – Water Reactors, AIME-TMS, (1999), 1.169–1.175.

[1.15] EFSING, P., PETTERSSON, K., Delayed hydride cracking in irradiated Zircaloy cladding, Zirconium in the Nuclear Industry – 12th International Symposium, ASTM STP 1354, eds. G.P. Sabol and G.D. Moan, ASTM, West Conshohocken, PA., (2000), 340–355.

[1.16] EDSINGER, K., DAVIES, J.H., ADAMSON, R.B., Degraded fuel cladding fractography and fracture behavior, Zirconium in the Nuclear Industry – 12th International Symposium, ASTM STP 1354, eds. G.P. Sabol and G.D. Moan, ASTM, West Conshohocken, PA., (2000), 316–339.

CHAPTER 2

DELAYED HYDRIDE CRACKING TESTING – STATE OF THE ART

2.1. General Description of the Phenomenon

Delayed hydride cracking is a sub-critical crack growth mechanism occurring in zirconium alloys as well as other hydride-forming materials that requires the formation of brittle hydride phases at the tip of a crack and subsequent failure of that hydride resulting in crack extension. The basic process is illustrated in Fig. 2.1.

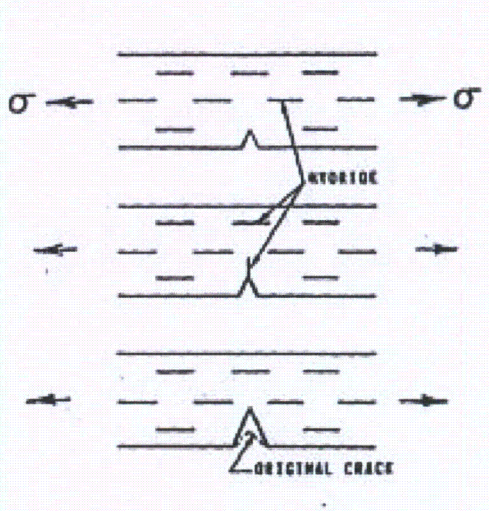

Fig. 2.1. A schematic illustration of a single step in DHC starting with a notch under stress (top), hydride precipitation at the notch (middle) and fracture of hydride and crack extension from the notch (bottom).

Hydrogen in solution in the zirconium alloy is transported to the crack tip by diffusion processes where it precipitates as a hydride phase. When the precipitate attains a critical condition, related to its size and the applied stress intensity factor, K_I, fracture ensues and the crack extends through the brittle hydride and arrests in the matrix. Each step of crack propagation results in crack extension by a distance approximately the length of the hydride. This step-wise progression may leave striations on the fracture surface corresponding to each step that can often be observed with a low power light microscope.

As with many other stable crack propagation mechanisms, the phenomenon of cracking can be generally described by the dependence of the crack growth rate or crack velocity on the applied stress intensity factor. The general shape of such a relationship has been shown to be similar to that demonstrated in many forms of environmentally assisted cracking and is illustrated in Fig. 2.2 [2.1, 2.2, 2.3]. This figure shows that, at stress intensities below a threshold, K_{IH}, cracks do not grow even though a quantity of hydride may accumulate at a crack tip under stress. In DHC, the transition to the plateau velocity portion of the velocity vs K_I curve is quite abrupt [2.4] and then the velocity does not change significantly with increasing K_I until the applied K_I approaches the fracture toughness corresponding to the initiation of unstable fracture for the material under test.

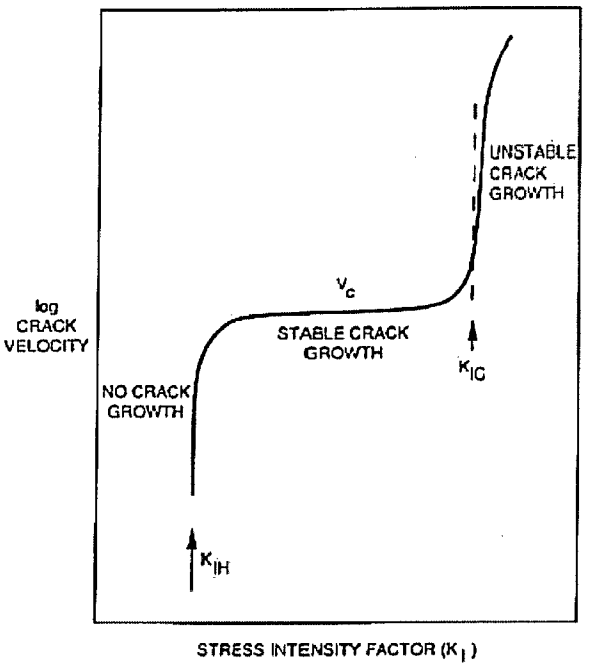

Fig. 2.2. A schematic representation of the relationship between crack velocity and stress intensity factor exhibited by the DHC phenomenon.

The velocity of the crack in the plateau region of the velocity-K_I curve has been found to have strong temperature dependence, as shown in Fig. 2.3. This temperature dependence reflects both the rate at which hydrogen in solution can be transported to the crack tip and the amount of hydride required to be formed for each fracture step in the propagation. Together, these determine the amount of hydrogen required to be transported per unit distance of crack growth The rate of transport of hydrogen to the crack tip is dependent upon the diffusion coefficient of hydrogen in the material, the amount of hydrogen available to be transported (the hydrogen dissolved in the metal) and the driving force for moving the hydrogen to the crack tip. Because the diffusion coefficient and the maximum amount of hydrogen available to be transported are both thermally activated phenomena, the crack velocity has the temperature dependence of a thermally activated process, decreasing with decreasing temperature.

The driving force for movement of hydrogen in solution to the crack tip is the gradient in the chemical potential of the hydrogen in solution that is determined by both the concentration and the stress state [2.5]. Hydrostatic tension reduces the chemical potential of hydrogen in solution in the material. Since the stress state near a crack tip under load is dependent upon the material yield stress, there is an expectation that the driving force can be higher in materials with higher yield strength. This would lead to a higher rate of diffusion of hydrogen to the crack tip and a higher crack velocity even if other factors (such as the amount of hydrogen required per unit length of crack extension) were unchanged.

These general features of the crack growth process were recognized in some of the initial studies of the phenomenon. However, understanding many of the details of the process remains an active area of investigation [2.6–2.10].

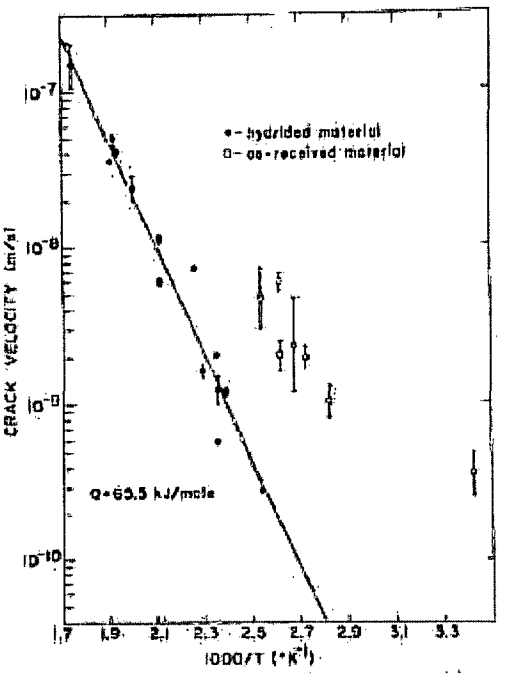

Fig. 2.3. The temperature dependence of the plateau in DHC velocity vs K_I [Ref. 2.4].

The amount of hydrogen dissolved in the metal and available for diffusion to the crack tip is a critical determinant of the cracking phenomenon. Some of the earliest experimental work on DHC, demonstrated that the upper temperature limit at which DHC could be observed corresponded closely with the temperature at which all hydrides could be dissolved on heating [2.11]. The hysteresis of the solubility of hydrogen in zirconium alloys [2.12–2.14], affects the crack growth rate that are relevant both to measurements of crack growth rates and to their prediction for the operating conditions of zirconium components in nuclear reactors. DHC crack growth rates have been observed to be dependent upon whether the crack growth temperature is approached by cooling or by heating [2.15]. These observations are a direct result of the hysteresis of the solubility of hydrogen in the material [2.16].

The purpose of this chapter is to review the phenomenon of DHC with emphasis on current understanding and how that understanding was used to establish a program of testing for this coordinated research project.

2.2. Models of DHC Cracking

The initial theoretical description of DHC was based on the model illustrated in Fig. 2.4 [2.2]. In this model, there is a hydride growing in the stress field of the crack tip.

The crack tip hydride grows due to the migration of hydrogen from hydrides in the bulk of the material at some characteristic distance from the crack tip. The driving force for the diffusion of the hydrogen is the difference in the chemical potential of hydrogen in the crack tip hydride due to the local hydrostatic stress field and the chemical potential of hydrogen in the hydrides under a reduced hydrostatic stress at the characteristic distance from the crack tip. Due to the positive partial molar volume of hydrogen in the hydrides, increasing tensile hydrostatic stress on a hydride reduces the chemical potential of hydrogen in that hydride. Therefore there exists

a chemical potential difference between hydrogen in the hydride at the crack tip compared with hydrogen in a hydride in the bulk. Assuming a condition of local chemical equilibrium of hydrogen at the interfaces between hydride and matrix, a chemical potential difference between these locations must exist for hydrogen in solution as well. This chemical potential difference drives the migration of the hydrogen in solution to the crack tip where it precipitates. In this model, the hydrides in the bulk dissolve to maintain the local hydrogen concentration in solution in the matrix at the hydride interface at the solubility limit for the temperature at which the cracking is occurring.

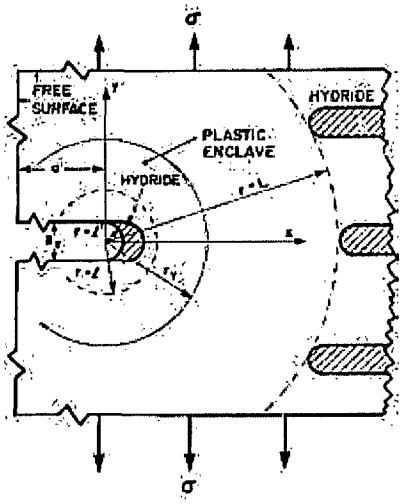

Fig. 2.4. The initial model for DHC developed by Dutton and Puls [Ref.2.2] showing the hydride growing at the crack tip and the hydrides in the matrix dissolving.

Assuming cylindrical symmetry about the crack tip, an expression for the crack velocity, V, according to this model was derived which had the following form:

$$V = G\, D_H C_H \{\exp({}^hV_H\, \Delta p/RT)$$

where:

- G is a function that includes geometry factors as well as the molar volumes of zirconium and hydride, and the composition of the hydride;
- D_H is the diffusion coefficient of hydrogen (a function of temperature);
- C_H is the solubility of hydrogen in zirconium in a stress-free state;
- ${}^hV_H$ is the partial molar volume of hydrogen in zirconium hydride;
- Δp is the difference in hydrostatic tensile stress between the crack tip and the bulk at a distance equal to the characteristic hydride spacing away from the crack tip;
- R is the gas constant; and
- T is the absolute temperature.

The dependence of the crack velocity on the diffusion coefficient and the solubility is explicit in this expression. The model assumed that the amount of hydride growth required for a given distance of crack growth was fixed and that the hydride growth could be assumed to be occurring continuously even though the process was recognized as being discontinuous in nature.

This model has been altered over the years but key features have been maintained. A major change in the model occurred when it was recognized that the assumed behaviour of the solubility of hydrogen in this model did not adequately reflect the observations and modeling of the phenomenon of hysteresis in the solubility of hydrogen in hydrogen-zirconium alloy systems. A revised model of DHC incorporating the hysteresis of the solubility was produced [2.17]. In this model, the hysteretic effects on the solubility of hydrogen are taken into account: there are two different expressions used for the solubility depending upon whether hydride is dissolving or precipitating. This model was able to provide some explanation for the different crack velocities obtained on heating and on cooling.

More recently, finite element modeling has been used to examine effects of temperature cycling and load changes on the accumulation of hydride at a flaw [2.18]. This model implicitly assumes different hydrogen solubility limits for dissolution and precipitation. It has been extended to account for the changing stress state at a flaw due to the formation of the hydride [2.19] and to model DHC velocities under temperature transients [2.20]. There are no simple expressions for crack velocities derived using these finite element models.

2.3. Hysteresis in the Solubility of Hydrogen in Zirconium

The observations of the behaviour of hydrogen in zirconium alloys indicate that there is a significant hysteresis in the solubility depending upon whether hydrides are dissolving or precipitating. These effects have been known for a long time [2.12, 2.13] and are seen using several techniques including differential scanning calorimetry, and measurements of changes in thermal expansion, electrical resistivity, and elastic modulus. In all cases, the effect is manifested as a difference between the concentration of hydrogen in solution in the metal in equilibrium with dissolving hydrides at a particular temperature and the concentration in equilibrium with precipitating hydrides at the same temperature. This is illustrated for Zircaloy material in Fig. 2.5 [2.21].

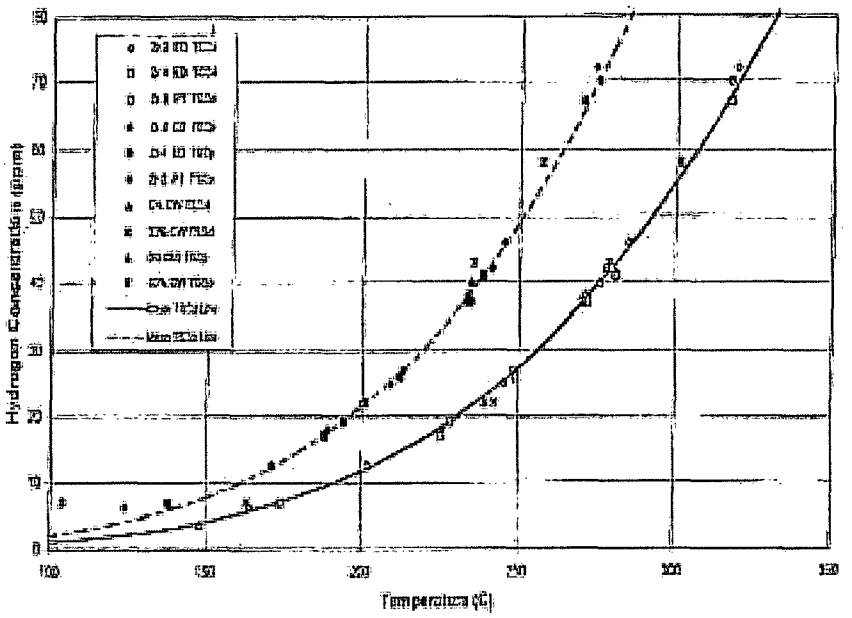

Fig. 2.5. The hysteresis in the solubility of hydrogen in Zircaloy observed using differential scanning calorimetry [Ref. 2.21].

These results were based on differential scanning calorimetry measurements of the zirconium-hydride transformation. Similar results have been obtained in Zr 2.5Nb alloys using elastic modulus measurements [2.14], (Figs 2.6 and 2.7). The modulus measurements clearly demonstrated that the amount of hydrogen in solution at a given temperature is dependent upon whether hydrides are dissolving or precipitating. Since the degree of modulus reduction is depends upon the amount of hydrogen in solution, by comparing the modulus at a given temperature with that in an unhydrided specimen, the amount of hydrogen in solution can be determined for each temperature. The complete solubility curve can be determined from a single specimen with sufficiently high hydrogen concentration. Such measurements have shown that the solubility limit associated with precipitation is itself dependent upon the thermal history of the specimen and two bounding solubility curves can be defined: one based upon precipitation of new hydrides (TSSP1) and the second based upon precipitation associated with growth of hydrides or precipitation at locations of pre-existing hydride (TSSP2).

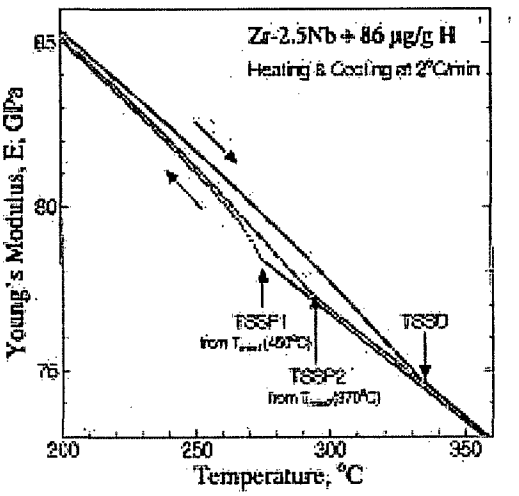

Fig. 2.6. Hysteresis in hydrogen solubility in Zr-2.5 Nb observed using dynamic elastic modulus measurements [Ref. 2.14].

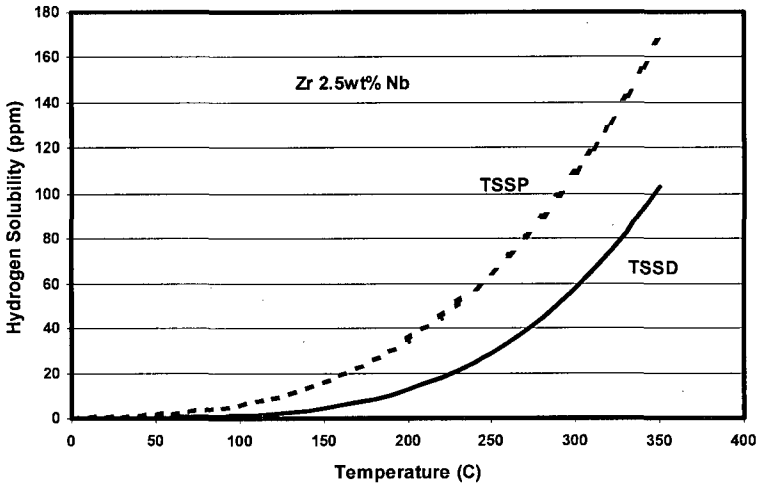

Fig. 2.7. The hydrogen solubility of Zr-2.5 Nb material measured using dynamic elastic modulus. The TSSP curve is that defined by TSSP1 in Reference 2.14.

The origin of this hysteresis is the internal stresses in the solid system developed during precipitation and dissolution of hydride caused by the 17% volume change associated with the transformation of alpha zirconium matrix to delta hydride [2.22]. If the system of hydrogen in zirconium with hydrides present could be completely stress free, (i.e. free of both internal and externally applied stresses), it would be expected that the equilibrium between hydrogen in solution and hydrogen in hydrides would be defined at a particular temperature by a single concentration of hydrogen in solution and this equilibrium would not be affected by the direction of approach in temperature to the temperature of interest. Some supersaturation could be required to nucleate hydrides on cooling due to the need to create new interfaces with characteristic surface energies. However, internal stresses develop within the system during the alpha zirconium to hydride transformation (and the reverse) and will be more intense near the hydrides themselves. These internal stresses and the plastic work associated with the formation and dissolution of hydrides are responsible for the solubility behaviour of hydrogen in zirconium alloys [2.23–2.25].

The solubility hysteresis appears to be very close to an equilibrium phenomenon because it is observed even when very slow heating and cooling rates are used or when material is charged with hydrogen isothermally [2.26]. If it is assumed that the solubility hysteresis is truly equilibrium behaviour, the chemical potential of hydrogen throughout the system can be assumed to be uniform at each temperature condition. The bulk concentration of hydrogen in solution away from the hydrides can be used as a measure of the chemical potential of hydrogen throughout the system at equilibrium. At a given temperature, the hydrogen concentration in solution in equilibrium with dissolving hydride is less that that in equilibrium with precipitating hydride. In this solid system with no externally applied stress, the chemical potential of hydrogen in a hydride undergoing dissolution is significantly lower than the chemical potential of hydrogen in a hydride that is precipitating.

It follows that non-equilibrium would exist if hydrides in a matrix were in another stress state. Chemical potential differences between hydrides in different stress states would produce local differences in the chemical potential of hydrogen in the surrounding matrices that would act to drive hydrogen towards the hydride in the higher tensile stress state.

The effect of thermal history on the concentration of hydrogen in solution of a specimen containing, for example, 60 ppm, can be illustrated by examining what occurs when the specimen is taken through a specific temperature sequence through heating and cooling. Referring to Fig. 2.8, as the temperature is increased from room temperature, the hydrogen concentration increases following the TSSD curve along AB. When the temperature begins to decrease, the concentration in solution is assumed not to change until the precipitation solvus is reached at point C. On further cooling, the concentration in solution drops following the precipitation solvus (TSSP) until point D. If the temperature is now increased again, the concentration in solution does not increase until the TSSD curve is reached. Consideration of similar temperature trajectories with different peak temperatures suggests that at a given temperature (such as the DHC test temperature), the concentration of hydrogen in solution in the bulk of the specimen could be made to vary from the TSSD concentration to the TSSP concentration. Thus the chemical potential driving force for DHC can be made to vary by changing the peak temperature attained immediately prior to the test temperature.

The difference in the stress states of the dissolving and precipitating hydrides causes the hysteresis. To change the stress state of a hydride from one state to the other, there must be a finite amount of hydrogen exchanged between the hydride and the matrix. Thus the assumption that the concentration in solution does not vary on cooling from the TSSD state to the TSSP state, i.e. along line BC in Fig. 2.8, cannot be strictly correct because a small change

in the concentration in solution is required to accommodate the hydrogen exchange between the matrix and the hydride necessary to change the stress state of the hydride.

2.4. Solubility Hysteresis and DHC Testing

Solubility hysteresis has very significant effects on DHC in zirconium alloys. The crack velocity and K_{IH} are both affected. These are discussed in turn.

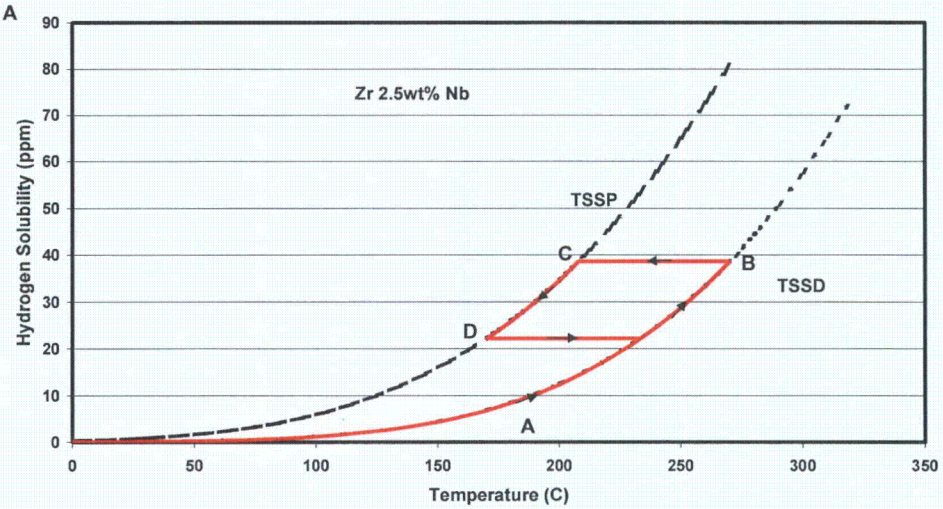

Fig. 2.8. The trajectory ABCD shows how hydrogen in solution varies during a temperature cycle.

For a DHC crack growing at isothermal conditions under a constant applied stress intensity, the rate of growth of the crack is determined by the chemical potential driving force for moving hydrogen to the crack tip from the surrounding material; the greater the chemical potential of hydrogen in the matrix, the higher the driving force and the larger velocity is a consequence. The corollary is that, at a given temperature, the DHC velocity may be a sensitive indicator of the chemical potential of hydrogen in the system.

This expectation is consistent with the observed behaviour in cracking tests. The crack velocity can be very sensitive to the precise thermal history of the test specimen immediately prior to the DHC crack growth test [2.15, 2.27]. Shek and Graham's result is shown in Fig. 2.9. In these tests, crack growth rates in unirradiated Zr-2.5 Nb specimens containing 60 ppm of hydrogen were measured at 250°C. Each specimen was heated to a different peak temperature before cooling to the test temperature. There are very large differences in the observed crack velocities with the highest velocities being obtained in specimens in which the hydrogen was all taken into solution at the peak temperature. The presence of hydrides in the bulk of the material is not a sufficient condition for cracks to grow with a measurable velocity by DHC: hydrides would certainly have been present in the bulk material for tests in which the peak temperature was simply the test temperature of 250°C and yet there was no indication of crack growth during the test. This result implies that the chemical potential of hydrogen in the system was too low to produce sufficient hydride at the crack tip to reach the critical state for fracture of the hydride. This result is also clear proof that the critical stress intensity factor for crack propagation is dependent upon the chemical potential of hydrogen in the system since no crack growth was observed at peak temperatures at or below 262°C.

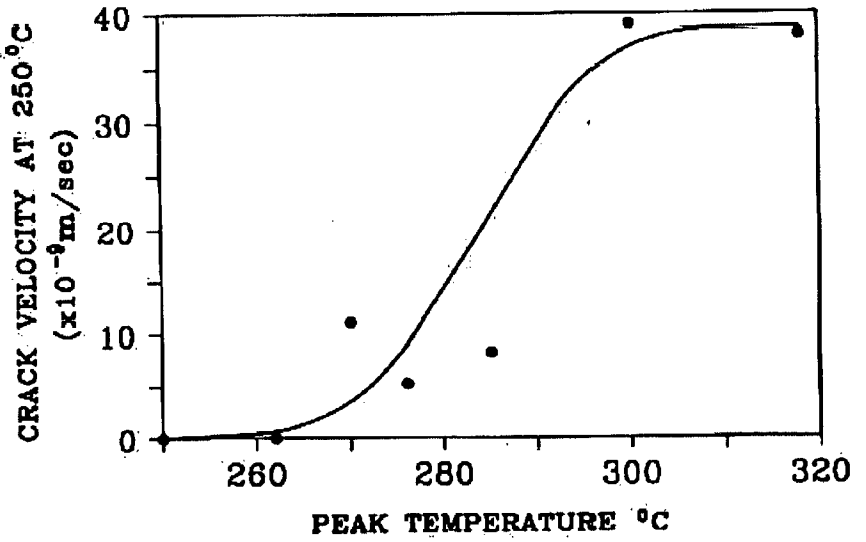

Fig. 2.9. DHC velocity measurements at 250℃ in CANDU pressure tube material showing the effect of peak temperature before testing [Ref. 2.27].

The DHC velocity measured at a test temperature will be the highest possible for that particular specimen at the test temperature when the concentration in solution (and hence the chemical potential of hydrogen in the bulk material) is maximized. Maximization for a particular specimen occurs either if all the hydrogen is in solution at the test temperature or if the hydrogen concentration in solution corresponds to the precipitation solvus. To find the maximum possible DHC velocity for a material, independent of the hydrogen concentration, there must be sufficient hydrogen in the specimens to achieve the precipitation solvus concentration at the test temperature and the thermal history of the sample must ensure that the concentration in solution is at the precipitation solvus level.

Figure 2.10 [2.16, 2.28] illustrates schematically the effects of solubility hysteresis on measure-ments of DHC crack velocities. For a specimen with a specific hydrogen concentration, the velocities can be measured after achieving the test temperature either through heating or cooling. If the specimen is heated to sequentially higher test temperatures, the velocities follow a profile similar to that described by $T_1T_2T_3T_4$. The maximum velocity occurs at T_2. When the velocities are measured after cooling from temperature T_4, the velocities follow the profile given by $T_4T_5T_6T_2$. The velocity at T_6 is the maximum for the specimen and this velocity is only achieved by cooling to T_6 from a sufficiently high temperature, T_4, such that all hydrogen was taken into solution. The decrease in velocity on heating above T_2 reflects a decreasing driving force since the total hydrogen available for transport continues to increase with increasing temperature. On cooling from T_4, the crack can grow at T_5 because there is now sufficient driving force to precipitate hydride at the crack tip in sufficient quantity to cause cracking. Upon further cooling to T_6, the velocity increases due to an increased driving force as the concentration of hydrogen required to precipitate at the crack tip decreases with temperature decrease, but the concentration in solution in the bulk material remains constant (all hydrides in the bulk dissolved).

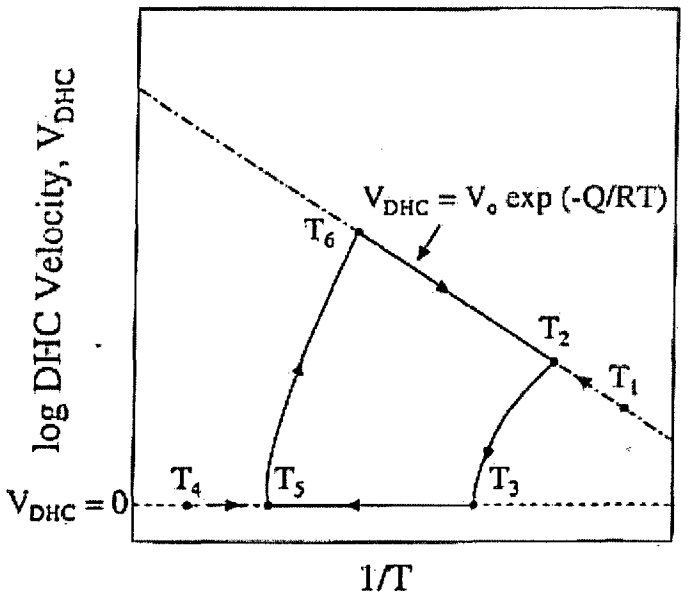

Fig. 2.10. A schematic diagram of the temperature dependence of the DHC velocity showing the effect of temperature history [Refs. 2.16, 2.28].

The schematic diagram makes it clear that the crack velocity is very dependent on the path of the temperature history immediately prior to the velocity measurement. It can be shown by consideration of other temperature histories that, at the same temperature, the velocity may be the maximum achievable or any lower velocity including zero. For this reason, to make a consistent inter-laboratory comparison of velocities, the temperature history to be followed immediately prior to the test temperature must be specified, as was done for the current co-ordinated research project.

The conditions under which hydrides nucleate and grow in the bulk of the material can influence the chemical potential of hydrogen in the bulk at a particular temperature [2.14]. Factors such as the maximum temperature to which the specimen was exposed prior to precipitation and the cooling rate, can modify the chemical potential and have been observed to modify the DHC crack growth rates [2.29]. There is a good correlation, in a specimen with fixed hydrogen concentration, between the temperature at which all hydride is dissolved on heating (the TSSD temperature) and the maximum temperature at which DHC can be observed when the test temperature is approached from a higher temperature [2.17]. In most cases the maximum temperature for DHC is slightly less than the TSSD temperature. This is the case even though, on cooling, hydrides do not form in the bulk of the specimen until the precipitation solvus temperature is attained, which can be as much as 50°C lower than the dissolution temperature. The reason for this observation has been explained by Eadie et al [2.30]. A very small difference between the partial molar volumes of hydrogen in solution in the matrix and hydrogen in the hydride means that there is little effect of stress on the solubility limit. However, the hydrostatic stress at the crack tip results in an elevated concentration of hydrogen in solution, due to the interaction of the partial molar volume of hydrogen in solution and the hydrostatic stress. The amplification is large enough at a sharp crack under load for the hydrogen concentration in solution at the crack tip to reach the precipitation solubility limit when the hydrogen concentration in solution far from the crack tip is close to the dissolution solvus concentration.

2.5. Conditions for Crack Tip Hydride Fracture

Fracture of the crack-tip hydride is a necessary requirement for the propagation of a crack by DHC. The detailed micro-mechanisms of such fracture are not yet well understood. However, a very useful approach for practical engineering assessments has been developed based on a process-zone model of hydride fracture [2.31, 2.32]. This model assumes that the hydrided zone at the crack tip can be considered as a fracture process zone similar to that proposed in the strip-yield fracture model [2.33, 2.34]. Within the process zone, the total stress acting in the crack-opening direction is a superposition of the usual K-type stress field due to the crack and a restraining stress due to the hydride. The hydride-induced restraining stress is assumed to be uniform over the process zone and decreases with an increased amount of hydride precipitation.

This assumption of stress uniformity is consistent with finite element modeling of hydride precipitation at crack tips that showed a condition of almost uniform stress in the crack-tip hydrided zone as the hydride developed [2.19]. The finite element model assumed that the hydride transformation strain was isotropic and that the condition for hydride precipitation was consistent with the precipitation solvus (i.e. the concentration in solution could not exceed TSSP for that temperature). It was observed that the stress within the crack tip region was reduced as the hydride precipitated, consistent with expectations. This same finite element model also suggested that the hydrides at the crack tip would take on a tapered shape. This shape of hydride was observed in low strength Zr-2.5Nb material in which the hydride size and shape prior to fracture could be clearly observed using light metallography [2.9]. The tapered shape of the hydride suggests that the amount of hydride required to be precipitated at the crack tip to generate a certain crack growth step length may be proportional to the square of the step length rather than simply proportional to the step length itself. The corollary of this observation is that the amount of hydrogen required to be transported to the crack tip to generate a certain amount of crack growth will be dependent on the crack-growth step size with larger steps requiring more hydrogen transport per unit length. Therefore, the expectation is that the crack velocity will be reduced in materials exhibiting large crack growth step sizes if other material characteristics are kept constant.

In the process-zone model, there are two conditions that must be met for fracture: a critical crack opening displacement, v_c, due to hydride precipitation must be attained, and, the uniform stress in the process zone must be above a critical value, p_c. The hydride must be sufficiently large and the stress along the hydride must be sufficiently high for fracture to occur. These parameters of the model are determined from values of K_{IH} and the stress required to cause fracture of long hydrides perpendicular to smooth surfaces. Good agreement between model predictions and crack initiation testing has been demonstrated for a range of flaw geometries [2.32].

During crack initiation and propagation in a DHC test, the conditions for crack tip hydride fracture must be repeatedly met for the crack to continue to propagate. When the load is first applied to a pre-cracked specimen after the DHC test temperature has been reached, there is always an incubation time required for the formation of the first hydride of the critical size required for fracture. This incubation time could be expected to be dependent upon the driving forces for hydrogen diffusion to the crack tip, the diffusion coefficient in the material and the amount of hydride required to form the critical hydride. These are the same parameters that ultimately determine the observed DHC crack velocity. In practice, incubation times are somewhat more variable than measurements of crack velocities.

Although, for simplification, the modelling of DHC has often used isotropic material properties, the crystallographic texture and material microstructure do affect the propagation of cracks by DHC. The crystallographic texture affects the precipitation of hydrides because hydride platelets have a crystallographic relationship with the metal from which they are formed. The transformation strains (metal to hydride) are also directionally related to the crystallography. The stress state of a crack tip is modified by the precipitation of hydride in a way that depends upon the orientation of the crack within the material (if that material is anisotropic). The critical hydride size and shape required for fracture will then be dependent upon the texture. DHC crack initiation and propagation in an anisotropic material will itself be anisotropic and that is what is observed [2.6, 2.7]. Crystallographic texture differences between materials will also produce differences in DHC characteristics, such as K_{IH} and crack velocity.

2.6. Co-ordinated Research Programme Testing

The testing procedure recommended for the DHC velocity measurement in the CRP was designed to maximize the velocity at each test temperature. Under all the test conditions in the test matrix (see Chapter 3, Section 3.3.3), the relationship between the hydrogen concentration in the specimen, the peak temperature achieved immediately prior to the test temperature and the DHC testing temperature were such that the concentration of hydrogen in solution was equal to the TSSP concentration at the crack tip for the test temperature.

Similarly, the applied stress intensity factor range (a minimum of 15 MPa$\sqrt{m}$) was sufficiently in excess of the usual range of K_{IH} for the materials tested (generally within a range of 4.5 to 10 MPa$\sqrt{m}$) that crack propagation should not be limited due to insufficient applied stress intensity factor.

2.7. Summary

A brief summary of the state of the art of the understanding of effects of hydrogen concentration in solution on DHC has been presented. The effects of hydrogen hysteresis on the expected driving force required to move hydrogen in solution to the crack tip have been discussed. The resulting effects on DHC testing have been shown to be consistent with observations reported in the literature. The defined test conditions for the CRP tests have been shown to meet the conditions required to maximize the crack growth rates at the test temperatures involved.

REFERENCES TO CHAPTER 2

[2.1] COLEMAN, C.E., AMBLER, J.F.R., "Delayed hydride Cracking in Zr-2.5wt%Nb Alloy", Reviews on Coatings and Corrosion, Vol.III, Freund, Israel, (1979), 105–157.

[2.2] DUTTON, R., NUTTALL, K., PULS, M.P., SIMPSON, L.A., "Mechanism of Hydrogen-Induced Delayed Hydride Cracking in Hydride Forming Materials", Metall. Trans.A, 8A, (1977), 1553–1562.

[2.3] COLEMAN, C.E., "Cracking of Hydride-forming Metals and Alloys", Comprehensive Structural Integrity, Elsevier, Eds. I. Milne, R.O. Ritchie and B. Karihaloo, 2003,Chapter 6.03, pp.103–161.

[2.4] SIMPSON, L.A., PULS, M.P., "The Effects of Stress, Temperature and Hydrogen Content on Hydride-Induced Crack Growth in Zr-2.5Nb", Metall. Trans.A, 10A, (1979), 1093–1105.

[2.5] LI, J.C.M., ORIANI, R.A., DARKEN, L.S., "The thermodynamics of a Stressed Solid", Phys. Chem. Neue. Folge, 49, (1966) 271–290.
[2.6] KIM, Y.S., KWON. S.C., KIM, S.S., Crack growth pattern and threshold stress intensity factor, KIH of Zr-2.5Nb alloy with the notch direction, J. Nucl. Mater., 280 (2000) 304–311.
[2.7] KIM, Y.S., PERLOVICH, Y., ISAENKOVA, M., KIM, S.S., CHEONG, Y.M., Precipitation of reoriented hydrides and textural change of α-zirconium grains during delayed hydride cracking of Zr-2.5%Nb pressure tube, J. Nucl. Mater. 297 (2001) 292–302.
[2.8] SINGH, R.N., KUMAR, N., KISHORE, R., ROYCHAUDHURY, S., SINHA, T.K., KASHYAP, B.P., "Delayed hydride cracking in Zr-2.5Nb pressure tube material", J. Nucl. Mat., 304, (2002), 189–203.
[2.9] SHEK, G.K., "The Effect of Material Properties, Thermal and Loading History on Delayed Hydride Cracking in Zr-2.5 Nb Alloys," PhD Thesis, University of Manchester, 1998.
[2.10] RESTA LEVI, M., SAGAT, S., "The Effect of Texture on Delayed Hydride Cracking in Zr-2.5Nb Alloy", Proceedings of the International Symposium on Environmental Degradation of Materials and Corrosion Control in Metals, 38th Annual Conference of Metallurgists, 29th Annual Hydrometallurgical Meeting of CIM, 1999 August, Quebec City, Quebec Also, AECL-report AECL-12045.
[2.11] COLEMAN, C.E., AMBLER, J.F.R., "Measurement of Effective Solvus of Hydrogen in Zr-2.5wt% Nb Using Acoustic Emission", Hydrogen in Metals, The Metallurgical Society of CIM Annual Volume, Can. Met. Quart., 17 (1978), 81–84.
[2.12] ERICKSON, W.H., HARDIE, D., "The Influence of Alloying Elements on the Terminal Solubility of Hydrogen in Alpha Zirconium", J. Nucl. Mats. 13,(1964), 254–262.
[2.13] SLATTERY, G., "The Terminal Solubility of Hydrogen in Zirconium Alloys between 30 and 400 °C", J. Inst. Met., 95, (1967), 43–47.
[2.14] PAN, Z.L., RITCHIE, I.G., PULS, M.P., "The terminal solid solubility of hydrogen and deuterium in Zr-2.5Nb alloys", J. Nucl. Mat. 228,(1996) 227–237.
[2.15] AMBLER, J.F.R,. "Effects of Direction of Approach to Temperature on Delayed Hydride Cracking Behaviour of Cold Worked Zr-2.5Nb", Zirconium in the Nuclear Industry: Sixth International Sym. STP 824, (1984) 653–674.
[2.16] SHI, S.Q., PULS, M.P., "Advances in the Theory of Delayed Hydride Cracking in Zirconium Alloys", Hydrogen Effects in Materials. Eds. A.W. Thompson and N.R. Moody, The Minerals, Metals and Materials Society, 1996, pp.611–621.
[2.17] PULS, M.P., "Effects of Crack Tip Stress States and Hydride-matrix Interaction Stresses on Delayed Hydride Cracking", Met. Trans. A, 21A, (1990), 2905–2917.
[2.18] EADIE, R.L., METZGER, D.R., LÉGER, M., "The Thermal Ratchetting of Hydrogen in Zirconium-Niobium – An Illustration using Finite Element Modelling", Scr. Metall. 29, (1993), 335–340.
[2.19] METZGER, D.R., SAUVÉ, R.G., "A Self-Induced Stress Model for Simulating Hydride Formation at Flaws", ASME PVP 326, Computer Technology:Application and Methodology", (1996), 137.
[2.20] METZGER, D.R., EADIE, R.L., Unpublished research.
[2.21] MCMINN, A., DARBY, E.C., SCHOFIELD, J.S., "The Terminal Solid Solubility of Hydrogen in Zirconium Alloys", Zirconium in the Nuclear Industry: Twelfth International Symposium, ASTM STP 1354, Eds. G.P. Sabol and G.D. Moan Eds., American Society for Testing and Materials, West Conshohocken, PA, 2000, 173–195.

[2.22] CARPENTER, G.J.C., "The Dilatational Misfit of Zirconium Hydrides Precipitated in Zirconium", J. Nucl. Mats. 48, (1973), 264–266.
[2.23] PULS, M.P., "On the Consequence of Hydrogen Supersaturation Effects in Zr Alloys to Hydrogen Ingress and Delayed Hydride Cracking", J. Nucl. Mats., 165, (1989),128.
[2.24] PULS, M.P., "The Effects of Misfit and External Stresses on Terminal Solid Solubility in Hydride Forming Metals", Acta Metall., 29, (1981), 1961.
[2.25] PULS, M.P., "Elastic and Plastic Accommodation Effects on Metal-Hydride Solubility", Acta Metall., 32, (1984), 1259–1269.
[2.26] PAN, Z.L., PULS, M.P., RITCHIE, I.G., "Measurement of hydrogen solubility during isothermal charging in a Zr alloy using an internal friction technique", J. of Alloys and Compounds, 211/212, (1994), 245–248.
[2.27] SHEK, G.K., GRAHAM, D.B., "Effects of Loading and Thermal Maneuvers on Delayed Hydride Cracking in Zr-2.5Nb Alloys", Zirconium in the Nuclear Industry: Eighth International Symposium, ASTM STP 1023, (1989), 89–110.
[2.28] CHEADLE, B.A., COLEMAN, C.E., AMBLER, J.F.R., "Prevention of Delayed Hydride Cracking in Zirconium Alloys", Zirconium in the Nuclear Industry: Seventh International Symposium, ASTM STP 939, (1987), 224–240.
[2.29] AMOUZOUVI, K.F., CLEGG, L.J., "The Effect of Heat Treatment on Delayed Hydride Cracking in Zr-2.5 Wt.Pct.Nb", Metall. Trans.A, 18A, (1987) 1687–1694.
[2.30] EADIE, R.L., MOK, D., SCARTH, D.A., LEGER, M., "The Hydrostatic Stress Field Around the Crack Tip in Zr 2.5% Niobium and Implications for Delayed Hydride Cracking", Scripta Met. 25, (1991), 497.
[2.31] SCARTH, D.A., SMITH, E., "Modelling Delayed Hydride Cracking in Zirconium Alloys," Proceedings of the IUTAM Symposium on Analytical and Computational Fracture Mechanics of Non-Homogeneous Materials, Edited by B.L. Karihaloo, Cardiff, U.K., June 2001, published by Kluwer, pp. 155-166.
[2.32] SCARTH, D.A., SMITH, E., "The Effect of Plasticity on Process-Zone Predictions of DHC Initiation at a Flaw in CANDU Reactor Zr-Nb Pressure Tubes," Proceedings of the 2002 ASME Pressure Vessels and Piping Conference, Vancouver, British Columbia, Canada, August 4-8, PVP-Vol. 437, pp. 19–30.
[2.33] DUGDALE, D.S., "Yielding of Steel Sheets Containing Slits," Journal of Mechanics and Physics of Solids, 8, (1960), 100–104.
[2.34] BILBY, B.A., COTTRELL, A.H., SWINDEN, K.H., "The Spread of Plastic Yield from a Notch," Proceedings, Royal Society of London, Vol. A-272, (1963), 304–314.

CHAPTER 3

EXPERIMENTAL PROGRAM

3.1. Philosophy

A three phase programme was set up to establish, in all the countries involved, a uniform and consistent laboratory practice to determine DHC velocity in the axial direction of pressure tubes. In the first phase, AECL's CRL, (Canada), as host laboratory, supplied participating countries with machined samples of Zr-2.5 Nb alloy each containing the same amount of hydrogen [3.1], Appendix 1[3]. Each country then performed DHC tests in a prescribed manner at a single temperature, 250°C [3.2], Appendix 2. Building on this experience, the second phase of the experimental programme consisted of each country producing their own samples out of segments of the same pressure tube, developing a hydriding method and charging the samples with the desired amount of hydrogen [3.3], Appendix 3, then testing them at various temperatures. In the third phase, each country made the same determinations on Zr-2.5 Nb material supplied by Lithuania and on their own material, if available. The procedures for these activities were documented in detail to ensure consistency. As a possible extension of this CRP, the feasibility of measuring DHC velocity in fuel cladding was explored by Sweden.

3.2. Materials

For Phases 1 and 2, an 800 mm long section of CANDU Zr-2.5 Nb pressure tube, identified as RX094-C2, was used. The section started approximately 0.185 m from the back end of the tube ("Back end" refers to the end of the tube that exits the extrusion press last.) The chemical composition of the original ingot material is given in Table 3.1 and the fabrication process flow chart is shown in Fig. 3.1. The ingot was melted four times. The dimensions of the finished tube are listed in Table 3.2 and the tensile properties are provided in Table 3.3. The initial microstructure, Fig. 3.2, consists of flattened α-grains about 0.5 μm thick surrounded by a grain boundary film of β-phase. The crystallographic texture is shown in Figure 3.3 and the fraction of resolved basal plane normals, F, in the three principal directions, radial, R, transverse, T and longitudinal, L, are summarized in Table 3.4.

For the common part of Phase 3, a section of RBMK Zr-2.5 Nb pressure tube in the TMT-1 condition was used. Tubes with this production schedule are used in the Ignalina Nuclear Power Plant, Unit 1, in Lithuania. The specified chemistry and some typical values of element concentration are incorporated in Table 3.1 [3.4]. The fabrication process flow chart for each version of RBMK pressure tubes is shown in Fig. 3.4. The dimensions of the finished tube are included in Table 3.2 and the tensile properties are provided in Table 3.3 The microstructure after the TMT-1 treatment, Fig.3.5, consists of α'-phase and between 10 and 20% untransformed α-phase. The crystallographic texture is shown in Fig. 3.6 and the F-values are included in Table 3.4.

[3] Appendices to this Report can be found in the CD-ROM attached on the inside back cover.

Table 3.1. Composition of test materials

Element	Materials			
	CANDU Tube	CANDU Tube	RBMK Specification	Indian HWR Tube
	RX094 (Ingot)	N429 (Ingot)	(Typical values for TMT-1)	100-2-3 (Measurements on typical tube)
Alloy:				
Niobium (wt%)	2.6	2.55	2.4-2.7	2.53
Oxygen (ppm)	1140	1172	1000 (400-700)	1226
Impurities (ppm)				
Aluminum	35	47	80	(29)
Beryllium			30	
Boron	<0.2	<0.25		(<0.25)
Cadmium	<0.2	<0.25	0.3	(<0.25)
Calcium			300	
Carbon	90	130	200 (30-70)	(95)
Chromium	<100	<80	200 (20-50)	200
Cobalt	<10	<10		(<10)
Copper	<25	<25	50	(27)
Hafnium	39	<40	500 (230-420)	(35)
Hydrogen	2	9	5 (2-3)	10 (4)
Iron	360	590	500 (80-250)	1300
Lead	<25	<25	50	(<25)
Magnesium		<10		(<10)
Manganese	<25	<25	20	(<25)
Molybdenum	<25	<25		(<25)
Nickel	<35	<25	200 (30-90)	<7
Nitrogen	24	42	60 (30-50)	56
Silicon	26	<60	200 (20-80)	(38)
Tantalum	<100	<200		(<100)
Tin	<25	<30		180
Titanium	<25	<25	70	(<25)
Tungsten	<25	<25		(<25)
Uranium	<1.0	<1.0		(<1.0)
Vanadium	<25	<25		(<25)

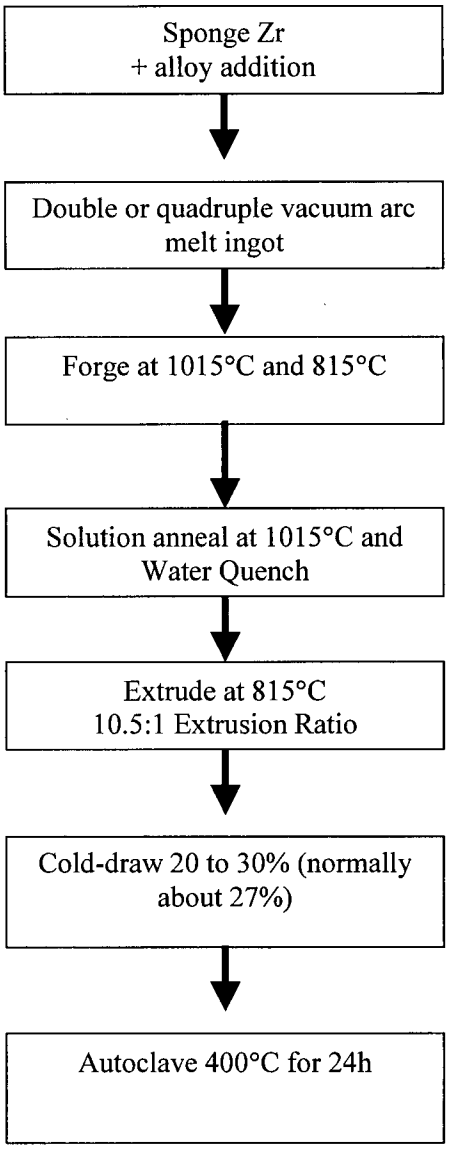

Fig. 3.1. Process flow chart for fabrication of CANDU pressure tubes.

Table 3.2. Dimensions of finished pressure tubes

Material	Inside diameter (mm)	Wall Thickness (mm)
CANDU	104	4.3
RBMK	80	4.0
Indian	82	3.7

Table 3.3. Tensile properties of test materials

Material	TEST DIRECTION L:longitudinal T:transverse	Test Temperature (°C)	0.2% Yield Stress (MPa)	UTS (MPa)	Total Elongetion (%)
CANDU Tube RX094	L	300	433	569	18
	T	20	803	889	22
	T	250	567	652	25
Tube N429	L	300	366	521	15
	T	250	585	673	13
RBMK TMT-1	L	20	580-640	680-720	20-24
	L	350	400-450	490-510	17-20
	T	20	659	760	25
	T	144	582	708	28
	T	182	546	655	24
	T	250	494	599	25
	T	300	484	555	27
Annealed	L	20	375-420	540-600	26-31
	L	300	229	336	27
	L	350	210-255	320-470	33-36
	T	20	483	520	20
	T	300	277	324	15
Indian 100-2-3	L	20	599	833	13
	L	300	426	587	14
	T	20	722	861	10
	T	250	531	641	12

Table 3.4. Resolved fraction of basal plane normals in the three principal directions of CANDU pressure tube RX094

Material	F_R	F_T	F_L
CANDU (RX094)	0.36	0.60	0.04
RBMK (TMT-1)	0.41	0.42	0.17
RBMK (Annealed)	0.47	0.46	0.07
Indian Tube	0.43	0.55	0.02

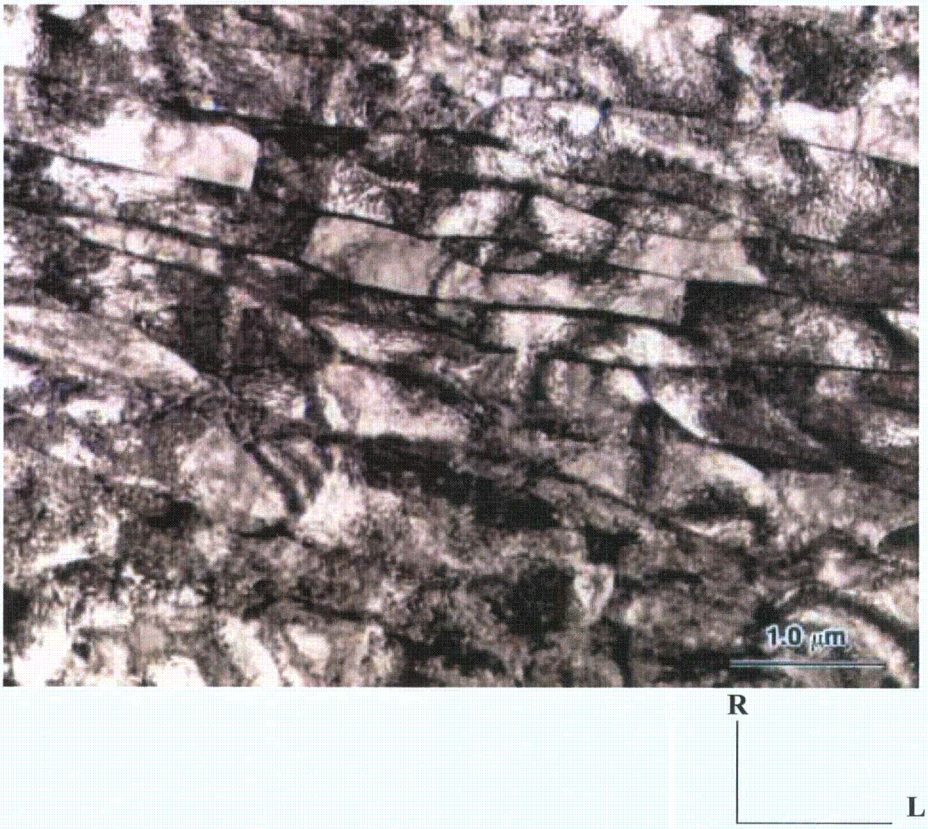

Fig. 3.2. Microstructure of CANDU pressure tube.

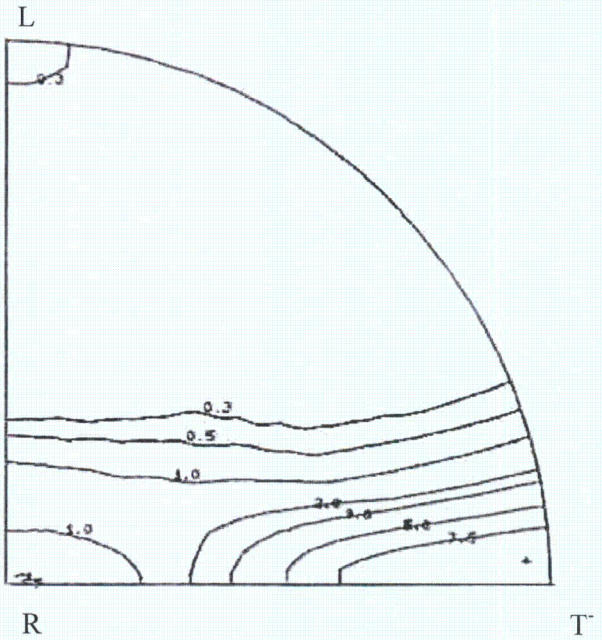

Fig. 3.3. Basal pole figure for CANDU tube RX094.

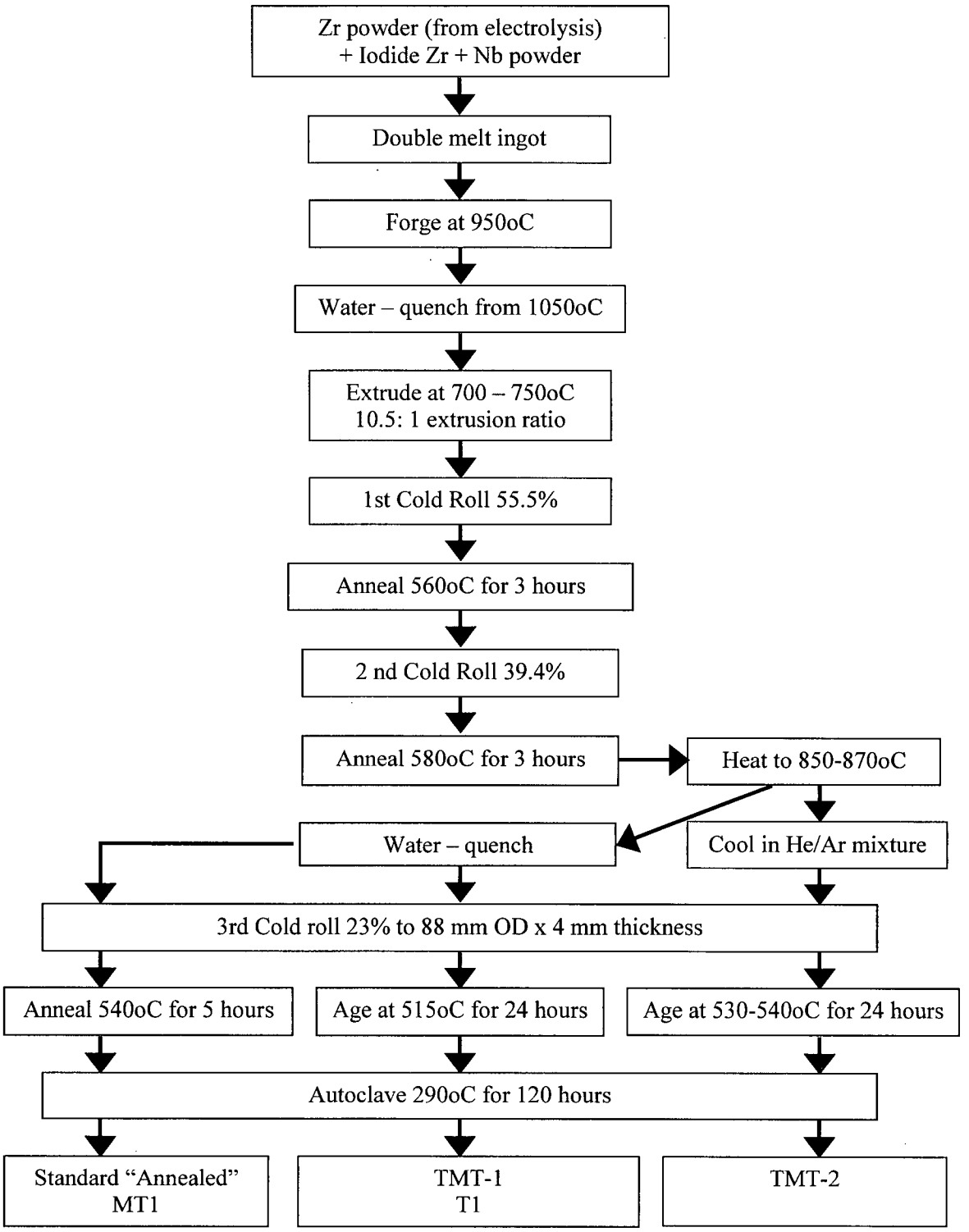

Fig. 3.4. Process flow chart for fabrication of RBMK pressure tubes.

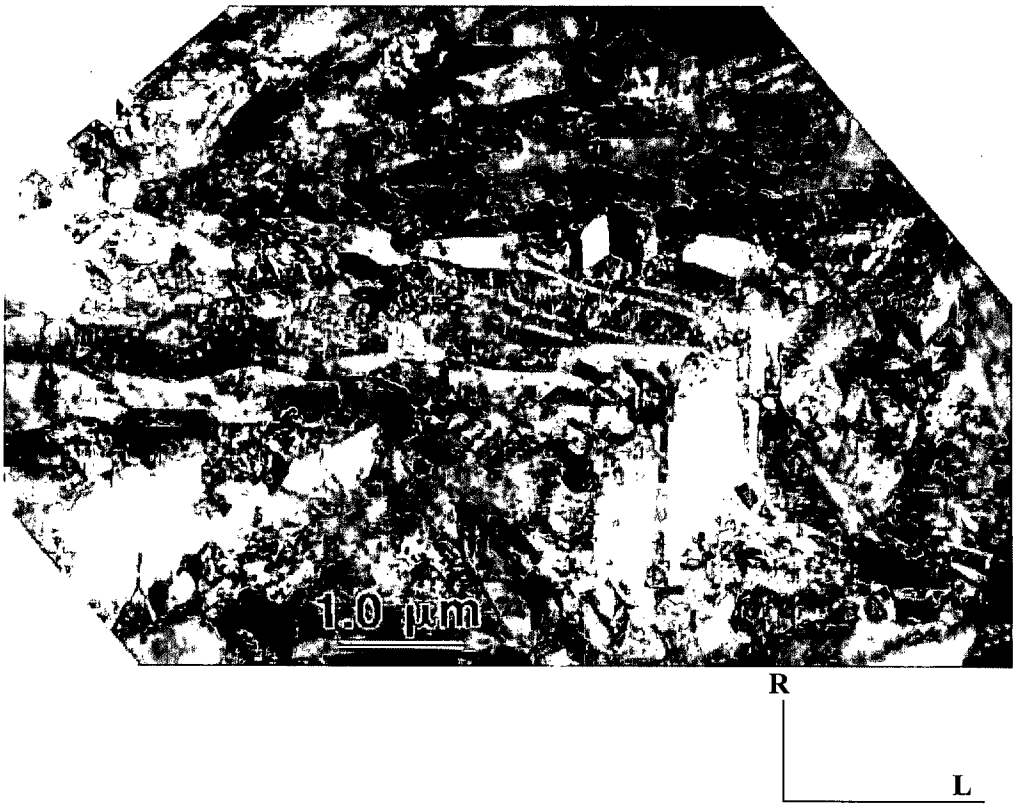

Fig.3.5. Microstructure of RBMK pressure tube with TMT-1 treatment.

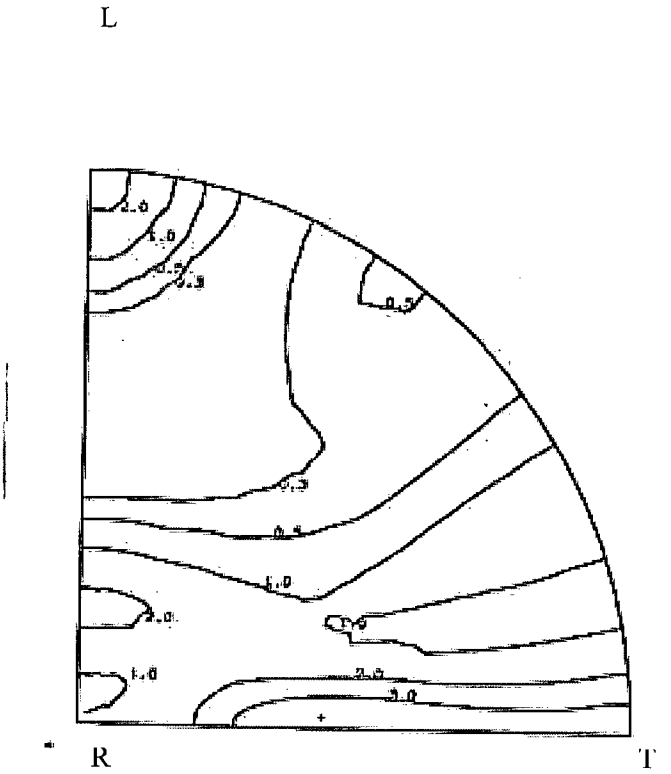

Fig.3.6. Basal pole figure for RBMK pressure tube in TMT-1 condition.

Other materials tested in Phase 3 are as follows:

Tube N429, typical of the CANDU reactor at Cernavoda, Unit 1, has attributes given in Tables 3.1 and 3.3. For this tube the ingot was melted twice. The microstructure and crystallographic texture are expected to be similar to those of Tube RX094.

Tube 100-2-3, made in India by the process depicted in Fig. 3.7, has the composition listed in Table 3.1 with dimensions and tensile properties included in Tables 3.2 and 3.3, respectively. The microstructure, Fig. 3.8, consists of elongated α-grains, 0.1 to 0.2 μm thick, surrounded by a thin layer of β-phase. The crystallographic texture, typical of this fabrication route is shown in Fig. 3.9 and the F-values are included in Table 3.4. For the tests on this material the hydrogen was added gaseously.

Some specimens were made from the other two routes for RBMK tubes, Fig. 3.4. Typical tensile properties are included in Table 3.3. The microstructure of annealed tubes contains elongated α-grains mixed with equiaxed α-grains and discontinuous β-phase at triple points and within the α-grains, Fig. 3.10. A typical crystallographic texture is shown in Fig. 3.11 with F-values in Table 3.4.

In summary, the properties of the sampled tubes were diverse. The anisotropy in properties tended to be higher in CANDU tubes than in RBMK tubes because of crystallographic texture and grain structure. The strengths at room temperature in the transverse direction were in the order CANDU (Canada), HWR (India), RBMK (TMT-1, Lithuania), RBMK (annealed, Russia). The range in strengths had several causes:

- RBMK material tends to have lower oxygen concentration than CANDU material,
- the microstructure provides lower strength in RBMK tubes than in CANDU tubes because of lower dislocation density and larger grain size,
- the high F_T in CANDU tubes leads to higher transverse strength than in RBMK tubes.

3.3. Specimen Preparation and Testing

The experiments involved adding known amounts of hydrogen to the Zr-2.5 Nb material, machining specimens and preparing a sharp crack, conducting the DHC test and evaluating the fracture surface.

3.3.1. Adding hydrogen

Several methods are available for adding hydrogen to zirconium alloys but the one chosen for this project, diffusing from a surface layer of hydride, combines good control with low temperatures [3.3]. The latter is important to minimise changing microstructure during specimen preparation, especially when dealing with irradiated materials.

The details of the procedure are given in Appendix 3. The hydride layer is formed electrolytically. After surface cleaning, the sample is placed into a bath containing 0.2 M H_2SO_4 at 65°C and electrolysis is performed at a current density of about 1.5 kA/m^2 using Pb (or other suitable metal) as anode. The hydride layer is examined metallographically to determine whether it is thick enough to supply the required concentration of hydrogen. Once a suitable layer is attained, the sample is heated, the temperature being determined by the TSS for dissolution to provide the target hydrogen concentration while the time of heating must be sufficient for the hydrogen to diffuse and attain the target concentration at the centre of the sample thickness. The efficacy of the preparation is determined by examining the resulting hydrides in the metal and by chemical analysis.

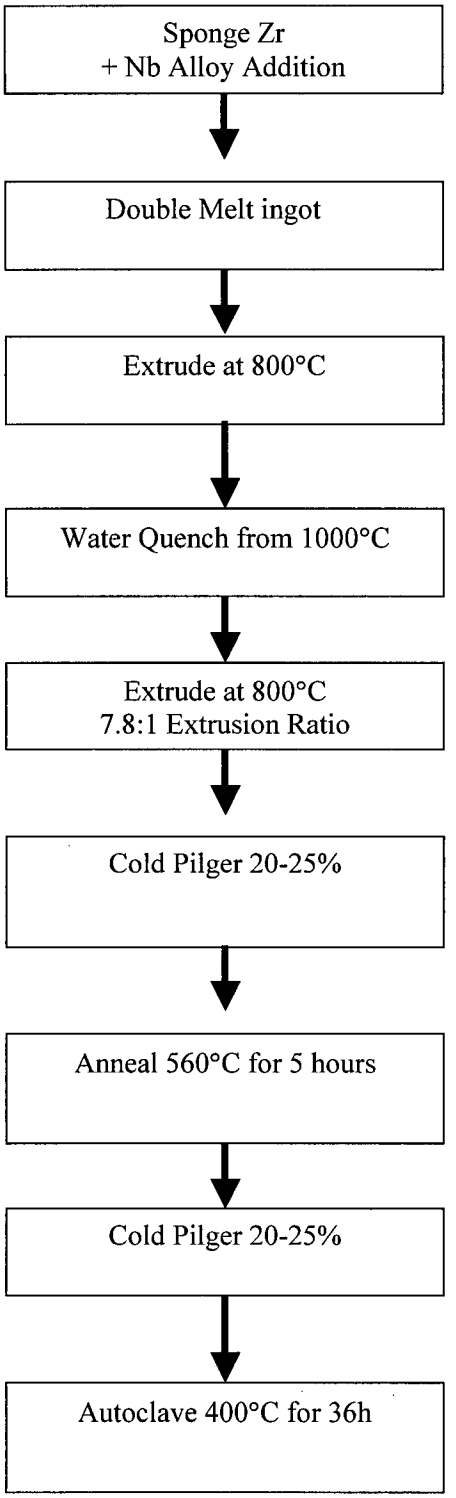

Fig. 3.7. Process flow chart for fabrication of Indian HWR pressure tubes.

Fig. 3.8. Microstructure of Indian HWR pressure tube. (Radial direction of the tube is vertical on the page and the longitudinal direction is horizontal.)

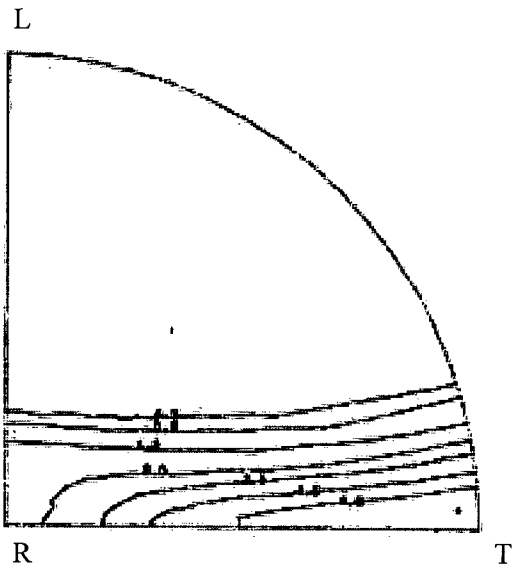

Fig.3.9. Basal pole figure for Indian HWR pressure tube.

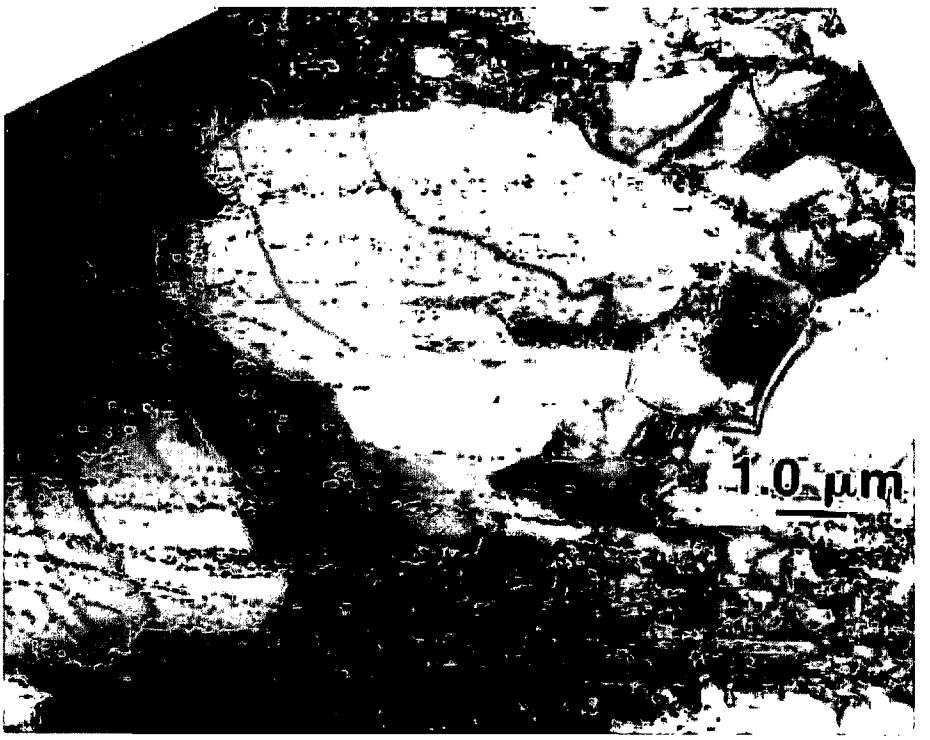

Fig. 3.10. Microstructure of annealed RBMK pressure tube (Radial direction of the tube is vertical on the page and the longitudinal direction is horizontal.)

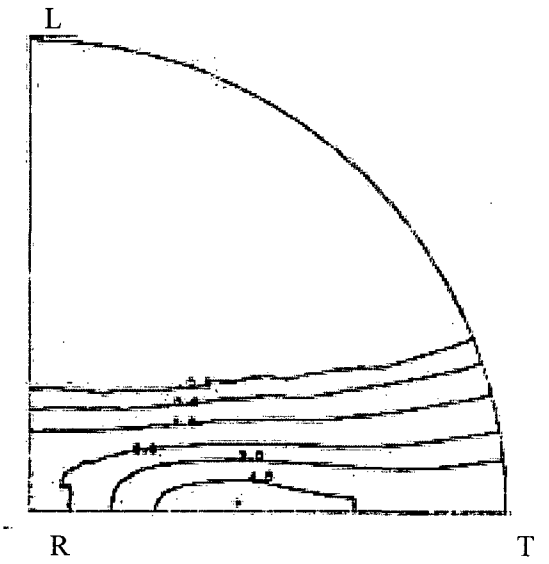

Fig.3.11. Basal pole figure for RBMK pressure tube in the annealed condition.

3.3.2. Test specimen

A detailed description of the test method [3.2] is given in Appendix 2. The test specimens were compact toughness specimens that met the requirements of ASTM E399, except for thickness and retention of the curvature, Fig. 3.12. The specimens were machined so that the crack grew in what was the longitudinal direction of the original tube on a plane with normal in the transverse direction of the original tube. A starter crack was grown about 1.7 mm from the notch by fatigue at room temperature, to give the recommended a_o/W ratio of 0.5 (where a_o is the crack length and W is the specimen width, with respect to the loading point.) K_I was calculated from equations given in ASTM E399. The maximum K_I was reduced during fatigue in up to six steps until it was less than the initial K_I for DHC testing.

3.3.3. DHC testing

To realize the maximum crack velocity, the test temperature must be attained by cooling from a peak temperature above the solvus temperature (with no under cooling), hydrides must be present at the test temperature and the maximum amount of hydrogen must be in solution. Since the latter two conditions are somewhat contradictory, the test temperature was set below the dissolution solvus temperature. A typical test sequence is given in Fig. 3.13. The full load, supplying an initial K_I of about 15 MPa$\sqrt{m}$, was applied about ½ hour after the test temperature had stabilized. After the crack extended about 1.5 mm, the load was removed and the specimen was cooled to room temperature. The end of the crack was marked by heat-tinting or post-test fatigue.

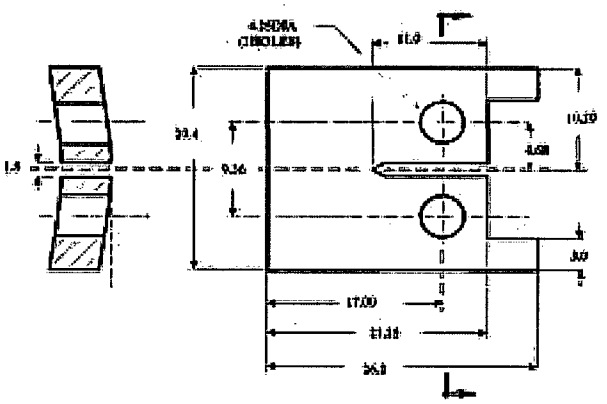

Fig. 3. 12. Schematic diagram of DHC compact toughness specimen.

The direct current, potential drop (dc pd) technique was used to evaluate the status of the crack during both fatigue pre-cracking and DHC testing. A constant current of about 8 A is large enough to provide a pd of about 5 mV across the specimen without excessive heating. The crack front tends to be curved. For fatigue, surface markers were useful to indicate the progress of the crack. After DHC, the amount of cracking was measured directly from the fracture surface once the two halves of the specimen were pulled apart. The crack length was evaluated by one of two methods. The area of DHC was estimated and the average crack length was calculated by dividing the crack area by the specimen thickness. Alternatively, the crack extension by DHC from the limit of fatigue cracking was averaged from measurements at nine equidistant intervals across the crack face.

DHC often required an incubation period, indicated by an increase in pd. The test time was taken as the difference of the total time under full load and the incubation time. DHC velocity was then crack extension by DHC divided by cracking time.

A test matrix was established where, in principle, each country measured DHC velocity on at least three specimens at three temperatures ranging from 283 °C down to 144 °C, with each temperature being covered by three countries, Table 3.5. At least nine results at each temperature were thought to provide a good statistical basis.

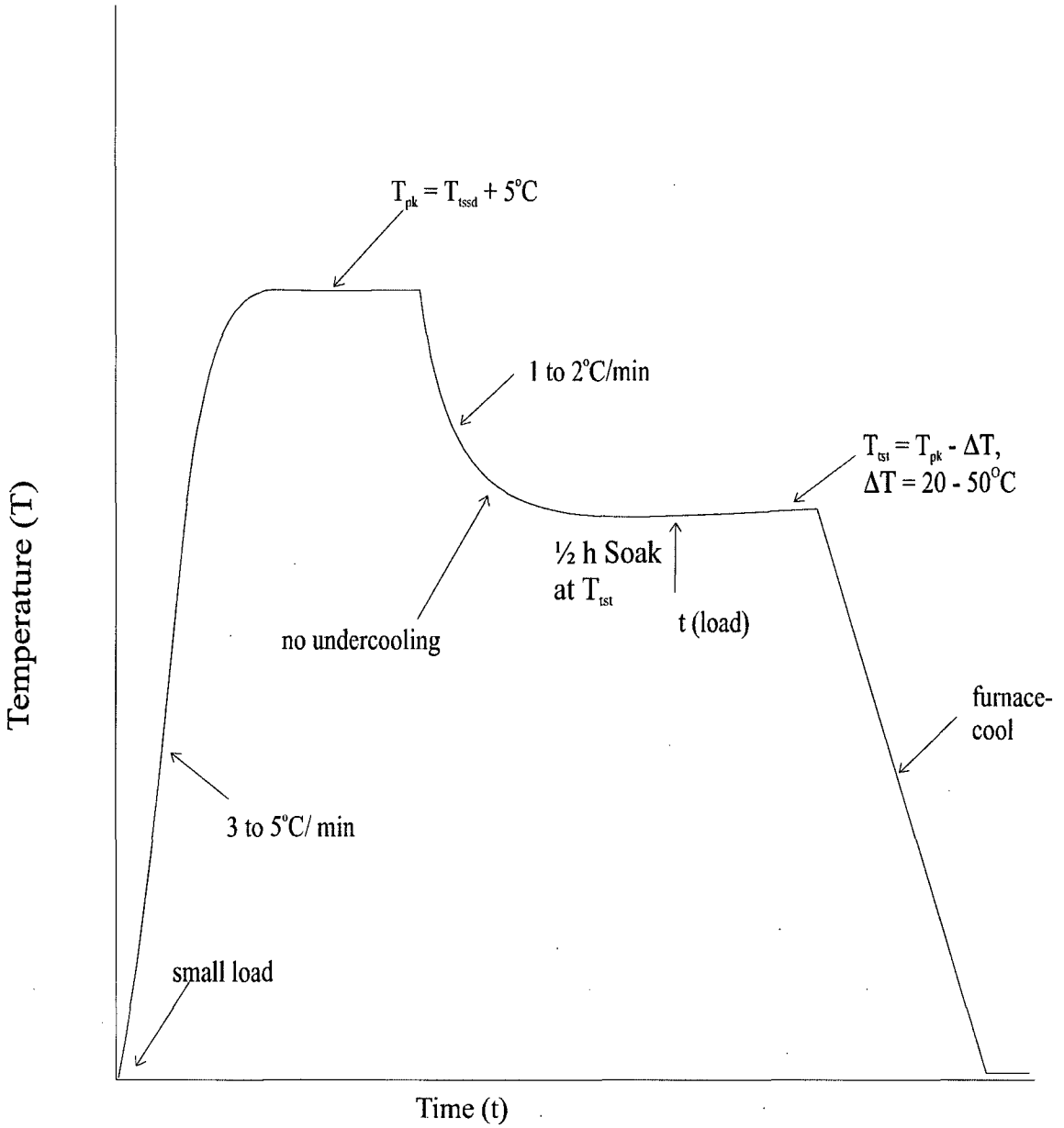

Fig. 3.13. Recommended temperature and loading history for DHC testing.

Table 3.5. Test matrix for Phases 1, 2, and 3

Peak Temperature (°C)	Test Temperature, (°C)	Hydrogen Concentration, ppm	Participating Countries
330	283	72	Russia, Lithuania, Argentina
315	250	58	ALL
295	227	45	Romania, Pakistan, Canada
285	203	38	Russia, Romania, India
275	182	34	ROK, China Argentina
275	162	31	Pakistan, China, India
275	144	29	Lithuania, ROK, Canada

In practice, because of some experimental difficulties some temperatures were lightly sampled. As one example, when the hydrogen concentration was not precisely known, the thermal cycle was altered. The peak temperature was set higher than the possible solvus temperature by a large margin, then the test temperature was reduced in steps to the temperature at which cracking started.

The distribution of hydrides was examined metallographically on the planes with their normal in the transverse and longitudinal direction. The fracture surfaces were examined, and, where found, striation spacings were estimated.

3.4. Hydrogen Analysis

Knowledge of hydrogen concentration is needed when assessing the response of zirconium alloys to hydrogen. During the CRP on DHC in zirconium alloys the participants were adding specific amounts of hydrogen to their test specimens. The hydrogen concentration is critical to the tests; too much hydrogen may cause hydrides to be present at the peak temperature reached before the lower test temperature is attained, while too little hydrogen may provide insufficient hydrogen for hydride precipitation during testing and give a false, low crack velocity.

Until recently, no standards were available for hydrogen in zirconium alloys and most laboratories use hydrogen in titanium as their standard. Samples of hydrogen in zirconium are currently prepared at AECL - Chalk River Laboratories to provide standards for zirconium alloys. Such samples require testing in several laboratories to enhance their status as standards. An inter-laboratory comparison by the CRP participants helped meet this requirement.

159 pellet specimens (approximately 200 mg) were cut from Zr-2.5Nb pressure tube material and prepared individually. Each pellet was heated to 950°C under vacuum to remove most of the initial dissolved hydrogen gas. The system was isolated from the vacuum pump and a known quantity of hydrogen gas was added from a calibrated volume. The pellet quantitatively absorbed the hydrogen gas during cooling from 950°C to room temperature.

The concentration assigned to each specimen (expressed in units of ppm) was based on the known mass of the pellet and the known amount of hydrogen to which it was exposed.

The target concentration for hydrogen addition was 47 ppm for each sample. The starting material may have a residual hydrogen concentration as high as 1 ppm after pre-extraction. After the standards were made, a problem with the temperature measurement was identified that may have introduced a systematic bias as high as 1 ppm. Therefore, the hydrogen concentration in the samples was expected to range from 47 to 49 ppm. Random samples were then analysed to determine the actual mean concentration and standard deviation of the population. The specimens were made in 4 batches (up to 49 specimens per batch). Ten samples were selected at random from each batch for a total of 40 specimens. These 40 random samples were analysed by hot vacuum extraction – isotope dilution mass spectrometry (HVE – IDMS)[3.5, 3.6]. The results from the 40 samples showed that the combined population was approximately normal with a mean value of 49.8 ppm and a standard deviation of 0.5 ppm (1% rsd). Although the mean value was somewhat higher than expected, the standard deviation of the distribution was ideal for the inter-laboratory comparison.

The remaining specimens from the 4 batches were mixed, and then randomly divided into 10 bottles with 10 specimens per bottle. Each bottle was labelled with a number from 1 to 10. Based on the Canadian determination, the H concentration of the 10 random samples in each bottle is expected (from probability theory) to have a standard deviation ≤ 0.7 ppm. Bottles #1 through #10 were sent to the IAEA coordinator for distribution to the participants who were asked to analyse them using their normal laboratory procedures. The remaining 19 specimens were placed in Bottle #11 and retained in Canada for later analysis. Each specimen in the bottles was weighed to the nearest 0.1 mg and recorded. The mass served to identify each specimen, except for a few samples where the masses were indistinguishable.

REFERENCES TO CHAPTER 3

[3.1] KIDD K. V., Preparation of Material and Specimens for the IAEA Co-ordinated Research Programme on Delayed Hydride Cracking. FC-IAEA-001, T1.20.13-CAN-273.63-01, November 1998.

[3.2] CHOUBEY, R., DHC Axial Velocity Test Procedure for IAEA Round-Robin Test Program, FC-IAEA-02, T1.20.13-CAN-27363-02, November 1998.

[3.3] LEPAGE, A. D., FERRIS, W. A. and LEDOUX, G. A., Procedure for adding Hydrogen to small sections of Zirconium alloys, FC-IAEA-03, T1.20.13-CAN-27363-03, November 1998

[3.4] NIKULINA, A.V., RESHETNIKOV, N.G., SHEBALDOV, P.V., AGEENKOVA, L.E., FOMIN, V.S., SHEVNIN, Yu.P., KOCHERGIN, S.A., Fabrication Technology of RBMK Zr-2.5Nb Pressure Tubes, Voprosy Atomnoy Nauki i Tekhniki, Ser. Materials Science and Novel Materials, 1990, issue 2 (36), pp. 46–54.

[3.5] GREEN, L. W., BICKEL, G. A., LEESON, P. K., JAMES, M. W. D., LAMARCHE, T. G. and H. Michel, A Hot Vacuum Extraction Mass Spectrometric System for Determination of H and D in Zirconium, Proceedings of the 2nd Alfred O. Nier Symposium on Inorganic Mass Spectrometry, Durango, Colorado, May 1994 (Available as part of AECL-11342, Jan. 1996, pp. 95–99.

[3.6] BICKEL, G.A., GREEN, L.W., JAMES, M.W.D., LAMARCHE, T.G., LEESON, P.K., MICHEL, H., The determination of hydrogen and deuterium in Zr-2.5 Nb material by hot vacuum extraction mass spectrometry, J. Nucl. Mater., 306, (2002), 21–29.

CHAPTER 4

RESULTS AND DISCUSSION

4.1. Source of Test Data

A typical test history, Fig. 4.1, shows the change in potential drop with changes in temperature and loading and subsequent cracking.

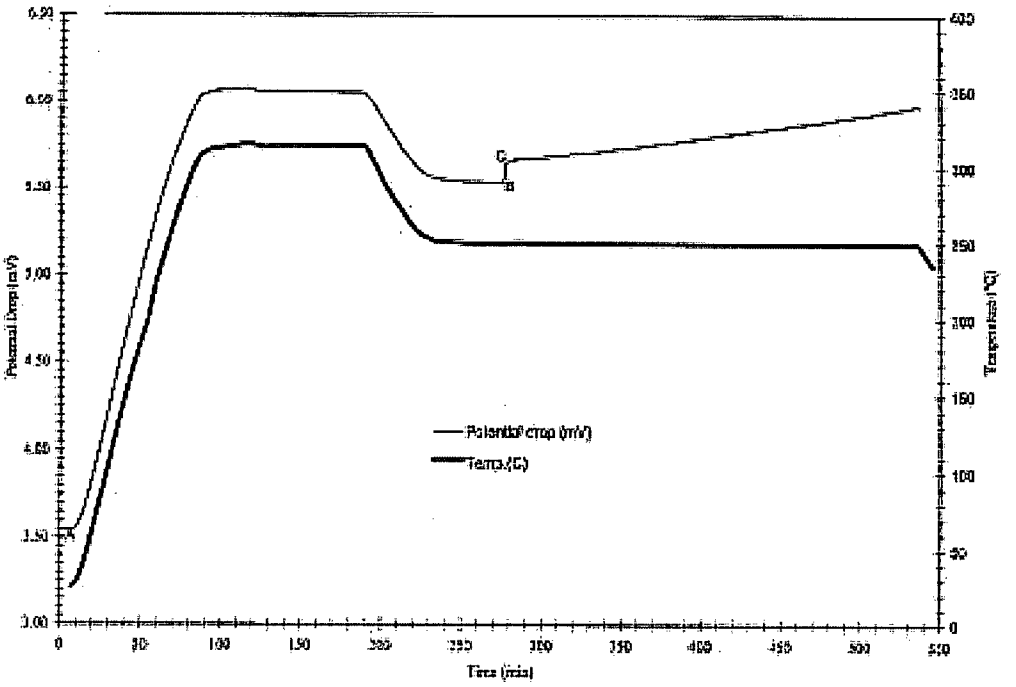

Fig. 4.1. Temperature and cracking history, as indicated by potential drop, during typical DHC test. A is start of test and the step at BC indicates the time of loading.

A typical fracture surface is depicted in Fig. 4.2 where the various stages of the test are visible as bands of different colour and roughness. Both fatigue cracks are characterized by a gently curved crack front. The DHC has a region where the crack is held up at each specimen surface corresponding to a less constrained stress state.

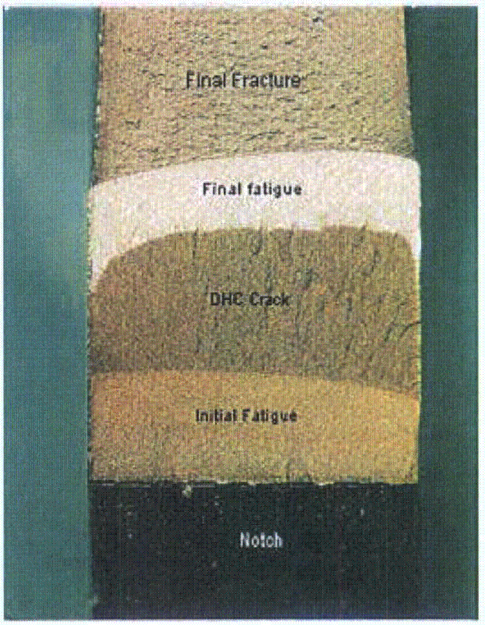

Fig. 4.2. Typical fracture surface of Zr-2.5 Nb after DHC testing.

4.2. Phase 1: Tests at 250°C on CANDU Pressure Tube

Details of each test are given in Appendix 4. The DHC velocities at 250°C are summarised in Table 4.1.

Table 4.1. Summary of DHC velocity of CANDU pressure tube at 250°C (m/s × 10^{-8}).

Argentina	Canada	China	India	ROK	Lithuania	Pakistan	Romania	Russia	Sweden
10.0	8.90	7.55	7.87	8.80	9.68	8.09	8.49	7.36	9.29
9.25	10.0	7.89	7.67	10.6	9.31	9.64	7.99	11.6	10.5
9.49	8.10	7.35	9.10	9.80	9.24	8.67	9.10	8.59	10.6
9.86	8.00	8.18	8.90	10.6	9.87	7.72	8.56	6.62	9.11
10.6	9.20	7.65	8.46	9.80	9.84	8.42	9.63	5.83	8.62
9.47	9.10	6.71	7.98	10.8	9.39	9.44	9.55	8.14	
8.95	8.30	8.62	8.50	10.2	9.86	8.63	8.96		
9.12	8.70	8.54	7.75		8.01				
8.54			7.49		8.58				
			8.14		9.35				
					7.34				
					8.89				
					8.22				

Average	9.48	8.79	7.81	8.19	10.1	9.04	8.66	8.90	8.02	9.62
Stdev	0.61	0.66	0.64	0.54	0.69	0.80	0.69	0.62	2.0	0.88

The mean value of all the data from 80 specimens is 8.86 × 10^{-8} m/s with a standard deviation of 1.07 × 10^{-8} m/s. The range of the mean value of each set of data is from 7.81 to 10.1 × 10^{-8} m/s while the standard deviation ranges from 0.54 to 2.0 × 10^{-8} m/s although most values are less than 0.7 × 10^{-8} m/s. The data can be reasonably represented by a normal distribution, Fig. 4.3. The tight distribution of the data can be attributed to the high level of control and consistency imposed by strict adherence to the test methods.

The mean value fits with data reported in the literature for tests at 250°C, Table 4.2. In early testing the importance of the various test conditions were not fully realised and, despite the specimens containing much hydrogen and K_I being large, the cracks grew more slowly than one would now expect. The main reason is that the peak temperature was too low to dissolve all the hydrogen. In later tests, with lower hydrogen concentrations but with peak temperatures greater than the solvus temperature for dissolution, the values spanned the current data.

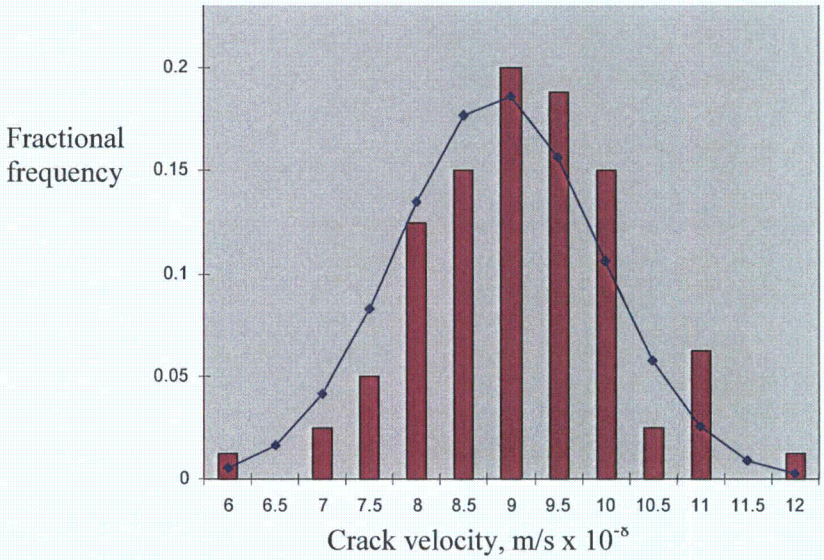

Fig. 4.3. Frequency distribution of crack velocities at 250°C. Continuous line is normal distribution.

Table 4.2. Reported values for DHC velocity in cold-worked Zr-2.5 Nb at 250°C

Hydrogen concentration (ppm)	DHC velocity range ($m/s \times 10^{-8}$)	Comment	Reference
150 to 400	0.9 to 3	K_I range from 15 to 45 MPa$\sqrt{m}$ Temperature history not well characterized	4.1
140	3 to 4	K_I range from 7 to 27 MPa$\sqrt{m}$ Peak temperature 290°C	4.2
55	11.8 ± 3.1	Initial K_I 17 MPa$\sqrt{m}$ Peak temperature greater than solvus temperature	4.3
40	5.9 ± 0.87		

Several factors could explain the distribution of the values in Table 4.1. DHC depends on the diffusion and solubility limit of hydrogen in zirconium, the growth and fracture of hydrides, and the local variation in grain structure. Each of these factors will have statistical variability;

consequently DHC will be inherently variable. Scatter from variation in material properties may be caused by variations in microstructure in the pressure tube. The microstructure in a cold-worked Zr-2.5 Nb pressure tube varies a small amount from end-to-end because of variation in temperature during extrusion, but over the length of tube used in these tests, 800 mm, such variation would be difficult to discern. The difference in results showed no correlation with position along the tube, Table 4.3, suggesting that some of the variation was caused by experimental vagaries.

Table 4.3. DHC velocity at 250°C at various positions in Tube RX094

Specimen group (see Appendix 1)	Distance from back end of tube RX094 (mm)	Crack velocity ($m/s \times 10^{-8}$)
100	1850 to 1918	8.54, 7.81
200	1920 to 1988	10.1, 9.04
300	1990 to 2058	8.66, 8.90
400	2060 to 2128	8.19, 8.02
500	2130 to 2198	9.66
1000	2480 to 2548	9.48, 9.03

Experimental factors that may affect the measurement of crack velocity are discussed below. Experiences from Phase 2 are included for completeness.

(1) Peak temperature

To maximize DHC velocity the zirconium alloy matrix should contain the maximum supersaturation of hydrogen [4.4]. This supersaturation can only be attained if all the hydrides are dissolved. Thus the peak temperature was set at least 5°C greater than the solvus temperature for hydride dissolution. For the range of hydrogen concentrations used at 250°C, the peak temperature had to be greater than between 298 and 306°C, and was set at 315°C to provide some margin on this factor. Some laboratories used peak temperatures lower than the recommended value, and consequently their values of crack velocity may be lower than expected, Table 4.4. For example, the values of crack velocity from China and India are the lowest and third lowest, respectively, and their peak temperatures were on the borderline of attaining full supersaturation.

(2) Under cooling at test temperature

Above a test temperature of about 180°C, if the test temperature is attained by heating, the crack velocity is less than the maximum value [4.4–4.8]. Hence we recommend that undercooling be avoided. In two early tests in Romania the test temperature of 250°C was attained after small undercoolings of about 2 and 2.5°C and the crack velocities were 6.3 and 5.7×10^{-8} m/s, respectively; with no undercooling the lowest value was 7.99×10^{-8} m/s. The values obtained after undercooling were excluded in determining the mean value of 8.9×10^{-8} m/s.

Table 4.4. Mean crack velocity at 250°C from various peak temperatures

Country	Hydrogen Concentration (ppm)	Solvus Temperature (°C)	Peak Temperature (°C)	Mean Crack Velocity ($m/s \times 10^{-8}$)
Argentina	57,59	298-300	313-315	9.48
Canada	57,59	298-300	315-320	8.79
China	59,59	300	305-308	7.81
India	59,63	300-306	304-305	8.19
Rep. of Korea	55,56	295-296	315	10.1
Lithuania	55,56	295-296	315	9.04
Pakistan	59,59	300	315-317	8.66
Romania	59,59	300	315	8.9
Russia	59,63	300-306	311-316	8.02
Sweden	56,60	296-302	319-321	9.66

(3) Cooling rate to test temperature

If Zr-2.5 Nb containing hydrogen in solution is cooled rapidly (>100°C/s) to below the solvus for precipitation, very small hydride precipitates form. The subsequent DHC velocity is much higher than in material that has been slowly cooled [4.9]. Thus in this test programme care was taken to control the cooling rate to the test temperature. In all the laboratories the cooling rate was between 1.0 and 2.7°C/min., Table 4.5, thus variation from differences in hydride size was minimised.

Table 4.5. Cooling rates used by each laboratory

Country	Cooling rate to test Temperature °C/min
Argentina	2.2
Canada	1 to 2
China	1.5
India	1
ROK	2.7
Lithuania	1.5
Pakistan	1.1
Romania	1.8
Russia	1 to 2
Sweden	1 to 2

(4) Actual test temperature

Crack velocity is sensitive to temperature through $V = A\exp(-Q/RT)$. As an illustration, using $A = 8.74 \times 10^{-3}$ and Q=50 kJ/mole, around 250°C, V changes by about 0.2×10^{-8}m/s per °C. Canada, India and Sweden reported small deviations from a test temperature of 250°C and the consequences are depicted in Fig. 4.4.

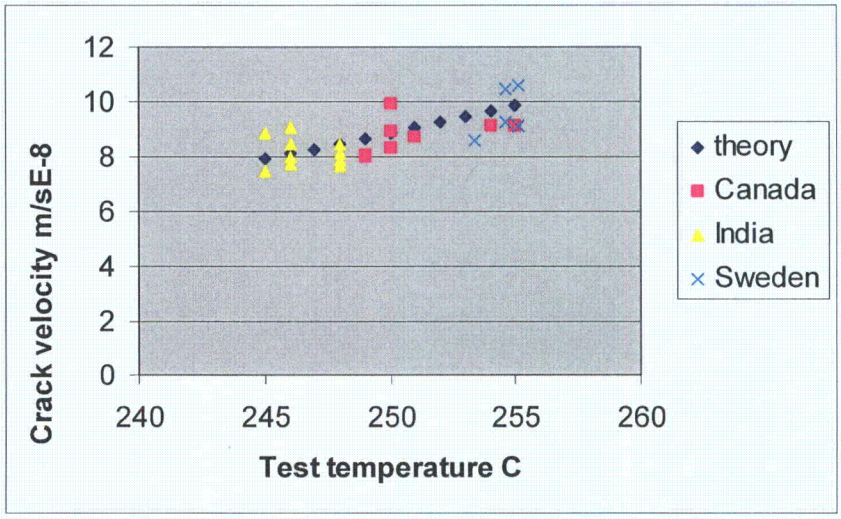

Fig. 4.4. Scatter in crack velocity as a consequence of deviation from 250 °C.

(5) Measurement of crack length

The two methods for measuring crack length were evaluated by ROK on six specimens. The nine-point method tends to miss specimen edges and the occasional longitudinal slit. (These slits are probably caused by the fracture of circumferential hydrides by the component of applied stress parallel with the crack plane in the thickness direction.) Since the crack front is retarded in these areas, the area method will provide a truer picture of the extent of fracture and will tend to produce lower values of crack growth than the discrete point method. The size of this difference is between 1 and 9%.

(6) Crack length

The recommended amount of crack growth by DHC is 1.5 mm. Although DHC velocity is reported to be independent of K_I over a wide range of K_I [4.2], crack growth should be limited to prevent changing the operating stress state from mostly plane strain to one of plane stress, as illustrated by the edge-effect. Since the exact crack length after fatigue pre-cracking was uncertain, there was a variation in initial values of K_I ranging from 13.3 to 20.0 MPa$\sqrt{m}$ with a mean value of 15.9 ± 1.7 MPa$\sqrt{m}$, close to the recommended value of 15 MPa$\sqrt{m}$. Most laboratories obtained seemingly valid results with crack growths in the range 0.86 to 4.0 mm; the mean crack growth by DHC in all the tests at 250°C was 1.91 ± 0.52 mm. The final K_I was in the range 19.8 to 40.3 MPa$\sqrt{m}$ with a mean value of 24.1 ± 4.5 MPa$\sqrt{m}$. Two contradictory observations were made. In early tests in China, crack growth longer than 4 mm appeared to induce plasticity that interfered with the DHC and slowed the crack growth; the final K_I values were up to 55 MPa$\sqrt{m}$ but the crack velocities were $<5 \times 10^{-8}$ m/s. (These results are excluded from the data set.) Alternatively, some results from Russia provide the opposite result; the crack growths varied from 1.5 to 2.28 mm and the derived velocities ranged from 5.8×10^{-8}m/s to 11.6×10^{-8}m/s. When all the results are pooled, no dependence or correlation between crack velocity and crack length or final K_I is observed, Figs 4.5 and 4.6, confirming expectations of K_I independence and suggesting that the latter results are a coincidence.

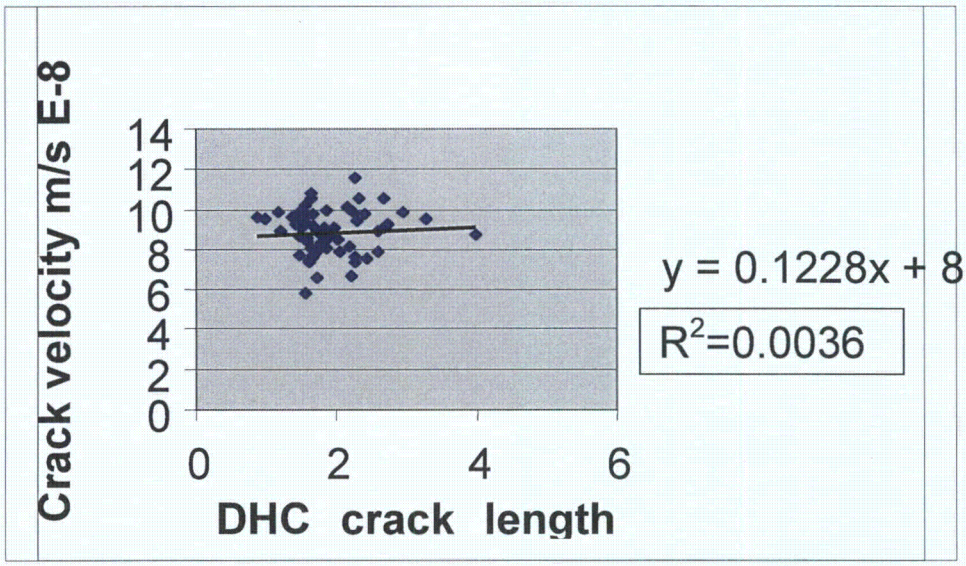

Fig. 4.5. Lack of dependence or correlation between amount of crack growth and DHC velocity at 250 ℃.

(7) Cracking time

Cracking starts after hydrides have grown at the initial crack tip and the conditions for cracking these hydrides has been established. Time is required to attain these conditions and a period of apparent inactivity, (for example, no change in the potential drop,) is observed between the initial application of the load and the start of cracking. This period is called the incubation time. An accurate assessment of incubation time depends on the sensitivity of the crack detection system, and in these experiments was very scattered. The time for the end of the test is established very accurately because it corresponds to the final unloading of the specimen. Thus the accuracy of the cracking time depends on observing the start of cracking. In the tests at 250°C the incubation time was usually very short, a few minutes, or even zero; occasionally cracking did not start for 20 min. and in one specimen the incubation time was 40 minutes. The mean incubation time, excluding the longest time, was 3.3±4.2 min. Since the average cracking time was 362±103 min., incubation time represents about 1% of the test time and any error in its value contributes little to the variation in crack velocity.

(8) Fatigue pre-cracking

If K_I is reduced during a test a new incubation period is required before cracking can restart [4.4, 4.5, 4.7]. Similarly if the final K_I during fatigue pre-cracking is greater than the starting K_I for the DHC test, crack initiation is much delayed. In some early tests in Romania cracks could not be initiated or the cracks propagated a small amount then stopped. This experience was attributed to pre-loading the crack by fatigue. When the final K_I of fatigue was lower than the DHC test load, the crack propagated by DHC at the expected rate. The results of these early tests are not included in the database.

(9) Loading rate

Another possible explanation of the variability in crack initiation was thought to be because of differences in specimen loading. For example, rapid application of the load may lead to plastic overload at the crack tip. A survey indicated that most laboratories used dead-weight loading that was applied manually at rates ranging from about 10 N/s up to 80 N/s. Since testing was successful with such a range of methods of loading, it was not considered further as contributing to variability.

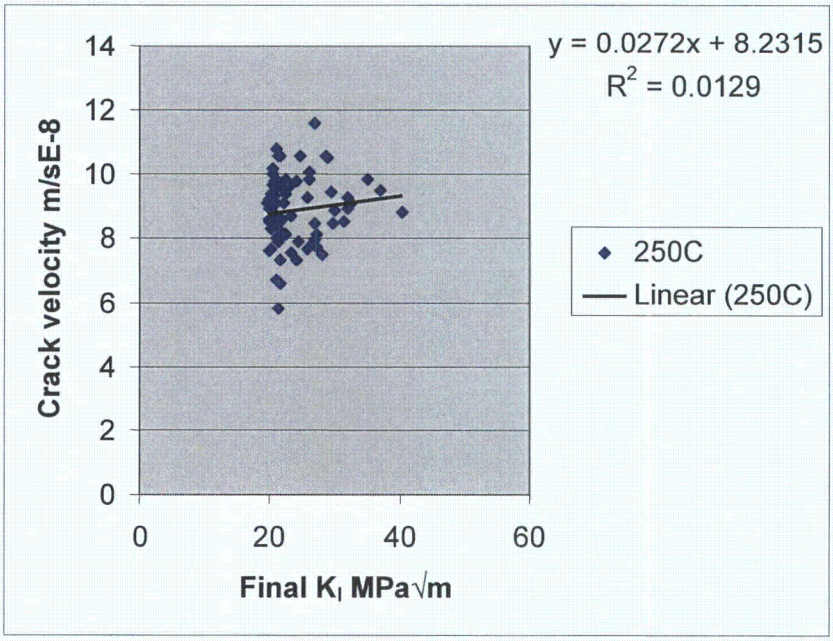

Fig. 4.6. Lack of dependence or correlation between DHC velocity and final K_I.

In summary, the chief experimental factors contributing to the variation in the values of crack velocity that have been accepted into the database, Table 4.1, appear to be variation in peak temperature and actual test temperature. The other factors considered appear to be under good control and contribute little to the scatter in data.

4.3. Phase 2: Tests at Other Temperatures on CANDU Pressure Tube

4.3.1. Specimen preparation

The formation of the hydride layer to supply hydrogen to the specimens was consistent within each laboratory but quite variable between each laboratory:

Country	Argentina	Canada	China	India	ROK	Lithuania	Pakistan	Romania	Russia
Hydriding rate μm/h	0.62	0.62	0.64 (CANDU) 2.5 (RBMK)	1.7	0.64	1.9	0.5 (CANDU) 1.6 (RBMK)	4.2	0.58

The hydriding rates of the CANDU tube RX094 could not be distinguished from those of the RBMK TMT-1 tube, except in China and Pakistan. Since the electrolyte, current density and electrolysing temperature were similar in all laboratories, the main source of variation was attributed to variation in surface preparation. For example, in Pakistan the hydriding rate after a final grinding with 1200 Emery paper was about 0.5 μm/hour while after pickling in 30% HNO_3/30%H_2SO_4/30%H_2O/10%HF the hydriding rate increased by a factor of two to four.

The final hydrogen concentration after annealing was also highly variable and did not correlate well with the expectation based on the TSSD [4.10], Fig. 4.7.

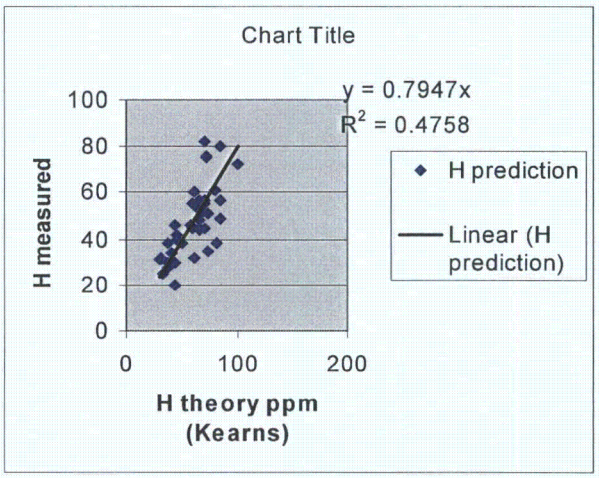

Fig. 4.7. Measured hydrogen concentrations after annealing hydride layers compared with expected hydrogen concentration based on Kearns' TSSD. Trend line forced through zero.

The sources of error are:

(a) insufficient time at the annealing temperature to allow the hydrogen concentration to approach equilibrium,
(b) errors in annealing temperature,
(c) insufficient hydride layer,
(d) retention of some hydride layer before hydrogen analysis,
(e) variation in hydrogen analysis.

Points (a), (b), c) and (e) could contribute to values of hydrogen concentration that are too low while points (b), (d) and e) could contribute to values of hydrogen concentration that are too high. It was outside the scope of this study to pursue in detail the sources of the variation although point (e) will be addressed in the section reporting on the inter-laboratory comparison of hydrogen analysis.

Typical distributions of hydrides are depicted in Figs 4.8 for CANDU material and Fig. 4 9 for RBMK TMT-1 material. In both materials the hydrides are well aligned with the direction of cold-work giving strong traces in the axial direction, as seen on the radial-axial sections. In the radial-transverse sections, the hydrides are still aligned but the traces are scattered about the transverse direction, but rarely approach the radial direction. Before testing the normals to the hydride plates are mostly in the radial direction, which is perpendicular to the expected plane of cracking. The length and breadth of the hydride traces are generally much smaller than 100 μm.

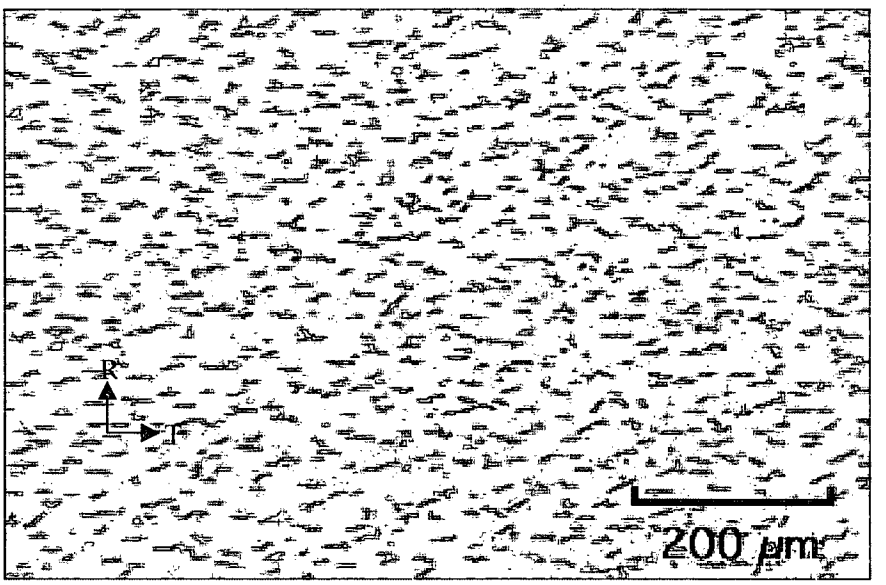

(a)

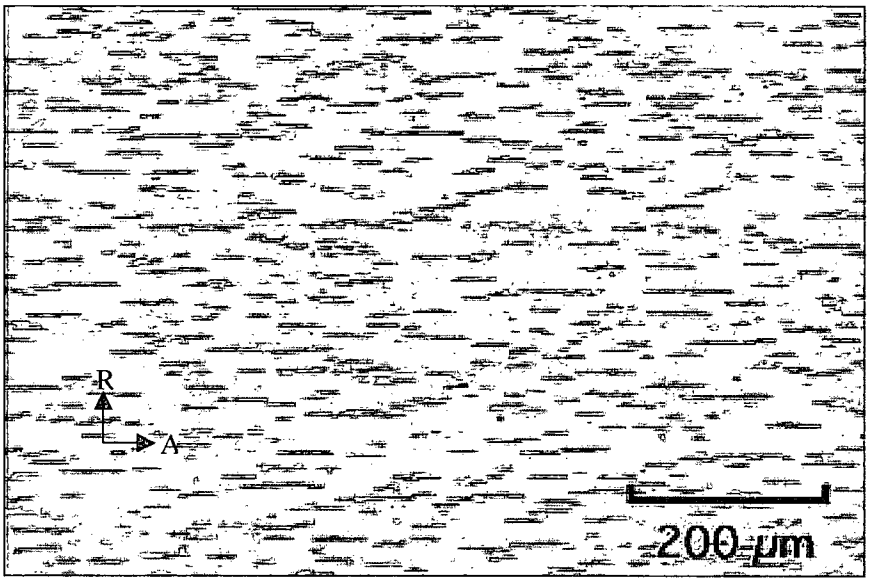

(b)

Fig. 4.8. Hydride distribution in CANDU pressure tube material with a hydrogen concentration of 79 ppm.: a - radial-transverse section; b – radial-axial section.

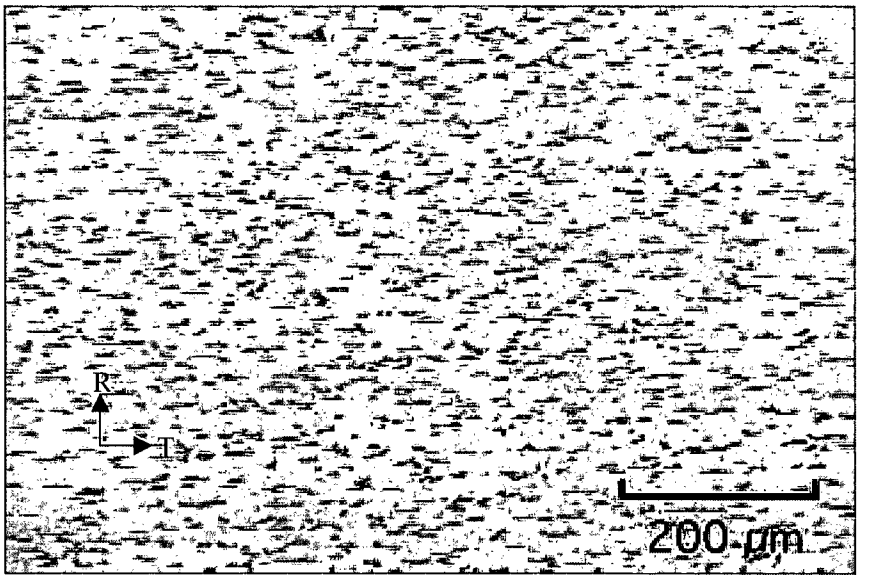

(a)

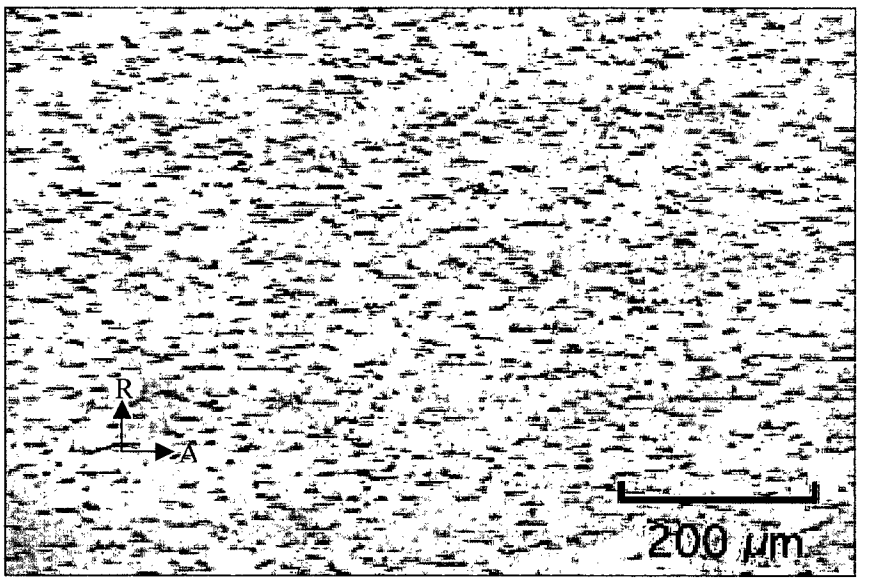

(b)

Fig. 4.9. Hydride distribution in RBMK TMT-1 pressure tube material with a hydrogen concentration of 76 ppm. a - radial-transverse section; b – radial-axial section.

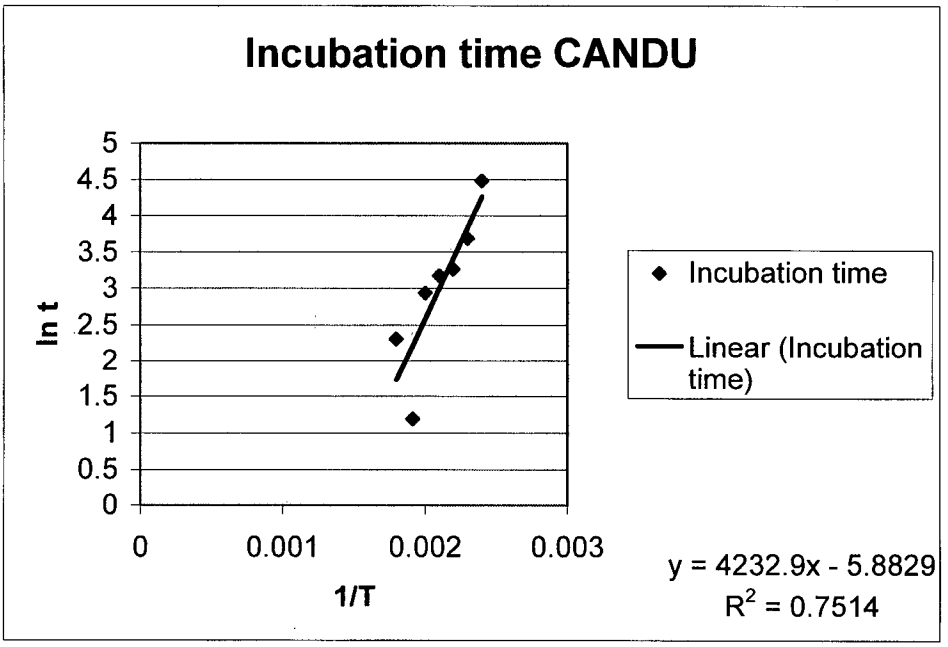

Fig. 4.10. Temperature dependence of mean incubation time for DHC in CANDU Zr-2.5 Nb pressure tube.

4.3.2. Results of DHC tests

Despite the mixed performance of the additions of hydrogen to the material, the DHC tests were successful, Appendix 4. The prescribed testing conditions were adhered to and the amounts of crack growth were not excessive. As with the first tests at 250°C, the incubation times to the start of continuous cracking were quite variable, with large dispersions, represented by the standard deviation and the range, Table 4.6. Contributing factors are the sensitivity of the crack monitoring equipment in resolving a change in potential drop and variations in the preparation of the starter-crack by fatigue. The incubation times consumed less than 5% of the total test time in all but five of the 89 tests, thus error in their determination contributed only a small error to the crack velocity.

Table 4.6. Summary of incubation times in CANDU Zr-2.5 Nb pressure tube RX094

Test Temperature °C	283	250	227	203	182	162	144
Mean value (min)	10	3.3	19	24*	26#	40	89
Standard deviation (min)	7.4	4.2	12	26*	16#	75	48
Maximum value (min)	27	40	36	84	61	190	162
Minimum value (min)	3	0	0	0.7	5	0.3	6

* Excludes values of 284 and 461 min. If these values are included, the mean value is 77 min. and the standard deviation is 138 min.
# Excludes values of 237 and 1489 min. If these values are included, the mean value is 166 min. and the standard deviation is 420 min.

The incubation time partly depends on the rate of arrival of hydrogen to the initial crack tip and thus it will tend to decrease as the test temperature is increased. This expectation is confirmed, Fig. 4.10, although the correlation is poor.
The crack velocities obtained at temperatures in the range 144°C to 283°C are summarized in Table 4.7. The standard deviations of the mean values range from 38% down to 8% of the mean while the range of values at any one temperature varies from a factor of 5.2 down to 1.3. The values of crack velocity have a clear and highly correlated temperature dependence described by $V = A\exp(-Q/RT)$. Fig. 4.11 and Fig. 4.12 depict the temperature dependence of the mean values and total data set, respectively, including the data from the tests at 250°C. The statistical parameters of the data set are summarised in Table 4.8. Q has a value of 45.4 kJ/mol based on the mean values and 47.9 kJ/mol based on all the data. Linearity is not verified using the total data. The correlation is higher but the confidence is lower using the mean values.

In the literature the value of Q has a wide range of values, 72 to 42 kJ/mol, with the current value being at the low end of the range. The main source of the discrepancy is the variety of temperature histories involved in the tests. The temperature dependence of DHC velocity arises through the temperature dependence of the solubility limit and diffusivity, which are responsible for transporting the hydrogen to the crack tip. The product of their activation energies over predict that for crack velocity, and other factors, such as the negative temperature dependence of the yield stress, are involved in describing the temperature dependence of V. These issues will be discussed further when the data from the other materials have been presented.

4.4. Phase 3: Tests On Other Materials

4.4.1. RBMK Zr-2.5 Nb with TMT-1 heat-treatment

A similar set of tests were performed on this material in the temperature range 144°C to 283°C with results qualitatively similar to those obtained on the CANDU tube. The complete results are included in Appendix 4.

Again the incubations times were very scattered, Table 4.9, but the mean values decreased with increasing test temperature, Fig. 4.13. The incubation time occupied over 5% of the test time in only seven of the 105 tests thus errors in crack velocity from this source are very low.

Although the data for both materials are very scattered, the mean values of the incubation times appear to be different, Fig. 4.14, with those for RBMK TMT-1 tube being longer than those for the CANDU tube.

The crack velocities obtained on the RBMK tube in the TMT-1 condition at temperatures in the range 144°C to 283°C are summarized in Table 4.10. The standard deviations of the mean values range from 36% down to 7% of the mean while the range of values at any one temperature varies from a factor of 4.5 down to 1.2. As with the CANDU material, the values of crack velocity have a clear and highly correlated temperature dependence described by $V = A\exp(-Q/RT)$. Figure 4.15 and Fig. 4.16 depict the temperature dependence of the mean values and total data set, respectively. Linearity of these plots is verified for both presentations of the data. The statistical parameters of the data set are summarised in Table 4.11. Q has a value of 54.3 kJ/mol based on the mean values and 55.5 kJ/mol based on all the data. The correlation is higher but the confidence is lower using the mean values.

Table 4.7. Summary of crack velocities in CANDU Zr-2.5 Nb pressure tube RX094

Test temperature °C	283	227	203	182	162	144
Crack Velocity 10^{-8} m/s	8.3	3.6	2.1	1.3	0.62	0.57
	6.3	4.4	2.0	1.4	0.60	0.59
	5.6	4.3	2.1	1.2	0.74	0.55
	6.9	4.0	1.8	0.58	0.87	0.52
	6.8	4.1	2.3	0.98	0.88	0.54
	17.7	3.8	1.9	2.0	0.79	0.57
	10.5	3.3	1.9	0.41	0.38	0.52
	10.8	5.7	3.2	2.2		0.59
	14.2	5.6	3.0	1.9		0.51
	9.5	6.0	2.5	1.9		0.49
	13.5	5.6	2.8	1.5		0.48
	14.1	5.2	2.1	1.5		0.45
		4.9	3.1	1.6		0.52
		4.2	1.6			0.54
		4.7	2.5			
		6.2	2.7			
		4.3	3.1			
		2.3	2.4			
			2.8			
			2.3			
			2.1			
			2.5			
Mean value	10.4	4.5	2.4	1.4	0.70	0.53
Standard deviation	3.8	0.98	0.46	0.53	0.18	0.041
Stdev/mean	0.37	0.22	0.19	0.38	0.26	0.08
Highest V/lowest V	3.2	2.6	2.0	5.2	2.3	1.3

Table 4.8. Statistical summary of DHC tests on CANDU Zr-2.5 Nb pressure tube

	Q kJ/mol	Standard Error on Q kJ/mol	Upper 95% Confidence of Q kJ/mol	Lower 95% Confidence of Q kJ/mol	A m/s	R^2
Mean values	45.4	2.76	52.5	38.3	2.33 10^{-3}	0.98
All data	47.9	1.03	50.1	45.8	8.31 10^{-3}	0.92

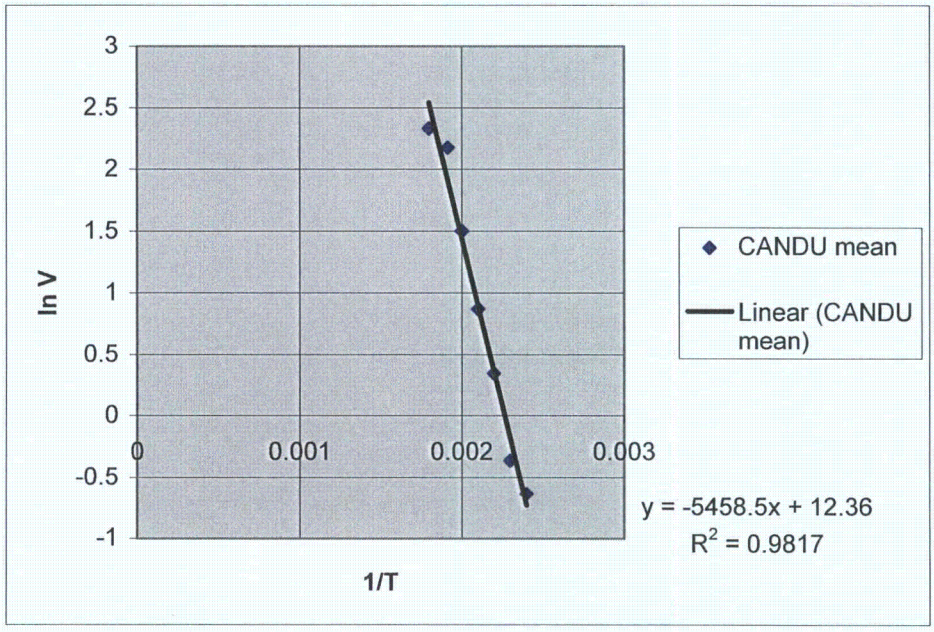

Fig. 4.11. Temperature dependence of mean velocity of DHC for CANDU Zr-2.5 Nb pressure tube RX094.

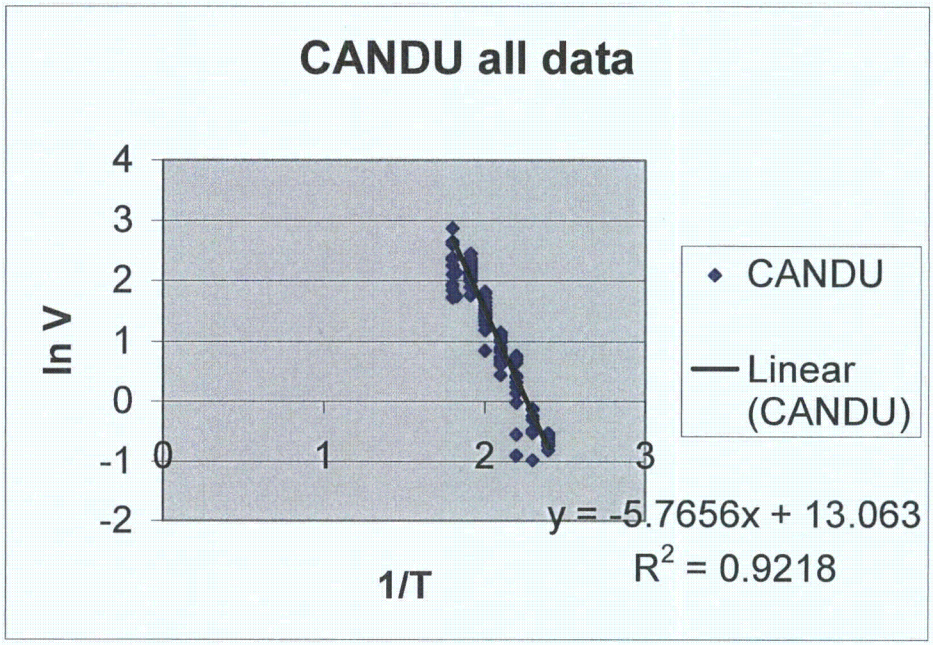

Fig. 4.12. Temperature dependence of velocity of DHC for CANDU Zr-2.5 Nb pressure tube RX094 based on all tests.

Table 4.9. Summary of incubation times in RBMK Zr-2.5 Nb pressure tube in TMT-1 condition

Test Temperature °C	283	250	227	203	162	144
Mean value (min)	37	25	29	56	123	660
Standard deviation (min.)	41	44	28	52	134	1080
Maximum value (min.)	120	172	66	148	347	3084
Minimum value (min.)	5	0	1	0	0	67

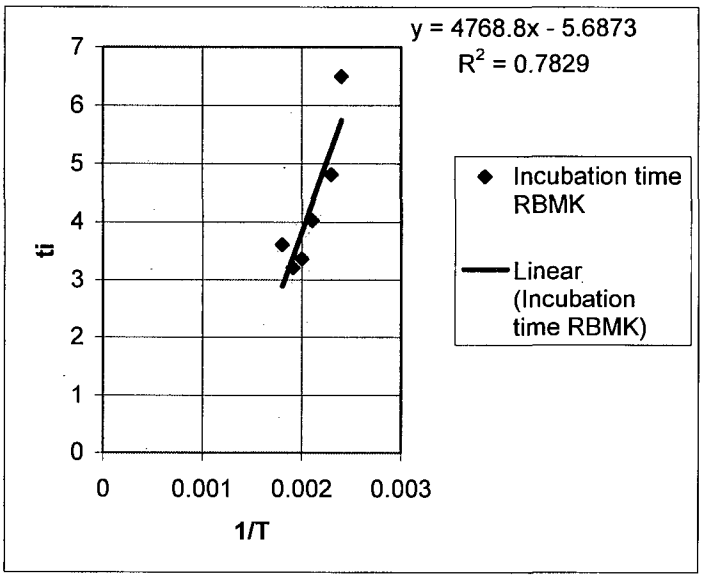

Fig. 4.13. Temperature dependence of mean incubation time for DHC in RBMK Zr-2.5 Nb pressure tube in TMT-1 condition.

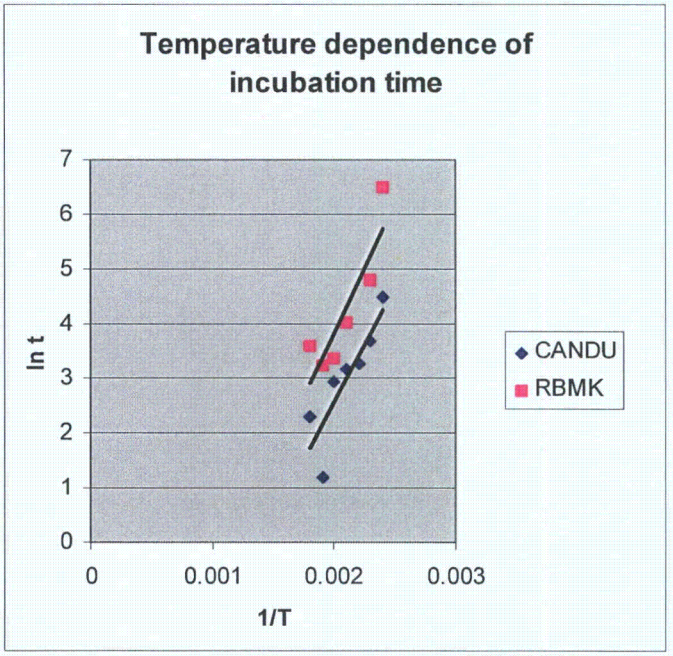

Fig. 4.14. Comparison of incubation times for DHC in CANDU and RBMK TMT-1 tubes.

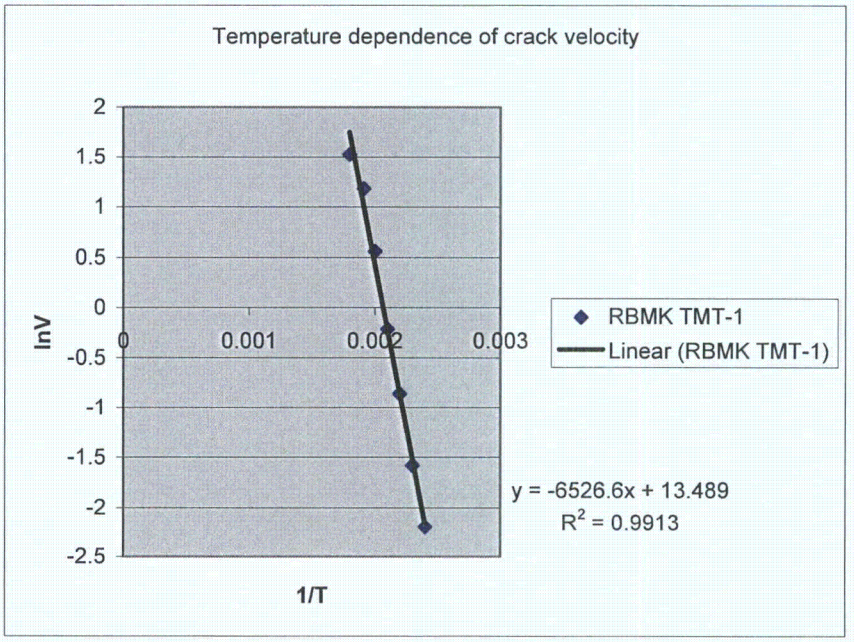

Fig. 4.15. Temperature dependence of mean velocity of DHC for RBMK TMT-1 Zr-2.5 Nb pressure tube.

Table 4.10. Summary of crack velocities in RBMK TMT-1 Zr-2.5 Nb pressure tube

Test temperature °C	283	250		227	203	182	162	144
	4.0	4.0	3.2	2.3	0.85	0.41	0.21	0.11
Crack velocity	3.7	4.0	3.0	2.0	0.54	0.44	0.23	0.11
m/s x10 ^{8}	4.8	3.8	3.3	2.1	1.0	0.43	0.20	0.12
	5.0	3.6	3.1	2.1	1.0		0.21	0.11
	4.3	3.7	3.6	2.0	1.0		0.19	0.11
	5.6	1.9	3.8	2.0	0.54		0.2	0.13
	5.9	1.6	3.7	1.9	0.80		0.22	0.13
	4.1	1.6	3.1	2.0	1.0			0.14
	4.0	1.7	3.9	2.0	0.99			0.094
	4.7	3.0	3.8	2.1	0.64			0.091
		2.6	4.0	2.0	0.71			0.095
		2.5	3.8	1.4	0.69			
		3.4	3.4	1.4	0.71			
		3.4	3.4	2.0				
		3.3	3.2	2.1				
		3.4	3.3	2.2				
		3.1	3.3	1.9				
		3.6	3.2	0.51				
		3.1	3.4	0.52				
		3.3	4.0	0.54				
			4.1					
Mean value	4.6	3.3		1.76	0.81	0.42	0.21	0.11
Standard deviation	0.74	0.64		0.63	0.19	0.013*	0.014	0.015
std.dev./mean	0.16	0.20		0.36	0.23	0.03*	0.07	0.14
Highest V/lowest V	1.6	2.7		4.5	1.9	1.1*	1.2	1.5

* Too few values to be statistically useful.

Table 4.11 Statistical summary of DHC tests on in RBMK TMT-1 Zr-2.5 Nb pressure tube

	Q kJ/mol	Standard Error on Q kJ/mol	Upper 95% Confidence of Q kJ/mol	Lower 95% Confidence of Q kJ/mol	A m/s	R^2
Mean values	54.6	2.26	60.1	48.4	7.3×10^{-3}	0.99
All data	55.5	1.4	58.3	52.7	1.01×10^{-2}	0.94

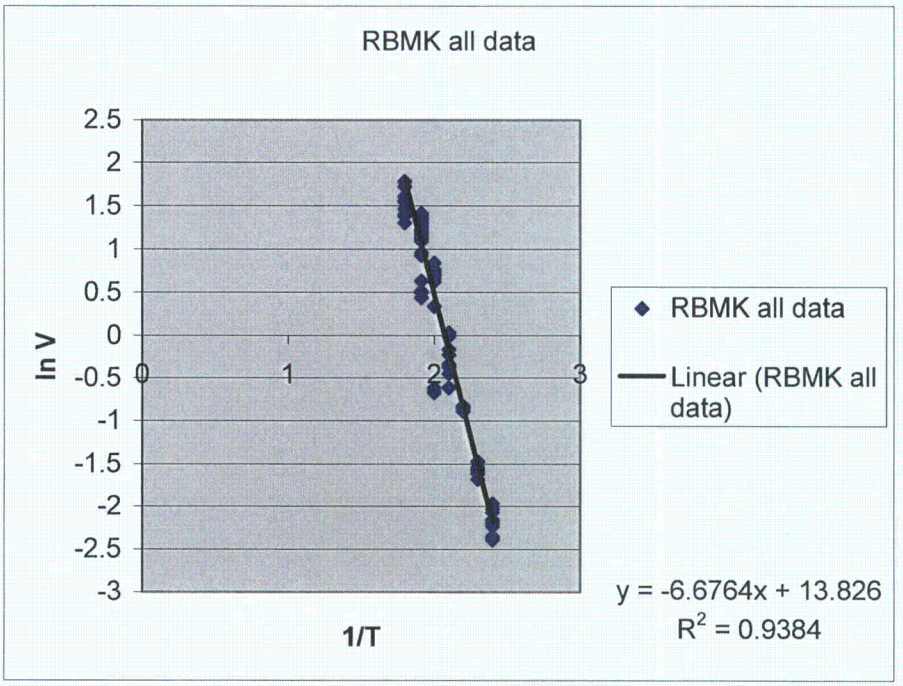

Fig. 4.16. Temperature dependence of velocity of DHC for RBMK TMT-1 Zr-2.5 Nb pressure tube based on all tests.

The mean values of crack velocity of the RBMK TMT-1 material appear much lower than those for the CANDU tube. The t-test was used to analyse both the total population and the mean values from each country at 250°C. The assumptions for validity for the t-test were examined. The DHC testing is considered to be random because each tube and the location of the test pieces were selected arbitrarily.

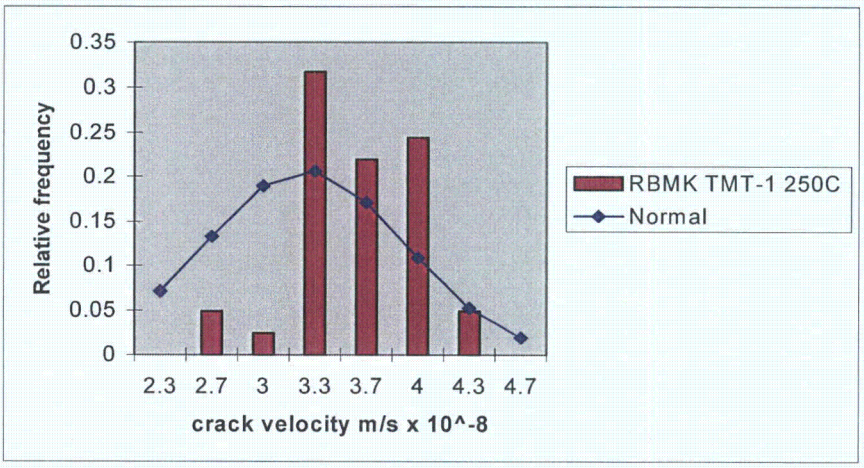

Fig. 4.17. Frequency distribution of crack velocities at 250℃ of RBMK TMT-1 pressure ube.

The data from the RBMK tube were not well represented by a normal distribution. Figure 4.17, although adherence to strict normality can be relaxed. The dispersions of the total sample population were quite distinct, so one has to be careful in case any difference is caused by the differences in dispersion rather than the means. The standard deviations of the total samples were 1.1 for CANDU and 0.64 for RBMK, while those of the means were similar, 0.74 versus 0.70. The t-values of 31 (total sample) and 17 (means) were so large and significant that the difference between the two tubes is real: the crack velocity in the CANDU tube was 2.7 times faster than in the RBMK TMT-1 tube at 250°C. This conclusion is further reinforced when the distributions of values are compared; they are clearly distinct, Fig. 4.18.

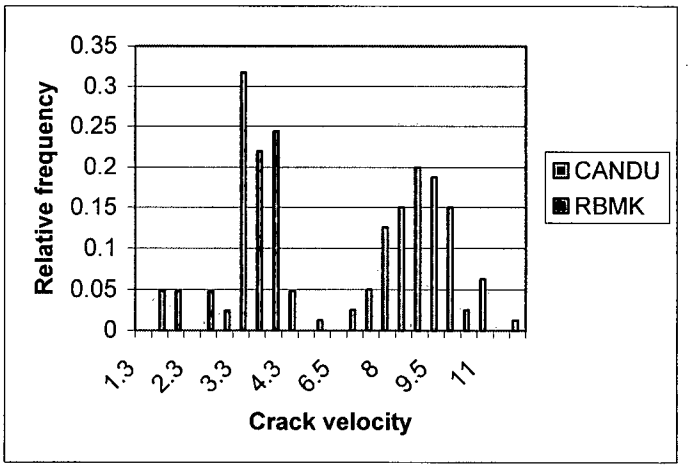

Fig. 4.18. Comparison of distributions of crack velocities at 250°C in CANDU and RBMK TMT-1 tubes (velocities have units of m/s x 10^{-8}).

Assuming that a similar analysis is valid at the other test temperatures, crack velocities were always greater in the CANDU tube than in the RBMK TMT-1 tube, with a possible increase in the ratio of velocities as the test temperature was lowered:

Temperature °C	283	250	227	203	182	162	144
CANDU/RBMK TMT-1: means	2.25	2.71	2.71	2.95	2.91	3.37	4.75

The difference in behaviour of the two tubes is also illustrated by the Arrhenius plot, Fig. 4.19:

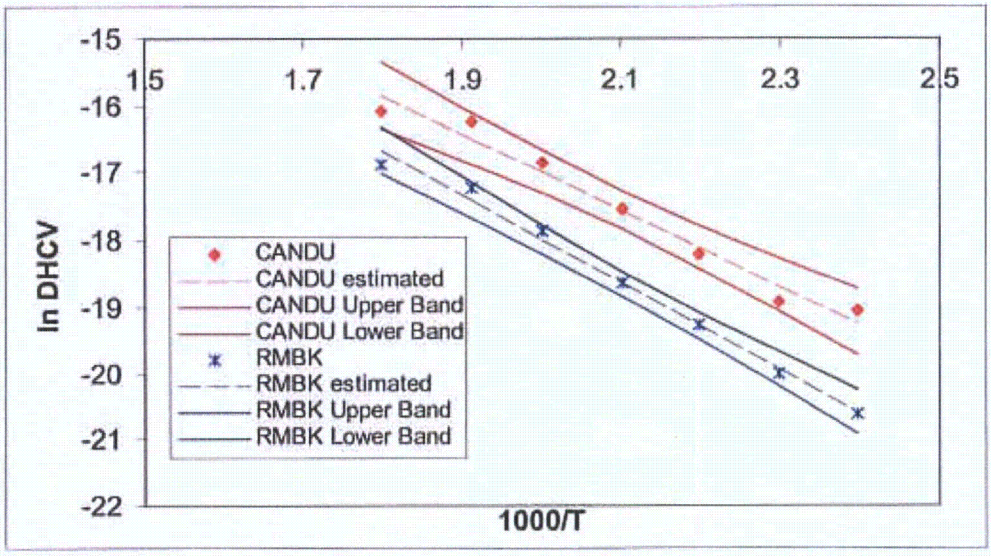

Fig. 4.19. Comparison of crack velocities of DHC in CANDU and RBMK TMT-1 tubes.

Having concluded that the crack velocities of the two tubes are clearly distinguishable over the whole range of test temperatures, we now consider their temperature dependencies. The values of Q in Tables 4.8 and 4.11, the ratios of the crack velocities and Fig. 4.19 all suggest that the RBMK TMT-1 tube has greater temperature dependence than the CANDU tube. However, statistically the temperature dependencies cannot be separated. This conclusion will be reinforced when the next sets of results are presented.

4.4.2. CANDU tube from Cernavoda

Velocity of DHC was measured at 250°C, 227°C and 203°C on specimens machined from tube 429. The results are included in Appendix 4 and summarised in Table 4.12.The values are slightly larger than those of tube RX094 although t-tests show they are essentially indistinguishable. The temperature dependence is also similar, Fig. 4.20, with an activation energy of 59.4 kJ/mol. This value is not very reliable because it is based on only three test temperatures. The technical significance of this result is that the two pressure tubes, which were chosen at random, one made from an ingot that was double melted and one from an ingot that was melted four times, have similar DHC behaviour, strongly suggesting that ingot preparation has no effect on the velocity of DHC [4.11].

Table 4.12. Summary of crack velocities in Cernovoda CANDU pressure tube 429

Test Temperature °C	250	227	203
Crack velocity $m/s \times 10^{-8}$	10.0 9.3 9.4	6.3 5.6 5.0 5.1 5.0 4.8 5.8 4.7	2.2 2.3 2.7 3.0 2.5
Mean value	9.6	5.3	2.5
Standard deviation	0.34	0.56	0.31
Difference of means (429-RX094) %	7.9	10.8	5.3

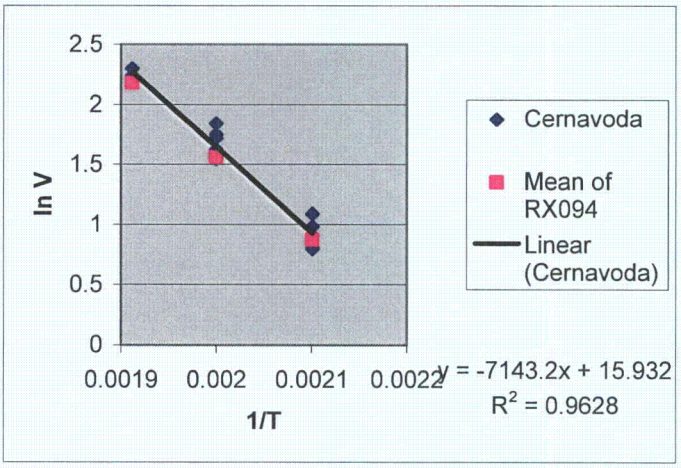

Fig. 4.20. Temperature dependence of DHC in Cernovoda Zr-2.5 Nb pressure tube 429.

4.4.3. HWR tube from India

Velocity of DHC was measured in the temperature range 283 to 162°C on specimens machined from tube 100-2-3. The results are included in Appendix 4 and summarised in Table 4.13.

Table 4.13. Summary of crack velocities in Indian HWR pressure tube 100-2-3

Test temperature °C	283	250	227	203	182	162
Crack velocity $m/s \times 10^{-8}$	16.2 17.7	8.5 9.2 8.1 7.2 6.3 6.6 6.8 8.2	4.2 4.5 3.5	2.6 2.3 1.6 1.9 2.1 1.9	0.96 0.97 1.0	0.56 0.80 0.47
Mean value Standard deviation	16.9 -	7.6 1.05	4.1 0.49	2.1 0.33	0.99 0.043	0.61 0.17
Difference in means ((100-2-3)-RX094)%	38.5	-16.5	-10.7	-16.7	-41.3	-14.7

Except at a test temperature of 283°C, the values are slightly lower than those of tube RX094, although t-tests show they are from the same population. The temperature dependence is also similar, Fig. 4.21, with an activation energy of 56.4 kJ/mol.

Again, tubes made from ingots with different melting practice and slightly different microstructure, have similar DHC behaviour [4.12].

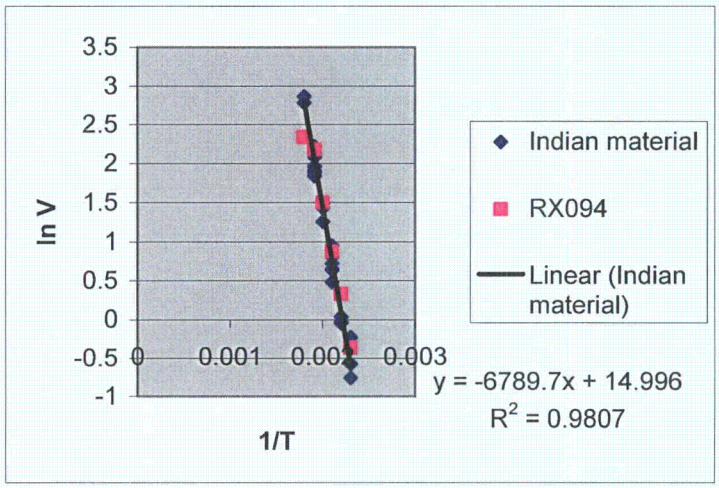

Fig.4.21. Temperature dependence of DHC in Indian Zr-2.5 Nb pressure tube 100-2-3.

4.4.4. Other RBMK materials

The velocity of DHC was measured at 250°C on specimens machined from a standard RBMK tube, from a standard tube in which the recrystallization treatment was absent and from a tube given the TMT-2 treatment. About 100 ppm hydrogen were added gaseously to all specimens. The results are included in Appendix 4 and summarised in Table 4.14.

Table 4.14. Incubation times and velocity of DHC at 250°C for three RBMK tubes

Material	RBMK Standard	RBMK no annealing	TMT-2
Incubation time	3240	29	160
Minutes	1244	18	140
	1560		197
Crack velocity	1.7	13.2	6.0
m/s 10^{-9}	3.2	17.1	6.1
	1.9		6.6
Mean value, V	2.3	15.2	6.3

Cracks were reluctant to grow in the standard RBMK material and the initial K_I used was higher than with other materials, about 21 MPa$\sqrt{m}$. The incubation times to the start of cracking were very long and the rate of cracking was low in this material. The other materials exhibited faster cracking but still lower than that in cold-worked Zr-2.5 Nb.

4.4.5. Alternative measurement method – CANDU Tube RX094

The standard method was not followed in Argentina because of difficulties in obtaining an accurate hydrogen analysis. This uncertainty led to uncertainty in what peak temperature to use and what test temperature to apply. The hydrogen concentration may be estimated by finding the temperature at which cracking starts after cooling from a temperature well above any reasonable solvus temperature for dissolution [4.13–4.15]. The test sequence was to heat to 330°C, well above the annealing temperature used for adding the hydrogen, cool to a trial test temperature, load the specimen and wait for the potential drop to indicate cracking. If no cracking was observed after a time that was several times the expected incubation time, the temperature was lowered. This process was followed until a temperature, T_c, was reached where cracking was detected, Fig 4.22. In this example, T_c was about 282°C. The value of T_c was related to the TSSP [4.15]. The crack front was marked either by overloading or heat-tinting, although the former gave erratic results in the RBMK TMT-1 material. On further lowering the test temperature, the crack grew and the velocity was estimated from the extent of cracking measured on the crack surface divided by the time of cracking as indicated by potential drop. As observed by Ambler [4.6], once cracking had initiated, with a reduction in temperature of about 10 to 20°C the crack velocity increased, passed through a maximum value then decreased as $V=Ae^{-Q/RT}$. Both of the common pressure tubes behaved in a similar manner, except cracking in the RBMK TMT-1 tube was about 2.5 times slower than in the CANDU tube, Fig. 4.23.

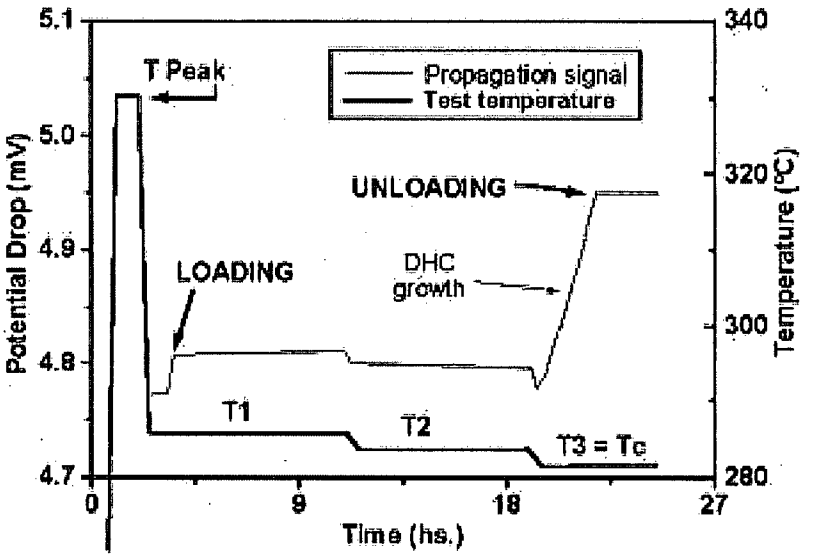

Fig. 4.22. Progressive cooling to evaluate the temperature at which DHC starts.

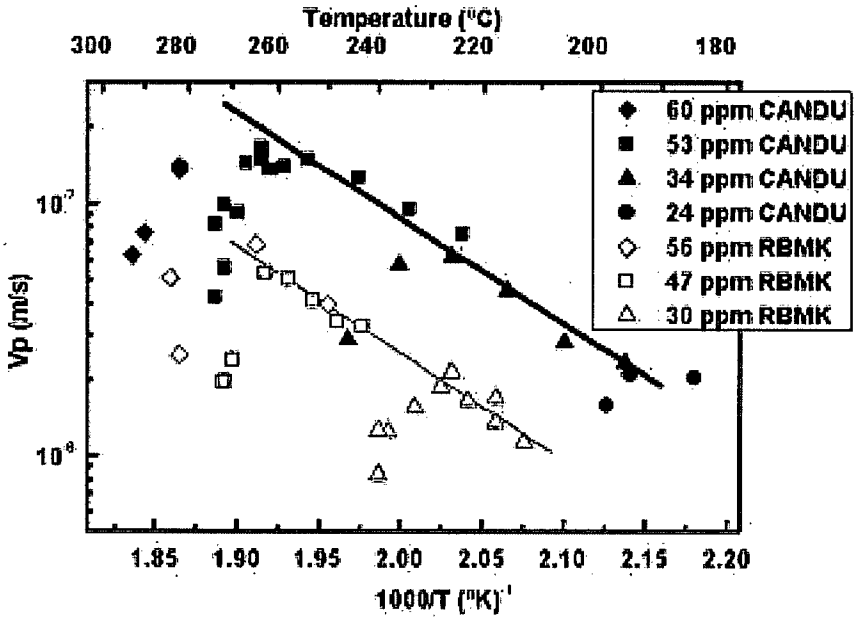

Fig. 4.23. Crack velocity as a function of inverse temperature during cooling showing maximum velocity below T_c followed by Arrhenius-behaviour at lower temperatures.

4.5. Striations

A prominent fractographic feature of DHC in Zr-2.5 Nb is the formation of striations perpendicular to the crack direction. Typical examples are shown in Fig. 4.24 for both the main pressure tubes.

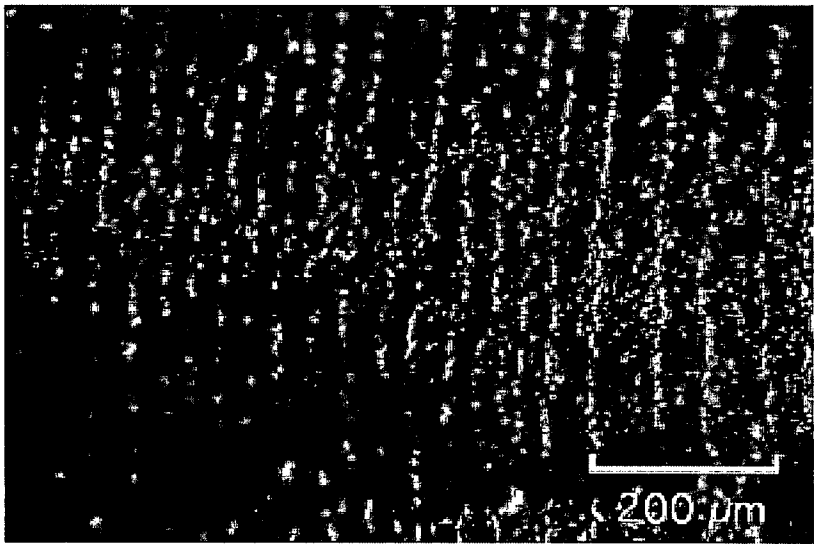

A)

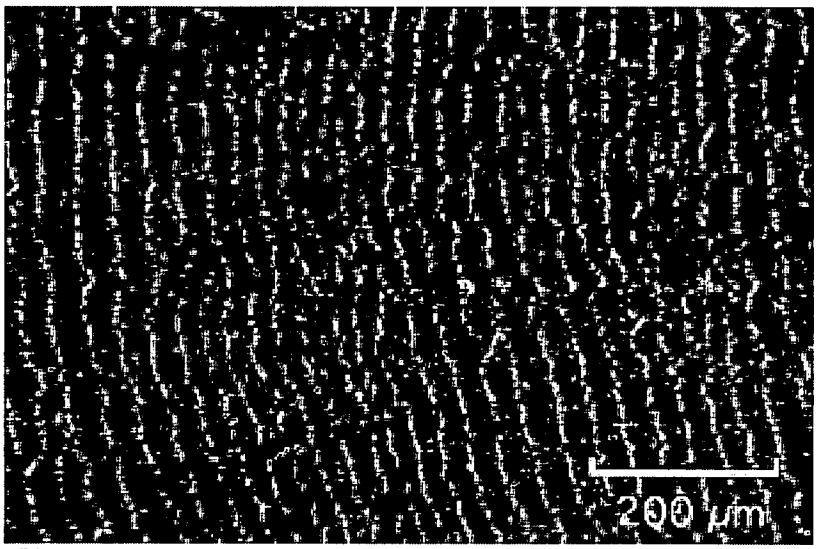

B)

Fig. 4.24. Striations formed by DHC at 283 °C. A) RBMK TMT-1 containing 76 ppm hydrogen, B) CANDU containing 79 ppm.

The light contrast arises from ductile fracture while the dark contrast is produced by cleavage of hydrides. The spacing between striations was measured by counting the number of striations within a known length of cracking and the results from four laboratories (Canada, ROK, Lithuania and the Russian Federation) are summarised in Table 4.15.

Striation spacing increases with increase in test temperature and appears to be larger in the specimens of the RBMK material than in the CANDU material. When compared with published values, those from CANDU material agree exactly with those of Nuttall and Rogowski [4.16] but when later measurements by Simpson and Puls [4.2] are added, they include the current values on RBMK TMT-1 material, Fig.4.25.

Table 4.15. Striation spacing of DHC at various temperatures on the two main materials

CANDU Tube RX094

Test temperature, °C	283	275	250	227	203	182	144
Striation spacing, μm	27.9	22.5	19.8	13.1	17.2	9.53	8.8
	28.8	24.2	20.0	14.5	16.4	10.8	8.0
	32.3		20.4	17.2	16.5	9.9	13.8
	29.1		22.1	16.4	16.7	10.0	12.9
	31.6		19.3	15.9	15.8	11.3	13.7
	29.6		24.8	16.1	9.8	12.0	11.5
			21.6		10.9	11.6	9.97
			20.8		12.6	9.8	10.3
			24.3			11.2	
			22.5				
			17.8				
			21.6				
			17.3				
			21.0				
			18.8				
			20.3				
Mean value, μm	29.9	23.4	20.8	15.5	14.5	10.7	11.1
Standard deviation	1.7	-	2.1	1.5	2.9	0.90	2.2

RBMK TMT-1

Temperature,°C	283	250	144
Striation spacing, μm	41.9	27	19.6
	43.2	26.3	23.3
	37.7	30.9	21.5
		32.4	
Mean value, μm	40.9	29.2	21.5

Early in the tests at 250°C on RBMK material in the annealed condition, the striation spacing was up to 200 μm but reduced as the test continued. In stress relieved material the average spacing was 45 μm while after the TMT-2 heat-treatment, spacings averaged 75 μm. All the striation spacings in each material of the current study can be reconciled as a linear function of the yield stress, Fig. 4.26.

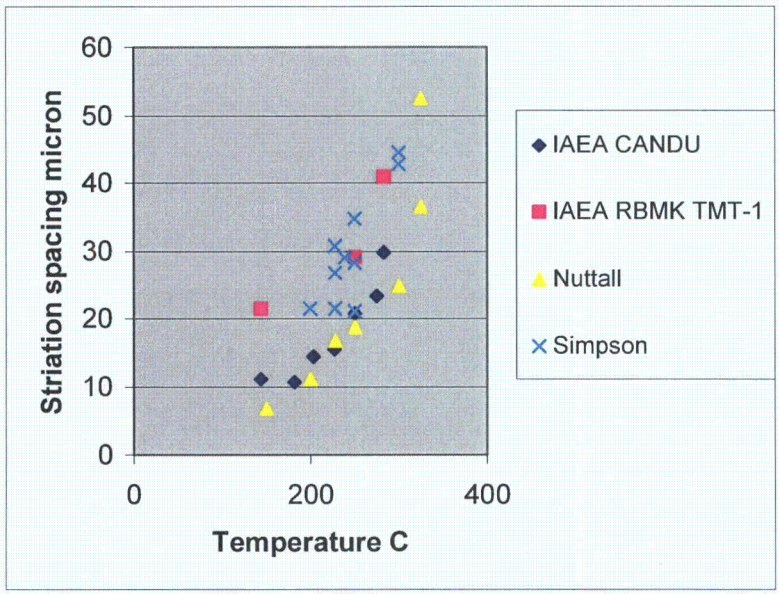

Fig. 4.25. Temperature dependence of striation spacing.

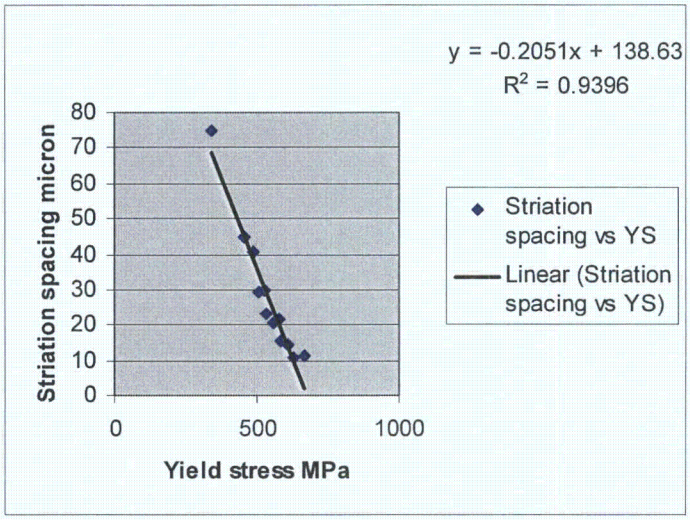

Fig. 4.26. Yield stress dependence of striation spacing.

4.6. Inter-Laboratory Comparison on Hydrogen Analysis

All of the participating laboratories (excluding Canada) used commercial inert gas fusion (IGF) instruments for the determination. (In Canada an isotope dilution method was used [4.17, 4.18] because the heat-transport fluid in a CANDU reactor is heavy water and one

needs to distinguish between deuterium and protium when estimating hydrogen ingress.) Any large variation between these instruments would reflect problems with standards, improper laboratory procedures or instrumental malfunctions. Table 4.16 is a synopsis of the instrumentation and methods used by each laboratory. The table also summarizes information on standards and blanks. Two laboratories reported that they used the ASTM analysis procedure for H in Ti [4.19]. This procedure is similar to that recommended by the instrument manufacturer. Presumably the other laboratories followed the instrument manufacturers recommended procedure.

Table 4.16. Synopsis of instruments and methods used by each laboratory

Country	Bottle	Equipment	Procedure	Standards	Blank
Argentina	1 & 3	LECO RH 404		Ti: LECO 502-154 and 762-741	
China	2	LECO RH 404		Ti	1 μg/g
India	4	LECO RH IE		Ti: LECO 762-741	1.1 ± 0.2 μg/g
ROK	5	LECO RH-404		Zr-2.5Nb: AECL 20HA and 100HA	0.05 μg/g
Lithuania	6	LECO RH-402		Ti	0.017 μg/g
Pakistan	7	STROHLIEN H-mat 251		Zr: NBS-358, Ti: AR-641	0.00001 μg/g
Romania	8 & 3	ELTRA OH-900	ASTM E 1447	Ti: AR 642	0.2 μg/g
Russia	9	LECO RH-404		Ti: LECO 762-741	0.28 μg/g
Sweden	10	ELTRA OH-900	ASTM E 1447	Ti: AR 648, NIST 352c, BCR No 318	0.4 μg/g
Canada	11	AECL HVE - IDMS	Custom	None	1.5 ± 0.4 μg/g

Results of the individual determinations are compiled in Table 4.17.

Table 4.17. Summary of analysis results from round robin on hydrogen analysis

Country	Argentina	China	India	ROK	Lithuania	Pakistan	Romania	Russia	Sweden	Canada A	Canada B
Bottle	1	2	4	5	6	7	8	9	10	11	11
H (μg/g)	41.0	48	45.8	46.6	57.9	49.5	29.3	47.6	49.8	46.7	47.1
	57.4	45	44.2	46.4	57.5	50.0	25.6	49.6	52.3	45.9	47.3
	60.1	49	46.3	47.7	57.5	50.0	25.1	48.8	50.0	46.8	46.9
	40.8	50	41.1	47.9	57.7	50.0	17.8	51.2	50.6	48.2	47.0
	61.7	45	42.3	48.7	57.9	50.0	35.0	49.2	51.2	47.3	47.3
	59.7	49	41.5	47.7	57.6	50.5	50.4	48.5	49.8	45.7	47.5
	59.9	49	44.4	47.1	59.2	50.5	32.6	48.4	50.1	47.1	47.0
	43.3	48	40.5	46.7		51.0	22.1	48.1	50.9	46.2	46.7
	46.2	49	44.2	47.1		51.0	16.5	52.9	51.2	47.0	47.1
	61.4	48	43.3	48.7			28.5	50.8	50.9	46.3	
Mean	53.2	48	43.4	47.5	57.9	50.3	28.3	49.5	50.7	46.7	47.1
Std Dev	9.1	1.7	2.0	0.8	0.6	0.5	9.8	1.7	0.8	0.7	0.2

4.6.1. Precision

The instrumental precision expected for repeat measurements is specified to be within 2% rsd (based on calibration by gas analysis) on the LECO RH-404 [4.20] and 1% rsd for the ELTRA OH-900 [4.21]. We assume that the other instrument models are competitive and offer similar precision. Considering the blank uncertainty and other uncertainties associated with the fusion step, a precision of 1–2 μg/g was anticipated from each laboratory. Most of the laboratories achieved that precision. This result confirmed that the samples were properly prepared with a small dispersion and were properly randomized. Argentina and Romania obtained a large dispersion initially. On investigation these laboratories confirmed that their instrument was malfunctioning. Five specimens from Bottle 3 were sent to these two laboratories and the subsequent results had a low dispersion:

	Hydrogen Concentration ppm					Mean	Standard Deviation
Argentina	53.3	53.2	53.1	53.0	53.4	53.2	0.16
Romania	54.3	54.4	56.2	52.8	54.3	54.4	1.2

The instrumental blank uncertainty may also contribute to the analysis precision. In Table 4.16, a wide range of blank values is reported. Some of the very low values reported are probably the residual blank after instrument compensation. The actual size of the blank should be determined and monitored routinely. The uncertainty on the blank must be known to calculate the precision of the sample analysis.

4.6.2. Bias

Assessment of the bias is hindered somewhat by the ambiguity in the known hydrogen concentration. The initial analysis of the 40 samples in Canada indicated the mean value was 49.8 μg/g. After 2 months of storage, the specimens in bottle #11 were analysed on two different HVE - IDMS instruments. The combined mean hydrogen concentration was found to be 46.9 μg/g. Such large systematic shifts are not seen on these instruments for analyses of deuterium in Zr standards, so it is thought that the original analysis was contaminated by background water from humid air providing an incorrect blank. High humidity may bias values since H_2O adsorbed on the surface of the sample reduces to H_2 during the fusion. The system blank does not account for this excess hydrogen introduced by the sample itself. However, there was no evidence that the observed relative biases correlate with differences in humidity.

Fig. 4.27 shows the results plotted relative to the mean value obtained in Canada (46.9 μg/g) and illustrates the relative biases between the laboratories. The results from Romania and Argentina are from the extra five specimens. Since all of the hydrogen in the Zr-2.5 Nb specimens came from the same source, the biases reflect differences in the performance of the individual laboratories.

The use of the standards may be the source for much of the bias. The standard deviation on some of the Ti standards is large. The laboratory operators must run a sufficient number of calibration standards to ensure that the calibration is not biased. For example, using LECO 762-741 certified with a standard deviation of 10 %, at least 16 calibration standards would

have to be analyzed to ensure that the calibration bias was < 5% at a level of confidence of 95%. Also Ti may not be a good surrogate for Zr. All laboratories used hydrogen in Ti as standards, except ROK. Zr standards had been provided to ROK by AECL under a commercial contract. Those standards were produced in the same way that the inter-laboratory specimens were produced. Therefore the agreement between Canada and ROK is expected to be good. More importantly, the differences between ROK and the other laboratories may be indicative of a real difference between Zr and Ti standards. For example, ROK measured the calibration factors for their instrument using both Ti and Zr standards, and obtained values of 1.3672 and 1.2591, respectively. The results suggest that more hydrogen is released from Zr than Ti. If the results with the high bias are corrected by the ratio of the two calibration factors, 0.9209, most of the values approach those of Canada and ROK, Fig. 4.28. The calibration factor for the Lithuanian results was reported as both 1.5366 and 1.3769 with the results being presented with the higher value in Fig. 4.27. These results were revised by 0.8194 in Fig. 4.28. The results from India tended to be slightly lower than those from Canada and ROK so they were not modified in Fig. 4.28.

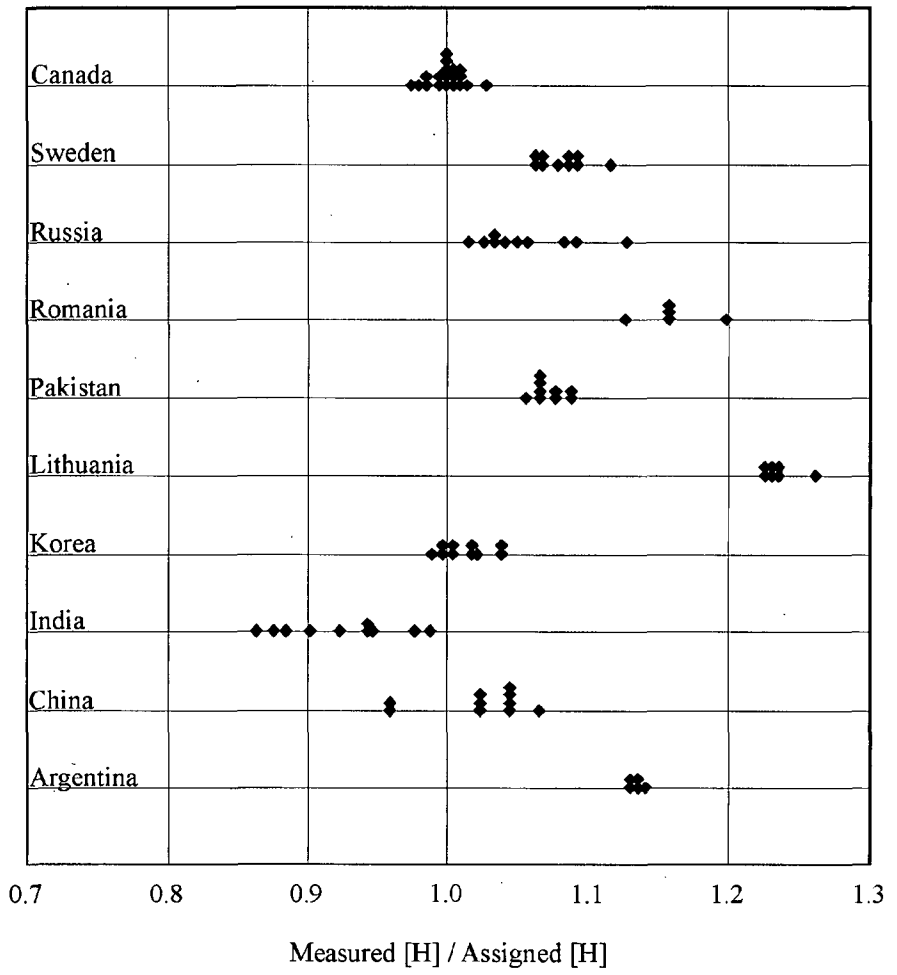

Fig. 4.27. Hydrogen analysis in each country relative to Canadian results.

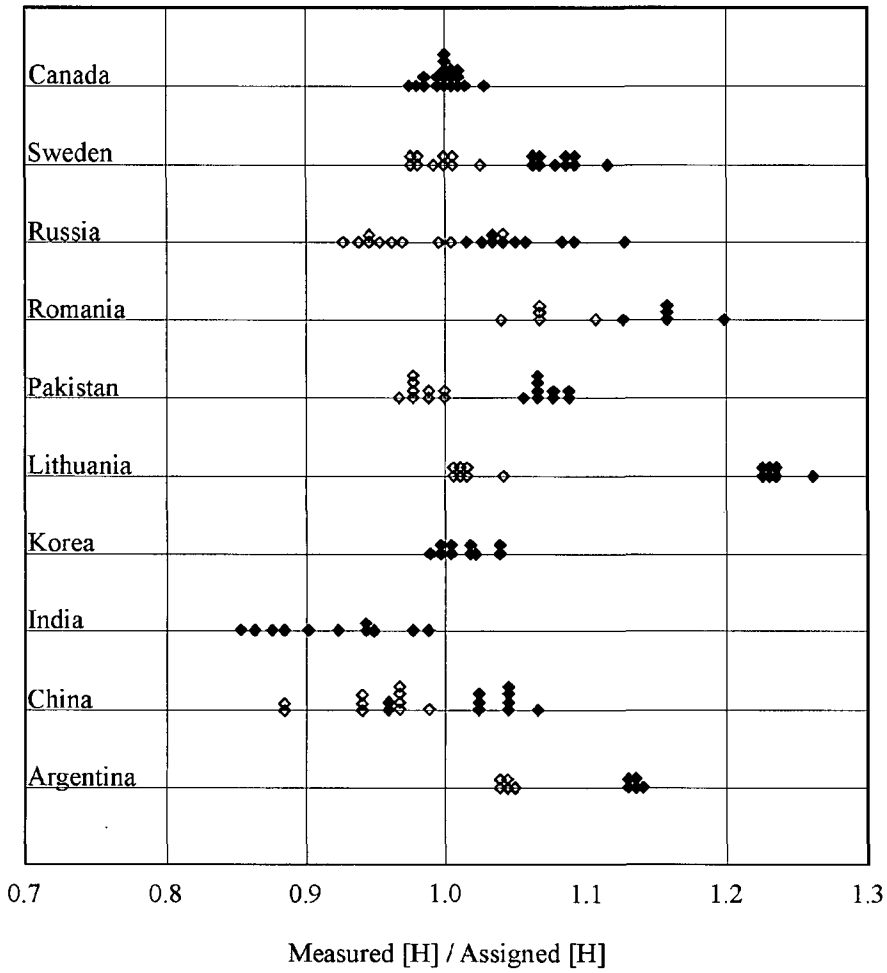

Fig.4.28. Hydrogen analysis results modified by the ratio of the calibration factors for Ti and Zr standards: open points; initial results from Fig. 4.27 are closed points.

The above corrections will not be exact because the calibration factors for Ti and Zr in the specific instruments will likely be different from those quoted, but the corrected results comply with those derived using Zr as a standard and with the initial hydrogen additions. If this approach is correct, standards appear to be specific to the particular metal. Thus measurements of hydrogen in Zr should use hydrogen in Zr for standards rather than hydrogen in Ti.

4.7. Discussion

The results presented in the previous sections show that this Co-ordinated Research Project has met its objectives. The methods for performing consistent measurements of DHC velocity in Zr-2.5Nb developed in Canada have been transferred to other countries. The general agreement on the values between the different laboratories on the two main test materials demonstrates the success of this transfer.

The main areas of inconsistency are with the additions of hydrogen and its analysis. Some latitude is available for DHC measurements so long as the temperature history of the tests meets the criteria for maximum crack velocity:

(a) The peak temperature must be equal to or exceed the solvus temperature for hydrogen dissolution, T_d [4.4].

This criterion is met so long as the peak temperature is greater than the annealing temperature used to diffuse the hydrogen into the specimen. Examination of the reported test conditions shows that this criterion was met, with the exceptions mentioned in Section 4.2. Some tests on other tubes may not have fully met this criterion. Three Indian tests at 250°C on tube 100-2-3 on specimens containing 80 ppm used a peak temperature of 306°C; depending on which TSSD is used [4.10, 4.22–4.24] T_d is between 317 and 329°C so hydrides would still have been present at the peak temperature. The crack velocities of these specimens were slightly lower, 6.3 to 7.15 $\times$ 10^{-8} m/s, than in similar specimens containing 60 ppm (T_d between 295 and 306°C) that had a peak temperature >319°C, 8.06 to 9.24 $\times$ 10^{-8} m/s. The peak temperature in the tests on the other RBMK materials, Table 4.14, were 325 to 330°C whereas with a hydrogen concentration of 100 ppm the preferred peak temperature is 335 to 348°C, thus the reported values of crack velocity may be slightly too low.

(b) The test temperature must always be attained by cooling.

Results of tests were rejected in which there was known undercooling before the test temperature, T_t, was reached and therefore the test temperature was attained by heating (Section 4.2).

(c) Hydrides must be available at the test temperature.

DHC can start when the solubility limit for precipitation is exceeded at the crack tip because of the transport of hydrogen into this high stress region. Thus the temperature at which cracking is possible, T_c, is between T_d and T_p, the solvus for precipitation. Over the current range of test conditions, based on crack incubation time detected by acoustic emission, [4.13, 4.14], T_d-T_c is in the range 6 to 17°C and T_c-T_p is in the range 41 to 52°C while the same quantities derived from cracking detected by potential drop [4.15] are 16 to 28°C and 30 to 42°C. To obtain the maximum crack velocity (minimum incubation time), the test temperature should be $\geq$ 15°C lower than T_c, that is, about 35 to 45°C below T_d or within 15 to 25°C of T_p. The results in Section 4.4.5, Figs 4.22 and 4.23, illustrate this situation. As the test temperature was lowered cracking was detected; this is T_c. As the temperature was lowered further the crack velocity increased to a maximum value; let us call this temperature T_m. With subsequent temperature reduction the crack velocity followed the Arrhenius relationship with all these values being the maximum value for that temperature. The relationship between T_c, T_m, T_d and T_p is summarised for these tests in Table 4.18. Included is a similar test on irradiated Zr-2.5 Nb, which fits the pattern [4.25].

A second illustration of the need to exceed a critical hydrogen concentration is the lower two results in Table 4.2. The test temperature of 250°C for the specimens containing 40 ppm did not meet the (T_c-15°C) criterion and thus the crack velocity was less than the maximum possible value; the specimens containing 55 ppm had sufficient hydrogen to crack at the maximum velocity because $T_t < T_c$-15°C.

Table 4.18. Test results indicating the temperature where the DHC velocity is maximized, T_m, and the relationship to the hydrogen solvus temperatures

Material	H ppm	T_c °C	T_m °C	T_c °C Literature	T_d °C	T_p °C
CANDU	24	201	189	218-227	234-242	175-206
	34	246	232	238-249	256-265	198-226
	53	276	263	268-278	286-296	232-254
	60	{300}	275-280	276-287	295-305	243-262
CANDU Irradiated	105	320-325	300-310	319-330	340-352	291-296
RBMK TMT-1	30	240	228	231-241	248-257	190-218
	47	275	263	260-270	277-287	223-246
	56	{284}	{278}	271-282	290-300	237-257

Having a test temperature below T_p guarantees the maximum crack velocity because hydrides are available throughout the specimen while the maximum hydrogen concentration in solution (supersaturated from cooling) is also available.

For the current tests, based on the reported hydrogen concentrations, maximum crack velocities were measured since the T_p criterion was met in all specimens tested at 203°C and below. In tests at 250 and 227°C the (T_c-15°C) criterion was met while in some tests at 283°C the (T_c-15°C) criterion was apparently borderline, which may account for some of the low values of crack velocity and the large standard deviation that were observed in the CANDU material, Table 4.7. In retrospect, the target hydrogen concentration for testing at 283°C should have been a little higher, say 85 to 90 ppm, to guarantee maximum velocities.

In Section 4.4.1 we concluded that DHC was 2 to 5 times slower in the RBMK TMT-1 material than in the CANDU tube. To judge whether these results represent members of the same population or not we need data from other tubes made to each representative specification. No further data are available on the RBMK material but several tests that met the criteria for maximum crack velocity have been done at 250°C on CANDU tubes other than the three reported here (Sections 4.2, 4.4.2, 4.4.3.) The results are summarised in Table 4.19. The best we can do is show whether or not the results on the RBMK TMT-1 tube are outside the distribution of the samples of CANDU data.

If so, and since these tubes were selected at random, we can conclude that the difference is because they were sampled from separate populations. The mean value of the results at 250°C on the RBMK TMT-1 tube was $3.3 \times 10^{-8} \pm 0.64$m/s (Table 4.10) which has less than 5% chance of being part of the distribution of results on CANDU material, that is: $(9.52–(2 \times 2.2)) > (3.3+(2 \times 0.64))$. We conclude that the results from each type of tube come from different populations.

Table 4.19. DHC velocity at 250°C in several CANDU tubes

Material	H ppm	Yield stress Mpa Transverse 250°C	Mean crack velocity m/s × 10^{-8}	Standard deviation (number of specimens) m/s × 10^{-8}	Reference
RX094	55 - 63	567	8.86	1.07 (80)	This report
429	65 - 67	585	9.6	0.34 (3)	This report
100-2-3	60 - 80	531	7.6	1.05 (8)	This report
"SMIRT-17"	170	606	7.0 (Interpolated value)		4.25
Tube A front	72	Not available	8.4	0.41 (6)	Choubey private communication
Tube A back	72	600	8.5	0.54 (6)	Choubey private communication
Tube B front	69	Not available	9.4	0.33 (6)	Choubey private communication
Tube B back	69	600	8.8	0.58 (6)	Choubey private communication
Tube C front	72	Not available	12.1	0.35 (6)	Choubey private communication
Tube C back	72	602	9.2	0.73 (6)	Choubey private communication
Tube D front	73	Not available	8.9	0.23 (6)	Choubey private communication
Tube D back	73	614	14.6	0.60 (6)	Choubey private communication
Tube E middle	63 - 71	567	6	0.30 (6)	Choubey private communication
Tube F	60	559	7.6 - 8.8		Shek private communication
Zr conference	55	Not available	11.8	3.1 (5)	4.3
		Mean value	9.52		
		Standard deviation	2.2		

The crack velocity is controlled by the solubility limit, C, diffusivity of hydrogen, D, and the ability to form and crack a hydride. The sources of the difference between the tube types are the parameters that affect each of the controlling factors: grain structure, crystallographic texture and strength. The interactions are complicated because strength is determined by the grain structure and texture as well as the chemical composition while grain structure and texture can affect DHC independently of strength. As examples:

(a) if the β-phase is continuous it can provide a pathway for rapid hydrogen diffusion and high crack velocities [4.26, 4.27],
(b) a tensile stress parallel to the basal plane normal promotes precipitation of hydrides with their platelet normals parallel with the stress and facilitates cracking whereas cracking is difficult when the tensile stress is perpendicular to the basal plane normal, [4.27–4.30],
(c) a high yield stress produces a high stress gradient at the crack tip and reduces the size of the hydride required for cracking and therefore facilitates DHC [4.4, 4.8, 4.31]. The latter effect is reflected in the dependence of the striation spacing on yield stress, Fig. 4.26.

The crack velocity was expected to be lower in the RBMK TMT-1 tube than in the CANDU tube because:

— it did not contain a continuous β-phase film in its grain boundaries as in the CANDU tube,
— the fraction of basal plane normals in the transverse direction was much lower in the RBMK
TMT-1 tube than in the CANDU tube,
— the yield stress was lower in the RBMK TMT-1 tube than in the CANDU tube.

To judge the relative importance of the microstructural features and strength, we compare the results on a CANDU tube given the same heat-treatment as TMT-1 [4.32]. The microstructure was similar to the RBMK tube but the strength was higher than in a cold-worked tube (estimated at 250°C by interpolation). The crack velocity (estimated by extrapolation of a fitted Arrhenius line) was intermediate between the values of the current two materials, Table 4.20. With the warning that only one tube is being sampled from each potential population, the results demonstrate that both microstructure and strength can independently affect crack velocity.

Table 4.20. Comparison of the factors affecting DHC velocity in Zr 2.5 Nb

Material	F_T	Continous β-phase	Yield stress, Mpa Transverse, 250°C	Crack velocity m/s × 10^{-8}
CANDU CW	0.6	Yes	567	8.9
CANDU HT	0.42	No	≈700	≈5.5
RBMK TMT-1	0.42	No	494 - 524	3.3

Difference in strength seems to be the main reason why the crack velocity in the standard annealed RBMK tube, (yield stress of 255-314 MPa) was about ten times slower than when the tube was only stress-relieved rather than annealed, providing a strength of 455 MPa, Table 4.14. Since texture is mostly established during extrusion, the texture of the two tubes should be similar. The β-phase stringers would be mostly decomposed by the intermediate anneal at 580°C so they should not play a major role in enhancing hydrogen diffusion. The importance of yield stress in controlling DHC velocity at 250°C is illustrated in Figure 4.29. Included in the figure are the current results, those in Tables 4.19 and 4.20 as well as the early results demonstrating the effect of strength [4.4] and results from a well-controlled irradiation [4.33] assuming the increase in strength is the main factor. Although the correlation holds over this wide range of yield stresses, it can be improved by taking into account the microstructure differences. To account for the temperature dependence of hydrogen migration V is normalized [4.31] by the solubility limit, ($C=1.2 \times 10^5 \exp(-35900/RT)$) [4.10] and diffusivity ($D = 2.17 \times 10^{-7}\exp(-35100/RT)$) [4.34].

The equation for the solubility limit was chosen because it provides a good representation of many data sets. To represent the materials where the β-phase was not continuous, the pre-exponential term in D was reduced by 50%. The activation energy was not changed to acknowledge that Q for crack velocity was similar for all the materials. To take into account texture, V was normalized by F_T, Table 3.4 [4.29]. The results, Fig. 4.30, show that the correlation is improved by 10%.

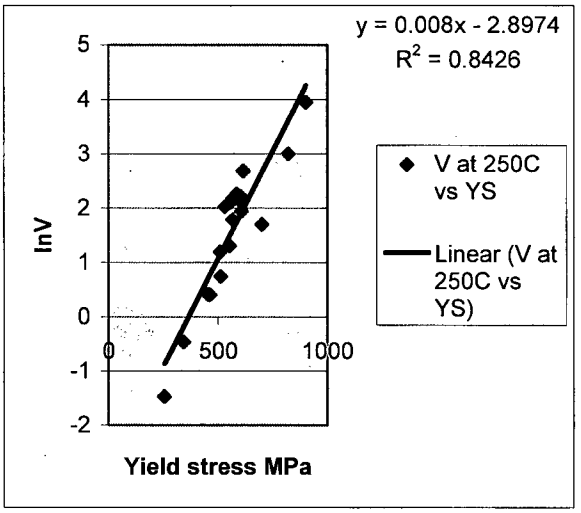

Fig. 4.29. Dependence of DHC crack velocity at 250°C in Zr–2.5 Nb on yield stress.

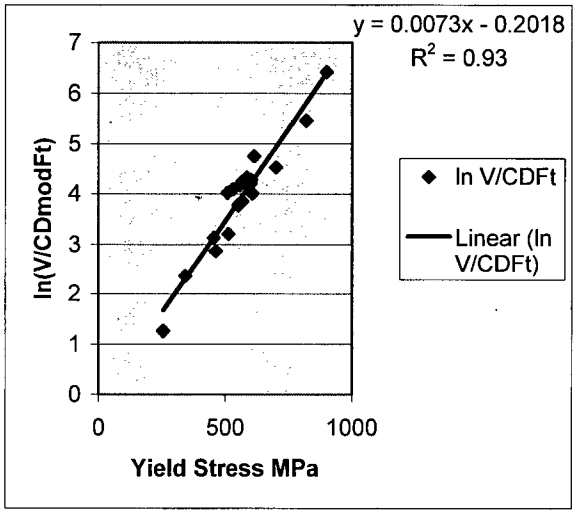

Fig.4.30. Dependence of normalized DHC crack velocity at 250°C in Zr–2.5 Nb on yield stress.

Despite the assumptions required because of lack of detailed information on some of the materials and the need to use representative values of C and D rather than values for the actual tubes, the analysis appears to depict the important factors in DHC velocity at one temperature.

The need for the normalization is more apparent when all the results at other test temperatures from this programme are plotted against strength, Fig. 4.31.

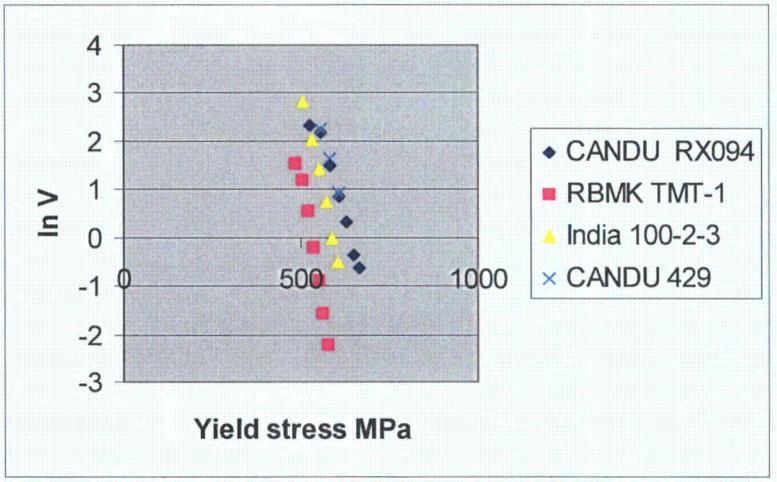

Fig.4.31. DHC velocity for the four test materials at various test temperatures as a function of yield stress.

Using the same normalization as above with the same equations for C and D, and the same values of F_T, the data are united, Fig. 4.32, although a better correlation is attained if the effect of texture is ignored, Fig. 4.33.

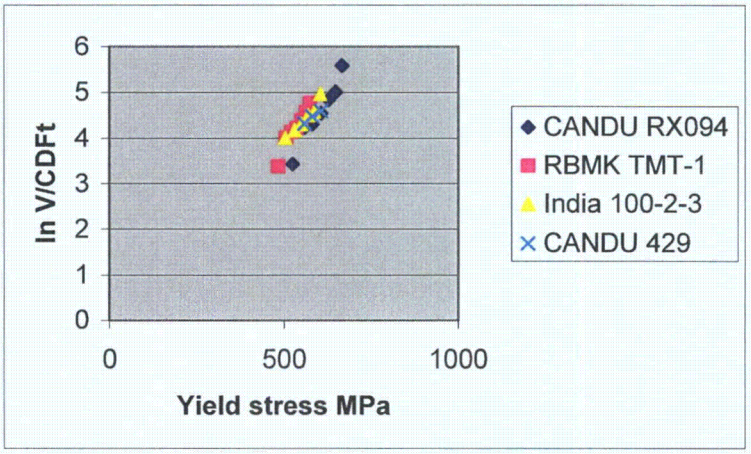

Fig. 4.32. Dependence on yield stress of normalized DHC velocity in the Zr-2.5 Nb tubes used in the current study.

When the data presented in Fig. 30 are combined with those in Fig. 4.32, they exhibit a clear but modest correlation with yield stress, Fig. 4.34. Thus the results of the test programme on Zr-2.5 Nb tubes made by different fabrication routes from material of different compositions and performed in different countries can be rationalized empirically through the expected temperature dependence of the main factors important to DHC — solubility limit of hydrogen, diffusivity of hydrogen and strength, and by taking into account microstructural features such as the distribution of β-phase and crystallographic texture.

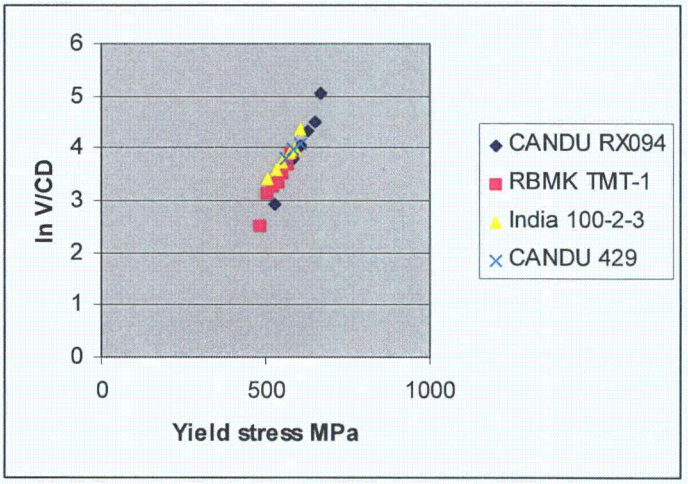

Fig. 4.33. Dependence on yield stress of normalized DHC velocity in the Zr-2.5 Nb tubes used in the current study, ignoring differences in texture.

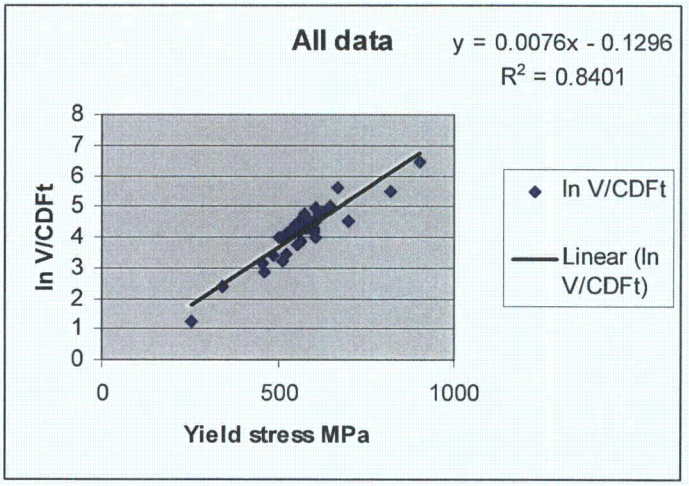

Fig. 4.34. Dependence on yield stress of normalized DHC velocity of all the various Zr-2.5 Nb materials tested over a wide temperature range.

REFERENCES TO CHAPTER 4

[4.1] DUTTON, R., NUTTALL, K., PULS, M.P., SIMPSON, L.A., Mechanisms of hydrogen induced delayed cracking in hydride forming materials, Met. Trans., 8A, (1977), 1553–1562.

[4.2] SIMPSON, L.A., PULS, M.P., The effects of stress, temperature and hydrogen content on hydride-induced crack growth in Zr-2.5 pct Nb, Met. Trans., 10A, (1979), 1093–1105.

[4.3] SAGAT, S., COLEMAN, C.E., GRIFFITHS, M., WILKINS, B.J.S., The effect of fluence and irradiation temperature on delayed hydride cracking in Zr-2.5 Nb, Zirconium in the Nuclear Industry-10th International Symposium, ASTM STP 1245, eds. A.M. Garde and E.R. Bradley, ASTM, West Conshohocken, PA, (1994), 35–61.

[4.4] SHEK, G.K., GRAHAM, D.B., Effect of loading and thermal maneuvers on delayed hydride cracking in Zr-2.5 Nb alloys, Zirconium in the Nuclear Industry-8th International Symposium, ASTM STP 1023, eds. L.F.P. Van Swam and C.M. Eucken, ASTM, West Conshohocken, PA, (1989), 89–110.

[4.5] AMBLER, J.F.R., COLEMAN,C.E., Acoustic emission during delayed hydrogen cracking in Zr-2.5 wt.%.Nb alloy, Proc. 2nd International Congress on Hydrogen in Metals, Paris, Pergamon Press, Oxford, (1977) Paper 3C10.

[4.6] AMBLER, J.F.R., Effect of approach to temperature on the delayed hydride cracking behavior of cold-worked Zr-2.5 Nb, Zirconium in the Nuclear Industry-6th International Symposium, ASTM STP 824, eds. D.G. Franklin and R.B. Adamson, ASTM, West Conshohocken, PA, (1984), 653–674.

[4.7] COLEMAN, C.E.,.CHEADLE,B.A., AMBLER, J.F.R., LICHTENBERGER, P.C., EADIE, R.L., Minimising hydride cracking in zirconium alloys, Can. Met. Quart., 24, (1985), 245–250.

[4.8] KIM, Y.S., KIM, S.S., CHEONG, Y.M., KIM, I.S., Governing factors for delayed hydride cracking in Zr-2.5 Nb tubes, Presented at Canadian Nuclear Society, June, 2003.

[4.9] AMOUZOUVI, K.F., CLEGG, L.J., Effect of heat treatment on delayed hydride cracking in Zr-2.5 wt pct Nb, Met. Trans., 18A, (1987), 1687–1694.

[4.10] KEARNS, J.J., Terminal solubility and partitioning of hydrogen in alpha zirconium, Zircaloy-2 and Zircaloy-4, J. Nucl. Mater., 20, (1967), 292–303.

[4.11] ROTH, M., CHOUBEY, R., COLEMAN, C.E., RITCHIE, I., Measurement of DHC in CANDU pressure tubes, 17th Int. Conf. Structural Mechanics in Reactor Technology, Prague, 2003, Paper G350.

[4.12] SINGH, R.N., KUMAR, N., KISHORE, R., ROYCHAUDHURY, S., SINHA, T.K., AND KASHYAP, B.P., Delayed hydride cracking in Zr-2.5Nb pressure tube material, J. Nucl. Mater., 304, (2002), 189–203.

[4.13] COLEMAN, C.E., AMBLER, J.F.R., Measurement of effective solvus temperature of hydrogen in Zr-2.5 wt% Nb using acoustic emission, Can. Met. Quart., 17, (1978), 81–84.

[4.14] COLEMAN, C.E., AMBLER, J.F.R., Solubility of hydrogen isotopes in stressed hydride-forming metals, Scripta Met., 17, (1983), 77–82.

[4.15] SHI, S.-Q., SHEK, G.K., PULS, M.P., Hydrogen concentration limit and critical temperature for delayed hydride cracking in zirconium alloys, J. Nucl. Mater., 218, (1995), 189–201.

[4.16] NUTTALL, K., ROGOWSKI, A.J., Some fractographic aspects of hydrogen-induced delayed cracking in Zr-2.5 wt. Percent Nb alloys, J. Nucl. Mater., 80, (1979),279–290.

[4.17] GREEN, L. W., BICKEL, G. A., LEESON, P. K., JAMES, M. W. D., LAMARCHE, T. G. and H. Michel, A Hot Vacuum Extraction Mass Spectrometric System for Determination of H and D in Zirconium, Proceedings of the 2nd Alfred O. Nier Symposium on Inorganic Mass Spectrometry, Durango, Colorado, May 1994 (Available as part of AECL-11342, Jan. 1996, pp. 95–99.

[4.18] BICKEL, G.A., GREEN, L.W., JAMES, M.W.D., LAMARCHE, T.G., LEESON, P.K., MICHEL, H., The determination of hydrogen and deuterium in Zr-2.5 Nb material by hot vacuum extraction mass spectrometry, J. Nucl. Mater., 306, (2002), pp. 21–29.

[4.19] ASTM E 1447, "Standard Test Method for Determination of Hydrogen in Titanium and Titanium Alloys by the Inert Gas Fusion Thermal Conductivity Method.

[4.20] LECO Corporation RH-404 Hydrogen Determinator Specification Sheet, LECO Corporation Application Bulletin: Determination of Hydrogen in Titanium.

[4.21] ELTRA GmbH Oxygen/Hydrogen Determinator OH900 Specifications, (www.eltragmbh.com).
[4.22] SLATTERY, G., "The Terminal Solubility of Hydrogen in Zirconium Alloys between 30 and 400 °C", J. Inst. Met., 95, (1967), 43–47.
[4.23] PAN, Z.L., Ritchie, I.G., Puls, M.P., The terminal solid solubility of hydrogen and deuterium in Zr-2.5Nb alloys, J. Nucl Mater., 228, (1996), 227–237.
[4.24] McMINN, A., DARBY, E.C., SCHOFIELD, J.S., Terminal solid solubility of hydrogen in zirconium alloys, Zirconium in the Nuclear Industry-12th International Symposium, ASTM STP 1354, eds. G.P. Sabol and G.D. Moan, ASTM, West Conshohocken, PA, (2000), 173–195.
[4.25] SAGAT, S., PULS, M.P., Temperature limit for delayed hydride cracking in Zr-2.5Nb alloys, 17th Int. Conf. Structural Mechanics in Reactor Technology, Prague, 2003, Paper G311.
[4.26] SIMPSON, L.A., CANN, C.D., The effect of microstructure on rates of delayed hydride cracking in Zr-2.5% Nb alloy., J. Nucl. Mater., 126, (1984), 70–73.
[4.27] COLEMAN, C.E., SAGAT, S., AMOUZOUVI, K.F., Control of microstructure to increase the tolerance of zirconium alloys to hydride cracking, AECL Report, AECL-9524, 1987.
[4.28] COLEMAN, C.E., Effect of texture on hydride reorientation and delayed hydrogen cracking in cold-worked Zr-2.5Nb, Zirconium in the Nuclear Industry-5th International Symposium, ASTM STP 754, eds. D.G. Franklin, ASTM, West Conshohocken, PA, (1982), 393–411.
[4.29] KIM, S.S., KWON, S.C., KIM, Y.S., The effect of texture variation on delayed hydride cracking behavior of Zr-2.5%Nb plate, J. Nucl. Mater., 273, (1999), 52–59.
[4.30] KIM, Y.S., KIM, S.S., KWON, S.C., IM, K.S., CHEONG, Y.M., Anisotropic threshold stress intensity factor, K_{IH} and crack growth rate in delayed hydride cracking of Zr-2.5Nb pressure tubes, Met. & Mat. Trans., 33A, (2002), 919–925.
[4.31] OH, J.Y., KIM, I.S., KIM, Y.S., A normalization method for relationship between yield stress and delayed hydride cracking velocity in Zr-2.5Nb alloy, J. Nucl. Sci. and Tech., 37 (2000), 595–600.
[4.32] CHOW, C.K., COLEMAN, C.E., KOIKE, M.H., CAUSEY, A.R., ELLS, C.E., HOSBONS, R.R., SAGAT, S., URBANIC, V.F., RODGERS, D.K., Properties of an irradiated heat-treated Zr-2.5Nb pressure tube removed from the NPD reactor, Zirconium in the Nuclear Industry-11th International Symposium, ASTM STP 1295, eds. E.R. Bradley and G.P. Sabol, ASTM, West Conshohocken, PA, (1996), 469–491.
[4.33] HOSBONS, R.R., DAVIES, P.H., GRIFFITHS, M., SAGAT, S., COLEMAN, C.E., Effect of long-term irradiation on the fracture properties of Zr-2.5Nb pressure tubes, Zirconium in the Nuclear Industry-12th International Symposium, ASTM STP 1354, eds. G.P. Sabol and G.D. Moan, ASTM, West Conshohocken, PA, (2000), 122–138.
[4.34] SAWATZKY, A., The diffusion and solubility of hydrogen in the alpha-phase of Zircaloy-2, J. Nucl. Mater., 2, (1960), 62–68.

CHAPTER 5

MEASUREMENT OF DHC VELOCITY IN FUEL CLADDING USING THE PIN-LOADING TENSION TEST

As indicated in Chapter 1, DHC is implicated in the development of long splits in some fuel cladding. A potential method for evaluating DHC is described below.

5.1. Method

The Pin-Loading Tension (PLT) technique has been used to characterise the fracture toughness in the axial direction of irradiated cladding [5.1-5.3]. A notched PLT-specimen is manufactured from the cladding tube, Fig. 5.1. The specimen is axially notched at both edges, with the notches at the front edge of the specimen being sharpened by fatigue.

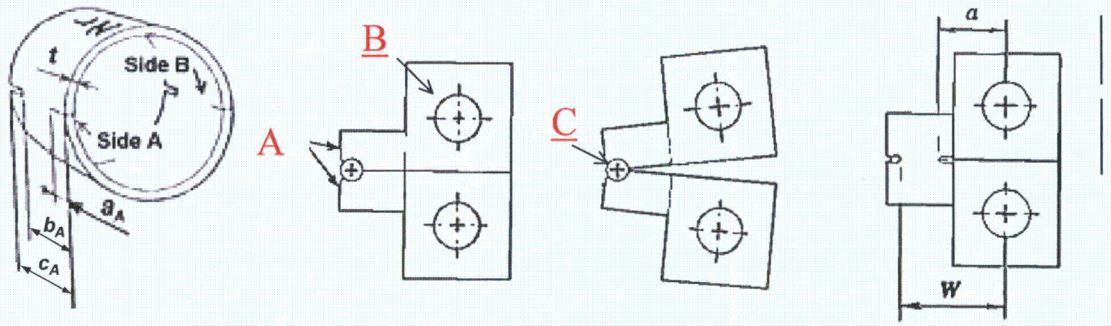

Fig. 5.1. Schematic diagram of the PLT specimen, fixture, and specimen-fixture assembly.

The PLT-fixture consists of two halves, which when placed together form a cylindrical holder A (see Fig. 5.1). The diameter of the holder allows it to be inserted into the tubular PLT-specimen, while maintaining a minimal interfacial gap. The fixture halves are loaded in tension through the pins B and have the capability of mutual rotation around the axis determined by a small pin C placed between the fixture halves at the end of the cylindrical holder. The rotation of the fixture halves is similar to the rotation of the halves of a compact specimen (CT) under tension, except that in the PLT-fixture, the rotation axis does not change its position when the crack propagates in the specimen.

The PLT specimen, pre-cracked by fatigue, can be used both for the fracture toughness evaluation and for the measurements of DHC velocities in fuel cladding materials. The crack extension during the testing can be monitored by measurement of DC potential drop, Fig. 5.2.

In the fracture toughness test the load and load-point displacement are monitored during the loading to plot the load-displacement record (LDR). After unloading, the crack extension area is marked by short-term fatigue, and the crack extension is measured on the both sides of the specimen. The average value of the crack extension is used for toughness evaluations.

The J-integral values are calculated from the LDR and plotted against the corresponding crack extensions. That plot represents a J-resistance curve of the specimen. The J-resistance curve is used to establish a crack initiation point, $J_{0.2}$, which is the J-integral value at the intersection of the 0.2 mm offset line and the J-resistance curve. The initial crack growth toughness, dJ/da, is obtained as a linear regression slope of the J-resistance curve between the 0.15- and 1.5-mm offset lines, Fig. 5.3.

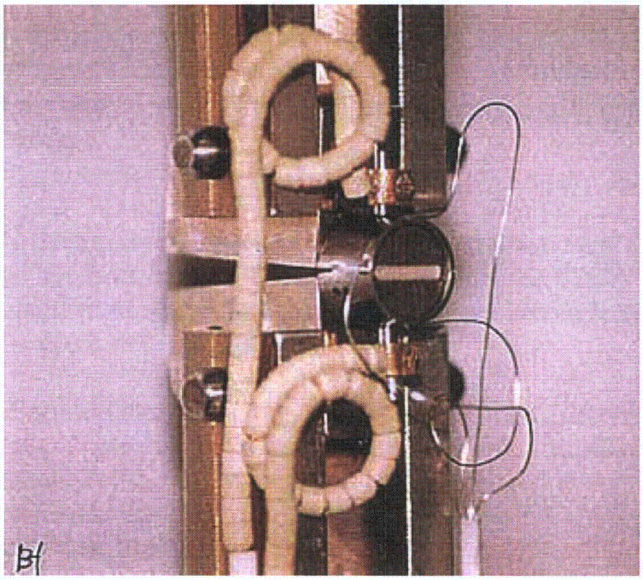

Fig. 5.2. The PLT specimen with attached DCPD probes mounted in the testing machine.

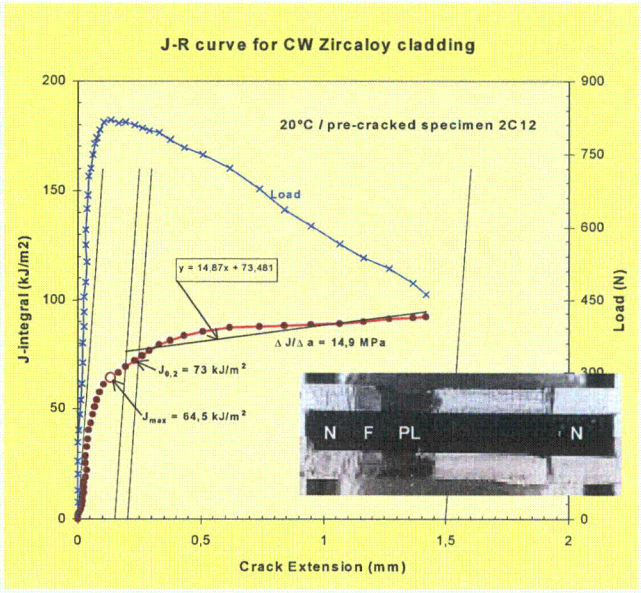

Fig. 5.3. An example of J-resistance curve and fracture surface of hydrided Zircaloy specimen (200 ppm) tested at 25°C.

The same experimental set-up has been used for the measurements of delayed hydride cracking velocity in Zircaloy cladding [5.4]. The PLT-specimens with two different lengths, 9 and 13 mm, were machined from Sandvik Zircaloy-4 lot 86080 (see Fig. 5.1). The tubing had an outside diameter of 9.5 mm and a wall thickness of 0.57 mm. The material had a final anneal of 480°C for 3.5 h and had a recovered cold-worked structure with 5 to 10% recrystallisation. The yield stresses at 20 and 385°C were 553 and 355 MPa, respectively. About 200 ppm hydrogen were added to the tubing electrolytically. The pre-cracked

specimens were heated in air to 315°C for one hour, cooled to the test temperature of 250°C, then loaded after a hold time of about one hour. To monitor crack growth under the constant load applied to the specimen, the DCPD technique was used. The loading of the specimen was usually accompanied by a step-wise increment of the DCPD reading followed by a gradual increase of the DCPD values, Fig. 5.4. Cracking was allowed to continue until the crack had grown about 2 mm. The load was then removed, the furnace opened and the specimen cooled down to room temperature. The unloading of the specimen was usually accompanied by a step-wise decrease of the DCPD reading (see Fig. 5.4). The end of the crack was marked by means of short-term fatigue. An example of specimen fracture surface obtained after the DHC test is also shown in Fig. 5.4.

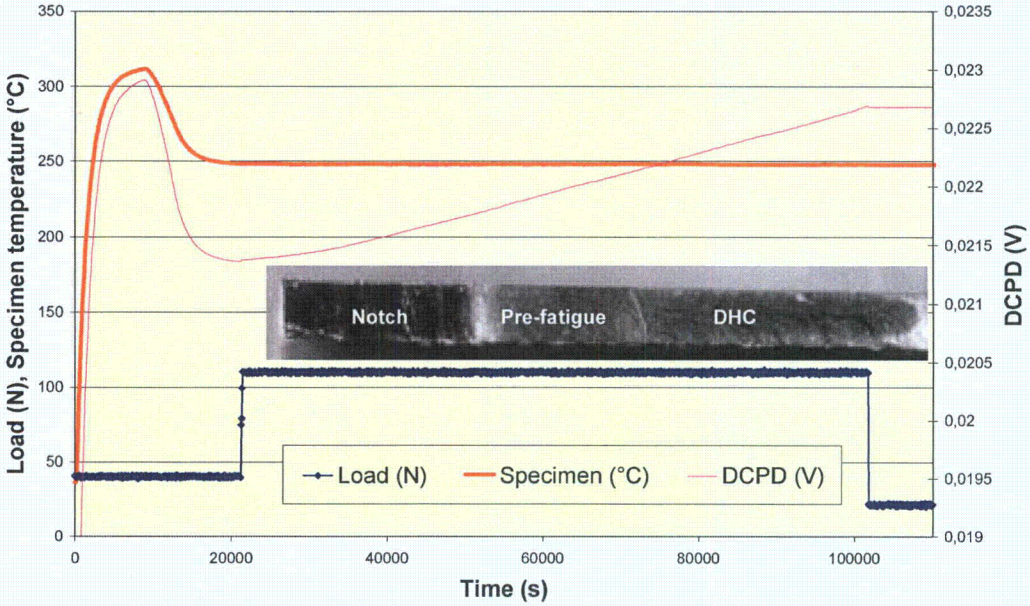

Fig. 5.4. An example of the data record for entire DHC test performed for hydrided Zircaloy cladding (200 wtppm). The DHC-crack area extended during the time under constant load of 110 N is clearly distinguished at the specimen fracture surface (one side of the specimen is shown).

5.2. Results

Independently of the specimen length, 9 or 13 mm, good reproducibility of the axial crack velocity, V_{DHC}, was observed, Table 5.1.

Table 5.1. Results of DHC tests at 250°C on Zircaloy-4 fuel cladding

Specimen	Test temp (°C)	Test temp 1000x(K^{-1})	DHC-crack (mm)	Incubation time (min)	Cracking time (min)	DHC velocity (m/s)
13-4	247.9	1.920	2.4	24	1398.0	2.8E-08
13-5	249.5	1.914	1.6	119	1032.5	2.6E-08
13-6	249.9	1.912	2.4	30	1294.0	3.0E-08
9-4	250.2	1.911	1.7	21	962.0	3.0E-08
9-5	248.1	1.919	2.1	14	1324.0	2.7E-08
9-6	251.1	1.908	1.6	19	875.0	3.0E-08

The V_{DHC}-values for identically tested specimens fell within the interval of 2.6×0^{-8} m/s to 3.0×10^{-8} m/s. Compared with the axial crack velocities obtained at 250°C in the Zr-2.5Nb pressure tube material, this range of values is below those for CANDU material, Table 4.1, but similar to those for RBMK TMT-1 material, Table 4.10. Contributors to the low value of V_{DHC} would be the low peak temperature that did not allow all the hydrogen to be dissolved and the moderate yield strength (430 MPa at 250°C,(by interpolation)), but separating these factors is beyond the scope of this report

The DHC-crack surface topography obtained in the present work for unirradiated cladding, Fig. 5.5, appears to reproduce the main topographical features observed for axial splits in failed fuel rods:

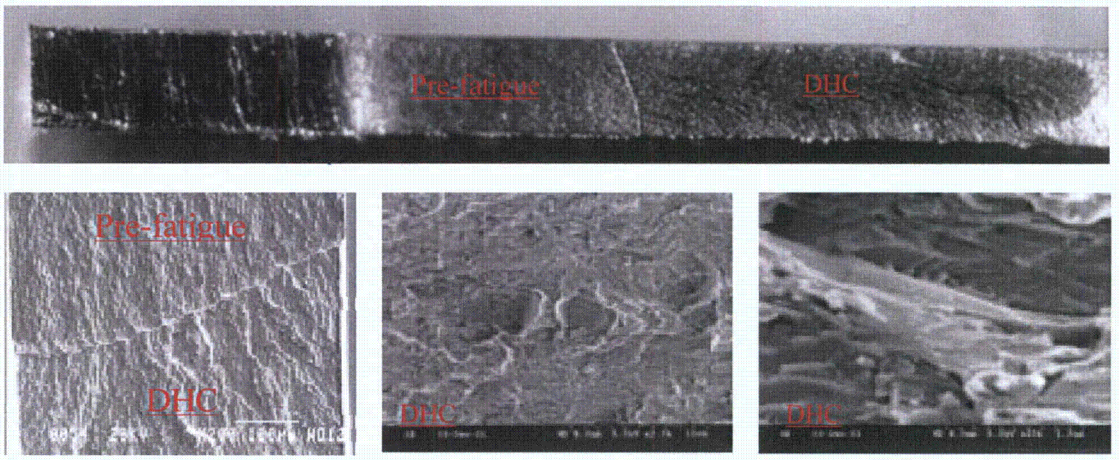

Fig. 5.5. Typical macroview of DHC fracture surface in unirradiated hydrided Zircaloy cladding and SEM photos of the same fracture surface (the SEM photos are the courtesy of K. Pettersson).

— the crack surface is macroscopically flat and oriented along the radial-axial plane of cladding;
— the clear "chevron" pattern is observed along the entire DHC-crack length;
— the notch length and fatigue crack length are longer at the inner surface of the specimen, while the DHC-crack propagates faster in the outer layers of the specimen;
— the fatigue crack propagates without specimen thinning while the specimen wall is thinned along the DHC-crack.

5.3. Summary

A method has been developed and demonstrated to measure the crack velocity of DHC in fuel cladding. The method is based on a previous method used for evaluating fracture toughness of fuel cladding and incorporates the knowledge developed in this CRP.

REFERENCES TO CHAPTER 5

[5.1] GRIGORIEV, V., JOSEFSSON, B., ROSBORG, B., Fracture toughness of Zircaloy cladding tubes. ASTM STP 1295, American Society for Testing and Materials, PA, 1996, pp. 431–447.

[5.2] GRIGORIEV, V., JOSEFSSON, B., ROSBORG, B., BAI, J., A novel fracture toughness testing method for irradiated tubing - Experimental results and 3D numerical evaluation. Transactions of the 14-th International Conference on Structural Mechanics in Reactor Technology (SMiRT-14), Vol. 2, Division C-4, 1997, pp. 57–64.

[5.3] LYSELL, G., GRIGORIEV, V., EFSING, P., Axial splits in failed BWR fuel rods. Presented at ANS International Topical Meeting on Light Water Reactor Fuel, Park City, Utah, USA, April 10–13, 2000.

[5.4] GRIGORIEV, V. JAKOBSSON, R., Application of the Pin-Loading Tension test to measurements of Delayed Hydride Cracking velocity in Zircaloy cladding. Report SKI-00:57 (November 2000).

CHAPTER 6

CONCLUSIONS AND RECOMMENDATIONS

6.1. Conclusions

1. The techniques for performing measurements of the rate of delayed hydride cracking in zirconium alloys have been transferred from the host laboratory to other countries.
2. By following a strict procedure, a very consistent set of values of crack velocity were obtained by both individual laboratories and between the different laboratories.
3. The results over a wide range of test temperatures from materials with various microstructures fitted into the current theoretical framework for delayed hydride cracking.
4. An inter-laboratory comparison of hydrogen analysis revealed the importance of calibration and led to improvements in measurement in the participating laboratories.
5. The success of the CRP in achieving its goals has led to the initiation of some national programmes.

6.2. Recommendations

1. Future work on delayed hydride cracking should be on equally well-characterized material with similarly controlled experimental procedures.
2. Based on the success of this CRP, it is recommended that further research should be initiated with the objective of evaluating delayed hydride cracking in fuel cladding to support understanding of long splits observed in some fuel.
3. Zirconium standards rather than titanium standards are recommended for calibration when analysing hydrogen in zirconium alloys.

LIST OF PARTICIPANTS

Alvarez, A.	Studsvik Nuclear, Sweden
Banerjee, S.	Bhabha Atomic Research Center, India
Bickel, G.A.	Atomic Energy of Canada Limited, Canada
Choubey, R.	Atomic Energy of Canada Limited, Canada
Coleman, C.E.	Atomic Energy of Canada Limited, Canada
Dobrea, D.	Institute for Nuclear Research, Romania
Gou, Yuan	Nuclear Power Institute of China, China
Grigoriev, V.	Studsvik Nuclear, Sweden
Grybenas, A.,	Lithuanian Energy Institute, Lithuania
Haddad, R.	Comision Nacional de Energia Atomica, Argentina
Jakobsson, R.	Studsvik Nuclear, Sweden
Kanwar Liaqat Ali	Pakistan Institute of Nuclear Science and Technology, Pakistan
Kim, Y.S.,	Korea Atomic Energy Research Institute, Republic of Korea
Leger, M.	Atomic Energy of Canada Limited, Canada
Levinskas, R.,	Lithuanian Energy Institute, Lithuania
Makarevicius, V.	Lithuanian Energy Institute, Lithuania
Markelov, V.A.	A.A. Bochvar All-Russian Scientific Research Institute of Inorganic Materials, Russian Federation
Pitigoi, V.	Institute for Nuclear Research, Romania
Radu V.	Institute for Nuclear Research, Romania
Ritchie, I.	International Atomic Energy Agency
Roth, M.	Institute for Nuclear Research, Romania
Singh, R.N.	Bhabha Atomic Research Center, India

Enclosure 16 to TN E-30577

McMinn, A., Darby, E. C., and Schofield, J. S., "The Terminal Solid Solubility of Hydrogen in Zirconium Alloys," *Zirconium in the Nuclear Industry: Twelfth International Symposium, ASTM STP* 1354, G. P. Sabol and G. D. Moan, Eds., American Society for Testing and Materials, West Conshohocken, PA, 2000, pp. 173-193 (associated with RAI 2-7)

Andrew McMinn,[1] *Edward C. Darby,*[1] *and John S. Schofield*[1]

The Terminal Solid Solubility of Hydrogen in Zirconium Alloys

REFERENCE: McMinn, A., Darby, E. C., and Schofield, J. S., **"The Terminal Solid Solubility of Hydrogen in Zirconium Alloys,"** *Zirconium in the Nuclear Industry: Twelfth International Symposium, ASTM STP 1354,* G. P. Sabol and G. D. Moan, Eds., American Society for Testing and Materials, West Conshohocken, PA, 2000, pp. 173–195.

ABSTRACT: An experimental program has been carried out to measure the terminal solid solubility (TSS) of hydrogen in Zircaloy. Unirradiated electron beam (EB) welded Zircaloy-2, EB-welded Zircaloy-4, Zircaloy-2 pressure tube, cold-worked β-quenched Zircaloy-2 forging, oxygen-strengthened tungsten inert gas (TIG) welded Zircaloy-4, and irradiated welded Zircaloy-2, welded Zircaloy-4, and Zircaloy-2 pressure tube materials were tested. A differential scanning calorimetry technique was used to measure the dissolution and precipitation temperatures for a range of hydrogen concentrations.

The TSS behavior of unirradiated EB welded Zircaloy-2 and Zircaloy-4, Zircaloy-2 pressure tube, and β-quenched Zircaloy-2 forging materials was very similar, indicating little influence of chemical composition or microstructure on TSS. There was a marked hysteresis between the dissolution (TSSd) and precipitation (TSSp) temperatures, and best fit equations are provided for the two curves.

Oxygen-strengthened TIG welded Zircaloy-4 exhibited markedly different solubility behavior to the other unirradiated materials. The oxygen addition increased the hydrogen solubility. Two explanations have been postulated for the effect, either an increase in the matrix strength or hydrogen trapping at the solute atoms. However, increasing the matrix strength in Zircaloy-2 by cold working did not increase hydrogen solubility.

Zircaloy-2 and Zircaloy-4 materials, irradiated to fluences in the range 5.5×10^{20} to 1.0×10^{22} n/cm^2 ($E > 1$ MeV) at temperatures in the range of 250 to 300°C, have higher dissolution and precipitation solubilities compared to those measured on unirradiated material. When the irradiation damage was annealed out at 500°C, the TSS temperatures tended to be restored to the unirradiated values. It has been hypothesized that the effect of irradiation is to trap hydrogen at the irradiation damage sites, although a second explanation involving the increase in matrix strength due to irradiation has also been considered.

For unirradiated Zircaloy, thermal history was found to affect TSSp but not TSSd. Increasing the peak temperature or the hold period at peak temperature reduced the TSSp temperature. This effect is considered due to a reduction of the "memory effect" in which preferential sites for hydride precipitation are removed by the annealing. Heating and cooling rates over the range 0.5 to 10°C/min had little effect on the measured dissolution and precipitation temperatures.

KEYWORDS: hydrogen, Zirconium, solubility

Zirconium alloys used for nuclear core structural components can be embrittled by the presence of hydrides. This can take the form of reduced ductility and fracture toughness [*1,2*] and sub-critical crack growth mechanisms such as delayed hydride cracking and environmental fatigue crack growth [*3–5*]. The solubility curves for hydrogen in zirconium

[1] Consultant, materials consultant, and consultant, respectively, Rolls-Royce, P.O. Box 2000, Derby, England, DE21, 7XX.

alloys are therefore important parameters as they define the conditions under which hydrides are present. The terminal solid solubility (TSS) dissolution curve defines the temperature (TSSd) and hydrogen concentration conditions for dissolution of hydrides on warmup. The precipitation curve defines the temperature (TSSp) and hydrogen concentration conditions for hydride precipitation on cooldown.

A literature review has revealed considerable scatter in published TSS data for zirconium and its alloys. This can be attributed partly to the variety of experimental techniques used, such as diffusion gradients [*6–8*], dialometry [*9,10*], calorimetry [*11*], pressure-composition-temperature relationships [*9,12–14*], internal friction [*15–17*], dynamic elastic modulus [*11,17,18*], metallography [*19*], resistivity [*20*], and neutron diffraction [*21*]. Most measurements have been made at temperatures above 300°C and only for the dissolution solubility. Less experimental data exist for the precipitation solubility, although data that do exist for Zircaloy show a marked difference (hysteresis) between the two solvii [*9,10*].

The inadequacies of the existing TSS database, and the concern over extrapolating high-temperature TSS measurements into the operating temperature region of nuclear reactor core components, meant there was a need to generate accurate TSS data on unirradiated and irradiated Zircaloy. The results of an experimental program to meet this need are presented in this paper.

TSS curves were generated for unirradiated zirconium alloys hydrided to hydrogen levels in the range 6 to 77 ppm. The materials tested included unirradiated electron beam (EB) welded Zircaloy-2, EB welded Zircaloy-4, Zircaloy-2 pressure tube, cold-worked β-quenched Zircaloy-2 forging, and oxygen-strengthened TIG welded Zircaloy-4, as well as irradiated EB welded Zircaloy-2 and Zircaloy-4, and Zircaloy-2 pressure tube. The TSS data were generated using a differential scanning calorimetry (DSC) technique. The tests allowed the effects of composition, microstructure, cold work, strength, and neutron irradiation on TSS to be investigated. The effects of thermal history on TSSp and TSSd were also investigated by varying the heating/cooling rates, the peak temperature reached before cooling, and the hold time at peak temperature.

Physical mechanisms have been proposed to explain the measured shifts in the solubility limit of hydrogen in irradiated Zircaloy that were observed in the DSC experiments reported here. The two main mechanisms proposed, irradiation trapping and yield strength effects, have been examined and the findings discussed together with the experimental data.

Experimental

Differential Scanning Calorimetry

The DSC technique was selected for this study because it is simple, relatively fast, and gives good reproducibility. Effects of material inhomogeneity are minimized because only small samples, typically weighting 300 mg, are tested. DSC is nondestructive, so repeat test runs on the same sample can be carried out. The technique is sensitive at low hydrogen levels, and TSSd has been measured for samples containing less than 10 ppm hydrogen. DSC has been used previously to measure the TSS of small irradiated samples removed from CANDU pressure tubes [*22*].

The operation of a differential scanning calorimeter is based on the measurement of the thermal response of a sample compared to a reference when the two are heated uniformly at a constant rate. Heat capacity is the usual property determined by measuring the changes in enthalpy in the sample. Enthalpy changes are often the result of phase transformations, and the dissolution and precipitation of zirconium hydride is a transformation that can be studied by DSC. This transformation occurs over a temperature range within the capabilities

of most calorimeters and is relatively rapid compared to other solid state phase transformations. Enthalpy changes are determined by measuring the differential heat flow between the test sample and reference, which are thermally isolated. Auxiliary heaters heat the two samples at a predetermined rate and maintain them at identical temperatures. The difference in heat flow is determined by the difference in power supplied to each individual heater. The heat flow is dependent on the enthalpy of transformation, the sample mass, and the overall reaction rate. The latter is dependent on the kinetics of the reaction and on the heating/cooling rate. The total enthalpy is determined by integrating the heat flow over time. A Zr-2.5Nb alloy sample with less than 2-ppm hydrogen was used as the reference to cancel out the heat-capacity effects of the matrix and maximize the differential nature of the measurement. Prior to, during, and after DSC testing, a number of calibrations were performed using a triple metal standard whose melting points and enthalpies are well known. The finite heat transfer characteristics of the DSC cell and the thermal mass of the sample cause the sample temperature to lag behind the measured temperature. When the calculated thermal lag was small (about 0.2°C), the correction was ignored since other experimental factors outweighed it. However, when the thermal lag was larger (about 1°C), a correction was made to the calculated TSS temperature. For the range of test temperatures in this study, the accuracy of the DSC technique is ±2°C.

Figure 1 illustrates a typical analysis of DSC heat flow and derivative heat flow curves on heating. The heat flow decreases with increasing temperature as heat is absorbed by the sample to dissolve hydrides. Once the last hydrides dissolve, the heat absorbed is no longer required and the curve swings upward. This discontinuity in the heat flow curve can be used to define TSS for different levels of bulk hydrogen. The drop in heat flow and the sharpness of the discontinuity increase with increasing hydrogen levels. Analysis yields three temperatures: a peak temperature (262.7°C in Fig. 1), a completion temperature (300.5°C), and a maximum slope temperature (284.8°C). The peak temperature represents the maximum deviation of the heat flow along a perpendicular to the interpolated baseline of the heat flow

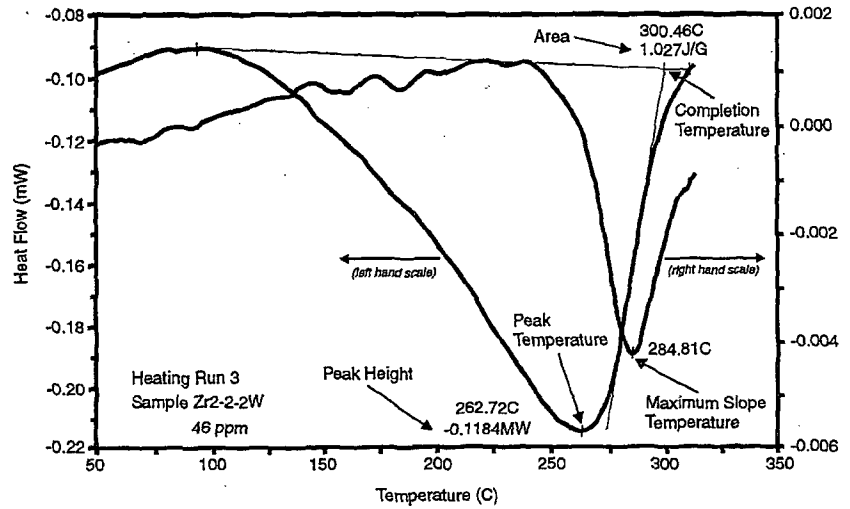

FIG. 1—*Typical DSC heat flow and derivative curves for a heating cycle.*

curve. The completion temperature is the temperature at which the interpolated baseline and the average dissolution discontinuity tangent intersect. Both these temperatures are sensitive to the characteristics of the interpolated baseline, which is assumed to be linear, but can exhibit curvature. The maximum slope temperature, which is derived from the maximum of the derivative heat flow curve, is not affected by the subjective nature of the interpolated baseline and has traditionally been used to define TSSd. In the idealized case, completion of hydride dissolution is marked by a sharp discontinuity, and the peak temperature, completion temperature, and maximum slope temperature would be identical. However, due to calorimeter response and hydride dissolution behavior, this ideal case is never realized.

Khatamian and Ling [*23*] have suggested recently that the peak temperature best represents TSSd for zirconium. Their justification is based on a better correlation between TSSd defined by peak temperature (rather than the maximum slope temperature) and the results obtained by Kearns [*6*] for unalloyed zirconium. The same comparison has been made for data reported in this paper, see Fig. 2. Although Kearns' relationship for the Zircaloys lies closer to the peak temperature than the maximum slope temperature, the correlation is not exact. Also included in Fig. 2 are the diffusion annealing temperatures used to hydride the samples tested. During hydriding, an equilibrium couple is set up between the Zircaloy with a low-hydrogen concentration and the hydride layer. As diffusion annealing establishes an equilibrium between hydrogen in solid solution and hydrides at a given temperature, the diffusion annealing temperature represents the equilibrium TSSd. The almost exact correlation between the diffusion annealing temperatures and the maximum slope temperatures derived from the DSC measurements indicate that, for the materials studied in this work, the maximum slope temperature best represents the temperature for complete hydride dissolution (TSSd).

The analysis of the heat flow curves on cooling is similar to the heating cycle analysis and is shown in Fig. 3. The major difference is that the curves are inverted and the maximum slope temperature, used to define TSSp, falls between the onset temperature and the peak temperature.

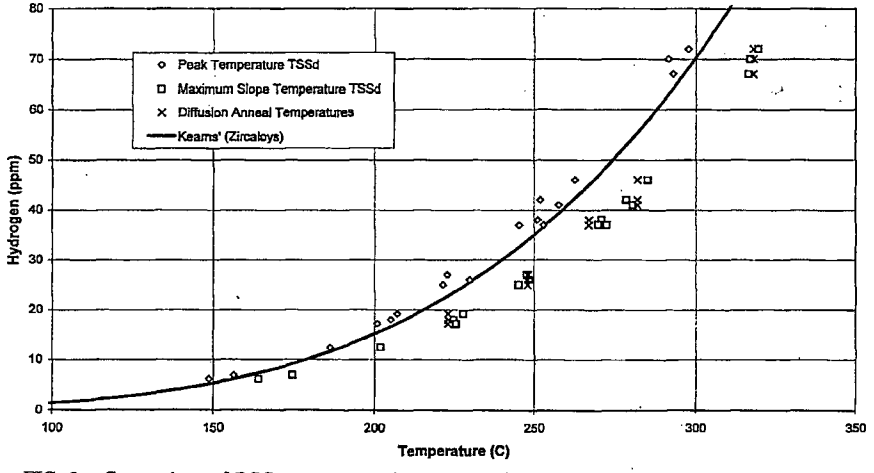

FIG. 2—*Comparison of DSC temperature definitions with Kearns' solubility curve and diffusion anneal temperatures.*

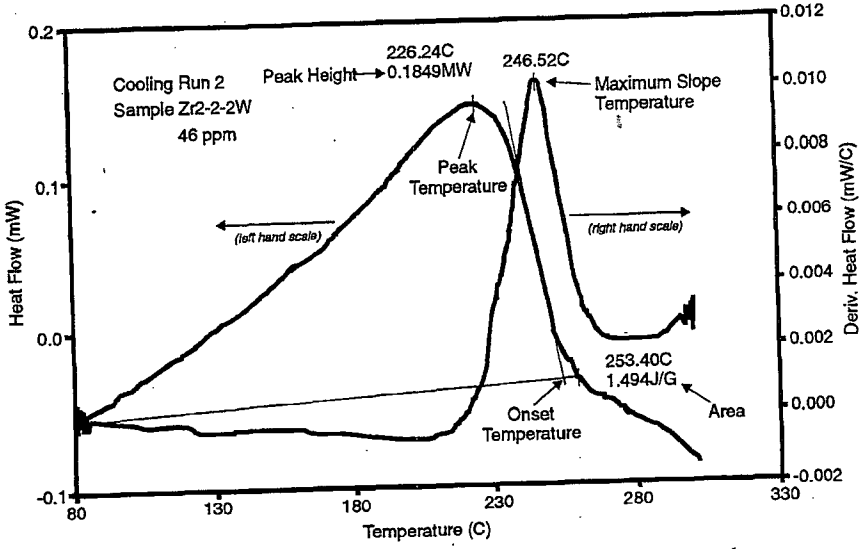

FIG. 3—*Typical DSC heat flow and derivative curves for a cooling cycle.*

Materials

TSS measurements were made on various unirradiated materials including EB welded Zircaloy-2 plate, EB welded Zircaloy-4 plate, Zircaloy-2 pressure tube, oxygen-strengthened TIG welded Zircaloy-4 plate, and a cold-rolled β-quenched Zircaloy-2 forging. The latter two materials were produced in an attempt to simulate the mechanical strength of irradiation-hardened material. Irradiated Zircaloy-2 and Zircaloy-4 materials were also tested. Typical yield strengths of these materials and their measured as-received hydrogen contents are given in Table 1.

The EB welded Zircaloy-2 and Zircaloy-4 plates had been vacuum annealed for 2 h at 760°C after welding. The Zircaloy-2 pressure tube had been extruded at 830°C, drawn (with intermediate anneals at 600°C), stress relieved at 400°C for 5 h, and then honed. The oxygen-strengthened material had been produced by depositing bead-on-plate TIG welds on a Zircaloy-4 plate with a cover gas containing a 0.75 vol% oxygen/argon mixture. The oxygen content of the welds was determined to be in the range 2540 to 2860 ppm, which compares to a typical oxygen content of 1000 to 1200 ppm in EB welded Zircaloy.

The beta-quenched Zircaloy-2 forging was tested in two conditions, as received (0% cold work) and after cross rolling to produce 30% cold work. The as-received material had a near random texture (Kearns' parameters $f_N = 0.365$, $f_T = 0.338$, and $f_L = 0.297$, where N, T, and L are the normal, transverse, and longitudinal directions of the forging) and a low yield strength, whereas the cold-rolled material had a strong texture ($f_N = 0.724$, $f_T = 0.152$, and $f_L = 0.124$) and higher strength (Table 1). The strength of the as-received forging was measured in the longitudinal direction. The strength of the 30% cross-rolled forging was measured in both the longitudinal and transverse directions and was similar in both directions. This is consistent with the texture parameters reported above. Cross rolling strengthens the material in the plane, as opposed to uniaxial rolling, which strengthens the material in

TABLE 1—*Room temperature yield strength of materials tested.*

Material	Yield Strength, MPa	Hydrogen Content Prior to Hydriding, ppm
Zircaloy-2 and 4 EB welded	380–430	6
Zircaloy-2 pressure tube	440–480	13
Zircaloy-4 oxygen strengthened	577–620	8
Zircaloy-2 β-quenched forging	294–358	4
Zircaloy-2 β-quenched forging 30% cold rolled	530–581	7
Zircaloy-2 and -4 irradiated	631–816	14–20
Zircaloy-2 pressure tube irradiated	730–790	75

one direction only. TSS measurements were also made after a 550°C stress relief, which was intended to remove the effects of the cold work but leave the strong texture unaltered.

Specimens were machined from irradiated Zircaloy-2 and Zircaloy-4 components, which had been irradiated to a fluence range of 5.5×10^{20} to 1.0×10^{22} n/cm^2, $E > 1$ MeV at temperatures in the range 250 to 300°C.

Hydriding

Test samples were hydrided by electrolytically depositing a surface hydride layer and then annealing to diffuse the hydrogen from the surface layer into the metal. Electrolytic hydriding was typically carried out in a bath of 0.1 *M* sulfuric acid at 90°C, using a current density of 100 to 120 mA/cm^2 for 72 h or less. The quality of the hydride layer was checked metallographically and was approximately 0.03 mm thick.

The individual welds and base plate materials were annealed at different temperatures and times to give estimated concentrations of 20, 30, 40, 50, 60, and 80-ppm hydrogen. During hydriding, an equilibrium couple is set up between the Zircaloy with a low-hydrogen concentration and the hydride layer. At the annealing temperature, the resulting hydrogen in solution equates to the equilibrium TSS. The Kearns' TSSd equation for Zircaloy was used to specify the annealing temperature required to obtain the target concentrations [5]. The annealing times were selected to give saturation through the sample thickness, although the annealing times for the cold-rolled material were minimized so as not to affect the degree of cold work in the material.

After annealing, the surface hydride layers were removed by grinding. Apart from the cold-rolled material and the irradiated material, the samples were then homogenized at 400°C for 48 h. DSC samples, measuring approximately 5 by 5 by 0.4 mm, were then removed from both the as-received and hydrided coupons using a slow-speed cutting wheel in order to minimize heating and cold working of the specimen surface, both of which could affect TSS.

Irradiated Zircaloy-2 samples were initially hydrided by diffusion annealing at 260°C, which, based on unirradiated material TSS data, would be expected to result in a hydrogen level of 32 to 36 ppm. However, measurements revealed a hydrogen level of 43 to 48 ppm.

This observation of different hydriding behavior is significant, as it provides independent support to the different solubility curves measured for the irradiated material (see later). Additional tests were carried out on irradiated samples with as-received hydrogen levels (Table 1) and hydrided to nominal hydrogen levels of 25, 35, and 55 ppm.

Experimental Procedures

The first set of TSS tests was carried out on the unirradiated EB weld, cold-worked pressure tube, and oxygen-strengthened materials, using a heating and cooling rate of 2°C/min. Specimens were heated in inert gas to 30°C above their predicted TSSd temperature and immediately cooled. Each specimen was given four identical thermal cycles, but only the data from the last three cycles were used to determine mean TSSd values. The first heating cycle may not produce reliable TSSd temperature data due to the unknown prior thermal history of the sample, and it is standard procedure to disregard the first heating cycle in determining TSSd. The first cooling run is used to determine TSSp because the relevant prior thermal history is known.

TSS tests were carried out on cold-worked material as described above, except a cooling rate of 10°C/min was used. After the initial DSC measurements on the 0 and 30% cold-rolled materials, the samples were annealed at 550°C for 1 h, and the experiments were repeated.

A series of tests were also carried out to determine the effects of thermal history on TSS. The tests included varying the peak temperature, the hold time at peak temperature, and the heatup and cooldown rates. The tests were performed on the same two samples of unirradiated EB welded Zircaloy-2, containing 25 and 46 ppm hydrogen, so that the results could be compared. The test conditions were as follows:

- A heating/cooling rate of 2°C/min to peak temperatures of 310, 350, and 400°C. The thermal cycle did not include a hold period at these peak temperatures.
- A heating/cooling rate of 2°C/min to peak temperatures of 350 and 400°C with hold periods of either 1 h or 24 h at the peak temperature.
- Identical (balanced) heating and cooling rates of 0.5, 5, or 10°C/min with no hold at peak temperature. The data could be compared directly to that obtained at 2°C/min.
- Dissimilar (imbalanced) heating (0.5 and 10°C/min) and cooling rates (10 and 0.5°C/min) were used on the specimen containing 25 ppm hydrogen. There was no hold at the peak temperature of 290°C.

The DSC procedures used for these tests were similar to those used for the first set of TSS tests. However, because of the varying thermal history of the tests, it was necessary to carry out a full enthalpy and temperature calibration at each heating rate.

Tests on irradiated material were carried out at two laboratories using procedures similar to those for unirradiated material. Comparative tests between the two laboratories on two unirradiated sample demonstrated good interlaboratory agreement. Repeat tests on irradiated material were initially carried out at heating and cooling rates of 2 and 10°C/min. As there was no significant difference in the TSS data, all other tests were carried out at a rate of 10°C/min. Specimens were heated to at least 30°C above the predicted unirradiated material TSSd temperature.

Following the initial DSC runs, all of the irradiated samples were given a 500°C anneal for 1 h in the calorimeter to remove the irradiation damage and hardening. The measurement of TSS was then repeated by cycling to the same peak temperature at the same heating and cooling rate.

The hydrogen concentrations in the DSC samples were determined using hot vacuum extraction mass spectrometry. The sample is heated in a quartz tube to 1100°C under a vacuum of 3×10^{-8} torr, and the extracted hydrogen is transferred to a mass spectrometer for isotopic analysis. The accuracy of the measurements was within 5 to 6% at the 2 sigma level for the size of sample and concentration ranges being measured.

Results

Unirradiated Material TSS Results

The TSS results for the EB welded Zircaloy-2, EB welded Zircaloy-4, and Zircaloy-2 pressure tube materials are presented graphically in Figs. 4 and 5. The data for these three materials exhibited little scatter and formed a tight distribution, indicating little effect of material composition or microstructure on TSS. There was a marked hysteresis between the TSSd and TSSp curves, which equated to a temperature difference of approximately 40°C. The TSSd data are compared to Kearns' mean dissolution line in Fig. 5, and it is seen that the materials tested had higher dissolution temperatures than predicted by the Kearns' correlation for Zircaloy [*6*].

The β-quenched forging was tested in four conditions: as-received and 30% cold worked, before and after annealing, and the results are presented graphically in Figs. 6 and 7. For hydrogen concentrations >22 ppm, the TSS data for the four conditions were very similar, indicating that neither cold work nor crystallographic texture have a significant effect on the TSS in this material. The TSS data were also very similar to that obtained on the other unirradiated materials of varying strength and texture. The data are compared to Kearns' Zircaloy correlation in Fig. 7, and again the materials generally exhibited higher TSSd temperatures than predicted by Kearns. The TSS data at the very low as-received hydrogen concentrations (especially the 7-ppm sample) indicate a shift in TSS on annealing to a higher-solubility temperature. Whether this is a real effect of cold work is debatable in light of other data, and the shift could represent a higher inherent scatter in the data at low temperatures and hydrogen concentrations.

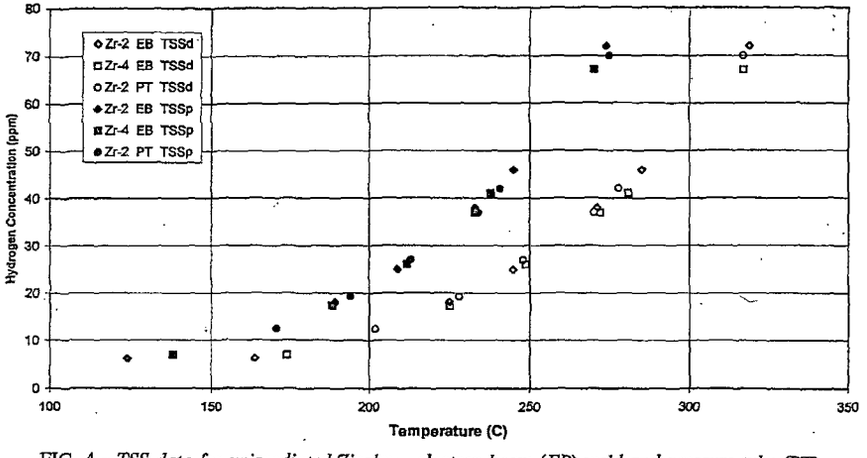

FIG. 4—*TSS data for unirradiated Zicaloy—electron beam (EB) weld and pressure tube* (PT).

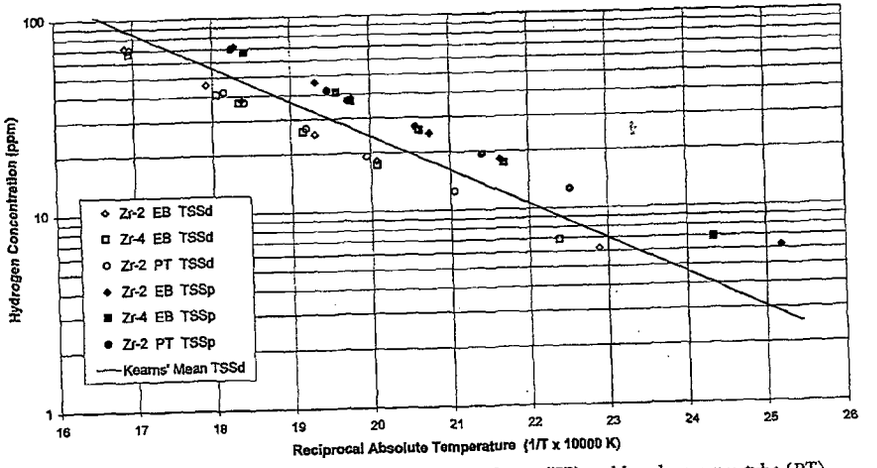

FIG. 5—*TSS data for unirradiated Zircaloy—electron beam (EB) weld and pressure tube* (PT).

Apart from the data obtained at hydrogen concentrations of 7 ppm or less, the TSS data for the cold-worked material were very similar to that obtained on EB welded and pressure tube Zircaloy materials. All of the data are plotted in Fig. 8. These data were statistically analyzed by linear regression in order to define the mean solubility curves. In line with previous representations, an Arrhenius functional form was used. Data for the annealed, cold-worked Zircaloy-2 were not included in the fit.

The mean solubility curves for dissolution and precipitation are plotted with the TSS data in Fig. 8 and are represented by the following equations:

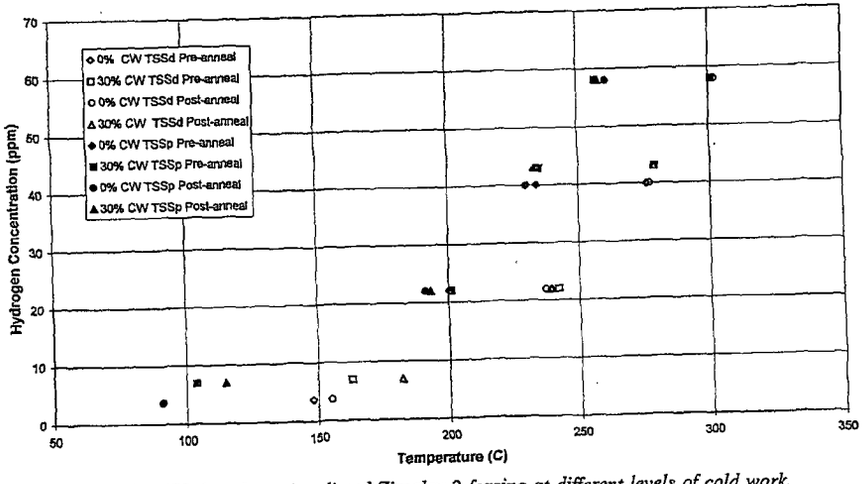

FIG. 6—*TSS data for unirradiated Zircaloy-2 forging at different levels of cold work.*

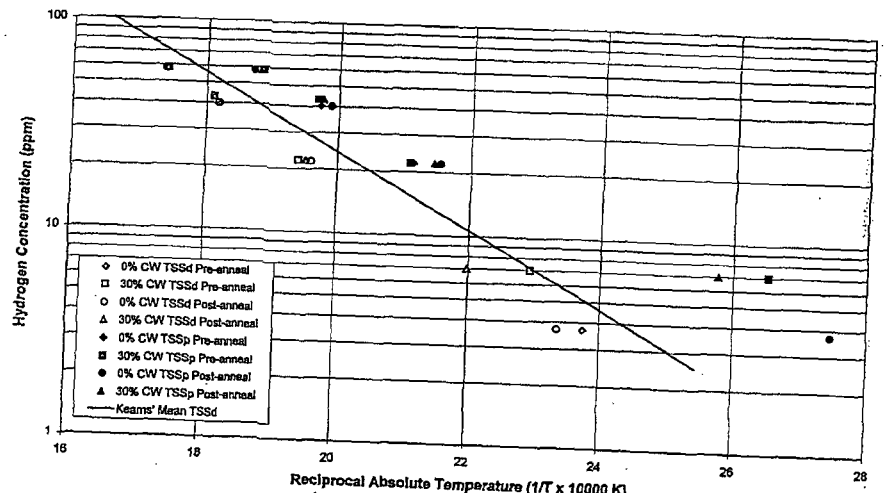

FIG. 7—*TSS data for unirradiated Zircaloy-2 forging at different levels of cold work.*

$$C_{du} = 106\,446.7 \exp\,[-4328.67/T] \quad (1)$$

$$C_{pu} = 138\,746.0 \exp\,[-4145.72/T] \quad (2)$$

where C_{du} and C_{pu} are the dissolution and precipitation hydrogen concentrations in ppm for unirradiated material, and T is the temperature in K.

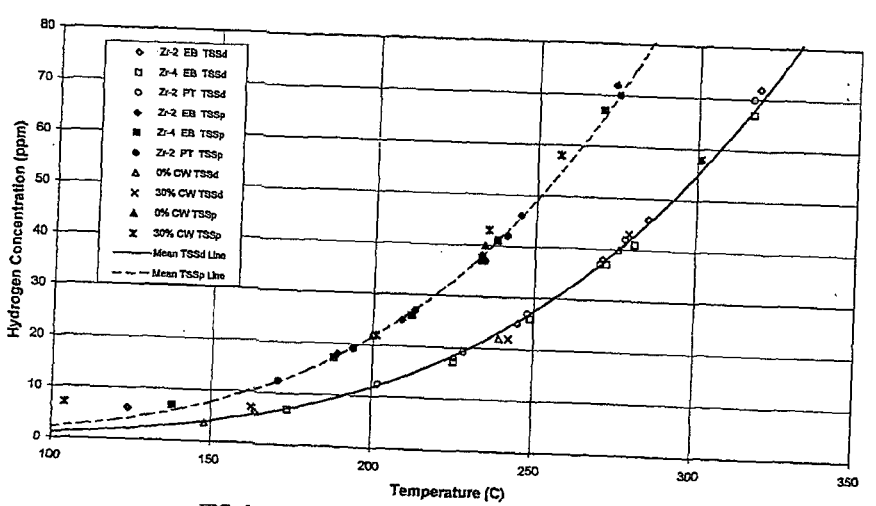

FIG. 8—*TSS data for unirradiated Zircaloy materials.*

In fitting the TSSp equation, the results for the lowest hydrogen concentration samples (≤7 ppm) were omitted as they deviated significantly from the Arrhenius fit (Figs. 5 and 7).

The oxygen-strengthened material exhibited a higher hydrogen solubility at a given temperature compared to the other unirradiated materials tested. The data are shown plotted against the best fit curves to the other data in Fig. 9. The results suggest that oxygen increases the hydrogen solubility, that is, it decreased the dissolution and precipitation temperatures. The scatter in the TSS data was larger in the oxygen-strengthened material compared to the other materials tested, and the reason for this is unclear.

Thermal History TSS Results

The results of the peak temperature variation tests are shown in Fig. 10. The TSSp temperature decreased with increasing peak temperature, whereas the TSSd on the second and subsequent heating cycles was unaffected. Reduction of the TSSp temperature with increasing peak temperature is considered to be due to a "memory effect" for hydride precipitation [*24–26*]. Effectively, high-peak temperatures "anneal out" favorable sites (dislocation networks) for hydride precipitation (prior hydride precipitation sites), thereby removing the "memory effect." For the 400°C peak temperature test, the TSSp temperature decreased with each calorimeter run, suggesting some residual "memory effect" between runs and further suggesting that a lowering of the TSSp temperature is both peak temperature and time dependent.

The results of the hold at peak temperature tests are shown in Fig. 11 for a peak temperature of 400°C. The TSSp temperatures decreased with increasing hold time, whereas the TSSd on the second and subsequent heating cycles was unaffected. The tests with a peak temperature of 350°C showed similar trends. The decrease in TSSp temperature is again believed to be due to a reduction of the "memory effect" on hydride precipitation, which is both time and temperature dependent. The effect of increasing the peak temperature and the hold period was therefore to increase the hysteresis between TSSd and TSSp.

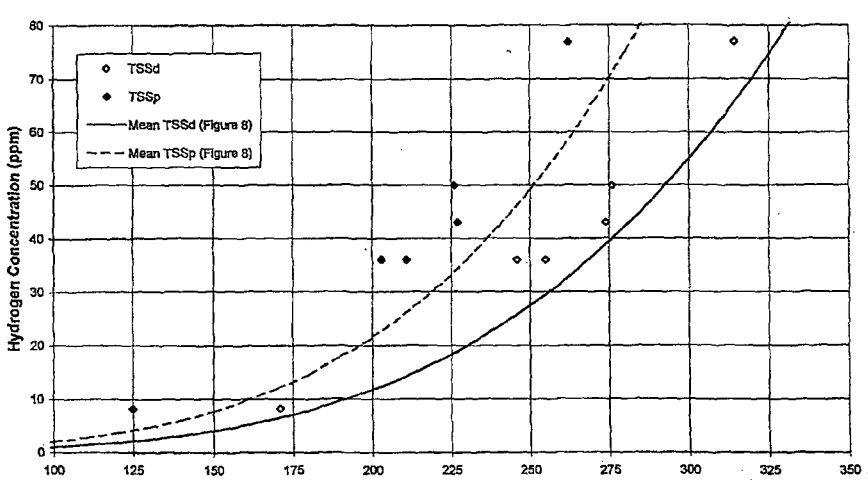

FIG. 9—*TSS data for oxygen-strengthened Zircaloy.*

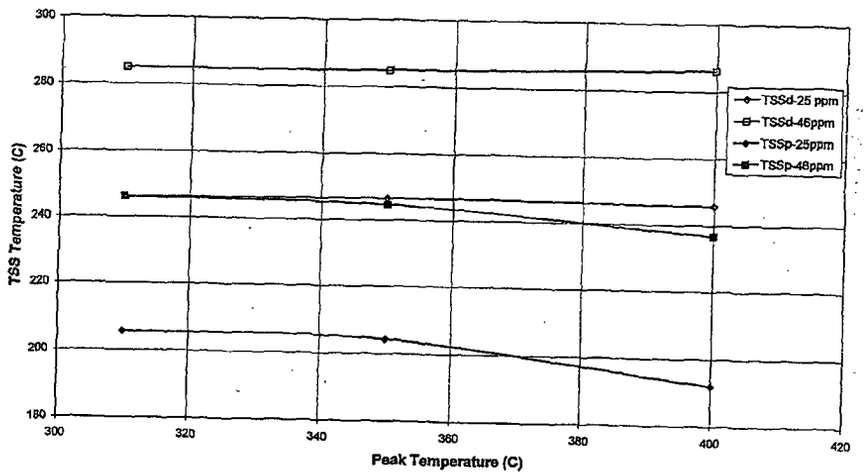

FIG. 10—*Effect of peak temperature on TSSd and TSSp.*

The results of the heating and cooling rate tests are shown in Fig. 12. The effect of varying heating and cooling rate on TSSd and TSSp temperatures was found to be very small over the range 0.5 to 10°C/min. The TSSd and TSSp temperatures varied only by 2 to 3°C for both the 25 and 46-ppm samples, with the faster heating/cooling rates giving slightly higher TSSd and slightly lower TSSp temperatures.

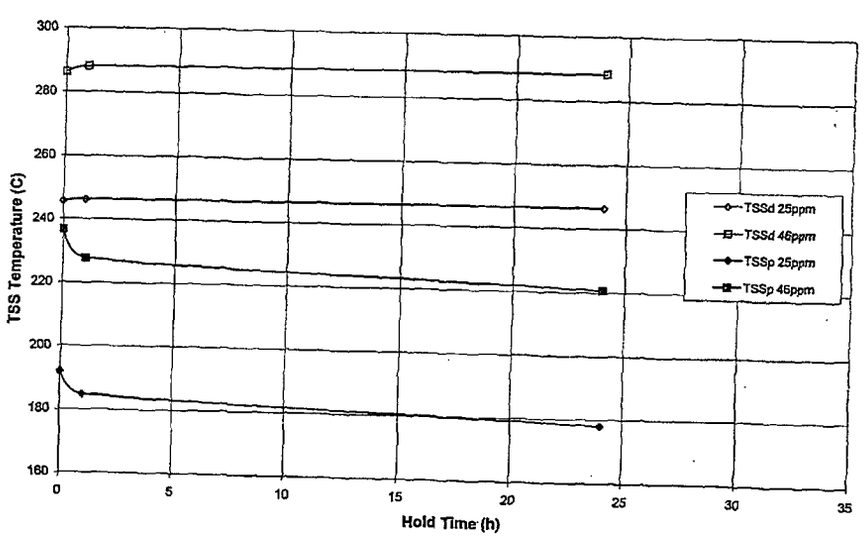

FIG. 11—*Effect of hold time at 400°C peak temperature on TSSd and TSSp.*

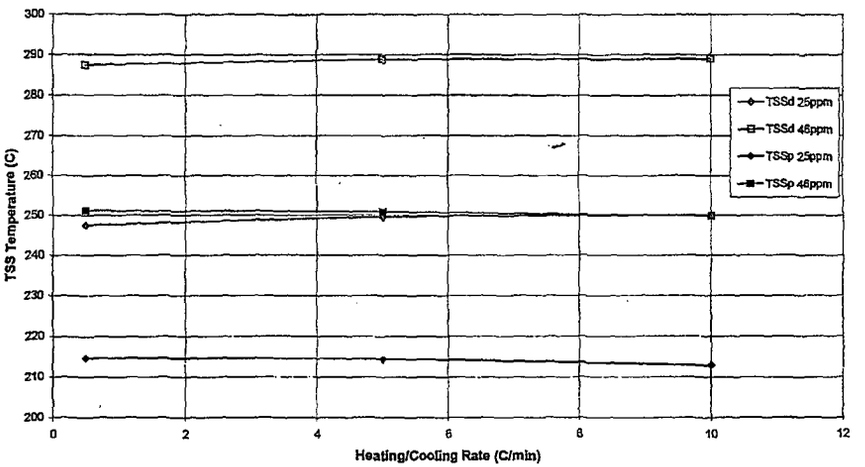

FIG. 12—*Effect of heating and cooling rate on TSSd and TSSp.*

The results of the imbalanced heating/cooling rate test showed that the TSSd and TSSp temperatures for the imbalanced rate tests were slightly higher than the balanced rate tests. Over the range of the imbalanced heating/cooling rates used, the measured TSS varied by no more than 6°C.

Irradiated Material TSS Results

The TSS data on irradiated material were generated at two different laboratories using different calorimeters and were found to be in good agreement. The TSSd and TSSp results for irradiated Zircaloy-2 and Zircaloy-4, before and after a thermal anneal, are presented in Figs. 13 and 14, respectively. Included in these figures are the mean TSSd and TSSp curves for unirradiated Zircaloy (Eqs 1 and 2). Neutron irradiation increased the solubility of hydrogen in Zircaloy-2 and Zircaloy-4, or put another way, irradiation lowered the solubility temperatures (both TSSd and TSSp) for the same bulk hydrogen concentration. There was a marked hysteresis between the irradiated material TSSd and TSSp data, with the precipitation temperature approximately 50 to 60°C lower than the dissolution temperature. The hysteresis was larger than that measured for unirradiated material (40°C).

Annealing out the irradiation damage shifted the measured TSSd and TSSp values back towards the unirradiated material equivalents. With the exception of the cold-worked pressure tube material, the TSSd data after annealing fell on the unirradiated material data curve, giving strong confirmation that the enhanced hydrogen solubilities measured for the irradiated samples are directly related to irradiation damage. After annealing, the TSSp data for all irradiated materials generally fell short of the unirradiated material data curve. This is believed to be due to a dual effect of the anneal in removing both irradiation damage (acts to increase TSSp) and hydride accommodation dislocations (acts to reduce TSSp).

Statistical analysis of the irradiated material TSS data, assuming an Arrhenius relationship as for the unirradiated material data, was carried out. It was found that a single Arrhenius relationship gave a good fit to the TSSd data over the complete temperature range. However, this was not the case for the TSSp data, and the best description of the TSSp was given by

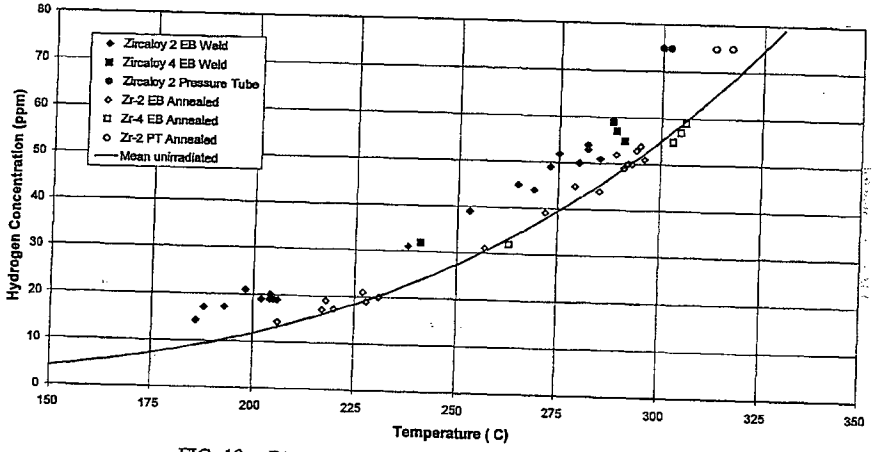

FIG. 13—*Dissolution solubility data for irradiated Zircaloy.*

two regression fits, one for TSSp < 170°C and one for TSSp > 170°C. The fits are shown plotted against the data in Fig. 15 and are defined as follows:

$$C_{di} = 24\,236.1 \exp[-3391.1/T] \tag{3}$$

$$C_{pi} = 212.1 \exp[-1003.6/T] \quad \text{for } T < 170°C \tag{4a}$$

$$C_{pi} = 66\,350.1 \exp[-3557.2/T] \quad \text{for } T > 170°C \tag{4b}$$

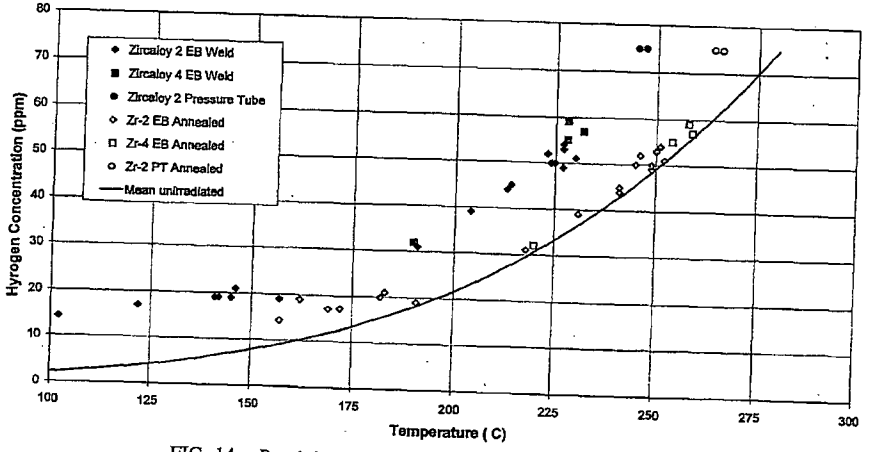

FIG. 14—*Precipitation solubility data for irradiated Zircaloy.*

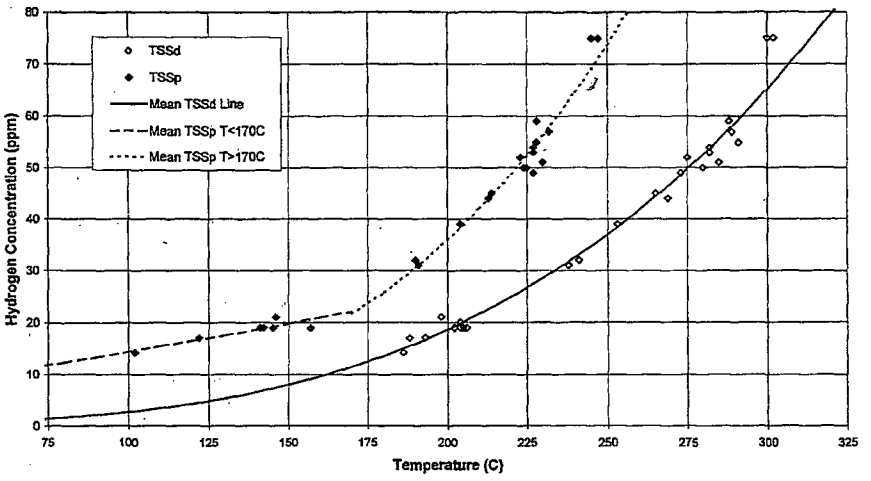

FIG. 15—*TSS data for irradiated Zircaloy.*

where: C_{di} and C_{pi} are the dissolution and precipitation hydrogen concentrations in ppm for irradiated material, and T is the temperature in K.

Although there was a consistent effect of irradiation on TSS, there did not appear to be a significant effect of fluence level on the measured irradiated material TSS values within the range of fluences tested (5.5×10^{20} to 1.0×10^{22} n/cm^2, $E > 1$ MeV).

There was little effect of peak temperature in the range 260 to 320°C on the measured TSSd and TSSp temperatures for irradiated Zircaloy. This is consistent with the unirradiated material data, in which an effect of peak temperature was not observed unless the peak temperature was above 350°C. Similarly, there was little effect of heating and cooling rate on irradiated Zircaloy TSS.

Discussion

Unirradiated Material Behavior

The TSS data indicate little difference in the dissolution and precipitation behavior between the EB welded Zircaloy-2, EB welded Zircaloy-4, Zircaloy-2 pressure tube, and cold-worked β-quenched Zircaloy-2 materials. Given the temperature uncertainty of ±2°C, the 5 to 6% error in hydrogen concentrations and the line-fitting errors, any apparent differences in the solubility lines suggested by these data are statistically insignificant. This observation is consistent with Kearns' assessment, which also found no significant difference in the dissolution solubility for Zircaloy-2 and Zircaloy-4 [6]. However, the dissolution temperatures measured in this study were higher than those measured by Kearns. The difference could be attributable to differences in experimental techniques, including measurement of hydrogen concentration. DSC is a dynamic method where the temperature must change in order to detect TSSd, whereas Kearns used an equilibrium diffusion couple technique in which, at equilibrium, the diffusion annealing temperature is the TSSd temperature. However, as described previously, the DSC maximum slope temperature was used to define TSSd, and

this temperature closely matched the diffusion annealing temperature. Thus, the differences between the data reported here and that of Kearns are considered to be real.

The observation that the precipitation solubility was essentially the same for the four materials is inconsistent with the data of Slattery [*10*], who observed a much lower precipitation temperature for Zircaloy-2 compared to Zircaloy-4. The difference could be due to different thermal histories used in Slattery's experiments, as differing peak temperatures, hold times, and cooling rates all affect the measured TSSp value. In addition, Slattery used dilatometry rather than DSC for measuring TSS, which could lead to different TSS values.

The Arrhenius plots of the TSS data suggest that the lowest hydrogen concentration points for the EB welded Zircaloy-2 and the cold-worked β-quenched Zircaloy-2 (and to a lesser extent EB welded Zircaloy-4) do not follow a simple Arrhenius relationship and exhibit a higher hydrogen solubility than extrapolation from higher concentrations would predict. This behavior has been observed by Daniel [*27*] and Mishra and Asundi [*15*]. The latter workers suggested that the deviation from the simple Arrhenius behavior at low hydrogen concentration may be due to the formation of the metastable gamma hydride phase in addition to the delta phase. There is also experimental evidence that, in Zr-2.5Nb, delta hydride converts to gamma hydride below 180°C [*21*]. TSSp and precipitation kinetics could be affected by the different hydride phase structures that may affect precipitate accommodation in the matrix.

The TSS of the oxygen-strengthened Zircaloy-4 TIG weld is clearly distinct from that measured for the other unirradiated materials. Oxygen addition, above that typically found in Zircaloy, increased the hydrogen solubility and suppressed the dissolution and precipitation temperatures. This result is contrary to the findings of Erickson and Hardie [*9*], who observed that the $\alpha/\alpha + \delta$ phase boundary in zirconium was not affected by oxygen additions up to 7700 ppm. There are at least two effects that could account for the different behavior of the oxygen-strengthened weld. The first could be due to hydrogen trapping caused by the additional oxygen solute atoms. The second effect could be the increase in matrix strength caused by the addition of oxygen.

Table 1 shows that at room temperature the oxygen-strengthened material was significantly stronger than other unirradiated materials, but not as strong as the irradiation-hardened materials. However, the strength differential between the oxygen-strengthened and unirradiated materials reduces with increasing temperature, and the diminishing strength differential would imply that the observed shift in TSS at higher temperature is not due to matrix strength, and the alternative mechanism of hydrogen trapping at oxygen solute atoms is favored by the authors. The lack of a significant influence of matrix strength is also indicated by the measurements made on the β-quenched Zircaloy-2 forging in the as-quenched and 30% cold-worked conditions. Although the cold-worked material was as strong as the oxygen strengthened material at room temperature, it did not exhibit a shift in TSS.

It is clearly very difficult to elucidate the exact mechanism behind the different TSS behavior of the oxygen-strengthened material based on the limited experiments reported there. There is little published in the literature that strongly supports either of the two mechanisms proposed. Although Kearns [*6*] has observed that cold work does not affect the TSS, Khatamian [*28*] has reported that dissolved oxygen does not trap hydrogen in Zr-2.5Nb. Further work would need to be carried out in order to understand the mechanisms behind the different TSS behavior of the oxygen-strengthened material.

Irradiated Material Behavior

The enhanced hydrogen solubility in irradiated Zircaloy-2 and Zircaloy-4 has been shown to be attributable to the irradiation damage. The temperature at which irradiation damage

anneals out can be obtained from the recovery of irradiated tensile properties. Data in the literature show some differences in the temperature for the onset of annealing, with a tendency for low fluence irradiation to anneal at a lower temperature than higher fluence. For example, Zircaloy-2 irradiated to 7.7×10^{19} n/m² (total neutrons) at 250°C showed a 50% recovery of the irradiation-induced yield stress after 1 h at 325°C [*29*]. Zircaloy-2 irradiated to 5.5×10^{19} n/cm² ($E > 1$ MeV) at 250°C exhibited a 50% recovery of the irradiation-induced hardness increase after annealing for 1 h at 380°C [*30*]. For Zircaloy-4 irradiated to 1.5×10^{21} n/cm² ($E > 1$ MeV), significant recovery did not occur until approximately 400°C for anneals of 1 h [*31*]. These studies are compatible with the recovery of the irradiation-induced TSS shift observed in this work for Zircaloy-2 and Zircaloy-4 irradiated to fluences in the range 5.5×10^{20} to 5.5×10^{21} n/cm² ($E > 1$ MeV). Partial recovery of the TSS shift was observed after 1 h at 400°C, and full recovery was observed after 1 h at 500°C.

The lack of a significant effect of fluence level on TSS, within the above range, can be explained by the fact that irradiation-induced increases in the defect density (⟨a⟩ component dislocation loops) and strength tend to build up rapidly with increasing fluence and then saturate. Data in the literature indicate that this saturation occurs in Zircaloy at a fluence level of approximately 2.0×10^{20} n/cm² ($E > 1$ MeV) [*32*].

It was observed, however, that Zircaloy-2 pressure tube (75 ppm) irradiated to a fluence level of 1×10^{22} n/cm² ($E > 1$ MeV) exhibited a greater shift in TSS from the unirradiated value and an incomplete recovery on annealing at 500°C for 1 h (Figs. 13 and 14). As discussed below, this difference in behavior might be attributable to the development of the irradiation-induced microstructure at high fluence through the formation of a high density of ⟨c⟩ component dislocation loops [*33*], which may be more resistant to recovery on annealing.

The differences in the dislocation density for the different material conditions (annealed, cold worked, and irradiated) are believed to account for the differences in hydrogen solubility through the trapping of hydrogen at dislocations. Dislocation density measurements on samples representative of the test materials indicate that, in the annealed condition, the density of ⟨a⟩ component dislocations (⟨a⟩ loops) is 0.08 to 0.17×10^{14} m^{-2}, and the density of ⟨c⟩ component dislocations (⟨c⟩ loops) is 0.01 to 0.03×10^{14} m^{-2}. The dislocation density of the cold-worked material was not measured, and values for cold-worked material are not readily available in the literature, but the density will be higher than in annealed material and will include a higher density of ⟨c⟩ loops. The dislocation density will increase with the level of cold work such that at high levels of cold work an effect on hydrogen solubility may be observed.

Irradiation modifies the dislocation structure, and the dislocation density will depend on the fluence level. The ⟨a⟩ loop density tends to saturate at low fluences, but ⟨c⟩ loops can evolve with increasing fluence. When the annealed material was irradiated to a fluence of 3 to 4.75×10^{21} n/cm², the density of ⟨a⟩ loops increased to 6.5 to 9.1×10^{14} m^{-2}, and the density of ⟨c⟩ loops increased to 0.12 to 0.47×10^{14} m^{-2}. These values are typical of the irradiated electron-beam-welded Zircaloy tested. Thus, there is approximately an order of magnitude increase in the ⟨c⟩ loop density and a two order of magnitude increase in the ⟨a⟩ loop density. At higher fluence levels, a further increase in the ⟨c⟩ loop density would be expected: the ⟨c⟩ loop density for the Zircaloy-2 pressure tube irradiated to a fluence of 1×10^{22} n/cm^{-2} is reported as 2.48×10^{14} m^{-2} [*33*].

The different TSS response to annealing of the irradiated pressure tube, compared to the irradiated weld material, is considered to be consistent with the differences in dislocation structure. The ⟨a⟩ loops will tend to anneal out, but the ⟨c⟩ loops are more likely to remain after annealing as trap sites for hydrogen. This is reflected by the higher hydrogen solubility of the annealed irradiated pressure tube when compared to unirradiated material. Further

measurements of dislocation densities for the materials tested would be needed to substantiate this theory.

It is therefore hypothesized that the effect of irradiation is to trap hydrogen at the irradiation damage sites, and this trapped hydrogen is not available to contribute to the hydride precipitation and dissolution processes. There is a considerable amount of data on hydrogen trapping at crystalline defects in transition metals, and there is clear evidence for hydrogen trapping at vacancy defects and dislocation lines in zirconium. Trap energies have been established for the important crystalline defects. The trap depth in zirconium is approximately 0.3 eV [*34*]. There is also experimental evidence that the irradiation-induced microstructure inhibits hydrogen diffusion during irradiation [*35*]. Although there is not direct experimental evidence to support the trapping of hydrogen at solutes, it is considered that solutes could be weak traps for hydrogen and that solute-defect complexes could be stronger traps.

An alternative hypothesis for the shift in TSS with irradiation is that it is due to the increase in matrix strength. Increasing matrix strength should make hydride precipitation less favorable because both elastic and plastic deformation are required to accommodate the substantial local volume change. Thus, hydrides only precipitate, grow, and dissolve in conjunction with dislocation activity, or plastic work, in the surrounding matrix. This matrix strength hypothesis and the hydrogen-trapping hypothesis have been assessed, and the likely magnitude of any effect on the solubility limit as a result of a change in yield strength due to irradiation or oxygen strengthening was found to be very small and insufficient to account for the increase in solubility. The assessment considered the effect of a uniformly applied hydrostatic stress on the solubility limit. At the solvus, hydrogen in solution is in equilibrium with hydrogen in the hydride, and the chemical potentials of hydrogen in both are equal. In the presence of a uniform stress, the chemical potential is lowered by a term involving the stress and the partial molar volumes of hydrogen in solution and in hydride. However, these partial molar volumes are approximately equal, so effectively the solvus in the presence of stress remains unchanged [*36*]. This approach was used to assess the change in solubility due to a change in yield strength by modeling the change in yield strength as the application of a compressive hydrostatic stress. It was found that the increase in yield strength due to either irradiation or oxygen strengthening would have caused only a 1 to 2% change in the solubility limit.

In contrast, the irradiation trapping mechanism is capable of producing effects of the magnitude required, providing sufficient traps can be identified. From consideration of theoretical models for hydrogen trapping [*35*], it can be concluded that isolated vacancies are incapable of trapping the required amount of hydrogen because their concentration during irradiation is too low. However, if dislocation loops are treated as traps, these defects are capable of trapping sufficient hydrogen. Based on typical dislocation densities in irradiated Zircaloy, a trap depth of 0.3 eV will trap a sufficient quantity of hydrogen to give the observed changes in the solubility limits.

Conclusions

1. Apart from the oxygen-strengthened material, there was no significant difference in either the TSSd or TSSp behavior for the unirradiated Zircaloy materials tested, suggesting little effect of material composition or microstructure on TSS.
2. Cold work and the associated increase in matrix strength level had little effect on the TSS in a β-quenched Zircaloy-2 forging material, except at low hydrogen concentrations.

3. The oxygen-strengthened TIG welded Zircaloy-4 exhibited markedly different solubility behavior to the other unirradiated materials tested. The oxygen addition increased the hydrogen solubility and suppressed the dissolution and precipitation temperatures. This effect is considered due to hydrogen trapping by the oxygen solute.
4. Increasing the peak temperature and/or the hold time at peak temperature in the thermal cycle decreased the TSSp temperature and increased the hysteresis between TSSd and TSSp. This is considered to be due to a reduction of the "memory effect" in which preferential sites (dislocation networks) for hydride precipitation are removed at higher temperatures. Heating and cooling rates over the range 0.5 to 10°C/min have little effect on the measured dissolution and precipitation temperatures.
5. Neutron irradiation significantly increases the solubility of hydrogen in annealed and cold-worked Zircaloy. This was observed in both weld and parent material. No difference in the effect of irradiation on TSS was observed for fluence levels in the range 5.5×10^{20} to 5.5×10^{21} n/cm^2 ($E > 1$ MeV), although there is evidence of a greater effect at higher fluence.
6. A thermal anneal to remove the irradiation damage tended to restore the TSS values to those measured on unirradiated Zircaloy, demonstrating that the increased solubility is directly related to irradiation damage.
7. It has been hypothesized that the shift in TSS in irradiated material is due to hydrogen trapping because the high density of irradiation-induced defects, in particular ⟨a⟩ and ⟨c⟩ loops, created during irradiation act as potent traps for hydrogen. The trap depth is expected to be approximately 0.3 eV. Trapped hydrogen is not available to contribute to the hydride precipitation and dissolution processes.
8. An alternative mechanism considered for the shift in TSS with irradiation involves the increase in matrix strength caused by neutron irradiation. However, the absence of a significant effect of cold work on TSS and theoretical considerations do not appear to support this hypothesis.

Acknowledgments

The application of DSC to the measurement of TSS in zirconium alloys was developed by K. Tashiro of Ontario Hydro Technologies. In addition, the contribution of the following to the work described in this paper is gratefully acknowledged. G. Shek and K. Tashiro of Ontario Hydro Technologies for hydriding and DSC measurements. J. van der Kuur, G. A. Bickle, and colleagues, Atomic Energy of Canada Limited, for hydriding, DSC measurements, and hydrogen analyses. C. English and P. Agnew, AEA Technology, for review and discussion on irradiation-trapping mechanisms.

References

[*1*] Kreyns, P. H. Bourgeois, W. F., White, C. J. Charpentier, P. L., Kammenzind, B. F., and Franklin, D. G., "Embrittlement of Reactor Core Materials," *Zirconium in the Nuclear Industry: Eleventh International Symposium, ASTM STP 1295*, E. R. Bradley and G. P. Sabol., Eds., American Society for Testing and Materials, 1996, pp. 758–782.

[2] Garde, A. M., Smith, G. P., and Pirek, R. C., "Effects of Hydride Precipitate Localization and Neutron Fluence on the Ductility of Irradiated Zircaloy-4" *Zirconium in the Nuclear Industry: Eleventh International Symposium, ASTM STP 1295*, E. R. Bradley and G. P. Sabol, Eds., American Society for Testing and Materials, 1996, pp. 407–430.

[3] Puls, M. P., "Assessment of Aging of Zr-2.5Nb Pressure Tubes in CANDU Reactors," *Nuclear Engineering and Design,* Vol. 171, 1997, pp. 137–148.
[4] Cheadle, B. A., Coleman, C. E., and Ambler, J. F. R., "Prevention of Delayed Hydride Cracking in Zirconium Alloys," *Zirconium in the Nuclear Industry: Seventh International Symposium, ASTM STP 939,* R. B. Adamson and L. F. P. Van Swam, Eds., American Society for Testing and Materials, 1987, pp. 224–240.
[5] Gee, C. F. Scott, P. M., and Truswell, A. E., "Factors Affecting Fatigue Crack Growth Rates in Zircaloy Components in Reactor Water Environments," *Proceedings, Fourth International Symposium on Environmental Degradation of Materials in Nuclear Power Systems—Water Reactors,* Jekyll Island, Georgia, 6–10 Aug. 1989, pp. 10–47 to 10–58.
[6] Kearns, J. J., "Terminal Solubility and Partitioning of Hydrogen in the Alpha-Phase of Zirconium, Zircaloy-2 and Zircaloy-4," *Journal of Nuclear Materials,* Vol. 22, 1967, pp. 292–303.
[7] Sawatzky, A. and Wilkins, B. J., "Hydrogen Solubility in Zirconium Alloys Determined by Thermal Diffusion," *Journal of Nuclear Materials,* Vol. 22, 1967, pp. 304–310.
[8] Kammenzind, B. F., Franklin, D. G., Peters, H. R., and Duffin, W. J., "Hydrogen Pickup and Redistribution in Alpha-Annealed Zircaloy-4," *Zirconium in the Nuclear Industry: Eleventh International Symposium, ASTM STP 1295,* E. R. Bradley and G. P. Sabol, Eds., American Society for Testing and Materials, 1996, pp. 338–370.
[9] Erickson, W. H. and Hardie, D., "The Influence of Alloying Elements on the Terminal Solubility of Hydrogen in Alpha-Zirconium," *Journal of Nuclear Materials,* Vol. 13, No. 2, 1964, pp. 254–262.
[10] Slattery, G. F., "The Terminal Solubility of Hydrogen in Zirconium Alloys Between 30 and 400°C," *Journal of Institute of Metals,* Vol. 95, 1967, pp. 43–47.
[11] Khatamian, D., Pan, Z. L., Puls, M. P., and Cann, C. D., "Hydrogen Solubility Limits in Excel, an Experimental Zirconium-based Alloy," *Journal of Alloys and Compounds,* Vol. 231, 1995, pp. 488–493.
[12] Mallet, M. W. and Albrecht, W. M., "Low-Pressure Solubility and Diffusion of Hydrogen in Zirconium," *Journal of Electrochemical Society,* Vol. 104, No. 3, March 1957, pp. 142–146.
[13] Erickson, W. H., "Hydrogen Solubility in Zirconium Alloys," *Electrochemical Technology,* Vol. 4, No. 5–6, May–June 1966.
[14] Ostberg, G., "Determination of Hydride Solubility in Alpha-Phase Zirconium, Zircaloy-2 and Zircaloy-4," *Journal of Nuclear Materials,* Vol. 5, No. 2, 1962, pp. 208–215.
[15] Mishra, S. and Asundi, M. K., "Determination of Solid Solubility Limit of Hydrogen in Alpha-Zirconium by Internal Friction Measurements," *Zirconium in Nuclear Applications, ASTM STP 551,* American Society for Testing and Materials, 1974, pp. 63–71.
[16] Ritchie, I. G. and Sprungmann, K. W., "Hydride Precipitation in Zirconium Studied by Low Frequency Pendulum Techniques," *Journal de Physique,* Colloque C9, Supplement 12, Tome 44, December 1983, pp. 313–318.
[17] Pan, Z. L., Ritchie, I. G., and Puls, M. P., "The Terminal Solid Solubility of Hydrogen and Deuterium in Zr-2.5Nb Alloys," *Journal of Nuclear Materials,* Vol. 228, 1996, pp. 227–237.
[18] Ritchie, I. G. and Pan, Z. L., "Internal Friction and Young's Modulus Measurements in Zr-2.5Nb Alloy Doped with Hydrogen," *M³D: Mechanics and Mechanisms of Material Damping, ASTM STP 1169,* V. K. Kinra and A. Wolfensen, Eds., American Society for Testing and Materials, 1992, pp. 385–395.
[19] Cann, C. D. and Atrens, A., "A Metallographic Study of the Terminal Solid Solubility of Hydrogen in Zirconium at Low Hydrogen Concentrations," *Journal of Nuclear Materials,* Vol. 88, 1980, pp. 42–50.
[20] Mishima, Y., Ishino, S., and Nakajima, S., "A Resistometric Study of the Solution and Precipitation of Hydrides in Unalloyed Zirconium," *Journal of Nuclear Materials,* Vol. 27, 1968, pp. 335–344.
[21] Root, J. H. and Fong, R. W. L., "Neutron Diffraction Study of the Precipitation and Dissolution of Hydrides in Zr-2.5Nb Pressure Tube Material," *Journal of Nuclear Materials,* Vol. 232, 1996, pp. 72–85.
[22] Tashiro, K. M., "Hydrogen Measurements by Differential Scanning Calorimetry," *Ontario Hydro Research Review,* No. 8, August 1993, pp. 29–30.
[23] Khatamian, D. and Ling, V. C., "Hydrogen Solubility Limits in α- and β-Zirconium," *Journal of Alloys and Compounds,* Vols. 253–254, 1997, pp. 162–166.
[24] Cameron, D. J. and Duncan, R. G., "On the Existence of a Memory Effect in Hydride Precipitation in Cold-Worked Zr-2.5%Nb," *Journal of Nuclear Materials,* Vol. 68, 1977, pp. 304–344.
[25] Carpenter, G. J. C., "The Precipitation of γ-Zirconium Hydride in Zirconium," *Acta Metallurgica,* Vol. 26, 1978, pp. 1225–1235.

[26] Carpenter, G. J. C., "The Dilatational Misfit of Zirconium Hydrides Precipitated in Zirconium," *Journal of Nuclear Materials,* Vol. 48, 1973, pp. 264–266.
[27] Daniel, A. R, "Terminal Solid Solubility of Hydrogen in Zircaloy-2," AECL Report 2453, Atomic Energy of Canada Limited, June 1966.
[28] Khatamian, D., "Hydrogen Traps in the Oxide-Alloy Interface Region of Zr-Nb Alloys," *Journal of Alloys and Compounds,* Vol. 231, 1995, pp. 722–729.
[29] Howe, L. M., AECL Report 1024, CR Met-922, Atomic Energy of Canada Limited, Chalk River, Ontario, 1960.
[30] Carpenter, G. J. C. and Watters, J. F., "Irradiation Damage Recovery in Some Zirconium Alloys," *Zirconium in Nuclear Applications, ASTM STP 551,* American Society for Testing and Materials, 1974, pp. 400–415.
[31] Adamson, R. B., "Irradiation Growth of Zircaloy," *Zirconium in the Nuclear Industry: Third International Symposium, ASTM STP 633,* American Society for Testing and Materials, 1977, pp. 326–343.
[32] Carpenter, G. J. C. and Northwood, D. O., "The Contribution of Dislocation Loops to Radiation Growth and Creep of Zircaloy-2," *Journal of Nuclear Materials,* Vol. 56, No. 19, 1975, pp. 260–266.
[33] Griffiths, M., Holt, R. A., and Rogerson, A., "Microstructural Aspects of Accelerated Deformation of Zircaloy Nuclear Reactor Components During Service," *Journal of Nuclear Materials,* Vol. 225, 1995, pp. 245–258.
[34] Lewis, M. B., "Deuterium-Defect Trapping in Ion-Irradiated Zirconium," *Journal of Nuclear Materials,* Vol. 125, 1984, pp. 152–159.
[35] Morikawa, H., "Influence of Irradiation in the Reactor on Hydrogen Diffusion in α-Zirconium," GKSS Report 81/E/8, GKSS-Forschungszentrum Geesthacht GmbH, 1981.
[36] Eadie, R. L. and Coleman, C. L., "Effect of Stress on Hydride Precipitation in Zirconium-2.5% Niobium and on Delayed Hydride Cracking," *Scripta Metallurgica,* Vol. 23, 1989, pp. 1865–1870.